STRUCTURAL MORPHOLOGY AND STABILITY OF TENSEGRITY STRUCTURES(Dissertation_全文)

AUTHOR(S):

ZHANG, Jingyao

STRUCTURAL MORPHOLOGY AND STABILITY OF TENSEGRITY STRUCTURES

Jingyao ZHANG

Kyoto University, Japan

A thesis submitted for the degree of

2007

Acknowledgements

Firstly, I would like to thank my family far in China. I could have achieved nothing without their encourages, although in this long distance. It is very lucky to have such a supportive family, and very sorry for not being able to spend enough time with them within the recent ten years.

My deepest thanks go to my supervisors at Kyoto, Professor Makoto Ohsaki and Professor Naoki Katoh, for their patient guidance and supports during the master's and doctoral programs. Their substantial supports, not only on research but also in daily life, enable me to grow up gradually in academics and manage an easy life in Japan. The beginning is the hardest. The great patience of Professor Ohsaki got me though this hardest stage. The advices on optimization and some other related subjects from Professor Katoh have been very helpful.

It has been a very good time to work with Dr. Simon D. Guest at Cambridge on symmetry and tensegrity structures; I could not have gone that far on this subject without the instructive discussions with him for the whole academic year. I was so lucky to have the opportunity to discuss with Professor Robert Connelly of Cornel University and Professor Patrick Fowler of University of Sheffield, during my stay at Cambridge. Some work in the dissertation, for example the stability conditions and star-shaped structures, were suggested and inspired by Professor Connelly.

Comments and suggestions by Professor Koji Uetani at Kyoto, from the viewpoint of an expert scientist in structural mechanics, on the doctoral dissertation are very beneficial. The discussions with Dr.

Yoshihiro Kanno at Tokyo on tensegrity as well as group representation theory, those with Professor Yoshikazu Araki at Kyoto on system identification, and those with Mr. R. Pandia Raj at Cambridge on tensegrity and symmetry are of great help. I would also like to thank every member, former and current, in the Ohsaki lab; they have established an ideal atmosphere for study. I shall also thank Professor Motoyuki Suzuki of Tohoku University, who brought me to Japan.

Lastly, I would like to thank those have helped me but not listed here. Any little help will be remembered in my mind. The financial supports from The Kyoto University Foundation and the EPSRC for my academic visit to Cambridge are greatly appreciated.

Contents

Chapter 0

PREFACE

This study is devoted to the development of powerful tools for morphology (form-finding) problem of tensegrity structures, as well as provision of conditions for their stability investigation. Many well-established mathematical theories, such as optimization techniques, graph theory and group representation theory, have been extensively applied for these purposes. The results derived in the study are expected to benefit the in-depth understanding of the distinct properties of tensegrity structures compared to conventional structures, as well as to inspire novel applications in any disciplines as long as their principles are applicable.

Tensegrity structures are featured by the fact that they are stabilized in a self-equilibrium state by the continuous components (cables) in tension and discontinuous components (struts) in compression. Although this kind of structures appear to be very simple, with the truss-like appearances, there involve many universal principles that are applicable to the structures in nature, from micro scale (e.g., viruses and cells) to macro scale (e.g., structure of cosmos). Tensegrity structures have been successfully applied in many different areas, such as architecture, mechanical engineering, bio-medical engineering, mathematics and arts etc, making use of the structures themselves or their principles.

Tensegrity structures share many common properties together with cable nets: (a) both of them carry prestresses in the members, and (b) they are treated as pin-jointed structures. It is because of the introduction of these prestresses that stabilizes the structures, which are usually unstable in the unstressed state due to the existence of mechanisms. On the other hand, some difficulties arise in the their

design problem, since configuration and prestresses are highly interdependent on each other, and hence neither of them can be determined without considering the other. The design process of determining such a balanced configuration together with the prestresses in the state of self-equilibrium is called *morphology* or *form-finding*.

However, the morphology methods developed for cable nets cannot be simply applied to tensegrity structures, because they differ in the facts that (a) tensegrity structures are usually free-standing, while cable nets are attached to supports, and (b) tensegrity structures consist of both compressive and tensile members, while cable nets carry only tension. For the morphology problem of tensegrity structures, several numerical and analytical methods, including adaptive force density method, direct approach and symmetry strategy, are proposed to satisfy different requirements by the designers.

Furthermore, the pattern of distribution of prestresses in tensegrity structures has great influence on their stability. Unlike cable nets that are always stable since they carry only tension, stability of tensegrity structures cannot be guaranteed by the introduction of prestresses. To be more specific, the structures with the same configuration can be super stable, prestress stable or even unstable dependent on distribution of prestresses. This leads to the difficulties in their design problem, but it is also an attractive point since we have the opportunity to design the structure according to our specific requirements.

0.1 Organization

This study deals with morphology and stability problems in the design of tensegrity structures. The relations among each chapter, the topics as well as mathematical tools are illustrated in Fig. 1.

Chapters 2 and 3 discuss the stability criteria for tensegrity structures, and then present the stability conditions, which is used to guide their design problem.

There are two categories for the morphology of tensegrity structures: begin from the assumptions that both of the configuration and prestresses are unknown as in Chapters 4 and 5, and determine the distribution of prestresses for the structure with given configuration as in Chapter 9.

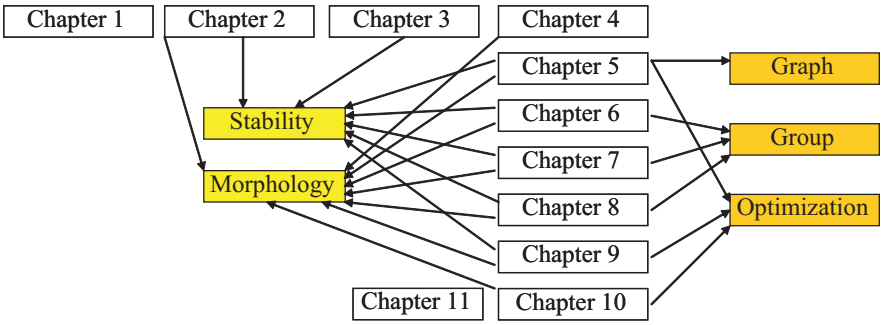

Figure 1: Relations between each chapter and the topics (on morphology and stability) as well as the mathematical tools (graph theory, group representation theory and optimization techniques).

The general super stability conditions for the structures with similar symmetry properties are available only by the analytical formulations for the block-diagonalization of the matrices presented in Chapter 6. The high level of symmetry of the structures is utilized to simplify stability investigation in Chapters 7, and 8, based on group representation theory.

Optimization techniques are utilized to find the optimal distribution of prestresses for the structures with multiple force modes in Chapter 9, as well as to search for the best measurement positions for the force identification in Chapter 10.

The detailed descriptions of each chapter are given as follows.

Chapter 1: Introduction

Chapter 1 introduces the basic concepts and principles of tensegrity structures, and investigates the applications in various areas. The existing studies on morphology and stability problems of tensegrity structures are briefly reviewed to provide background and motivation of the study.

Chapter 2: Basics

This chapter considers general pin-jointed structures. Formulations of the self-equilibrium equations of a pin-jointed structure are presented in two different ways: those with respect to nodal coordinates, and those with respect to prestresses. To avoid ending up in a lower dimensional structure,

a free-standing tensegrity structure has to satisfy the non-degeneracy condition, which is presented based on the solution space of nodal coordinates defined by the self-equilibrium equations.

Stiffness matrices are formulated for general pin-jointed structures. Three stability criteria—stability, prestress stability and super stability—are then defined and discussed in detail, based on these formulations. The discussions on the stability properties of pin-jointed structures enable us to divide them into three different categories: (a) trusses, (b) tensile structures, and (c) tensegrity structures. Tensegrity structures consist of both compressive and tensile members, and their stability are not clear unlike the structures in the other two categories.

Chapter 3: Stability Conditions

It is firstly proved that a stable tensegrity structure must satisfy the condition that the geometry matrix is of full rank. Further study shows that a tensegrity structure is guaranteed to be super stable, if the following two conditions are also satisfied in addition to the above-mentioned necessary condition: (a) the geometrical stiffness matrix is positive semi-definite; (b) the geometrical stiffness matrix is of minimum rank deficiency for non-degeneracy condition.

Stability conditions of tensegrity structures are also discussed based on linear dependency of the null-spaces of the linear and geometrical stiffness matrices. Prestress stability is demonstrated to be the necessary but not the sufficient condition for stable structures.

Chapter 4: Adaptive Force Density Method

Form-finding of a tensegrity structure by the proposed adaptive force density method is divided into two design stages: (1) to find the feasible force densities starting from the given initial values, and (2) to uniquely determine the self-equilibrated configuration (in terms of nodal coordinates). An efficient numerical method is presented for determining for feasible force densities that satisfy the non-degeneracy condition presented in Chapter 2.

The method has great advantage in guaranteeing super stable structures during the form-finding process.

To have more control over geometrical properties of the structure, geometrical constraints, such as symmetry and z-coordinates, that can be formulated in linear forms with respect to the force densities as well as the nodal coordinates, are incorporated into the two design stages of form-finding process.

Chapter 5: Direct Approach

To have precise control over member directions of a tensegrity structure, the structure is modelled as a directed graph. Self-equilibrated configuration of the structure, described in terms of components of prestresses and nodal coordinates in each direction, is determined by specifying the independent components consecutively in the proposed method. Furthermore, the non-degeneracy condition of the structure modeled by a directed graph is derived in terms of necessary rank deficiency of the modified equilibrium matrix by an effective algorithm.

Chapter 6: Symmetry-adapted Formulations

The stiffness matrices, the equilibrium matrix and the force density matrix are rewritten in symmetry-adapted (block-diagonal) forms in an analytical manner by transforming the current coordinate systems into the symmetry-adapted systems. Computation cost can then be significantly reduced by considering only the non-trivial blocks in their diagonals, which are of much smaller dimensions compared to the original matrices. In stead of using transformation matrices as in conventional numerical approaches, a direct strategy is presented for the analytical derivation of these blocks for the structures with dihedral symmetry, based on group representation theory. Computational costs are further reduced since the transformation matrices are no longer necessary. More importantly, these analytical formulations make it possible to find the general conditions for the super stability of prismatic and star-shaped structures Chapters 7 and 8, respectively.

Chapter 7: Prismatic Structures

Self-equilibrated configurations of prismatic tensegrity structures with dihedral symmetry are determined by considering only self-equilibrium of the representative nodes. Tt is proved that the prismatic structures are super stable, if and only if the horizontal cables are connected to adjacent nodes, using the analytical formulations presented in Chapter 6. It is further demonstrated that prestress stability of this class of structures is dependent on connectivity of the members, and is related to their geometry realization (height/radius ratios), if they are not super stable; moreover, the ratio of axial stiffness to prestress is another critical factor for their stability.

Chapter 8: Star-shaped Structures

Star-shaped tensegrity structures are also of dihedral symmetry, and have similar appearance to the prismatic structures. However, they have very different stability properties since the existence of center nodes introduce more mechanisms into the structure. Based on the symmetry-adapted formulations presented in Chapter 6, we prove that the star-shaped structures are super stable if and only if they have odd number of struts and the struts are as close to each other as possible.

Numerical investigation also indicates that this class of structures are prestress stable if their height/radius ratios are large enough. It is discovered that some prestress stable structures may have multiple stable configurations, and has been successfully traced by numerical analysis and confirmed by physical models.

Chapter 9: Force Design

Distribution of prestresses can be written as a linear combination of the independent force modes satisfying the self-equilibrium equations. For a structures with multiple force modes, it gives us the opportunity to make the structure as strong as possible by carefully selecting the prestresses. For this purpose, a bi-objective optimization problem is presented to maximize stiffness of the structure as well as to minimize the force deviation from target values. The curve of Pareto optimal solutions for these two objective functions is derived using the constrained approach, in order to let the

designers have the freedom to choose a solution according to their preference as a trade-off between the objectives.

Chapter 10: Force Identification

Distribution of prestresses of prestressed structures in service or under construction is necessary to be identified for their health monitoring, evaluation and maintenance. The identification error is formulated taking consideration of the measurement errors of the nodal coordinates as well as prestresses. We then study the problem of finding the optimal measurement positions such that the identification error is minimized with the specified number of measurement devices. This combinatorial optimization problem is solved by combining the basic idea of simulated annealing and stingy method, which shows the versatility in dealing with different preassumptions.

Chapter 11: Summaries

The proposed methods for morphology and derived conditions for stability of tensegrity structures are briefly summarized in this chapter.

Future studies to have deeper understanding of tensegrity structures are also discussed:

- Some tensegrity structures may consist of unstressed cables, which have zero stiffness in compression. Conventional stability investigation does not work well for these cases, since initially stressed members remain stressed, and therefore, do not lose their stiffness subject to infinitesimal displacements. To verify the stability of this kind of structures, several optimization problems are under consideration.
- When the symmetry operations of translations are also taken into account, the self-equilibrated configuration can be derived similar to the way for the structures with symmetry of point group, as illustrated by a two-dimensional structure with translation of unit cells in one single direction. However, the symmetry-adapted formulations for stiffness matrices presented in Chapter 6 may not work well since the structures

with space symmetry are intrinsically infinite, such that their stability problems need more further investigations.

0.2 Publications

The publications related to the study (to be) published in journals and (to be) presented in international and local conferences are listed as follows.

Journal Papers:

[J1] J.Y. Zhang and M. Ohsaki, Form-finding of self-stressed structures by an extended force density method. *Journal of the International Association for Shell and Spatial Structures*, 46, pp. 159–166, 2005.

[J2] J.Y. Zhang, M. Ohsaki and Y. Kanno, A direct approach to design of geometry and forces of tensegrity systems. *Int. J. Solids, Structures*, 43(7-8), pp. 2260–2278, 2006.

[J3] J.Y. Zhang and M. Ohsaki, Adaptive force density method for form-finding problem of tensegrity structures. *Int. J. Solids, Structures*, 43(18-19), pp. 5658–5673, 2006.

[J4] M. Ohsaki and J.Y. Zhang, Stability conditions of prestressed pin-jointed structures. *Int. J. Non-Linear Mechanics*, 41, pp. 1109-1117, 2006.

[J5] J.Y. Zhang and M. Ohsaki, Form-finding of tensegrity structures subjected to geometrical constraints. *Int. J. Space Structures*, 21(2), pp. 183–195, 2006.

[J6] J.Y. Zhang and M. Ohsaki, Stability conditions for tensegrity structures. *Int. J. Solids, Structures*, 44, pp. 3875–3886, 2007.

[J7] J.Y. Zhang and M. Ohsaki, Force identification of prestressed pin-jointed structures. *Computers and Structures*, submitted.

[J8] J.Y. Zhang, S. Guest and M. Ohsaki, Symmetric prismatic tensegrity structures I. configuration and stability. *Int. J. Solids, Structures*, to be submitted.

[J9] J.Y. Zhang, S. Guest and M. Ohsaki, Symmetric prismatic tensegrity structures II. symmetry-adapted formulations. *Int. J. Solids, Structures*, to be submitted.

[J10] M. Ohsaki, J.Y. Zhang and Y. Ohishi, Force design of tensegrity structures by enumeration of vertices of feasible region. *Int. J. Space Structures*, to be submitted.

[J11] J.Y. Zhang, S.D. Guest and M. Ohsaki, Star-shaped tensegrity structures. *Int. J. Solids, Structures*, to be submitted.

Conference Papers (with review):

[C1] J.Y. Zhang, M. Ohsaki and Y. Araki, Optimal measurement positions for identifying stress distribution of membrane structures using cable net approximation. *Proc. of the 3rd China-Japan-Korea Joint Symposium on Optimization of Structures and Mechanical Systems*, Kanazawa, Japan, pp. 547–552, Nov., 2004.

[C2] M. Ohsaki, J.Y. Zhang and J. Kimura, An optimization approach to design of geometry and forces of tensegrities. *Proc. of Symposium of International Association for Shell and Spatial Structures* , Bucharest, Romania, pp. 603–610, Sep., 2005.

[C3] J.Y. Zhang and M. Ohsaki, Form-finding of self-stressed structures by an extended force density method. *Proc. of Symposium of International Association for Shell and Spatial Structures*, Bucharest, Romania, pp. 93–100, Sep., 2005.

[C4] J.Y. Zhang, S. Guest and M. Ohsaki, Symmetric prismatic tensegrity structures. *Proc. of Symposium of International Association for Shell and Spatial Structures* (CD-ROM), Beijing, China, Oct., 2006.

[C5] J.Y. Zhang and M. Ohsaki, Multiobjective optimization for force design of tensegrity structures. *Proc. of the 4th China-Japan-Korea Joint Symposium on Optimization of Structures and Mechanical Systems* (CDROM), Kunming, China, Nov., 2006.

[C6] J.Y. Zhang, M. Ohsaki and S.D. Guest, Multi-stable tensegrity structures. *2006 Structural Analysis and Morphogenesis Colloquium*, pp. 105–110, Nagoya, Japan, Nov., 2006.

[C7] J.Y. Zhang and M. Ohsaki, Optimization methods for force and shape design of tensegrity structures. *Proc. of 7th World Congress on Structural and Multidisciplinary Optimization*, Soul, Korea, May, 2007.

[C8] J.Y. Zhang and M. Ohsaki, Optimization approach to force identification of prestressed pin-jointed structures. *Proc. of Symposium of International Association for Shell and Spatial Structures*, Venice, Italy, Dec., 2007. (to appear)

Oral Presentation (in Japanese):

[L1] J.Y. Zhang, M. Ohsaki and Y. Araki, Optimal measurement positions for identifying stresses of membrane structures modeled by cable net. *Summaries of Technical papers of Annual Meeting, AIJ*, Hokkaido, Japan, B-1, pp. 915–916, 2004.

[L2] M. Ohsaki, J.Y. Zhang and H. Tagawa, Shape optimization of beams with horizontal haunch and RBS considering elasto-plastic responses. *AIJ Kinki Branch*, Vol. 45, pp. 349–352, 2005.

[L3] J. Kimura, M. Ohsaki and J.Y. Zhang, Optimization method for determination of axial forces and shape of tensegrity structures. *Summaries of Technical papers of Annual Meeting, AIJ*, Kinki, Japan, B-1, pp. 941–942, 2005.

[L4] J.Y. Zhang and M. Ohsaki, A method for the form-finding problem of tensegrity structures by eigenvalue analysis of equilibrium matrix. *Summaries of Technical papers of Annual Meeting, AIJ*, Kinki, B-1, pp. 943–944, 2005.

[L5] M. Ohsaki, J.Y. Zhang and H. Tagawa, Shape optimization of beams with horizontal haunch and RBS considering elasto-plastic responses. *Summaries of Technical papers of Annual Meeting, AIJ*, Kinki, B-3, pp. 715–716, 2005.

[L6] M. Ohsaki and J.Y. Zhang, Form-finding and stability conditions for tensegrity structures. *2005 Annual Conference of The Japan Society for Industrial and Applied Mathematics*, pp. 78–79, 2005.

[L7] M. Ohsaki and J.Y. Zhang, Eigenvalue analysis for shape design and stability conditions for tensegrity structures. *The 55th Nat. Cong. of Theoretical & Applied Mechanics*, pp. 121–122, 2006.

[L8] M. Ohsaki and J.Y. Zhang, Design of tensegrity structures by optimization methods. *Proc. of International Conference on Computational Methods*, Hiroshima, April, 2007.

[L9] J.Y. Zhang and M. Ohsaki, Multi-stable star-shaped tensegrity structures. *AIJ Kinki Branch*, June, 2007.

[L10] J.Y. Zhang and M. Ohsaki, Form-finding of tensegrity towers. *Summaries of Technical papers of Annual Meeting, AIJ*, Kyusyu, B-1, Aug., 2007.

Chapter 1

INTRODUCTION

Weakness indicates strength.

—Tao Te Ching , by Lao-Tzu

Tensegrity structures are constructed by weak and global components (cables) that are flexible in unstressed state, together with strong and local components (struts); but they exhibit sufficient capability of resisting external loads while properly prestressed. The one-dimensional cables and struts are the simplest structural elements, and are most comprehensible since they carry only axial forces, either tension or compression. However, tensegrity structures might be one of the most 'complicated' structures in the world—they 'exist' universally, from virus in micro field to cosmos in macro.

For example, in the micro field, response of living cells subject to environmental changes can be interpreted and predicted by tensegrity models; in the mediate scale, body of an animal can be modeled as a tensegrity structure—skeletons and muscles respectively are the compressive members (struts) and tensile members (cables); and in the macro world, structure of the cosmos can also be regarded as a tensegrity structure, where the planets are the nodes and their interactions are the invisible members.

Since the invention of tensegrity structures by the artists, there have been a number of successful applications of their principles in many academic and non-academic fields, such as arts, bio-medical engineering, mechanical engineering and

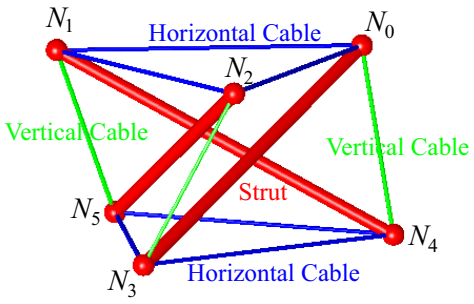

Figure 1.1: The simplest tensegrity structure in three-dimensional space. Struts are denoted by thick lines and cables by thin lines. A class of structures similar to this one will be revisited in Chapters 6 and 7 for their self-equilibrated configurations and stability properties.

mathematics etc. There are also some applications in architectural engineering, in the form of lightweight structures.

In this introduction chapter, Section 1 introduces the basic concepts and applications of tensegrity structures, and Section 2 reviews the existing researches for the morphology and stability problems of tensegrity structures.

1.1 Concepts and Applications

This section introduces the basic concepts of tensegrity structures firstly, and then some applications of their principles in various academic and non-academic fields, including arts, architecture, mechanical engineering, biomedical engineering and mathematics.

1.1.1 Basic Concepts

The term of *tensegrity* was created by Richard Buckminster Fuller as a contraction of 'tensional integrity' (Fuller, 1975). It refers to the integrity of stable structures as being based in a synergy between the balanced continuous tensile components and discontinuous compressive components. The tensile components that carry only tension are called *cables*, and the compressive components that carry compression are *struts*. Struts push the nodes away, while cables intend to

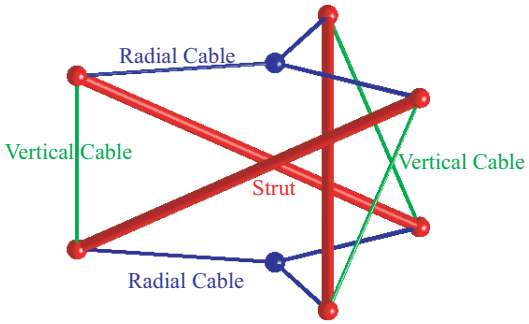

Figure 1.2: The simplest star-shaped prismatic tensegrity structure with dihedral symmetry. This structure is stable although the number of members is smaller than that is necessary according to the Maxwell's rule. Stability of this class of structures is investigated in Chapter 8.

pull them back, which makes all the nodes stay in the state that they are unmoved and balanced, the so-called *self-equilibrium state*. For example, Fig. 1.1 shows the simplest, and perhaps the most well-known, (prismatic) tensegrity structure in three-dimensional space. It is in the state of self-equilibrium, and composed of six nodes and twelve members; each node is connected by three cables shown as thin lines and one strut as thick line in the figure. The struts make no physical contact to any others.

Relation between struts and cables can be described as, isolated islands of compressive components (struts) are floating in an ocean of tension provided by tensile components (cables). In other words, struts are local components of a tensegrity structure, while cables are global. This distinct characteristics is very useful for long-span structures that cover large space, since materials can be effectively made use.

A structure is said to be *stable* if it returns to its initial configuration subject to any small disturbance. Stability of trusses that are composed of straight members connected at their ends by frictionless joints can be validated by the Maxwell's rule. In the paper by Maxwell (1864), he showed that a three-dimensional frame (truss) having n joints (nodes) requires in general $3n - 6$ bars (members without prestresses) to render it stable; i.e., a truss is stable if the number of bars m

satisfies

$$m = 3n - 6 \tag{1.1}$$

where 6 is the number of rigid-body motions of a structure in three-dimensional space. However, the Maxwell's rule is usually not applicable to tensegrity structures, although they have similar appearance and properties compared to trusses except for the existence of prestresses. Tensegrity structures can be stable with less members required by the Maxwell's rule as for conventional trusses. Consider the example structure, called star-shaped prismatic tensegrity structure, as shown in Fig. 1.2 for instance. The structure consists of eight nodes and twelve members, hence we have

$$m = 12 < 3n - 6 = 3 \times 8 - 6 = 18 \tag{1.2}$$

which indicates that the structure is not stable according to the Maxwell's rule in Eq. (1.1). However, this structure is indeed 'super' stable, regardless of materials that it is made of and level of prestresses, as will be discussed in Chapter 8 in detail.

In the cases of tensegrity structures, stability is ensured by the proper distribution of prestresses together with their self-equilibrated configurations. Based on their stability properties, trusses and tensegrity structures are classified into two different categories in Chapter 2.

Tensegrity structures were originally born in art. Their distinct mechanical properties as well as mathematical principles have then attracted great attentions of scientists and engineers in many different fields. The remaining of this section is devoted to brief introductions of their applications.

1.1.2 Applications in Arts

Tensegrity structures were invented by artists, and obtained their initial development in the field of art. Among the pioneers, Kenneth Snelson, David Georges Emmerich and Richard Buckminster Fuller should be remembered for their contribution to the initial development of tensegrity structures in the earliest stage. Motro (1992, 1996, 2003) gave a detailed history of development of tensegrity structures from their beginning to most recent.

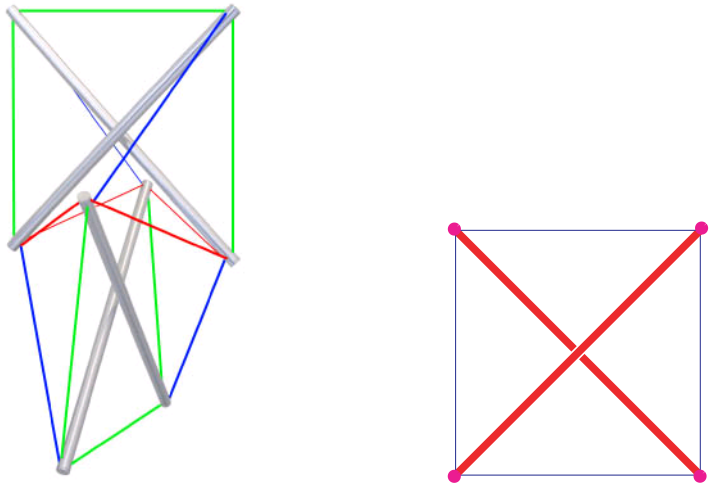

(a) X-shape structure (b) the simplest 2D tensegrity structure

Figure 1.3: The X-shape tensegrity structure in (a), courtesy of K. Snelson and *http://www.kennethsnelson.net*, is an assemble of the two-dimensional modules in (b), one to the other. The picture is a reproduction of X-shape tensegrity structure created by Snelson in 1948.

Tensegrity structure was first explored by Snelson, when he was experimenting to build flexible modular towers. In the summer of 1948, R.B. Fuller, who was his teacher at Black Mountain College, posed the question whether one can build a model to illustrate the structural principle of nature, which was observed to rely on that continuous tension embraces isolated compression elements. Fuller came up with the idea of the X-shape tensegrity structure as shown in Fig. 1.3 after several experiments, as the answer to this question.

In 1968, Snelson built an eighteen-meter-high "Needle Tower" as shown in Fig. 1.4, which is perhaps one of the most well-known tensegrity artwork in the world. The structure was constructed from the simplest three-dimensional tensegrity structure as shown in Fig. 1.1 as modules being assembled one to another. (This class of structures are studied as example structures for the proposed form-finding method in Chapter 4.) More artworks of tensegrity structures are available from the links published on our website: *http://tensegrity.AIStructure.com*

Besides high art, the idea of tensegrity structures has penetrated into low art as well: some baby toys employ the same principles as Snelson's original tensegrity structures.

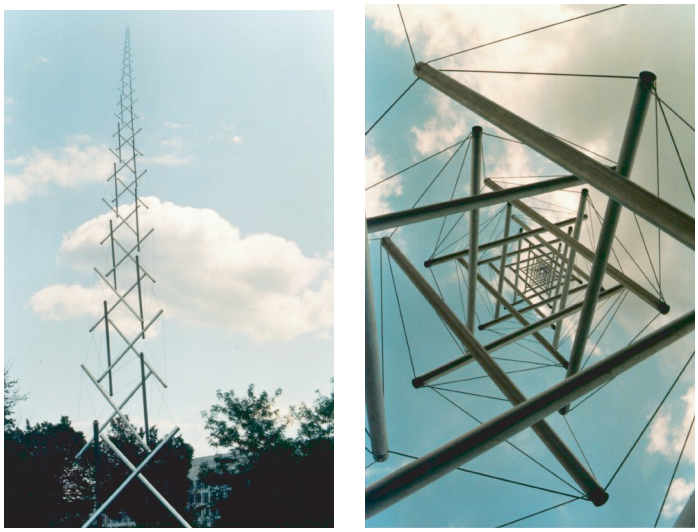

(a) side view (b) bottom view

Figure 1.4: Needle tower by Kenneth Snelson in 1968. It has been standing at the Hirshhorn Museum and Sculpture Garden, Smithsonian Institution, Washington D.C. since its construction.

Tensegrity structures had been regarded only as artworks for a long time until they attracted attentions of researchers in academics. After that, the community of tensegrity structures has been growing up much faster, and many of their important properties were discovered by theoretical studies. The in-depth understanding of them has also inspired novel applications as long-span structures in architectural engineering.

1.1.3 Applications in Architecture

Tensegrity structures are ideal structural forms for long-span structures because

- Introduction of prestress greatly enhance the stiffness of the tensegrity structures, such that they can be built with less materials to obtain the same capacity of resisting external loads.
- The struts in compression that are sensible to member buckling can be made much slender since they are local components of the tensegrity structures, and therefore, are much shorter than those of cables.

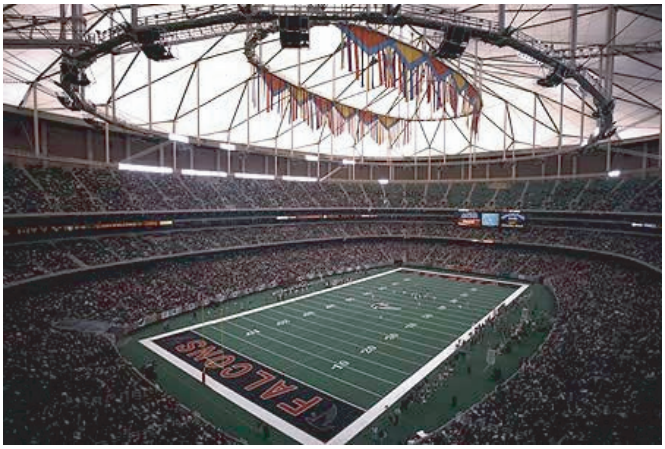

Figure 1.5: Inside view of the Georgia Dome, a special tensegrity structure. It was built in Atlanta U.S. in 1992 for the Atlanta Summer Olympic Games. It is a multi-purpose public stadium, that can be used for American football, concert, basketball and gymnastics.

- The cables are in tension such that they can make use of the high-strength materials without considering member buckling.
- Complex joints are not necessary since the struts in compression are connected by flexible cables.

The followings introduce the applications of tensegrity structures in architectural engineering as a structural system (cable dome) or as a structural component.

1.1.3.1 Cable Domes

David Geiger proposed and designed a permanent structure as an architectural form, called *cable dome* or *tensegrity dome*, in a competition of hall for the 1996 Atlanta Summer Olympic games in U.S. Construction of the dome was accomplished in 1992, at a cost of 214 million US dollars. The structure has a height of 82.5 meters, a length of 227 meters, a width of 185 meters, and a total floor area of 9,490 m^2. It seats 71,228 for football, up to 75,000 for concerts, and up to 40,000 for basketball and gymnastics. The great success aroused the interests and enthusiasms of many structural engineers and researchers, and a number of

Figure 1.6: Example of a pair of tensegrity structures used as frames to support a membrane roof, constructed at Chiba in Japan in 2001. (Architectural design by A. Fujii and structural design by K. Kawaguchi.) The left photo is the interior view of the building, the upper-right photo is its exterior view and the lower right is one of the tensegrity structure under construction. The photos are kindly provided by one of the designer, Professor K. Kawaguchi at the University of Tokyo.

tensegrity domes with different styles were built after that. However, difficulties in management and maintenance of prestresses during and after construction are the barriers for their further applications in architectural engineering. This problem is dealt with in Chapter 10 for their force identification.

1.1.3.2 Structural components

As another example, Fig. 1.6 shows a pair of tensegrity structures that are used as structural components in a building to support the roof made in membrane (Kawaguchi and Ohya, 2004). The structure was built in Chiba in Japan in 2001. One of the tensegrity structure is ten-meter high and the other is seven-meter high. Both of them are similar to the prismatic structure with three struts as shown in Fig. 1.1, but with three additional 'vertical' cables connecting to

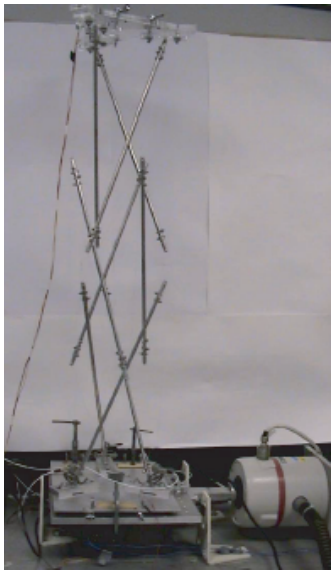

Figure 1.7: Vibration control of a three-stage tensegrity tower. Vibration on the top of the structure is to be reduced where enforced vibration is introduced at the bottom via shake table. The picture is courtesy of Professor R.E. Skleton.

the struts to ensure safety. An isolated strut is placed between the tensegrity structure and the membrane roof, and connected to the top of the structure.

1.1.4 Applications in Mechanical Engineering

Configuration of a tensegrity structure can be actively controlled by adjusting the prestresses introduced in the structure, because of the high interdependency between the self-equilibrated configuration and prestresses. Making use of this property, a number of 'smart' structures have been studied in mechanical engineering.

Tensegrity structure has predictable and linear response over a wide range of different shapes. And control systems (sensors and actuators) can be easily embedded and implemented in members, because they carry only axial forces. These advantages of tensegrity structures attracted some researchers to use them as smart structures, of which shapes are actively adjusted and controlled to satisfy different requirements in different circumstances.

For example, Fig. 1.7 is a three-layer tensegrity tower, which was used by Chan

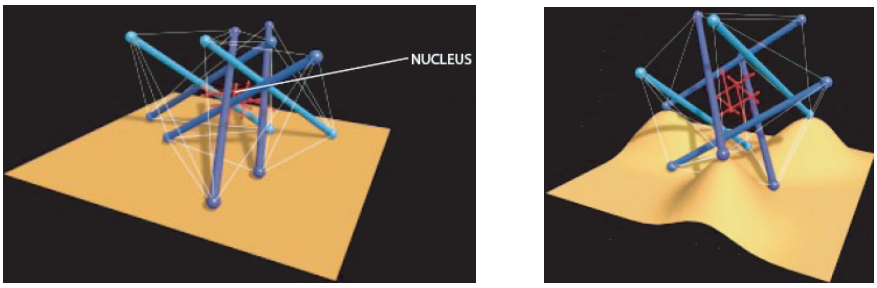

(a) shape on a flat surface (b) shape on a curved surface

Figure 1.8: Tensegrity model of a living cell, which interprets the different shapes of cells while placed on different surfaces. A living cell becomes flatter when it is placed on a flat surface as in (a), and becomes more spherical on a curved surface. The figures are taken from the introduction paper on applications of tensegrity structures in biology by Ingber (1998). The pictures are courtesy of Scientific American, Inc.

et al. (2004) for actively control of its vibration in real time. The structure is placed on a shake table, and the goal is to reduce vibration of the top of the structure. For this purpose, piezoelectric actuators and sensors used to adjust member lengths and measure internal forces are embedded in the members. Movie of the experiment is available from homepage of Structural Systems and Control Laboratory at UCSD in U.S.: *http://maeweb.ucsd.edu/ skelton/laboratory/SSCL.htm*

Principles of tensegrity structures can also be found in biomedical engineering, at various scales.

1.1.5 Applications in Biomedical Engineering

Tensegrity structures also aroused the interests in the biomedical community. The principles of tensegrity apply at essentially every detectable size scale in the body. At the macroscopic level, the 206 bones that constitute our skeleton are pulled up against the force of gravity and stabilized in a vertical form by the pull of tensile muscles, tendons and ligaments. In other words, bones can be regarded as struts and muscles (tendons and ligaments) as cables. At the other end of the scale, proteins and other key molecules in the body also stabilize themselves through the principles of tensegrity. Researchers in biomedical engineering were initially interested in using tensegrity structure as a model for the structure of viruses

(Caspar and Klug, 1962), for the purpose of interpretation of their structural behavior subject to change of external environment. Their increasing interests were extended to cellular structures at the microscopic level researches (Ingber, 1993).

Previously, biologists generally viewed the cell as a viscous fluid or gel surrounded by a membrane, much like a balloon filed with molasses. Cells were known to contain an internal framework, or cytoskeleton, composed of three different types of molecular protein polymers. But their role in controlling cell shape was poorly understood. For example, it was experimentally known that isolated cells behave differently when they are placed on different surfaces: they spread out and flatten when they are attached to a rigid glass or plastic culture dish, and contract to become more spherical when affixed to a flexible rubber substrate. This phenomenon has not been well interpreted until the tensegrity model for them was proposed—a smaller spherical tensegrity structure representing the nucleus is contained within a larger structure consisting of six struts as shown in Fig. 1.8.

Other than arts and engineering, tensegrity structures are not only studied in mathematics, mainly on their stability (structural rigidity in the language of mathematics), but also applied to solve some challenging mathematical problems.

1.1.6 Applications in Mathematics

Particle packing is an interesting as well as important problem, among the many applications of tensegrity structures in the field of mathematics. It studies how the particles can be packed together to occupy the minimum space. In other words, particle packing is to study what is the maximum volume that can be occupied by hard-particles of uniform of size and shape, when they are poured into a container with a given shape. An example of the problem is illustrated in Fig. 1.9 (Weiss, 2004). This problem has been a persistent scientific problem (many still open) for hundreds of years. The study on it helps scientists better understand the behavior of disordered materials ranging from powders to glassy solids, and could also lead to denser ceramic materials that might improve heat shields for furnaces and reduced-porosity glass with exceptional transparency.

Figure 1.9: Packing problem in mathematics using principles of tensegrity structures. In packing problem, the maximum number of objects with a given shape (M&M's chocolate candies for instance) is to be searched for a container with given configuration (e.g., the spherical container as in the figure). The picture is courtesy of Science News.

In any packing problems, the centers of hard-particles must keep a minimum distance but can be as far apart as desired. Thus, it can be regarded as a tensegrity with invisible struts. Furthermore, the particle packing problem can be formulated as a problem of detecting stability (rigidity in mathematics) of the tensegrity structures associated with the contact graph of the packing. The particle centers correspond to nodes of the structure, and interparticle contacts correspond to the members. The lengths of the cables are not allowed to decrease, which models the impenetrability constraints. A linear programming algorithm for detecting stability in hard sphere packing (equivalently, tensegrity structures) was proposed (Donev *et al.*, 2004).

1.2 Study Background and Existing Studies

This section introduces the background for our study on morphology and stability problems of tensegrity structures, and discusses the existing studies on them.

1.2.1 Study Background

Nodes of a tensegrity (or generally prestressed) structure stay in a state of self-equilibrium under the interaction of prestresses in its members, where struts with negative forces push the nodes away and cables with positive forces pull them back. Because of the high interdependence of prestresses and self-equilibrated configuration of a tensegrity structure, they have to be determined taking consideration of the other. The process of determination of them is called *form-finding* or *morphology*[1].

The difficulties in form-finding problem of tensegrity structures are to find the self-equilibrated configuration that satisfies specific properties required by the designers, as well as to derive the solutions in an efficient way. Some of the existing methods for the problem may not be efficient enough so that they can only be used for relative simple structures, and some others may lose the chance to have further insight into properties of the structures. To provide efficient analytical and numerical methods for form-finding problem of tensegrity structures is one of the main objectives in this study. The proposed methods should be comprehensible enough and robust, furthermore, should lead to in-depth understanding of their structural properties.

A stable tensegrity structure is in a state of self-equilibrium when no external loads are considered; however, self-equilibrium of a structure does naturally mean that it is stable! This can be explained from the viewpoint of energy: a structure has extreme value, either maximum or minimum, of strain energy (equivalent to total potential energy in this case since no external loads are applied), when it is in a state of self-equilibrium.

Stability of a structure is equivalent to positive definiteness of its tangent stiffness matrix, which is the second-order derivative of energy with respect to displacements (Thompson and Hunt, 1984). Stability of trusses carrying no prestresses can be easily verified by Maxwell's rule, which will be further discussed

[1]The term 'morphology' here is used to indicate the study dealing with the self-equilibrated configurations of tensegrity structures. Originally, it can mean: 1, The branch of biology that deals with the form and structure of organisms without consideration of function; 2, The form and structure of an organism or one of its parts.

in Chapter 2. Stability investigation of tensegrity structures is much more complicated due to the fact that prestresses are also involved in the tangent stiffness. On the other hand, this also provides the opportunity for a tensegrity structure to be stable with less members than that are necessary for a truss according to the Maxwell's rule, and much more important stability properties that are to be studied in the thesis.

Before introduction to our achievements on morphology and stability problem of tensegrity structures that are summarized in the next section, existing studies on them are briefly reviewed as follows.

1.2.2 Existing Studies on Morphology

In the early stage, tensegrity structures were studied by purely geometric approach, mainly by artists, where regular and convex polyhedra were usually used as references (Pugh, 1976). New self-equilibrated configurations were found (invented) by making physical models by trial and error, and mimicing polyhedra that were already known. Many interesting and even amazing tensegrity structures have been found by this kind of purely geometric approaches. The methods made the first and one of the most important contributions to the development of tensegrity structures by exploring and spreading the special structural philosophy behind this kind of structures. However, configurations determined by this kind of methods are restricted by knowledge on geometry of existing objects and intuition of human beings. More systematical ways certainly desired in practical design of tensegrity structures, and many excellent methods have been proposed after the structures attracted attentions of researchers in academics, especially in mathematics and engineering.

Tibert and Pellegrino (2003) presented a review paper for the existing methods for form-finding problem of tensegrity structures. The most recent review paper for this problem is by Juan and Tur (2007). These existing methods are briefly summarized as follows.

Symmetry Method:

For the structures with high level of symmetry, self-equilibrium equations of the whole structure can be simplified to that of its representative nodes. This way,

it is possible to derive analytical solutions even for complicated structures with large number of nodes and members. For example, Connelly and Terrell (1995) presented the general solution for symmetric prismatic tensegrity structures, and derived a catalogue of symmetric structures belonging to permutation group that are published on http://mathlab.cit.cornell.edu/visualization/tenseg/tenseg.html.

Optimization Method:

With the fixed lengths for cables, self-equilibrated configuration of a tensegrity structure can be determined by solving the optimization where total length of struts is to be maximized (Pellegrino, 1986).

Dynamic Relaxation Method:

The dynamic relaxation method and force density method were initially developed for form-finding problem of cable nets and tensile membrane structures Barnes (1999); Schek (1974).

In the dynamic relaxation method, the structure is enforced to deform from an initial configuration with zero velocities by the unbalanced loads. Deformation of the structure obeys the fictitious dynamic equations, and all nodal velocities are set to zero when the structure has local maximum of total kinetic energy. By repeating the above-mentioned process, the structure arrives at a self-equilibrated configuration when the local maximum of total kinetic energy becomes sufficiently small (Motro, 1984; Zhang *et al.*, 2006).

Force Density Method:

Equilibrium equations of a tensegrity structure can be written as product of the force density matrix and nodal coordinates. To make the force density matrix satisfy non-degeneracy condition, which will be presented in Chapter 2, Vassart and Motro (1999) proposed an analytical method to find the force densities of members in symbolic or semi-symbolic forms. The method provides opportunity to look inside the relation between different force densities, but is only applicable to relatively simple structures because symbolic computations are much time consuming and the analytical force densities may lose their meaning while there are too many. In Chapter 4, we will present a more powerful numerical method based on the similar idea, where stability can also be guaranteed in the form-finding process.

In fact, the symmetry method mentioned previously also belongs to the family of force density method, where force densities are involved in the self-equilibrium equations of representative nodes.

Internal Coordinate Method:

Self-equilibrium equations of a structure can be written as product of the equilibrium matrix in internal coordinate (members) system and prestresses. The equilibrium matrix should be singular so as to let the structure carry non-trivial prestresses. For this purpose, Sultan *et al.* (2001) used symbolic manipulation software, e.g. Maple or Mathematic, to derive the nodal coordinates that satisfies this condition.

Energy Method:

A structure is in a state of equilibrium when it has extreme value of energy, and is stable when the energy is locally minimum. Based on this idea, Connelly and Whiteley (1996) presented the energy method for determination of the self-equilibrium configurations of a stable structure. The energy method is equivalent to the force density method, so that they can also be classified in the family of force density method.

Each method mentioned above has its own merits and disadvantages as well. Among these, the force density method is considered to be most efficient and suitable to searching for new configuration with the given topology. The force density method may lead to much deeper insight into properties of tensegrity structures, which will be further discuss in the follows of the study.

1.2.3 Existing Studies on Stability

The stability criterion that the tangent stiffness matrix is positive definite is widely adopted in structural engineering. Since prestresses also contribute to stiffness of the structure, their influence should be further investigated to guide designs and applications in practice. For this purpose, there are two other stability criteria adopted in the community of tensegrity structures: prestress stability where stiffness of each member is assumed to be infinite, and super stability which indicates that the structure is always stable for any (conventional) materials and level of prestresses.

Assuming the members have infinite stiffness, the tangent stiffness matrix is reduced to the quadratic form of the geometrical stiffness matrix with respect to mechanisms that lie in the null-space of the linear stiffness matrix. Stability of the structure was then believed to be able to be verified by positive definiteness of the quadratic form (Calladine and Pellegrino, 1991). As discussed in Chapter 2, we will show that this is only the necessary but not the sufficient condition for stability of a tensegrity structure.

Connelly and Whiteley (1996) gave a detailed investigation on the second-order stability (prestress stability) of tensegrity structures. Furthermore, Connelly (1982, 1999) presented the necessary and sufficient conditions for the super stability of tensegrity structures. However, these conditions are descriptive in terms of mathematical terminologies, and not easy to understand and implement in computers, which motivates our studies on more comprehensible stability conditions.

Moreover, for the high level of symmetry of some tensegrity structures, the block-diagonalization of the relevant matrices might lead to thorough understanding the the whole class of structures with similar properties. Chapter 6 will present the analytical formulations for the studies on the structures with dihedral symmetry—the prismatic and star-shaped structures in Chapters 7 and 8, respectively.

Chapter 2

BASICS

This chapter is to provide basic definitions and formulations for further investigation of and discussions on tensegrity structures in the following chapters.

Definitions and formulations are presented for general pin-jointed structures, including the tensegrity structures. Topology is described in terms of graph theory and configuration in nodal coordinates. The equilibrium equations of a structure is formulated with respect to prestresses (member forces) with the equilibrium matrix and nodal coordinate with the force density matrix, respectively. The stiffness matrices are then formulated in terms of the equilibrium and force density matrices. Three stability criteria—stability, prestress stability, and super stability—are defined and discussed based on the positive definiteness of the stiffness matrices. The general pin-jointed structures are classified into (a) trusses, (b) tensile structures, and (c) tensegrity structures, based on the discussions of their stability properties.

To ensure that the final configuration of a tensegrity structure will not degenerate into the space with lower dimensions, the non-degeneracy condition is presented in terms of rank deficiency of the force density matrix.

2.1 Configuration

This section is to introduce the basic assumptions for all the studies on tensegrity structures in this dissertation, and to present the means of description of topology using graph theory as well as that of configuration in terms of nodal coordinates.

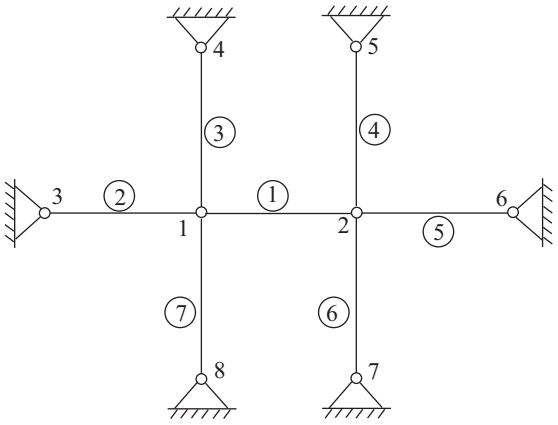

Figure 2.1: A two-dimensional cable net. The structure consists of both fixed and free nodes.

2.1.1 Assumptions

To presented the formulations for pin-jointed structures, the following assumptions that are widely used in structural engineering are adopted:

[L1] Members are straight and are connected by pin joints at their ends.

[L2] Self-weight of the structure is neglected, and no external loads are considered for its morphology and stability problem.

[L3] Member failure, such as yielding or buckling, is not considered.

[L4] All members of the structure are in stressed state, such that lose of stiffness of cable in compression is not taken into consideration in its stability investigation.

[L5] Stability investigation is based on up to second order of the energy.

From the assumptions (a) and (b), pin-jointed structures transmit only axial forces, if forces exist in the structures. that only axial forces, either in compression or tension, are transmitted by the members.

2.1.2 Topology

The way that the members of a pin-jointed structure are connected by the nodes is called *topology* or *connectivity* of the structure.

Because the members of the pin-jointed structures connect the nodes in the shortest paths, graph theory is used to describe the connectivity (topology) of them (Harary, 1969; Kaveh, 1992). The vertexes and edges in graph theory are the nodes and members of the structure, respectively. And the incidence matrix describing the topology of the structure is called *connectivity matrix* in the study.

Let k denote a member, and let i and j $(i < j)$ denote two nodes. If member k is connected to the nodes i and j, then the ith and jth elements of the kth row of the connectivity matrix $\mathbf{C}^s$ are 1 and -1, respectively; otherwise, if nodes i and j are not connected by the member k, then the corresponding elements in $\mathbf{C}^s$ are zero. Hence, the connectivity matrix $\mathbf{C}^s$ can be written as follows

$$\mathbf{C}^s_{(k,p)} = \begin{cases} 1 & \text{for } p = i \\ -1 & \text{for } p = j \\ 0 & \text{for other cases} \end{cases} \tag{2.1}$$

A pin-jointed structure usually has two types of nodes: fixed nodes and free nodes. The fixed nodes are attached to supports, and therefore, they cannot have any displacement even subject to external loads, whereas the displacements of the free nodes are not constrained. For example, the two-dimensional structure as shown in Fig. 2.1 has two free nodes 1 and 2, and is attached to the fixed nodes 3–8.

Suppose that a structure has m members, n free nodes and n^f fixed nodes. For convenience, the fixed nodes are preceded by the free nodes in the numbering sequence. Thus, the connectivity matrix $\mathbf{C}^s \in \Re^{m\times(n+n^f)}$ can be partitioned into two parts as

$$\mathbf{C}^s = (\mathbf{C},\ \mathbf{C}^f) \tag{2.2}$$

where $\mathbf{C} \in \Re^{m\times n}$ and $\mathbf{C}^f \in \Re^{m\times n^f}$ describe the connectivities of the members by the free and fixed nodes, respectively.

For example for the structure as shown in Fig. 2.1, the connectivity matrices $\mathbf{C}^s \in \Re^{7\times 8}$, $\mathbf{C} \in \Re^{7\times 2}$ and $\mathbf{C}^f \in \Re^{7\times 6}$ of the whole structure, the free and fixed

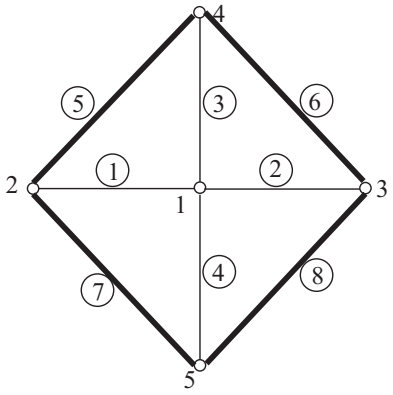

Figure 2.2: A two-dimensional tensegrity structure. The structure is free-standing, i.e., it has no fixed nodes.

nodes are written as follows, respectively

$$\mathbf{C}^s = \begin{array}{c|cc|cccccc} & 1 & 2 & 3 & 4 & 5 & 6 & 7 & 8 \\ \hline ① & 1 & -1 & 0 & 0 & 0 & 0 & 0 & 0 \\ ② & 1 & 0 & -1 & 0 & 0 & 0 & 0 & 0 \\ ③ & 1 & 0 & 0 & -1 & 0 & 0 & 0 & 0 \\ ④ & 0 & 1 & 0 & 0 & -1 & 0 & 0 & 0 \\ ⑤ & 0 & 1 & 0 & 0 & 0 & -1 & 0 & 0 \\ ⑥ & 0 & 1 & 0 & 0 & 0 & 0 & -1 & 0 \\ ⑦ & 1 & 0 & 0 & 0 & 0 & 0 & 0 & -1 \\ \hline & \multicolumn{2}{c|}{\mathbf{C}} & \multicolumn{6}{c}{\mathbf{C}^f} \end{array}$$

If a structure has only free nodes, then it is said to be *fress-standing*, because the rigid-body motions (see the detailed descriptions of the rigid-body motions in Chapter 3) have not been constrained and it can be freely transformed in the space preserving relative positions between the nodes and members. Tensegrity structures interested in the study are always free-standing, thus the connectivity matrix becomes

$$\mathbf{C}^s = \mathbf{C} \tag{2.3}$$

For example, the free-standing tensegrity structure in the two-dimensional space as shown in Fig. 2.2 consists of five free nodes and eight members. The

connectivity matrix $\mathbf{C}(=\mathbf{C}^s \in \Re^{8\times5})$ of the structure is

$$\mathbf{C}=\mathbf{C}^s=\begin{array}{c|ccccc} & 1 & 2 & 3 & 4 & 5 \\ \hline ① & 1 & -1 & 0 & 0 & 0 \\ ② & 1 & 0 & -1 & 0 & 0 \\ ③ & 1 & 0 & 0 & -1 & 0 \\ ④ & 1 & 0 & 0 & 0 & -1 \\ ⑤ & 0 & 1 & 0 & -1 & 0 \\ ⑥ & 0 & 0 & 1 & -1 & 0 \\ ⑦ & 0 & 1 & 0 & 0 & -1 \\ ⑧ & 0 & 0 & 1 & 0 & -1 \end{array}$$

2.1.3 Geometry

Consider a pin-jointed structure in d-dimensional (d=2 or 3) space. Let $\mathbf{x}$, $\mathbf{y}$, $\mathbf{z}$ ($\in \Re^n$) and $\mathbf{x}^f$, $\mathbf{y}^f$, $\mathbf{z}^f$ ($\in \Re^{n^f}$) denote the nodal coordinates of the free and fixed nodes in x-, y- and z-directions, respectively.

The coordinate differences u_k, v_k and w_k of the member k connecting to nodes i and $j(i<j)$ in x-, y- and z-directions can be respectively calculated as follows

$$u_k = x_i - x_j, \qquad v_k = y_i - y_j, \qquad w_k = z_i - z_j \tag{2.4}$$

From the definition of the connectivity matrix, which has only two non-zero elements in its k-row, 1 and -1 corresponding to the nodes i and j connected by the member k, Eq. (2.4) can be rewritten as

$$\begin{aligned} u_k &= \mathbf{C}_k\mathbf{x} + \mathbf{C}_k^f\mathbf{x}^f \\ v_k &= \mathbf{C}_k\mathbf{y} + \mathbf{C}_k^f\mathbf{y}^f \\ w_k &= \mathbf{C}_k\mathbf{z} + \mathbf{C}_k^f\mathbf{z}^f \end{aligned} \tag{2.5}$$

where $\mathbf{C}_k$ and $\mathbf{C}_k^f$ denote the k-th rows of $\mathbf{C}$ and $\mathbf{C}^f$, respectively. Hence, we can have the *coordinate difference vectors* $\mathbf{u}$, $\mathbf{v}$ and ($\mathbf{w} \in \Re^m$) as follows by combination of the coordinate differences in Eq. (2.5) for all members

$$\begin{aligned} \mathbf{u} &= \mathbf{C}\mathbf{x} + \mathbf{C}^f\mathbf{x}^f \\ \mathbf{v} &= \mathbf{C}\mathbf{y} + \mathbf{C}^f\mathbf{y}^f \\ \mathbf{w} &= \mathbf{C}\mathbf{z} + \mathbf{C}^f\mathbf{z}^f \end{aligned} \tag{2.6}$$

In some cases, it might be more convenient for us to use the diagonal form of a vector, which is denoted by the capital letter. For example, $\mathbf{U}$, $\mathbf{V}$ and $\mathbf{W}(\in$

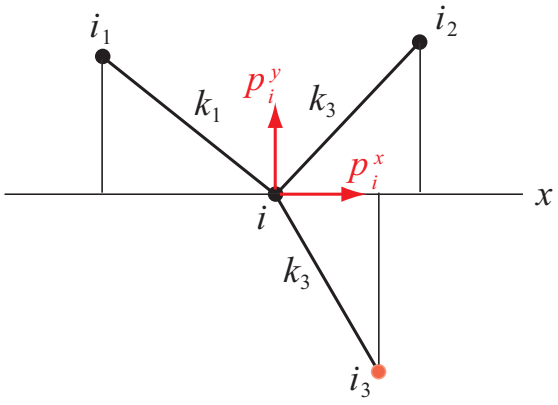

Figure 2.3: Equilibrium of a free node subject to external loads applied at the node.

$\Re^{m\times m}$) are the diagonal forms of the coordinate difference vectors $\mathbf{u}$, $\mathbf{v}$ and $\mathbf{w}$, respectively.

Because the length l_k of member k has the following relation with the its coordinate differences

$$l_k^2 = u_k^2 + v_k^2 + w_k^2$$

the *length vector* $\mathbf{l} \in \Re^m$ can be written as follows using the coordinate difference vectors

$$\mathbf{l}^2 = \mathbf{u}^2 + \mathbf{v}^2 + \mathbf{w}^2 \tag{2.7}$$

The diagonal form of $\mathbf{l}$ is denoted by $\mathbf{L}(\in \Re^{m\times m})$.

2.2 Equilibrium Analysis

In this section, the equilibrium equations are written as linear forms with respect to the prestresses by the equilibrium matrix, and with respect to the nodal coordinates by the force density matrix.

2.2.1 Equilibrium Matrix

Let $\mathbf{s} \in \Re^m$ denote the *prestress vector* of the structure, the k-th element s_k of which is the prestress (axial force) of member k.

Consider a free node i as shown in Fig. 2.3, which is connected by nodes $i_j (j = 1, 2, \ldots)$ as members k_j. A node is in a state of equilibrium only if the internal forces (prestresses) of the members are equilibrated by the external forces $\mathbf{p}$ applied on that node. Hence, the equilibrium equation of node i in x-direction can be written as

$$p_i^x = \sum_j s_{k_j}(x_{i_j} - x_i)/l_{k_j} \tag{2.8}$$

Because $(x_{i_j} - x_i)$ is the coordinate difference u_{k_j} of member k_j in x-direction, and the non-zero elements in the i-th column of $\mathbf{C}$ correspond to the nodes that are connected to the node i as members, the equilibrium equation of the free node i in x-direction can be rewritten as follows

$$p_i^x = \mathbf{C}_i^\top \mathbf{U}\mathbf{L}^{-1}\mathbf{s}$$

where $\mathbf{C}_i^\top$ denotes the ith row of the transpose of $\mathbf{C}$, and $\mathbf{L}^{-1}$ is the inverse of the length matrix $\mathbf{L}$. $\mathbf{C}_i^\top \mathbf{U}$ in the equation ensures that the coordinate differences are pointing from node i to nodes i_j, which is consistent with $(x_{i_j} - x_i)$ in Eq. (2.8).

Hence, the equilibrium equation for all the free nodes in x-direction is

$$\mathbf{p}^x = \mathbf{C}^\top \mathbf{U}\mathbf{L}^{-1}\mathbf{s} \tag{2.9}$$

Similarly, the equilibrium equations in y- and z-directions can be written as

$$\begin{aligned} \mathbf{p}^y &= \mathbf{C}^\top \mathbf{V}\mathbf{L}^{-1}\mathbf{s} \\ \mathbf{p}^z &= \mathbf{C}^\top \mathbf{W}\mathbf{L}^{-1}\mathbf{s} \end{aligned} \tag{2.10}$$

Writing

$$\mathbf{D} = \begin{pmatrix} \mathbf{D}^x \\ \mathbf{D}^y \\ \mathbf{D}^z \end{pmatrix} \begin{pmatrix} \mathbf{C}^\top \mathbf{U}\mathbf{L}^{-1} \\ \mathbf{C}^\top \mathbf{V}\mathbf{L}^{-1} \\ \mathbf{C}^\top \mathbf{W}\mathbf{L}^{-1} \end{pmatrix} \tag{2.11}$$

the equilibrium equations with respect to the prestresses in a linear form can be combined as

$$\mathbf{D}\mathbf{s} = \mathbf{p} = \begin{pmatrix} \mathbf{p}^x \\ \mathbf{p}^y \\ \mathbf{p}^z \end{pmatrix} \tag{2.12}$$

The matrix $\mathbf{D} \in \Re^{dn \times m}$ is called the *equilibrium matrix*.

2.2.2 Force Density Matrix

Let the prestress s_k to member length l_k denote the *force density* q_k of member k; i.e., $q_k = s_k/l_k$. The *force density vector* $\mathbf{q} \in \Re^m$ of the structure can then be calculated by

$$\mathbf{q} = \mathbf{L}^{-1}\mathbf{s} \tag{2.13}$$

Because the multiplication $\mathbf{Ab}$ of a diagonal matrix $\mathbf{A}$ with a vector $\mathbf{b}$ is equal to $\mathbf{Ba}$, where $\mathbf{A}$ and $\mathbf{B}$ are the diagonal versions of the vectors $\mathbf{a}$ and $\mathbf{b}$, respectively; i.e., $\mathbf{Ab} = \mathbf{Ba}$, the equilibrium equations (2.9) and (2.10) in each direction can be written as follows by using Eqs. (2.6) and (2.13)

$$\begin{aligned} \mathbf{C}^\top\mathbf{Qu} &= \mathbf{C}^\top\mathbf{QCx} + \mathbf{C}^\top\mathbf{QC}^f\mathbf{x}^f = \mathbf{p}^x \\ \mathbf{C}^\top\mathbf{Qv} &= \mathbf{C}^\top\mathbf{QCy} + \mathbf{C}^\top\mathbf{QC}^f\mathbf{y}^f = \mathbf{p}^y \\ \mathbf{C}^\top\mathbf{Qw} &= \mathbf{C}^\top\mathbf{QCz} + \mathbf{C}^\top\mathbf{QC}^f\mathbf{z}^f = \mathbf{p}^z \end{aligned} \tag{2.14}$$

where $\mathbf{A}$ is the diagonal version of $\mathbf{q}$.

Denote $\mathbf{E} \in \Re^{n\times n}$ and $\mathbf{E}^f \in \Re^{n\times n^f}$ as

$$\begin{aligned} \mathbf{E} &= \mathbf{C}^\top\mathbf{QC} \\ \mathbf{E}^f &= \mathbf{C}^\top\mathbf{QC}^f \end{aligned} \tag{2.15}$$

where $\mathbf{E}$ is called the *force density matrix* or stress matrix (Connelly, 1982). Note that the force density matrix $\mathbf{E}$ is not the diagonal version of the force density vector $\mathbf{q}$.

Instead of using $\mathbf{C}$ and $\mathbf{A}$ as Eq. (2.15), the force density matrix $\mathbf{E}$ can also be written directly from the force densities. Let $\mathcal{J}$ denote the set of members connected to free node i. The (i,j)-component $\mathbf{E}_{(i,j)}$ of $\mathbf{E}$ is given as

$$\mathbf{E}_{(i,j)} = \begin{cases} \sum_{k\in\mathcal{J}} q_k & \text{for } i = j \\ -q_k & \text{if nodes } i \text{ and } j \text{ are connected by member } k \\ 0 & \text{for other cases} \end{cases} \tag{2.16}$$

For example, the force density matrix $\mathbf{E}$ of the structure as shown in Fig. 2.1 can be written directly from Eq. (2.16) as

$$\mathbf{E} = \begin{pmatrix} q_1+q_2+q_3+q_7 & -q_1 \\ -q_1 & q_1+q_4+q_5+q_6 \end{pmatrix}$$

Obviously, $\mathbf{E}$ is always square and symmetric, and moreover, it is positive definite if all members are in tension; i.e. $q_k > 0$ $(k = 1, 2, \ldots, m)$.

As comparison, the force density matrix $\mathbf{E}$ of the two-dimensional tensegrity structure as shown in Fig. 2.2 is

$$\mathbf{E} = \begin{pmatrix} q_1+q_2+q_3+q_4 & -q_1 & -q_2 & -q_3 & -q_4 \\ -q_1 & q_1+q_5+q_7 & 0 & -q_5 & -q_7 \\ -q_2 & 0 & q_2+q_6+q_8 & -q_6 & -q_8 \\ -q_3 & -q_5 & -q_6 & q_3+q_5+q_6 & 0 \\ -q_4 & -q_7 & -q_8 & 0 & q_4+q_7+q_8 \end{pmatrix}$$

Apparently, the force density matrix is symmetric.

When the external loads are absent in Eq. (2.14) and there exist prestresses in the members, the structure is said to be in a state of *self-equilibrium*. The self-equilibrium equations of the structure can be written as follows by using Eq. (2.14)

$$\begin{aligned} \mathbf{E}\mathbf{x} &= -\mathbf{E}^f\mathbf{x}^f \\ \mathbf{E}\mathbf{y} &= -\mathbf{E}^f\mathbf{y}^f \\ \mathbf{E}\mathbf{z} &= -\mathbf{E}^f\mathbf{z}^f \end{aligned} \tag{2.17}$$

Because the connectivity of a structure is usually regarded to be constant, $\mathbf{E}$ and $\mathbf{E}^f$ defined in Eq. (2.15) are also constant if the force densities are assigned or determined a priori. This way, the non-linear self-equilibrium equation Eq. (2.17) with respect to the unknown nodal coordinates $\mathbf{x}$, $\mathbf{y}$ and $\mathbf{z}$ are transformed into a set of linear equations, because they are the only unknown parameters in the equations.

If the force density matrix $\mathbf{E}$ is full-rank, the unknown coordinates $\mathbf{x}$, $\mathbf{y}$ and $\mathbf{z}$ of the free nodes can be uniquely determined as

$$\begin{aligned} \mathbf{x} &= -\mathbf{E}^{-1}\mathbf{E}^f\mathbf{x}^f \\ \mathbf{y} &= -\mathbf{E}^{-1}\mathbf{E}^f\mathbf{y}^f \\ \mathbf{z} &= -\mathbf{E}^{-1}\mathbf{E}^f\mathbf{z}^f \end{aligned}$$

Hence, the configuration of the structure described in terms of nodal coordinates can be uniquely determined. This is the original idea of the *force density method* for the form-finding problem of cable nets, which transforms the non-linear self-equilibrium equations into a set of linear equations by the introduction of force density. Because the cable nets consist of only cables, the prestresses of which

are always positive (tensile), the force density matrix $\mathbf{E}$ of this kind of structures are always positive definite, and therefore, Eq. (2.17) always has unique solution (Schek, 1974).

The tensile membrane structures hold the most basic characteristics as the cable nets—both of them have only tensile members with positive prestresses, although membrane is a kind of continuous materials while cable is discrete. Hence, the basic idea of the force density method can also be applied to the form-finding problem of the tensile membrane structures, by substituting the membrane materials by the cables based on the principle of virtual work (Maurin and Motro, 1998).

However, the same idea cannot be simply applied to the form-finding problem of tensegrity structures. The force density matrix of a tensegrity structure is always rank deficient, because of its being free-standing, and therefore, not invertible for the unique determination of the configuration in the case of tensegrity structures. Moreover, the existence of struts with negative prestresses can make the rank deficiency of the force density matrix even larger. As will be discussed in the next section, the force density matrix of a tensegrity structure should have the right rank deficiency in order to ensure a non-degenerate configuration in the interested space. This is one of the motivation for us to extend the excellent idea of the force density method to the problem of tensegrity structures, which is called *adaptive force density method*, presented in Chapter 4.

2.3 Non-degeneracy Condition

From the definition in Eq. (2.15) or Eq. (2.16), the force density matrix of a tensegrity structure has rank deficiency of at least one, because the sum of its elements in each row or column is always equal to zero. This is caused by the fact that the tensegrity structures are free-standing without any fixed nodes. Hence, the self-equilibrium equations of the tensegrity structures can be written as follows

$$\begin{aligned} \mathbf{E}\mathbf{x} &= \mathbf{p}^x = \mathbf{0} \\ \mathbf{E}\mathbf{y} &= \mathbf{p}^y = \mathbf{0} \\ \mathbf{E}\mathbf{z} &= \mathbf{p}^z = \mathbf{0} \end{aligned} \tag{2.18}$$

Define rank deficiency r^E of $\mathbf{E}$ as

$$r^E = n - \text{rank}(\mathbf{E}) \tag{2.19}$$

From Eq. (2.18), we know that the solution space of the self-equilibrium equation in each direction is spanned by r^E independent vectors.

If a structure lies in a space with less dimensions than d, then the structure is said to be *degenerate* in the d-dimensional space. For example, the structure in Fig. 2.2 is degenerate in the three-dimensional space, because it can lie in a two-dimensional space (e.g., the plane parallel to the paper). From the definition of degeneracy of a structure in d-dimensional space, we have the following lemma:

Lemma 2.1 *The nodal coordinate vectors are linearly independent if the structure is non-degenerate.*

Proof. Suppose the coordinate vectors $\mathbf{x}$, $\mathbf{y}$ and $\mathbf{z}$ of a three-dimensional structure are linearly dependent. Thus, we have the following equation

$$\beta_1\mathbf{x} + \beta_2\mathbf{y} + \beta_3\mathbf{z} = \mathbf{0} \tag{2.20}$$

where the arbitrary coefficients β_1, β_2 and β_3 cannot be equal to zero simultaneously.

Since Eq. (2.20) is an equation of a plane, the three-dimensional structure can then lie in the plane defined by Eq. (2.20). Hence, the structure is degenerate in the three-dimensional space, which conflicts with the assumption of non-degeneracy of the structure. Therefore, the nodal coordinate vectors $\mathbf{x}$, $\mathbf{y}$ and $\mathbf{z}$ in three-dimensional space are linearly independent, if the structure is non-degenerate.

Two-dimensional case can be proved similarly, which completes the proof. □

Furthermore, for the tensegrity structure, r^E should satisfy the following non-degeneracy condition in order to have the non-degenerate configuration in the interested space with specific dimensions.

Lemma 2.2 Non-degeneracy Condition for Tensegrity Structures: *If a tensegrity structure is non-degenerate in d-dimensional space, then the rank deficiency r^E of its force density matrix should hold the following relation*

$$r^E \geq d + 1 \tag{2.21}$$

Proof. Let $\mathbf{x}_0$, $\mathbf{y}_0$ and $\mathbf{z}_0$ be defined as

$$\begin{aligned} \mathbf{x}_0 &= \alpha_0^x \bar{\mathbf{I}} \\ \mathbf{y}_0 &= \alpha_0^y \bar{\mathbf{I}} \\ \mathbf{z}_0 &= \alpha_0^z \bar{\mathbf{I}} \end{aligned}$$

where all the elements of the vector $\bar{\mathbf{I}} \in \Re^n$ are equal to 1, and the coefficients α_0^z, α_0^y and α_0^z can have arbitrary values. Since the sum of the elements of any row of $\mathbf{E}$ is always equal to zero for a tensegrity structure, it is obvious that $\mathbf{x}_0$, $\mathbf{y}_0$ and $\mathbf{z}_0$ are the solutions of Eq. (2.18). Accordingly, the solutions of Eq. (2.18) can be combined to a general form as

$$\begin{pmatrix} \mathbf{x} \\ \mathbf{y} \\ \mathbf{z} \end{pmatrix} = \begin{pmatrix} \mathbf{x}_0 \\ \mathbf{y}_0 \\ \mathbf{z}_0 \end{pmatrix} + \sum_{i=1}^{r^E-1} \begin{pmatrix} \alpha_i^x & 0 & 0 \\ 0 & \alpha_i^y & 0 \\ 0 & 0 & \alpha_i^z \end{pmatrix} \begin{pmatrix} \boldsymbol{\sigma}_i \\ \boldsymbol{\sigma}_i \\ \boldsymbol{\sigma}_i \end{pmatrix} \tag{2.22}$$

where $\boldsymbol{\sigma}_i$ is in the null-space of $\mathbf{E}$ such that $\mathbf{E}\boldsymbol{\sigma}_i = \mathbf{0}$.

From Eq. (2.22), we have the following properties for the configuration of the tensegrity structure with different rank deficiency of the force density matrix:

[L1] If $r^E = 1$, all nodes degenerate into one node $(\alpha_0^x, \alpha_0^y, \alpha_0^z)$, which is called *base node* here.

[L2] If $r^E = 2$, Eq. (2.22) defines a line that passes through the base node.

[L3] Eq. (2.22) forms a two-dimensional space (plane) in the case of $r^E = 3$, and a three-dimensional space if $r^E = 4$. Both of these solution spaces contain the base node.

Therefore, in order to obtain a non-degenerate tensegrity structure in d-dimensional space, rank deficiency r^E of its force density matrix should be equal to or larger than $d + 1$, which completes the proof. □

Note that the condition $r^E \geq d+1$ is only the necessary condition but not sufficient for the non-degeneracy of a tensegrity structure. From Lemma 1, linear independence of the coordinate vectors should also be satisfied in addition to the non-degeneracy condition to ensure a non-degenerate tensegrity structure in d-dimensional space.

2.4 Stiffness Matrices

The stiffness matrices, including the tangent, linear (material, or first-order), and geometrical (second-order) stiffness matrices, of a general pin-jointed structure, with and without prestresses, are formulated in this section in the field of elastic systems with small strain.

Let e_k and A_k denote the Young's modulus and cross-sectional area of member k, respectively. The lengths of member k in the prestressed and initial unstressed states are denoted by l_k and l_k^0, respectively. Assuming that struts and cables are made of linear elastic materials; i.e., the strain-stress relation is linear, its force density q_k can then be written as follows when the strain is small

$$\begin{aligned} q_k = \frac{s_k}{l_k} &= \frac{1}{l_k}\left(e_k A_k \frac{l_k - l_k^0}{l_k^0}\right) \\ &= e_k A_k \left(\frac{1}{l_k^0} - \frac{1}{l_k}\right) \end{aligned}$$

Let $\mathbf{L}_0$ and $\mathbf{L}$ denote the diagonal matrices of which the kth diagonal elements are l_k^0 and l_k, respectively. $e_k A_k$ of member k are denoted by the (k,k) element of the diagonal matrix $\hat{\mathbf{K}}$. Hence, we have the following equation for all the force densities

$$\mathbf{A} = \hat{\mathbf{K}}(\mathbf{L}_0^{-1} - \mathbf{L}^{-1}) \tag{2.23}$$

The equivalent nodal load vectors in x-, y- and z-directions, which are compatible to the deformation of the structure, are denoted by $\mathbf{f}^x$, $\mathbf{f}^y$ and $\mathbf{f}^z$, respectively. The following relations hold from the equilibrium equations:

$$\begin{aligned} \mathbf{f}^x &= \mathbf{E}\mathbf{x} + \mathbf{E}^f\mathbf{x}^f \\ \mathbf{f}^y &= \mathbf{E}\mathbf{y} + \mathbf{E}^f\mathbf{y}^f \\ \mathbf{f}^z &= \mathbf{E}\mathbf{z} + \mathbf{E}^f\mathbf{z}^f \end{aligned} \tag{2.24}$$

The tangent stiffness matrix $\mathbf{K} \in \Re^{3n\times 3n}$ of a structure is defined by partial differentiation of the equivalent nodal load vector $\mathbf{f} = (\mathbf{f}^{x\top}, \mathbf{f}^{y\top}, \mathbf{f}^{z\top})^\top \in \Re^{3n}$ with respect to nodal coordinate vector $\mathbf{X} = (\mathbf{x}^\top, \mathbf{y}^\top, \mathbf{z}^\top)^\top \in \Re^{3n}$, which can be written as

$$\mathbf{K} = \frac{\partial \mathbf{f}}{\partial \mathbf{X}} = \begin{pmatrix} \frac{\partial \mathbf{f}^x}{\partial \mathbf{x}} & \frac{\partial \mathbf{f}^x}{\partial \mathbf{y}} & \frac{\partial \mathbf{f}^x}{\partial \mathbf{z}} \\ \frac{\partial \mathbf{f}^y}{\partial \mathbf{x}} & \frac{\partial \mathbf{f}^y}{\partial \mathbf{y}} & \frac{\partial \mathbf{f}^y}{\partial \mathbf{z}} \\ \frac{\partial \mathbf{f}^z}{\partial \mathbf{x}} & \frac{\partial \mathbf{f}^z}{\partial \mathbf{y}} & \frac{\partial \mathbf{f}^z}{\partial \mathbf{z}} \end{pmatrix} \tag{2.25}$$

Partial differentiation of Eq. (2.24) with respect $\mathbf{x}$ results in

$$\frac{\partial \mathbf{f}^x}{\partial \mathbf{x}} = \left(\frac{\partial \mathbf{E}}{\partial x_1}\mathbf{x} + \frac{\partial \mathbf{E}^f}{\partial x_1}\mathbf{x}^f, \frac{\partial \mathbf{E}}{\partial x_2}\mathbf{x} + \frac{\partial \mathbf{E}^f}{\partial x_2}\mathbf{x}^f, \ldots, \frac{\partial \mathbf{E}}{\partial x_n}\mathbf{x} + \frac{\partial \mathbf{E}^f}{\partial x_n}\mathbf{x}^f \right) + \mathbf{E} \tag{2.26-1}$$

$$\frac{\partial \mathbf{f}^y}{\partial \mathbf{x}} = \left(\frac{\partial \mathbf{E}}{\partial x_1}\mathbf{y} + \frac{\partial \mathbf{E}^f}{\partial x_1}\mathbf{y}^f, \frac{\partial \mathbf{E}}{\partial x_2}\mathbf{y} + \frac{\partial \mathbf{E}^f}{\partial x_2}\mathbf{y}^f, \ldots, \frac{\partial \mathbf{E}}{\partial x_n}\mathbf{y} + \frac{\partial \mathbf{E}^f}{\partial x_n}\mathbf{y}^f \right) \tag{2.26-2}$$

$$\frac{\partial \mathbf{f}^z}{\partial \mathbf{x}} = \left(\frac{\partial \mathbf{E}}{\partial x_1}\mathbf{z} + \frac{\partial \mathbf{E}^f}{\partial x_1}\mathbf{z}^f, \frac{\partial \mathbf{E}}{\partial x_2}\mathbf{z} + \frac{\partial \mathbf{E}^f}{\partial x_2}\mathbf{z}^f, \ldots, \frac{\partial \mathbf{E}}{\partial x_n}\mathbf{z} + \frac{\partial \mathbf{E}^f}{\partial x_n}\mathbf{z}^f \right) \tag{2.26-3}$$

where x_i denotes the x-coordinate of free node i. By using the definitions $\mathbf{E} = \mathbf{C}^\top\mathbf{Q}\mathbf{C}$ and $\mathbf{E}^f = \mathbf{C}^\top\mathbf{Q}\mathbf{C}^f$ in Eq. (2.15), where $\mathbf{C}$ and $\mathbf{C}^f$ are constant, we obtain

$$\frac{\partial \mathbf{E}}{\partial x_i} = \mathbf{C}^\top \frac{\partial \mathbf{A}}{\partial x_i}\mathbf{C}, \quad \frac{\partial \mathbf{E}^f}{\partial x_i} = \mathbf{C}^\top \frac{\partial \mathbf{A}}{\partial x_i}\mathbf{C}^f \tag{2.27}$$

Because the member lengths $\mathbf{L}_0$ in the unstressed state is constant, the partial differentiation of $\mathbf{A}$ with respect to the x_i can be written as follows from Eq. (2.23)

$$\frac{\partial \mathbf{Q}}{\partial x_i} = \hat{\mathbf{K}}(\mathbf{L}^{-1})^2 \frac{\partial \mathbf{L}}{\partial x_i} \tag{2.28}$$

Moreover, $\hat{\mathbf{K}}$ are considered to be constant, since the members are assumed to be linear elastic that e_k is constant and the changes of cross-sectional areas A_k can be neglected while the strains are very small. From Eq. (2.7), partial differentiation of $\mathbf{L}$ with respect to x_i leads to

$$\frac{\partial \mathbf{L}}{\partial x_i} = \mathbf{L}^{-1}\left(\mathbf{U}\frac{\partial \mathbf{U}}{\partial x_i} + \mathbf{V}\frac{\partial \mathbf{V}}{\partial x_i} + \mathbf{W}\frac{\partial \mathbf{W}}{\partial x_i} \right) \tag{2.29}$$

From Eq. (2.5), we have

$$\frac{\partial \mathbf{U}}{\partial x_i} = \mathrm{diag}(\mathbf{C}_i), \quad \frac{\partial \mathbf{V}}{\partial x_i} = \mathbf{0} \quad \frac{\partial \mathbf{W}}{\partial x_i} = \mathbf{0} \tag{2.30}$$

where $\mathbf{C}_i$ is the ith column of $\mathbf{C}$.

From Eqs. (2.27)–(2.30), we obtain

$$\begin{aligned}\frac{\partial \mathbf{E}}{\partial x_i}\mathbf{x} + \frac{\partial \mathbf{E}^f}{\partial x_i}\mathbf{x}^f &= \mathbf{C}^\top \hat{\mathbf{K}}(\mathbf{L}^{-1})^3 \mathbf{U}\mathrm{diag}(\mathbf{C}_i)(\mathbf{C}\mathbf{x} + \mathbf{C}^f\mathbf{x}^f) \\ &= \mathbf{C}^\top \hat{\mathbf{K}}(\mathbf{L}^{-1})^3 \mathbf{U}\mathrm{diag}(\mathbf{C}\mathbf{x} + \mathbf{C}^f\mathbf{x}^f)\mathbf{C}_i \\ &= \mathbf{C}^\top \hat{\mathbf{K}}(\mathbf{L}^{-1})^3 \mathbf{U}^2\mathbf{C}_i\end{aligned} \tag{2.31}$$

Using Eq. (2.31) and letting $\mathbf{D}_x = \mathbf{C}^\top \mathbf{U}\mathbf{L}^{-1}$, Eq. (2.26-1) can be written as

$$\begin{aligned}\frac{\partial \mathbf{f}^x}{\partial \mathbf{x}} &= \mathbf{C}^\top \hat{\mathbf{K}}(\mathbf{L}^{-1})^3 \mathbf{U}^2\mathbf{C} + \mathbf{E} \\ &= \mathbf{D}_x \hat{\mathbf{K}}\mathbf{L}^{-1}\mathbf{D}_x^\top + \mathbf{E} = \mathbf{D}_x \bar{\mathbf{K}}\mathbf{D}_x^\top + \mathbf{E}\end{aligned} \tag{2.32}$$

where the diagonal matrix $\bar{\mathbf{K}}(= \hat{\mathbf{K}}\mathbf{L}^{-1})$ is called the *axial stiffness matrix*, the diagonal elements $A_k e_k / l_k$ are the axial stiffness of the corresponding members k. Similarly, Eqs. (2.26-2) and (2.26-3) can be written as

$$\frac{\partial \mathbf{f}^y}{\partial \mathbf{x}} = \mathbf{D}_\mathbf{y} \bar{\mathbf{K}}\mathbf{D}_x^\top \tag{2.33}$$

and

$$\frac{\partial \mathbf{f}^z}{\partial \mathbf{x}} = \mathbf{D}_z \bar{\mathbf{K}}\mathbf{D}_x^\top \tag{2.34}$$

respectively, where $\mathbf{D}_y = \mathbf{C}^\top \mathbf{V}\mathbf{L}^{-1}$ and $\mathbf{D}_z = \mathbf{C}^\top \mathbf{W}\mathbf{L}^{-1}$ as defined in Eq. (7.3).

Let $\mathbf{I} \in \Re^{3\times 3}$ denote an identity matrix, and $\mathbf{D}^\top = (\mathbf{D}_x^\top, \mathbf{D}_y^\top, \mathbf{D}_z^\top)$. From Eqs. (2.32)–(2.34) and the similar equations for partial differentiation with respect to $\mathbf{y}$ and $\mathbf{z}$, the tangent stiffness matrix $\mathbf{K}$ defined in Eq. (2.25) can be written as the sum of the linear stiffness matrix $\mathbf{K}_E$ and the geometrical stiffness matrix $\mathbf{K}_G$ as follows

$$\mathbf{K} = \mathbf{D}\bar{\mathbf{K}}\mathbf{D}^\top + \mathbf{I} \otimes \mathbf{E} = \mathbf{K}_E + \mathbf{K}_G \tag{2.35}$$

where $\otimes$ denotes tensor product.The stiffness matrices derived above is equivalent to those by Murakami (2001), Guest (2006) or Masic *et al.* (2005).

In this formulation, the stressed equilibrium state is considered as the reference state. It can be easily observed that the stiffness matrices $\mathbf{K}_E$, $\mathbf{K}_G$ and $\mathbf{K}$ are all symmetric, because $\bar{\mathbf{K}}$ and $\mathbf{E}$ are symmetric.

It can also be easily observed that the linear stiffness matrix is independent on the initial lengths l_k^0 of the members but only dependent on the current lengths l_k

after deformation by the introduction of prestresses. In the case that the structure has no prestresses, the geometrical stiffness matrix vanishes, and we have $l_k = l_k^0$ because no member is deformed.

The tangent stiffness matrix presented above can be used for any pin-jointed structure in the field of elastic systems with small strain, since we have not used any further assumptions. Note that the rigid-body motions should be appropriately constrained in the analysis of tensegrity structures, because they are free-standing.

2.5 Stability Criteria

Based on the positive definiteness of the stiffness matrices and linear dependence of their eigenvectors, we introduce three stability criteria – stability (minimality of energy), prestress stability and super stability, which will be extensively used in the study for the stability investigation of the tensegrity structures.

Super stability implies stability, which implies prestress stability for the tensegrity structures. Hence, super stability is the strongest criterion and the prestress stability is the weakest among these three.

2.5.1 Statical and Kinematical Determinacy

From Eq. (2.12), the self-equilibrium equation with respect to the prestresses, where there is no external load applied on the structure; i.e., $\mathbf{p} = \mathbf{0}$, can be written as

$$\mathbf{Ds} = \mathbf{0} \tag{2.36}$$

Denote the rank of $\mathbf{D}$ by r^D; i.e.,

$$r^D = \text{rank}(\mathbf{D})$$

If the rank r^D of $\mathbf{D}$ is less than the number m of members, i.e. $r^D < m$, there can exist non-trivial prestresses ($\mathbf{s} \neq \mathbf{0}$) in the members, and the structure is said to be *statically indeterminate*, because we cannot uniquely determine the prestresses in the structure without any further information.

On the other hand, if $r^D = m$, the structure is *statically determinate*. The structure cannot contain any prestresses while no external loads are applied.

Let $\mathbf{d} \in \Re^{dn}$ denote (infinitesimal) nodal displacements corresponding to the external loads $\mathbf{p}$ applied on the structure. And let $\mathbf{e} \in \Re^m$ denote the extensions of the member lengths due to $\mathbf{p}$. The member extensions $\mathbf{e}$ are related to the small displacements $\mathbf{d}$ by the kinematical relations via the *compatibility matrix* $\mathbf{H} \in \Re^{m \times dn}$:

$$\mathbf{Hd} = \mathbf{e}$$

From the conservation of energy, we know that the work done to the structure by the external loads should be equal to the increase of strain energy stored in the structure in the field of small displacement for the elastic conservative systems. Hence, we have

$$\frac{1}{2}\mathbf{p}^\top \mathbf{d} = \frac{1}{2}\mathbf{s}^\top \mathbf{e}$$

From the relationship between the external loads $\mathbf{p}$ and the prestresses s in Eq. (2.12), we know that

$$\mathbf{s}^\top \mathbf{D}^\top \mathbf{d} = \mathbf{s}^\top \mathbf{Hd}$$

Because the small displacements $\mathbf{d}$ are arbitrary, the above equation can be ensured to be true only if the following relation holds, based on the principle of virtual work (Calladine, 1978; Livesley, 1975)

$$\mathbf{H} = \mathbf{D}^\top$$

Thus, the kinematical relation of the structure can be written as follows by the transpose $\mathbf{D}^\top$ of the equilibrium matrix

$$\mathbf{D}^\top \mathbf{d} = \mathbf{e} \tag{2.37}$$

When there is no member is extended, we have

$$\mathbf{D}^\top \mathbf{d} = \mathbf{0} \tag{2.38}$$

which will be very useful for your discussions on the stability.

If the structure is free-standing in d-dimensional space, it has $r^b = d(d+1)/2$ rigid-body motions. (This will be explicitly demonstrated in Chapter 3). So

Table 2.1: Statical and kinematical determinacy of pin-jointed structures

	Statically		Kinematically	
	Determinate	Indeterminate	Determinate	Indeterminate
$r^D - m$	$=0$	> 0		
$r^D - dn - r^b$			$=0$	> 0

the null-space of $\mathbf{D}^\top$ has at least r^b independent solutions for a free-standing structure.

If there exists a non-trivial displacement $\mathbf{d}(\neq \mathbf{0})$ that is not a rigid-body motion preserves the member lengths; i.e., Eq. (2.38) is satisfied, then the structure is said to be *kinematically indeterminate*, and this displacement is called *mechanism* of the structure. Otherwise, the structure is *kinematically determinate* such that there is no displacement can preserve the member lengths except for the rigid-body motions.

The statical and kinematical determinacy of the pin-jointed structures are summarized in Table 2.1, where r^b is the number of rigid-body motions that have not been constrained.

The number of states of prestresses n^s and modes of mechanisms n^m can then be very easy to calculate from the numbers of nodes n and members m and the rank r^D of the equilibrium equation $\mathbf{D}$ as follows for a d-dimensional structure (Pellegrino and Calladine, 1986)

$$\begin{aligned} n^s &= m - r^D \\ n^m &= dn - r^D - r^b \end{aligned} \tag{2.39}$$

This naturally leads to the generalized Maxwell's rule by Calladine (1978)

$$n^s - n^m = m - dn - r^b \tag{2.40}$$

For example, consider the simple structures as in Fig. 2.4, which consist of two members and three nodes, two of them are fixed. All the rigid-body motions have been constrained, so we have $r^b = 0$. Hence, $n^s - n^m = 2 - 2 = 0$.

Rank of the equilibrium matrix of the structure in Fig. 2.4.(a) is two, and that of Fig. 2.4.(b) is one. Therefore, we know that the first structure is statically and kinematically determinate, and the second is indeterminate with one states of prestresses ($n^s = 1$) along the members and one mode of (infinitesimal) mechanism ($n^m = 1$) perpendicular to the members.

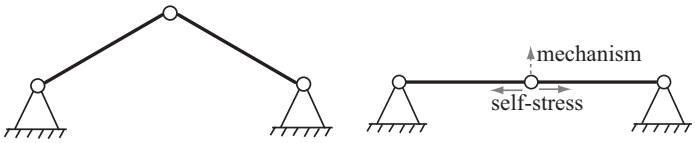

(a) determinate (b) indeterminate

Figure 2.4: Statical and kinematical determinacy of a two-dimensional structure. (a) is a statically and kinematically determinate structure, and (b) is a statically and kinematically indeterminate structure than has one mechanism and one pre-stresses mode.

2.5.2 Stability Criteria

When we discuss the stability of a structure in the study, the rigid-body motions of the structure are assumed to be properly constrained; i.e., the zero eigenvalues and eigenvectors of the stiffness matrices corresponding to the rigid-body motions are not considered.

2.5.2.1 Stability (Minimality of Energy)

Because a structure always tends to transform to the configuration with lower potential energy (it is equivalent to the stain energy when no external loads exist), it can be in equilibrium if only if the stationary condition of the energy is satisfied from the viewpoint of energy.

Moreover, the structure is said to be *stable*, if it has to stability return back to the original equilibrium configuration after a deformation subject to some small disturbances (displacements). This means that the stable structure has the (local) minimality of (strain) energy at the original configuration, and any disturbances to the structure would increase the energy stored in the structure. Hence, equilibrium of the structure does not naturally implies stability, but stability does imply equilibrium.

When the structure has strict (local) minimum energy, the Hessian of the energy must be positive definite (Thompson and Hunt, 1984). This leads to our definition for the stability of a structure:

Definition 2.1 Stability:

A structure is stable, if it strictly has the local minimum (strain) energy, or the Hessian of the energy (the tangent stiffness matrix excluding the rigid-body

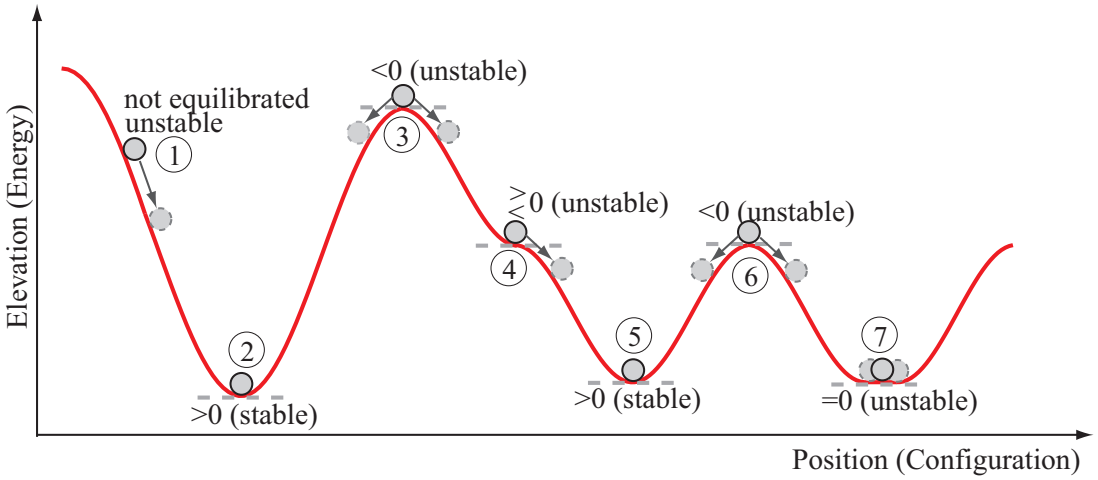

Figure 2.5: Stability of a structure in view of energy. A structure is state of self-equilibrium when it has extreme value of energy; and is stable if its energy is locally minimum in the vicinity.

motions for the free-standing structures) is positive definite; i.e., for any small displacements $\mathbf{d}$ *the quadratic form* Q *of the tangent stiffness matrix is positive:*

$$Q = \mathbf{d}^\top \mathbf{K}\mathbf{d} > 0 \tag{2.41}$$

Note that the structure may still be stable for the case $Q = 0$, but need further investigation of higher-order than second terms of the energy. Because $\mathbf{K}\mathbf{d}$ is the external loads applied to the structure from the formulation of the tangent stiffness matrix in Eq. (2.25), the quadratic form Q is twice of the work done by the external loads. Eq. (2.41) means that the increase of energy stored in the structure, converted from the work done by external loads, is strictly positive.

This stability criterion is widely adopted in the field of structural engineering. Note that material properties are usually involved in the stability of a structure, except that the structure is super stable, which will be introduced later.

However, a structure is stable only if it can return to its initial configuration subject to small disturbances. Hence, the structure should have (local) minimum strain energy so as to be stable associated with the current configuration.

It might be clearer to consider a ball subject to gravity, e.g., as shown in Fig. 2.5, to illustrate the concept of stability. In the figure, position of the ball

represents configuration of the structure, the elevation represents the strain energy, and gravity can be considered as prestresses that tend to move the nodes. If the ball is in a such position that its gradient is not equal to zero (stationary condition of the energy is not satisfied), e.g., position①, the ball cannot stay at current position and will move down to the position with smaller elevation (energy) indicated by the ball with dotted boundary. Hence, the structure is not in equilibrium in this case.

If the gradient of the curve at some specific position is equal to zero (stationary condition of the energy is satisfied), the ball can maintain its current position if no disturbances are applied on it. Hence, this indicates the ball (structure) is in equilibrium. However, the structure tends to move to a position with lower or the same elevation by only a little disturbance if the second-order of the curve is not positive. These cases can be found in positions ③, ④, ⑥ and ⑦ in Fig. 2.5.

Only in the positions with strictly local minimum elevation (energy), such as ② and ⑤, can the ball be stable against small disturbances (displacements) in any directions.

Interestingly, there are some structures, called multi-stable structures, may have more than one local minimum energy so that they can be stable with several different configurations. In Chapter 10, we will introduce an interesting multi-stable tensegrity structures with star-like shapes, and trace their multi-stable behaviors.

2.5.2.2 Prestress Stability

As the tangent stiffness matrix can be written as the sum of the linear and geometrical stiffness matrices, the quadratic form Q of it with respect to a small displacement $\mathbf{d}$ can be written as

$$Q = \mathbf{d}^\top \mathbf{K}\mathbf{d} = \mathbf{d}^\top \mathbf{K}_E\mathbf{d} + \mathbf{d}^\top \mathbf{K}_G\mathbf{d} = Q_E + Q_G$$

If the structure is kinematically indeterminate, then there exist mechanisms $\mathbf{d}$ that make $\mathbf{K}_E\mathbf{d} = \mathbf{0}$, and therefore, $Q_E = 0$. Hence, we have the following equation for the mechanism $\mathbf{d}$

$$Q = 0 + Q_G$$

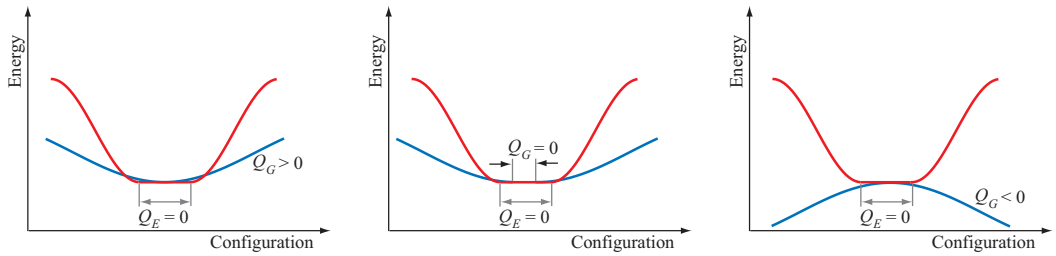

(a) stable ($Q_G > 0$) (b) unstable ($Q_G = 0$) (c) unstable ($Q_G < 0$)

Figure 2.6: Energy and stability of the kinematically indeterminate structures. Linear stiffness of a kinematically indeterminate structure is positive semi-definite; and positive definiteness of the tangent stiffness matrix is sensitive to the contribution but that of the geometrical stiffness matrix.

From the definition of stability, we know that the structure is possible to be stable ($Q > 0$) if and only if $Q_G > 0$. Note that $Q > 0$ is the necessary but not sufficient condition as will discussed later. This can also be explained intuitively by the figures in Fig. 2.6.

Write the mechanisms, which lie in the null-space of the transpose of the equilibrium matrix, or equivalently in the null-space of the linear stiffness matrix, as the columns of the *mechanism matrix* $\mathbf{M}$. From Eqs. (2.35) and (2.38), the quadratic form $\mathbf{Q}$ of the tangent stiffness matrix $\mathbf{K}$ with respect to the mechanisms $\mathbf{M}$ turns out to be equal to that of the geometrical stiffness matrix:

$$\mathbf{Q} = \mathbf{M}^\top \mathbf{K} \mathbf{M} = \mathbf{M}^\top \mathbf{K}_G \mathbf{M} \tag{2.42}$$

Let λ and $\mathbf{d}$ denote an eigenvalue and its corresponding eigenvector of the linear stiffness matrix $\mathbf{K}_E$. We have

$$\mathbf{K}_E \mathbf{d} = \lambda \mathbf{d}$$

Let a be a positive value. Then $a\lambda$ is an eigenvalue of $a\mathbf{K}_E$. Suppose that $\mathbf{K} = a\mathbf{K}_E + \mathbf{K}_G$, so that the value of a can represent the scale of the axial stiffness of the members by considering $\mathbf{K}_E = \mathbf{D}(a\bar{\mathbf{K}})\mathbf{D}^\top$.

If $a \to \infty$ (or a is sufficiently large) and $\lambda \neq 0$, we have

$$\mathbf{K}\mathbf{d} = a\mathbf{K}_E\mathbf{d} + \mathbf{K}_G \cong a\mathbf{K}_E\mathbf{d} = a\lambda\mathbf{d} \tag{2.43}$$

from which, we know that $a\lambda$ is the eigenvalue of $\mathbf{K}$ when a is large enough. In this case, we can consider only the positive definiteness of quadratic form of the geometry stiffness matrix with respect to the mechanisms as in Eq. (2.42) to investigate the stability of the structure.

Assuming that the axial stiffness of the members is infinite or large enough, here comes the definition of prestress stability:

Definition 2.2 Prestress Stability:

If the quadratic form $\mathbf{A}$ *defined in Eq. (2.42) of the geometrical stiffness matrix with respect to the mechanisms, where rigid-body motions have been excluded, is positive definite, then the structure is said to be prestress stable.*

Obviously, the concept of minimality of energy is stronger than the prestress stability, especially when there exit negative eigenvalues in the force density matrix, or the geometrical stiffness matrix as well. This will be investigated in more detail later in the chapter. For the special case that there exist no infinitesimal mechanisms in the structure, the quadratic form of the geometrical stiffness matrix vanishes, and the structure is also said to be prestress stable.

If a structure is prestress stable with negative eigenvalues in the geometrical stiffness matrix, then it can be stable with the positive definite tangent stiffness matrix when the axial stiffness is relatively very high compared to the level of self stresses. So, it is sufficient and more convenient to consider only the prestress stability instead of the minimality of energy, because the material properties do not need to be considered.

Hence, we usually investigate the prestress stability of the tensegrity structures instead of the minimality of energy in the study, in order to avoid the confusions in the selection of materials.

2.5.2.3 Super Stability

If the geometrical stiffness matrix is positive semi-definite, and $\mathbf{Q}$ in Eq. (2.42) is positive definite, then the structure can be guaranteed to be stable, no matter what materials the structure is made of. This is much stronger than the concept of stability, and hence, named *super stability* (Connelly and Whiteley, 1996), which is defined as

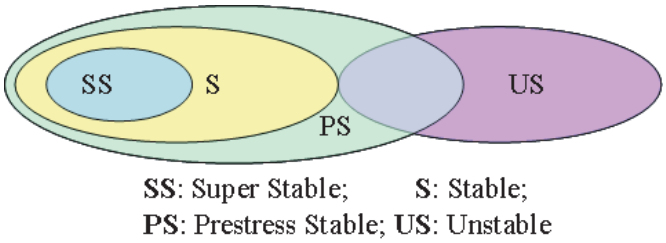

Figure 2.7: Relationships among the stability criteria: stability, prestress stability and super stability. A super stable tensegrity structure is stable, a stable structure is prestress stable. A structure can be either stable or unstable, so the shaped area of the prestress stability (PS) in the figure except for those of stability (S) and unstability (US) is indeed empty, although it is not in the figure for the convenience of illustrating their relationships.

Definition 2.3 Super Stability:

If the force density matrix is positive semi-definite and there exists no mechanism that make the quadratic form $\mathbf{Q}$ *of the geometrical stiffness in Eq. (2.42) equal to zero, then the structure is super stable.*

If a structure is super stable, then it is always stable, irrespective of the selection of materials or level of self stresses. The necessary conditions and sufficient conditions for the super stability of a tensegrity structures will be presented in Chapter 3.

In these three stability criteria, super stability is the strongest and the prestress stability is the weakest. Super stability implies stability (with the strict minimum energy), which implies prestress stability for tensegrity structures. The relations among them can be illustrated in Fig. 2.7.

Hence, we are usually interested in finding the super stable tensegrity structures if it is possible. Prestress stability is the second choice if super stability of the structures is not available. But in some cases, prestress stable tensegrity structures can be multi-stable, which might be interesting and useful for some special purposes, as will be presented in Chapter 10.

2.6 Classification

In this section, the pin-jointed structures are classified into three types: trusses, tensile structures, and tensegrity structures, based on their stability properties.

By investigation of the quadratic form of the linear stiffness matrix, we may have the following two statements for its positive definiteness based on the kinematical determinacy.

Statement 2.1 *If the structure is kinematically determinate, then the linear stiffness matrix* $\mathbf{K}_E$ *is positive definite, i.e., its quadratic form* Q_E *with respect to any non-trivial vector* $\mathbf{d}(\neq \mathbf{0})$ *excluding the rigid-body motions is positive:*

$$Q_E = \mathbf{d}^\top \mathbf{K}_E \mathbf{d} > 0 \tag{2.44}$$

Proof. Since the axial stiffness matrix $\bar{\mathbf{K}}$ for a elastic system is positive definite, i.e. to any arbitrary non-trivial vector $\bar{\mathbf{d}}(\neq \mathbf{0})$ we have

$$\bar{\mathbf{d}}^\top \bar{\mathbf{K}} \bar{\mathbf{d}} > 0 \tag{2.45}$$

On the other hand, if the structure is kinematically determinate, there exist extensions in some of the members corresponding to any non-trivial nodal displacements $\mathbf{d}(\neq \mathbf{0})$, we can then have the following relation:

$$\mathbf{D}^\top \mathbf{d} \neq \mathbf{0} \tag{2.46}$$

By using this non-trivial vector $\mathbf{d}$, the quadratic form of $\mathbf{K}_E$ can be written as

$$\mathbf{d}^\top \mathbf{K}_E \mathbf{d} = (\mathbf{D}\mathbf{d})^\top \bar{\mathbf{K}} (\mathbf{D}\mathbf{d}) \tag{2.47}$$

By letting $\bar{\mathbf{d}} = \mathbf{D}\mathbf{d}$, the statement is clearly true by observing Eqs. (2.45) and (2.46), which completes the proof. ◻

Statement 2.2 *If the structure is kinematically indeterminate, then the linear stiffness matrix is positive semi-definite.*

Table 2.2: Quadratic form of the linear and geometrical stiffness matrix.

	kinematically		statically		
	determinate	indeterminate	determinate	indeterminate	
				tensile [a]	tensegrity[b]
Q_E	> 0	≥ 0			
Q_G			$= 0$	> 0	indefinite[c]

[a] All prestresses are tension.
[b] Consist both of tensile and compressional prestresses.
[c] It can be positive, zero or negative.

Proof. If the structure is kinematically indeterminate, then the extensions $\mathbf{D}^\top\mathbf{d}$ of members might be equal to zero by some non-trivial nodal displacements $\mathbf{d}(\neq \mathbf{0})$, and therefore, the quadratic form of the geometrical stiffness in Eq. (2.47) turns out to be zero.

Except for the ones that make $\mathbf{D}^\top\mathbf{d} = \mathbf{0}$, we can know from Statement 2.1 that Eq. (2.47) is positive.

Summarily, the statement can be proved. □

Furthermore, we can have the following discussions on the statically determinate and indeterminate pin-jointed structures:

[L1] If the structure is statically determinate, Eq. (2.36) has only trivial solution ($\mathbf{s} = \mathbf{0}$). Hence, its geometrical stiffness vanishes, and the quadratic form of the geometrical stiffness matrix must be always equal to zero ($Q_G = 0$).

[L2] As have been pointed out by Schek (1974) that if the structure is statically indeterminate and all the members are in tension, i.e. all the force densities q_k are positive, and there is no isolated points, then the force density matrix $\mathbf{E}$ is positive definite. So the geometrical stiffness matrix $\mathbf{K}_G$ is positive definite in this case from its definition in Eq. (2.35).

Denote $\mathbf{d}(\neq \mathbf{0})$ as a nontrivial vector. The statements discussed above about the quadratic form of the linear stiffness matrix $\mathbf{K}_E$ and the geometrical stiffness matrix $\mathbf{K}_G$ can be summarized in Table 7.2.

Note that the *tensile structure* denotes the structure that is self-equilibrated by the introduction of prestresses with all members in tension. This can include the cable nets and tensile membrane structures, which can be discretized and substituted by cable net models. Tensile structure has to be suspended to some fixed nodes (supports) so as to obtain its self-equilibrium state and stability.

Based on the stability criterion concerning minimality of energy, we have the following statement for a stable structure that is a statically and kinematically indeterminate.

Statement 2.3 *For a statically and kinematically indeterminate structure, the introduction of prestress stiffens the infinitesimal mechanisms if the structure is stable.*

Proof. For a structure that is kinematically indeterminate, there exists a non-trivial displacement $\mathbf{d}(\neq \mathbf{0})$ that make the following equation hold

$$\mathbf{K}_E\mathbf{d} = \mathbf{0}$$

If the structure is stable, the quadratic form Q of the tangent stiffness matrix with respect to the mechanism $\mathbf{d}$ must be positive:

$$Q = \mathbf{d}^\top\mathbf{K}\mathbf{d} = \mathbf{d}^\top\mathbf{K}_G\mathbf{d} > 0 \tag{2.48}$$

Thus, it is clear that the mechanisms of a kinematically indeterminate structure are stiffened and stablized by the introduction of prestresses, because the geometrical stiffness matrix is not trivial if there exist prestresses within the structure. □

By using the stability criterion in terms of minimality of energy and the quadratic forms of the linear and geometrical stiffness matrices listed in Table 7.2, it is very easy to have the following conclusions:

CASE 1 : A kinematically and statically determinate pin-jointed structure is stable. This is the most simple stable structural form, e.g. a conventional truss structure.

CASE 2 : A kinematically determinate and statically indeterminate pin-jointed structure is stable if the introduced prestresses are sufficiently small or the axial stiffness of the materials is large enough. This has been shown in Eq. (7.34), and a detailed discussion can also be found in the necessary and sufficient conditions for the stability in Lemma 3.8 in Chapter 3.

CASE 3 : A structure that is kinematically indeterminate and statically determinate is unstable.

CASE 4 : For a kinematically and statically indeterminate structure, we can have the following two cases:

a : If all the members are in tension, the structure is stable. Hence, the tensile structures, including cable nets and tensile membrane structures, are stable.

b : If the members of the structure consist of both compressional and tensile members, it is not direct to draw a conclusion whether it is stable or not. The stability of this kind of structures will be discussed in Chapter 3 in detail.

Based on the above discussions, we classify the pin-jointed structures into the following three types:

Type I *truss*, which falls in CASE 1;

Type II *tensile structure*, which falls in CASE 4.a;

Type III *tensegrity structure*, which falls in CASE 2 and CASE 4.b.

In the remaining of the study, we will mainly deal with the stability and morphology (form-finding) of the tensegrity structures, the Type III pin-jointed structures.

2.7 Discussions and Conclusions

To formulate the equilibrium equations of a pin-jointed structure, we need to describe connectivity relation between nodes and members, which is also called *topology*, of the structure. Graph theory turns out to be convenient for this purpose, where topology of a structure is modeled as a graph: nodes of the structure correspond to vertices of the graph, and members are edges. Equilibrium equations of the structure can then be easily formulated in terms of connectivity matrix which describes its topology in a matrix form, by considering equilibrium of each node in each direction. Equilibrium equations are formulated in two different forms for further study: product of the equilibrium matrix and prestresses, and that of the force density matrix and nodal coordinates.

It is proved by solution space of nodal coordinates that the force density matrix should have enough rank deficiency, say, at least $d+1$ for the d-dimensional case, to ensure a non-degenerate structure. This condition will be demonstrated to be important for the presentation of the adaptive force density method in Chapter 4 for the form-finding problem of tensegrity structures, as well as for the symmetry strategy in Chapter 6 while considering singularity of specific blocks of the symmetry-adapted force density matrix.

Formulations of the stiffness matrices, including the tangent, linear (material), and geometrical stiffness matrices, are given by considering the partial deferential of the force density matrix with respect to the nodal coordinates. The formulations agree with those formulated in some other ways, and it is shown to have a simple form such that the linear stiffness is constructed from the equilibrium matrix, while the geometrical stiffness is directly from the force density matrix. This will be extensively used in Chapter 3 for presentation of stability conditions, and in other chapters for stability investigation.

Three stability criteria—stability, prestress stability and super stability—that are used in the study for stability investigation of tensegrity structures are introduced based on positive definiteness of the stiffness matrices. Among these stability criteria, super stability indicates stability, which indicates prestress stability; however, the reverse relation is not always true. From the viewpoint of

stability, pin-jointed structures are divided into trusses and prestressed structures, and prestressed structures are further classified into tensile structures and tensegrity structures. Trusses carry no prestresses, and are stable only if they are kinematically determinate; tensile structures, including cable nets and tensile membrane structures, that carry only tension are super stable; and stability of tensegrity structures that carry both tension and compression in their members is not apparent and need further investigation, which will be discussed in Chapter 3 in more detail.

Chapter 3

STABILITY CONDITIONS

This chapter is to present stability conditions for tensegrity structures.

The rigid-body motions need be extracted out from stability investigation of a tensegrity structure that is free-standing, since the structure will not deform subject to these motions. From the formulation of the geometrical stiffness matrix and non-degeneracy condition presented in Chapter 2, we may have noticed that the geometrical stiffness matrix has much more zero eigenvalues than the number of rigid-body motions. It would be a good question to ask how other non-rigid-body motions corresponding to these zero eigenvalues influence stability of the structure. This chapter is to answer such a question, with the presentation of a necessary stability condition. Further study shows that the structure is guaranteed to be super stable if two more conditions are satisfied at the same time.

Moreover, linear independence between the null-spaces of the linear and geometrical stiffness matrices provides another way for stability investigation of tensegrity structures. Some important stability properties of tensegrity structures were found from this view of point.

3.1 Affine Motions

We begin with affine motions to identify the non-rigid-motions lying in the null-space of the geometrical stiffness matrix.

An *affine motion* is a motion that preserves colinearity and ratios of distances; i.e., all points lying on a line are transformed to points on a line, and ratios of the

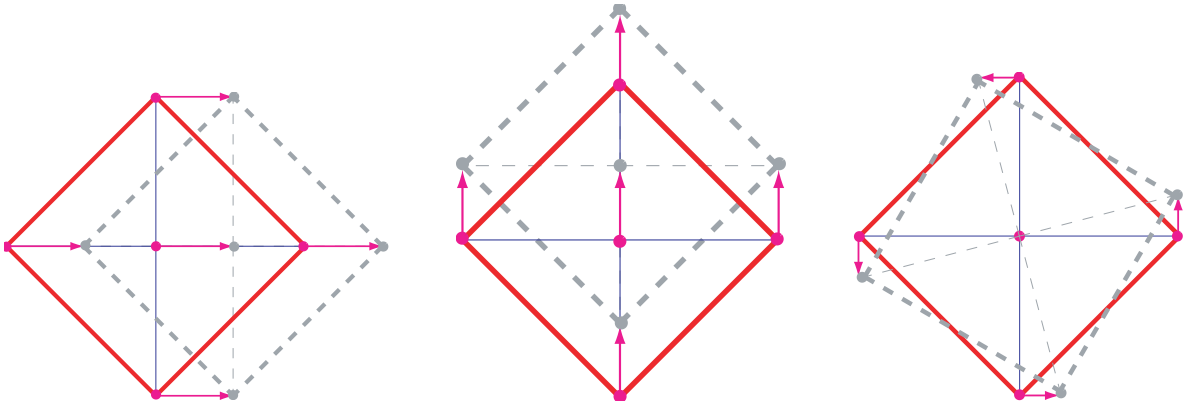

(a) translation in x-direction (b) translation in y-direction (c) rotation about z-axis

Figure 3.1: Rigid-body motions of a two-dimensional tensegrity structure.

distances between any pairs of the points on the line are preserved (Weisstein, 1999). However, an affine motion does not necessarily preserve angles or lengths. Hence, any triangle can be transformed into another by an affine motion.

There are d^2+d independent affine motions in d-dimensional space. In general, an affine motion can be a linear combination of *rotation*, *translation*, *dilation*, and *shear*. The rotation and translation of the structure are rigid-body motions of a structure, because they always preserve the member lengths (distances between the nodes). Thus, only dilation and shear, which are called *non-trivial affine motions* in the study, should be considered for the investigation of stability. It is shown in this section that the rigid-body motions lie in the null-spaces of both the linear and geometrical stiffness matrices, and the non-trivial affine motions do also lie in the null-space of the geometrical stiffness matrix if the structure is non-degenerate.

Thus, half of the $d^2 + d$ affine motions of a free-standing tensegrity structure in d-dimensional space are the rigid-body motions, and the other half are the non-trivial affine motions.

For example, for a tensegrity structure in two-dimensional space, there exist six affine motions. The three rigid-body motions and the three non-trivial affine motions are shown in Figs. 3.1 and 3.2, respectively. The solid and dashed lines in the figures denote the members before and after transformation, respectively.

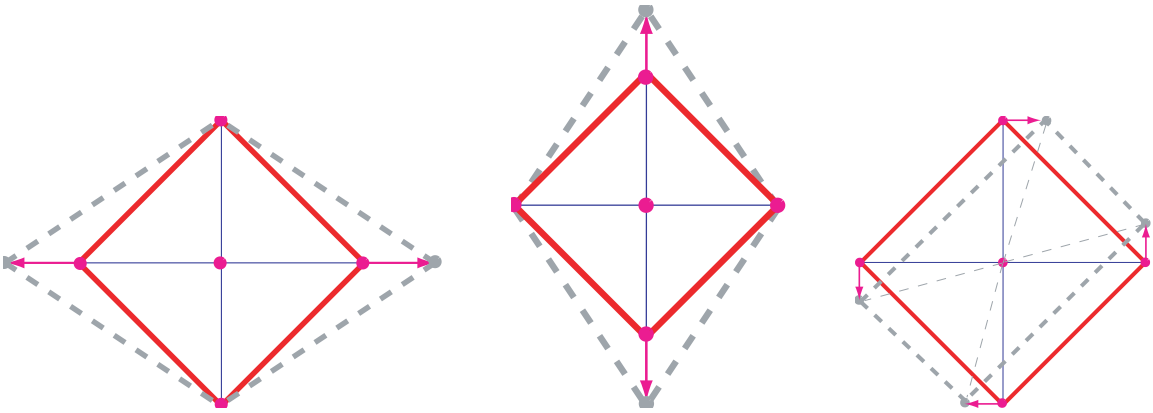

(a) dilation in x-direction (b) dilation in y-direction (c) shear in xy-plane

Figure 3.2: Non-trivial affine motions of a two-dimensional tensegrity structure.

3.1.1 Rigid-body Motions

A free-standing structure in d-dimensional space in Cartesian coordinate system has $(d^2+d)/2$ independent rigid-body motions: translation in each direction and rotation about each axis. With respect to the rigid-body motions, the quadratic form Q of the tangent stiffness matrix $\mathbf{K}$ is always equal to zero irrespective of the geometrical and mechanical properties of the structure, because the member lengths are not changed by these motions (displacements), and therefore, the strain energy of the structure does not change.

3.1.1.1 Translation

The translation vectors $\mathbf{d}_x^r$, $\mathbf{d}_y^r$ and $\mathbf{d}_z^r$ in x-, y- and z-directions are written as

$$\mathbf{d}_x^r = \begin{pmatrix} \mathbf{i} \\ \mathbf{0} \\ \mathbf{0} \end{pmatrix} \quad \mathbf{d}_y^r = \begin{pmatrix} \mathbf{0} \\ \mathbf{i} \\ \mathbf{0} \end{pmatrix} \quad \mathbf{d}_z^r = \begin{pmatrix} \mathbf{0} \\ \mathbf{0} \\ \mathbf{i} \end{pmatrix} \tag{3.1}$$

where all the elements of the identity vector $\mathbf{i} \in \Re^n$ are 1.

From the formulations of the linear $\mathbf{K}_E$ and geometrical $\mathbf{K}_G$ stiffness matrices in Eq. (2.35), the following equations always hold for any translation $\mathbf{d}_i^r$ ($i \in \{x, y, z\}$):

$$Q_E = (\mathbf{d}_i^r)^\top \mathbf{K}_E \mathbf{d}_i^r = 0, \quad Q_G = (\mathbf{d}_i^r)^\top \mathbf{K}_G \mathbf{d}_i^r = 0$$

Therefore, the translations in Eq. (3.1) are the rigid-body motions.

3.1.1.2 Rotation

In order to show that rotations about the axes are also the rigid-body motions, the quadratic forms Q_G and Q_E of the geometrical and linear stiffness matrices are considered separately.

For the case of the geometrical stiffness matrix, the rotation can be any arbitrary angle about the axes, while the angle should be infinitesimal for the case of the linear stiffness matrix. For simplicity, only the rotation about z-axis is considered. The formulation can be easily extended to the rotations about x- and y-axes.

1. Rotation of Geometrical Stiffness Matrix

Let $\bar{x}_i$, $\bar{y}_i$ and $\bar{z}_i$ denote the new coordinates of node i by the rotation about z-axis through an arbitrary angle θ. The relation between the new and old coordinates of node i can be written as

$$\begin{pmatrix} \bar{x}_i \\ \bar{y}_i \\ \bar{z}_i \end{pmatrix} = \begin{pmatrix} c & -s & 0 \\ s & c & 0 \\ 0 & 0 & 1 \end{pmatrix} \begin{pmatrix} x_i \\ y_i \\ z_i \end{pmatrix} = \mathbf{r} \begin{pmatrix} x_i \\ y_i \\ z_i \end{pmatrix}$$

where $c = \cos\theta$ and $s = \sin\theta$.

Let $\bar{\mathbf{X}}$ and $\mathbf{X}$ denote the new and old generalized coordinate vectors, respectively. The relation between $\bar{\mathbf{X}}$ and $\mathbf{X}$ can be written as

$$\bar{\mathbf{X}} = \mathbf{R}\mathbf{X}$$

where $\mathbf{R}$ is written as follows by an identity matrix $\mathbf{I}^n \in \Re^{n\times n}$

$$\mathbf{R} = \mathbf{r} \otimes \mathbf{I}^n = \begin{pmatrix} c\mathbf{I}^n & -s\mathbf{I}^n & \\ s\mathbf{I}^n & c\mathbf{I}^n & \\ & & \mathbf{I}^n \end{pmatrix}$$

The displacement $\mathbf{d}^r$ of a structure is equal to the nodal coordinate differences $\bar{\mathbf{X}} - \mathbf{X}$ after and before the transformation; i.e., $\mathbf{d}^r = \bar{\mathbf{X}} - \mathbf{X}$. Thus, we have the following relation for the displacement $\mathbf{d}^r$

$$\mathbf{K}_G\mathbf{d}^r = \mathbf{K}_G\bar{\mathbf{X}} - \mathbf{0} = \mathbf{K}_G\mathbf{R}\mathbf{X} = \mathbf{R}\mathbf{K}_G\mathbf{X} = \mathbf{0} \tag{3.2}$$

from the definitions of $\mathbf{K}_G$ and $\mathbf{R}$. Hence, the quadratic form Q_G of $\mathbf{K}_G$ with respect to $\mathbf{d}^r$ vanishes.

2. Rotation for Linear Stiffness Matrix

Consider member k connecting nodes i and j, of which the coordinate vectors are denoted by $\mathbf{X}_i$ and $\mathbf{X}_j$, respectively. The displacements of nodes i and j are denoted by $\mathbf{d}_i$ and $\mathbf{d}_j$, respectively. The elongation e_k of member k for small rotation about z-axis is written as

$$\begin{aligned} e_k &= \frac{1}{l_k}(\mathbf{X}_i - \mathbf{X}_j)^\top(\mathbf{d}_i - \mathbf{d}_j) \\ &= \frac{1}{l_k}(\mathbf{X}_i - \mathbf{X}_j)^\top(\mathbf{r} - \mathbf{I}^d)(\mathbf{X}_i - \mathbf{X}_j) \\ &= \frac{1}{l_k}(c-1)(u_k^2 + v_k^2) \\ &\simeq -\frac{1}{l_k}\theta^2(u_k^2 + v_k^2) \end{aligned}$$

which vanishes if θ is small; hence the member length extension equation Eq. (2.38) is satisfied for all members ($k = 1, \ldots, m$), and the following equation holds for the rotation $\mathbf{d}^r$ about z-axis by a small angle θ

$$\mathbf{K}_E\mathbf{d}^r = \mathbf{0} \tag{3.3}$$

Thus, the quadratic form of $\mathbf{K}_E$ with respect to $\mathbf{d}^r$ vanishes.

Because both of the quadratic forms of $\mathbf{K}_G$ and $\mathbf{K}_E$ with respect to the rotation about z-axis are zero, this rotation is a rigid-body motion. Similar approach can be used to verify that the rotations about x- and y-axes are also rigid-body motions.

So far, we have demonstrated that translations and rotations in the affine motions are the rigid-body motions. The linear combination of these motions is certainly a rigid-body motion too.

3.1.2 Non-trivial Affine Motions

By applying dilation, the structure expands or contracts in one direction and remains unchanged in the perpendicular directions. Directions of these motions $\mathbf{d}_x$, $\mathbf{d}_y$ and $\mathbf{d}_z$ ($\in \Re^{dn}$) of a structure in the three-dimensional space can be written as follows by using the nodal coordinate vectors

$$\mathbf{d}_x = \begin{pmatrix} \mathbf{x} \\ \mathbf{0} \\ \mathbf{0} \end{pmatrix}, \quad \mathbf{d}_y = \begin{pmatrix} \mathbf{0} \\ \mathbf{y} \\ \mathbf{0} \end{pmatrix}, \quad \mathbf{d}_z = \begin{pmatrix} \mathbf{0} \\ \mathbf{0} \\ \mathbf{z} \end{pmatrix} \tag{3.4}$$

Fig. 3.2(a) and (b) show the two dilations $\mathbf{d}_x$ and $\mathbf{d}_y$ in x- and y-directions of a two-dimensional tensegrity structure, respectively.

The shears $\mathbf{d}_{xy}$, $\mathbf{d}_{xz}$ and $\mathbf{d}_{yz}$ ($\in \Re^{dn}$) in xy-, xz- and yz-planes can be defined as

$$\mathbf{d}_{xy} = \begin{pmatrix} \mathbf{y} \\ \mathbf{x} \\ \mathbf{0} \end{pmatrix}, \quad \mathbf{d}_{xz} = \begin{pmatrix} \mathbf{z} \\ \mathbf{0} \\ \mathbf{x} \end{pmatrix}, \quad \mathbf{d}_{yz} = \begin{pmatrix} \mathbf{0} \\ \mathbf{z} \\ \mathbf{y} \end{pmatrix} \tag{3.5}$$

In the shears $\mathbf{d}_{ij}$ ($i, j \in \{x, y, z\}$), the motion in i-direction is proportional to the nodal coordinates in j-direction, and vice versa. We have only one shear $\mathbf{d}_{xy}$ for the two-dimensional case as shown in Fig. 3.2(c).

It is apparent from the self-equilibrium equations with respect to the nodal coordinates in Eq. (2.18) and definition of the geometrical stiffness matrix $\mathbf{K}_G$ in Eq. (2.35) that the non-trivial affine motions $\mathbf{d}_{i(j)}$ presented above lie in the null-space of $\mathbf{K}_G$ as

$$\mathbf{K}_G \mathbf{d}_{i(j)} = \mathbf{0}$$

Because the non-trivial affine motions defined above are dependent on the nodal coordinates, while the rigid-body motions are not, the non-trivial affine motions and the rigid-body motions are linearly independent. Hence, the following lemma, which shows that the non-trivial motions are linearly independent, ensures that the dilations and shears together with the rigid-body motions span the whole space of the affine motions:

Lemma 3.1 *The non-trivial affine motions defined in Eqs. (3.4) and (3.5) of a non-degenerate tensegrity structure in d-dimensional space are linearly independent.*

Proof. Consider the three-dimensional case. Let an arbitrary affine motion $\mathbf{d}(\in \Re^{dn})$ be denoted as the linear combination of the affine motions defined in Eqs. (3.4) and (3.5) by the the coefficients β_k ($k = 1, \ldots, 6$) as follows

$$\mathbf{d} = \beta_1 \mathbf{d}_x + \beta_2 \mathbf{d}_y + \beta_3 \mathbf{d}_z + \beta_4 \mathbf{d}_{xy} + \beta_5 \mathbf{d}_{xz} + \beta_6 \mathbf{d}_{yz} \tag{3.6}$$

By incorporating Eqs. (3.4) and (3.5), Eq. (3.6) can be divided into

$$\begin{aligned}\mathbf{d} &= (\mathbf{d}_1^\top, \mathbf{d}_2^\top, \mathbf{d}_3^\top)^\top \\ \mathbf{d}_1 &= \beta_1\mathbf{x} + \beta_4\mathbf{y} + \beta_5\mathbf{z} \\ \mathbf{d}_2 &= \beta_4\mathbf{x} + \beta_2\mathbf{y} + \beta_6\mathbf{z} \\ \mathbf{d}_3 &= \beta_5\mathbf{x} + \beta_6\mathbf{y} + \beta_3\mathbf{z}\end{aligned}$$

From Lemma 2.1, we know that the coordinate vectors $\mathbf{x}$, $\mathbf{y}$ and $\mathbf{z}$ of a non-degenerate (free-standing) structure in three-dimensional space are linearly independent. Thus, $\mathbf{d}_1 = \mathbf{d}_2 = \mathbf{d}_3 = \mathbf{0}$ is satisfied if and only if

$$\begin{aligned}\beta_1 = \beta_4 = \beta_5 = 0 \\ \beta_4 = \beta_2 = \beta_6 = 0 \\ \beta_5 = \beta_6 = \beta_3 = 0\end{aligned}$$

Hence, $\mathbf{d} = \mathbf{0}$ is satisfied if and only if

$$\beta_k = 0 \quad \text{for } k = 1, \ldots, 6$$

Therefore, the non-trivial affine motions are linearly independent. Linear independence can also be shown for the two-dimensional case, which concludes the proof. □

When the force density matrix $\mathbf{E}$ of a d-dimensional non-degenerate tensegrity structure has the minimum rank deficiency $d+1$, the rank deficiency of $\mathbf{K}_G$ is $d(d+1)$ from its definition in Eq. (2.35). Therefore, in this case, the affine motions, including the rigid-body motions and the non-trivial affine motions, span the whole null-space of $\mathbf{K}_G$. This will be presented as one of the necessary and sufficient conditions for the super stability of a tensegrity structure later.

3.2 Necessary Stability Condition

Because the tangent stiffness matrix is the sum of the linear and geometrical stiffness matrices and the linear stiffness matrix is always positive (semi-)definite, if there exist some prestress modes that let $\mathbf{K}_G$ be positive semi-definite, the structure is highly possible to be stable concerning with the positive definiteness of the tangent stiffness matrix. However, there should be no non-trivial motion $\mathbf{d}$, excluding the rigid-body motions, that satisfies the following condition:

$$\mathbf{d}^\top \mathbf{K}_E \mathbf{d} = \mathbf{d}^\top \mathbf{K}_G \mathbf{d} = 0 \tag{3.7}$$

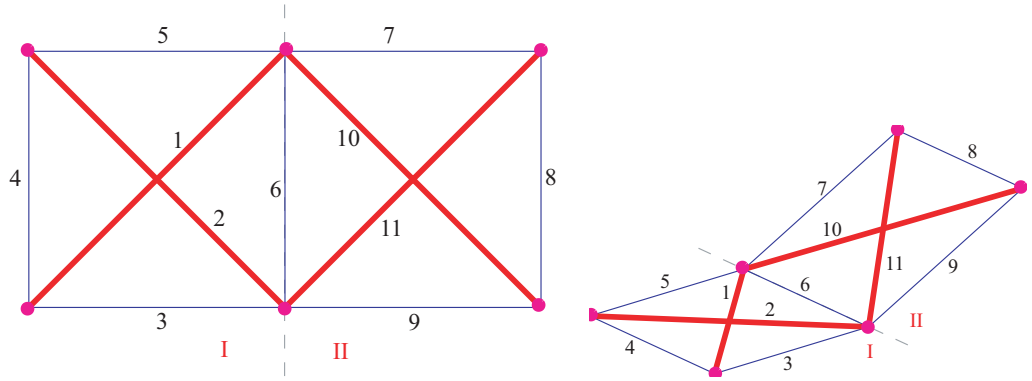

(a) top view (b) perspective view

Figure 3.3: An unstable tensegrity structure. The structure has semi-definite force density matrix which is one of the conditions for super stability; however, it is not stable in three-dimensional space because there exists a finite mechanism about the member 6.

For example, consider the three-dimensional tensegrity structure as shown in Fig. 3.3. The members lie on two intersecting planes I and II. The geometrical stiffness matrix $\mathbf{K}_G$ is positive semi-definite for this structure with the proper signs of the prestresses; i.e., tension for cables and compression for struts. However, obviously the structure is not stable because the two planes can relatively rotate about the intersecting line without external loads; i.e., there exist non-trivial motions excluding rigid-body motions that satisfy Eq. (3.7).

Connelly (1982) presented conditions for the stability of tensegrity structures in the terminologies of mathematics based on structural rigidity. However, it might be more comprehensible for engineers to understand the problems by utilizing the stability criteria with respect to the stiffness matrices. The purpose of this section is to present a necessary condition for the stability of tensegrity structures. It is also proved that the necessary conditions derived in different ways are equivalent. Hence, the discrepancy in the stability conditions between the fields of engineering and mathematics is resolved.

3.2.1 Geometry Matrix

Because the non-trivial affine motions presented in Eqs. (3.4) and (3.5) are linearly independent from Lemma 3.1, any non-trivial affine motion $\mathbf{d}$ can be

written as the linear combination of the six non-trivial affine motions as

$$\mathbf{d} = \alpha_x \mathbf{d}_x + \alpha_y \mathbf{d}_y + \alpha_z \mathbf{d}_z + \alpha_{xy} \mathbf{d}_{xy} + \alpha_{xz} \mathbf{d}_{xz} + \alpha_{yz} \mathbf{d}_{yz} \tag{3.8}$$

where the following equation is always satisfied

$$\mathbf{K}_G \mathbf{d} = \mathbf{0}$$

Hence, the quadratic form Q of $\mathbf{K}$ with respect to $\mathbf{d}$ is reduced to

$$Q = \mathbf{d}^\top \mathbf{K} \mathbf{d} = \mathbf{d}^\top \mathbf{K}_E \mathbf{d} = (\mathbf{D}^\top \mathbf{d})^\top \bar{\mathbf{K}} (\mathbf{D}^\top \mathbf{d}) \tag{3.9}$$

Because $\mathbf{K}_E$ is positive semi-definite, Q in Eq. (8.16) cannot be negative. The only possibility for the structure with positive semi-definite force density matrix being unstable is that $Q = 0$. In this case, Eq. (2.38) ($\mathbf{Dd} = \mathbf{0}$) holds because the axial stiffness matrix $\bar{\mathbf{K}}$ is positive definite for the usual materials. This indicates that the member lengths of the structure are not changed by the non-trivial affine motions.

For the shear $\mathbf{d}_{xy}$, for example, we have the following relation from Eq. (7.3):

$$\begin{aligned} \mathbf{D}^\top \mathbf{d}_{xy} &= \begin{pmatrix} \mathbf{D}_x^\top & \mathbf{D}_y^\top & \mathbf{D}_z^\top \end{pmatrix} \begin{pmatrix} \mathbf{y} \\ \mathbf{x} \\ \mathbf{0} \end{pmatrix} \\ &= \mathbf{D}_x^\top \mathbf{y} + \mathbf{D}_y^\top \mathbf{x} = \mathbf{L}^{-1}(\mathbf{U}\mathbf{C}\mathbf{y} + \mathbf{V}\mathbf{C}\mathbf{x}) = 2\mathbf{L}^{-1}\mathbf{U}\mathbf{v} \end{aligned} \tag{3.10}$$

Similarly, we have

$$\begin{aligned} &\mathbf{D}^\top \mathbf{d}_x = \mathbf{L}^{-1}\mathbf{U}\mathbf{u}, \quad \mathbf{D}^\top \mathbf{d}_y = \mathbf{L}^{-1}\mathbf{V}\mathbf{v}, \quad \mathbf{D}^\top \mathbf{d}_z = \mathbf{L}^{-1}\mathbf{W}\mathbf{w}, \\ &\mathbf{D}^\top \mathbf{d}_{xz} = 2\mathbf{L}^{-1}\mathbf{U}\mathbf{w}, \quad \mathbf{D}^\top \mathbf{d}_{yz} = 2\mathbf{L}^{-1}\mathbf{V}\mathbf{w} \end{aligned} \tag{3.11}$$

Substituting Eq. (3.8) into Eq. (2.38) and using Eqs. (8.19) and (8.20), we obtain

$$\mathbf{Dd} = \mathbf{L}^{-1}\mathbf{A}\boldsymbol{\alpha} = \mathbf{0} \tag{3.12}$$

where $\boldsymbol{\alpha} = (\alpha_x, \alpha_y, \alpha_z, 2\alpha_{xy}, 2\alpha_{xz}, 2\alpha_{yz})^\top$ and

$$\mathbf{A} = \begin{pmatrix} \mathbf{U}\mathbf{u}, & \mathbf{V}\mathbf{v}, & \mathbf{W}\mathbf{w}, & \mathbf{U}\mathbf{v}, & \mathbf{U}\mathbf{w}, & \mathbf{V}\mathbf{w} \end{pmatrix} \tag{3.13}$$

The matrix $\mathbf{A} \in \Re^{m \times d(d+1)/2}$ is called the *geometry matrix*, because it is related only to the geometry (nodal coordinates and topology) of the structure.

For the two-dimensional tensegrity structures, the geometry matrix $\mathbf{A} \in \Re^{m\times 3}$ becomes

$$\mathbf{A} = \begin{pmatrix} \mathbf{Uu}, & \mathbf{Vv}, & \mathbf{Uv} \end{pmatrix} \tag{3.14}$$

Thus, $\mathbf{A}$ is an m-by-$(d^2+d)/2$ matrix for a d-dimensional structure.

Because the inverse $\mathbf{L}^{-1}$ of the length matrix $\mathbf{L}$ is positive definite, Eq. (8.21) has a non-trivial solution $\boldsymbol{\alpha} \neq \mathbf{0}$, if and only if the rank of $\mathbf{A}$ is less than $(d^2+d)/2$. From this discussion, we have the following necessary stability condition for tensegrity structures based on the rank of the geometry matrix $\mathbf{A}$:

Lemma 3.2 *If a d-dimensional tensegrity structure is stable, then the rank of the geometry matrix $\mathbf{A}$ defined in Eq. (8.22) or Eq. (8.23) is equal to $(d^2+d)/2$.*

Proof. The space spanned by the non-trivial affine motions is a sub-space of the null-space of the geometrical stiffness matrix. If the rank of $\mathbf{A}$ is less than $(d^2+d)/2$, then there exist non-trivial motions in this sub-space that make the quadratic form Q equal to zero from Eqs. (8.16) and (8.21). Therefore, the structure is unstable. Hence, the lemma has been proved. □

Note that if a d-dimensional structure is degenerate, the nodal coordinate vectors are linearly dependent and so are the coordinate difference vectors. Thus, rank of $\mathbf{A}$ must be less than $(d^2+d)/2$ and the structure is unstable in d-dimensional space.

It is also observed from the size of $\mathbf{A}$ that a tensegrity structure can never be stable if the number m of members is less than $(d^2+d)/2$, which is equal to three and six in two-dimensional and three-dimensional spaces, respectively.

3.2.2 Comparison with Existing Condition

Connelly (1982) presented the equivalent necessary condition as in Lemma 3.2 for the stability of a tensegrity structure in the terminology of mathematics:

Condition by Connelly (1982): *The member directions do not lie on the same conic at infinity.*

Let the coordinates of node i be denoted as $\mathbf{p}_i = (x_i, y_i, z_i)^\top \in \Re^d$. By applying the affine motion defined by the transformation matrix $\mathbf{T} \in \Re^{d\times d}$ and translation vector $\mathbf{t} \in \Re^d$, $\mathbf{p}_i$ is transformed to $\bar{\mathbf{p}}_i$ as

$$\bar{\mathbf{p}}_i = \mathbf{T}\mathbf{p}_i + \mathbf{t} \tag{3.15}$$

Suppose that nodes i and j are connected by member k. The *member direction* of member k is given as $\mathbf{p}_i - \mathbf{p}_j$.

If the directions $\mathbf{p}(\in \Re^d)$ in the d-dimensional space lie on a *conic at infinity* denoted by C, then C can be defined as follows by $\mathbf{p}$ and a non-trivial symmetric matrix $\mathbf{N}(\in \Re^{d\times d})$:

$$C = \{\mathbf{p} \mid \mathbf{p}^\top \mathbf{N}\mathbf{p} = 0\} \tag{3.16}$$

If the structure has a non-trivial motion preserving the lengths of all members, the (strain) energy of the structure does not change; therefore, the structure is unstable. This is the basic idea of Connelly (1982), which can be expressed by the following lemma:

Lemma 3.3 *The member lengths are preserved by some affine motions if all member directions of the structure lie on the same conic at infinity.*

Proof. From the affine transformations of nodes i and j as in Eq. (3.15), the following equation holds if the length of member k, which is connected by nodes i and j, does not change by the affine motion:

$$\begin{aligned} |\bar{\mathbf{p}}_i - \bar{\mathbf{p}}_j|^2 - |\mathbf{p}_i - \mathbf{p}_j|^2 &= (\bar{\mathbf{p}}_i - \bar{\mathbf{p}}_j)^\top(\bar{\mathbf{p}}_i - \bar{\mathbf{p}}_j) - (\mathbf{p}_i - \mathbf{p}_j)^\top(\mathbf{p}_i - \mathbf{p}_j) \\ &= (\mathbf{p}_i - \mathbf{p}_j)\mathbf{T}^\top\mathbf{T}(\mathbf{p}_i - \mathbf{p}_j) - (\mathbf{p}_i - \mathbf{p}_j)^\top\mathbf{I}^d(\mathbf{p}_i - \mathbf{p}_j) \\ &= (\mathbf{p}_i - \mathbf{p}_j)(\mathbf{T}^\top\mathbf{T} - \mathbf{I}^d)(\mathbf{p}_i - \mathbf{p}_j) \\ &= 0 \end{aligned} \tag{3.17}$$

where $\mathbf{I}^d \in \Re^{d\times d}$ is an identity matrix, and $\mathbf{p}_i - \mathbf{p}_j$ is the member direction of member k.

Let $\mathbf{N} = \mathbf{T}^\top\mathbf{T} - \mathbf{I}^d$ and $\mathbf{p} = \mathbf{p}_i - \mathbf{p}_j$. By comparing Eq. (3.17) with Eq. (3.16), the member directions $\mathbf{p}_i - \mathbf{p}_j$ of the structure lie on the same conic at infinity defined by $\mathbf{N}(= \mathbf{T}^\top\mathbf{T} - \mathbf{I}^d)$ if all member lengths of the structure are preserved. □

The following lemma shows that Connelly's condition is equivalent to our necessary stability condition in Lemma 3.2:

Lemma 3.4 *The rank of the geometry matrix* $\mathbf{A}$ *is equal to* $(d^2+d)/2$*, if and only if the member directions do not lie on the same conic at infinity.*

Proof. Consider the three-dimensional case ($d = 3$). Since $\mathbf{N} \in \Re^{d\times d}$, which defines the conic at infinity in Eq. (3.16), is a symmetric matrix, it can be written as a linear combination of $(d^2+d)/2$ symmetric matrices

$$\begin{aligned}\mathbf{N} = \quad & \alpha_x \begin{pmatrix} 1 & 0 & 0 \\ 0 & 0 & 0 \\ 0 & 0 & 0 \end{pmatrix} + \alpha_y \begin{pmatrix} 0 & 0 & 0 \\ 0 & 1 & 0 \\ 0 & 0 & 0 \end{pmatrix} + \alpha_z \begin{pmatrix} 0 & 0 & 0 \\ 0 & 0 & 0 \\ 0 & 0 & 1 \end{pmatrix} \\ & + \alpha_{xy} \begin{pmatrix} 0 & 1 & 0 \\ 1 & 0 & 0 \\ 0 & 0 & 0 \end{pmatrix} + \alpha_{xz} \begin{pmatrix} 0 & 0 & 1 \\ 0 & 0 & 0 \\ 1 & 0 & 0 \end{pmatrix} + \alpha_{yz} \begin{pmatrix} 0 & 0 & 0 \\ 0 & 0 & 1 \\ 0 & 1 & 0 \end{pmatrix}\end{aligned} \tag{3.18}$$

Because $\mathbf{N}$ is a non-trivial matrix, the coefficients α_i cannot be zero at the same time.

The member direction $\mathbf{p}$ of member k connecting nodes i and j $(i < j)$ is written as

$$\mathbf{p} = \mathbf{p}_i - \mathbf{p}_j = \begin{pmatrix} u_k \\ v_k \\ w_k \end{pmatrix} \tag{3.19}$$

where u_k, v_k and w_k are the kth elements of the coordinate difference vectors $\mathbf{u}$, $\mathbf{v}$ and $\mathbf{w}$, respectively.

Substituting Eqs. (3.18) and (3.19) into Eq. (3.16), we have

$$\mathbf{p}^\top \mathbf{N} \mathbf{p} = \alpha_x u_k^2 + \alpha_y v_k^2 + \alpha_z w_k^2 + 2\alpha_{xy} u_k v_k + 2\alpha_{xz} v_k w_k + 2\alpha_{yz} v_k w_k = 0 \tag{3.20}$$

If the member directions lie on the same conic at infinity, all member directions of the structure should satisfy Eq. (3.20), and the equations Eq. (3.20) for all members k $(= 1, \ldots m)$ can be combined to a matrix form as

$$\mathbf{B}\boldsymbol{\alpha} = \mathbf{0} \tag{3.21}$$

where $\boldsymbol{\alpha}^\top = (\alpha_x, \alpha_y, \alpha_z, 2\alpha_{xy}, 2\alpha_{xz}, 2\alpha_{yz})^\top$. It is easy to observe that $\mathbf{B} = \mathbf{A}$.

If the member directions do not lie on the same conic at infinity, then Eq. (3.21) has no non-trivial solution for the coefficient vector $\boldsymbol{\alpha}$. Hence, the rank of the matrix $\mathbf{B}$ or $\mathbf{A}$ is $(d^2+d)/2$.

Conversely, if the rank of $\mathbf{A}$ is $(d^2+d)/2$, then there exists no non-trivial solution $\boldsymbol{\alpha}$ for Eq. (3.21); i.e., there exists no matrix $\mathbf{N}$ satisfying Eq. (3.20) for all members; hence, the member directions do not lie on the same conic at infinity. □

The necessary stability condition derived in Lemma 3.2 is considered to be more applicable than Connelly's descriptive condition, because only the rank of the well-established geometry matrix constructed from the nodal coordinates and connectivity of the structure needs to be investigated.

3.3 Stability Conditions

This section presents the sufficient and necessary conditions for the super stability of a tensegrity structure, based on the discussion of necessary condition in the previous section.

Furthermore, based on the study of the linear dependence of the eigenvectors of the linear and geometrical stiffness matrices, we investigate the stability conditions of the tensegrity structures concerning the minimality of energy.

Note that when we discuss the stability, the rigid-body motions are not taken into consideration. They are assumed to be properly constrained or the zero eigenvalues and the corresponding eigenvectors in the stiffness matrices are implicitly ignored.

3.3.1 Super Stability Conditions

From Lemma 3.2, we have known that the rank of the geometry matrix must have rank of $d(d+1)/2$ for a stable tensegrity structure in d-dimensional space.

Because the affine motions can span the whole null-space of the geometrical stiffness matrix if the force density matrix has the minimum rank deficiency, the structures are guaranteed to be super stable, irrespective of selection of materials and level of prestresses, if the two more conditions for the force density matrix

(the geometrical stiffness matrix as well) are satisfied addition to the necessary stability condition (Connelly, 1999). Accordingly, we have the following Lemma for the super stability of a tensegrity structure.

Lemma 3.5 *If the following three conditions are all satisfied, then the d-dimensional tensegrity structure is super stable:*

[L1] The force density matrix $\mathbf{E}$ *has the minimum rank deficiency* $d+1$.

[L2] $\mathbf{E}$ *is positive semi-definite.*

[L3] The rank of the geometry matrix $\mathbf{A}$ *is* $(d^2+d)/2$.

Proof. If condition (1) is satisfied, then the affine motions, which are the linear combination of the rigid-body motions and the non-trivial affine motions, can span the whole null-space of $\mathbf{K}_G$.

Since $\mathbf{A}$ has rank of $(d^2+d)/2$ from condition (3), there exists no non-trivial affine motion in this space that leads to $Q=0$.

From condition (2), both of the linear and geometrical stiffness matrices are positive semi-definite, and Q cannot have a negative value.

Therefore, the structure is super stable, irrespective of the selection of materials and level of prestresses, and the lemma can be proved. □

Lemma 3.5 shows us that if we want to obtain a super stable tensegrity structure, the force density matrix should be positive semi-definite with the proper rank deficiency $(d+1)$. This leads to the strategy of the adaptive force density method proposed in Chapter 4 for the form-finding problems of tensegrity structures.

However, the necessary stability condition should also be satisfied in order to ensure a stable structure. For example, consider the unstable structure in Fig. 3.3 again, which satisfies the first two sufficient conditions but violates the third listed in Lemma 3.5.

The tensegrity structure consisting of six nodes and eleven members. Members 1–6 and 6–11 lie in two different planes I and II, respectively. Planes I and II

are not parallel and intersect along member 6. Hence, the structure is in three-dimensional space; i.e., $d = 3$.

The structure has two modes of prestresses. The prestress mode in one plane does not affect that of the members in the other plane except the common member 6. The force density matrix $\mathbf{E}$ is positive semi-definite, with two positive and four zero eigenvalues, if the axial forces are properly assigned to the members – tension to the cables and compression to the struts. The non-degeneracy condition for a tensegrity structure in three-dimensional space is satisfied, because the rank deficiency of $\mathbf{E}$ is four. Therefore, conditions (1) and (2) in Lemma 3.5 are satisfied.

However, the structure is not stable, and of course, can never be super stable. Suppose that one of the planes is rotated about member 6 by an arbitrary angle without moving the members in the other plane. All member lengths remain unchanged and the structure is still in a state of self-equilibrium with the same prestresses after transformation. This motion is actually a finite mechanism.

Using Eq. (8.22), we obtain the 11-by-6 geometry matrix $\mathbf{A}$ for this three-dimensional structure. The rank of $\mathbf{A}$ is five, which is less than the necessary value of six. Therefore, the structure cannot be stable in three-dimensional space from Lemma 3.2, which agrees with the existence of the finite mechanism as described above.

3.3.2 Stability Conditions (Minimality of Energy)

Let λ_i^E and $\mathbf{\Psi}_i^E$ denote the ith eigenvalue and eigenvector, respectively, of the linear stiffness matrix $\mathbf{K}_E$. The jth eigenvalue and eigenvector of the geometrical stiffness matrix $\mathbf{K}_G$ are denoted by λ_j^G and $\mathbf{\Psi}_j^G$, respectively. Eigenvectors of $\mathbf{K}_E$ and $\mathbf{K}_G$ are ortho-normalized so as to satisfy

$$\mathbf{\Psi}_i^{E\top}\mathbf{\Psi}_j^E = \mathbf{\Psi}_i^{G\top}\mathbf{\Psi}_j^G = \begin{cases} 1 & \text{for } i = j \\ 0 & \text{for } i \neq j \end{cases} \tag{3.22}$$

The eigenvectors $\mathbf{\Psi}_i^E$ are linearly independent, and any nontrivial vector $\mathbf{d}$ ($\neq \mathbf{0}$) in the nodal displacement space can be written as a linear combination of $\mathbf{\Psi}_i^E$ as

$$\mathbf{d} = \sum_i \alpha_i \mathbf{\Psi}_i^E \tag{3.23}$$

where α_i is the coefficient for the corresponding eigenvector. The eigenvectors $\mathbf{\Psi}_j^G$ are also linearly independent and span the same nodal displacement space as Eq. (3.23); i.e.

$$\mathbf{d} = \sum_j \gamma_j \mathbf{\Psi}_j^G \tag{3.24}$$

where γ_j is the coefficient.

Hence, the quadratic form Q of the tangent stiffness matrix $\mathbf{K}$ with respect to the nodal displacement $\mathbf{d}$ can be written as follows by using Eqs. (3.22)–(3.24):

$$\begin{aligned} Q = \mathbf{d}^\top \mathbf{K} \mathbf{d} &= \mathbf{d}^\top \mathbf{K}_E \mathbf{d} + \mathbf{d}^\top \mathbf{K}_G \mathbf{d} \\ &= \sum_i \alpha_i^2 \lambda_i^E + \sum_j \gamma_j^2 \lambda_j^G \end{aligned} \tag{3.25}$$

Moreover, $\mathbf{\Psi}_i^E$ can be written as a linear combination of $\mathbf{\Psi}_j^G$ as

$$\mathbf{\Psi}_i^E = \sum_j \kappa_j \mathbf{\Psi}_j^G \tag{3.26}$$

where

$$\sum_j \kappa_j^2 = 1$$

is derived from Eq. (3.22).

Note from the definition of $\mathbf{K}_G$ in Eq. (2.35) that all λ_j^G are proportional to the scale of the force densities; i.e. if $\mathbf{q}$ is scaled by c to $c\mathbf{q}$, then the eigenvalues of $\mathbf{K}_G$ become $c\lambda_j^G$.

It can also be easily observed that if all the eigenvalues of $\mathbf{K}_E$ and $\mathbf{K}_G$ are positive, the quadratic form in Eq. (3.25) is positive, and the corresponding structure is stable. However, $\mathbf{K}_E$ usually has zero eigenvalue(s), because tensegrity structures are usually kinematically indeterminate. Moreover, $\mathbf{K}_G$ must have zero eigenvalues for the tensegrity structure because of the non-degeneracy condition, and even can have even negative eigenvalues depending on the values of the force densities.

Let $\mathcal{J}_0^E$, $\mathcal{J}_+^E$, $\mathcal{J}_-^G$, $\mathcal{J}_0^G$ and $\mathcal{J}_+^G$ denote the set of indices of the eigenvalues for which $\lambda_i^E = 0$, $\lambda_i^E > 0$, $\lambda_j^G < 0$, $\lambda_j^G = 0$ and $\lambda_j^G > 0$, respectively. For a kinematically indeterminate structure, the set $\mathcal{J}_0^E$ is not empty. Thus, the mechanism which

preserves the member lengths is denoted by $\mathbf{\Psi}_i^E$ $(i \in \mathcal{J}_0^E)$, and the external loads $\mathbf{p}$ applied on the structure in this case if $\mathbf{K}_G \mathbf{\Psi}_i^E$.

Based on the linear dependence of the eigenvectors $\mathbf{\Psi}_i^E$ $(i \in \mathcal{J}_0^E)$ and $\mathbf{\Psi}_j^G$ $(j \notin \mathcal{J}_+^G)$, we have the following sufficient condition for the unstable tensegrity structures.

Lemma 3.6 *If an eigenvector $\mathbf{\Psi}_i^E$ $(i \in \mathcal{J}_0^E)$ of $\mathbf{K}_E$ can be expressed as a linear combination of the eigenvectors $\mathbf{\Psi}_j^G$ $(j \notin \mathcal{J}_+^G)$ of $\mathbf{K}_G$, then the structure is unstable.*

Proof. The quadratic form Q for an eigenvector $\mathbf{\Psi}_i^E$ $(i \in \mathcal{J}_0^E)$ is written as

$$Q = \mathbf{\Psi}_i^{E\top} \mathbf{K} \mathbf{\Psi}_i^E = \mathbf{\Psi}_i^{E\top} \mathbf{K}_G \mathbf{\Psi}_i^E = \sum_{j \notin \mathcal{J}_+^G} \kappa_j^2 \lambda_j^G \leq 0$$

Hence, we have at least one vector that results in non-positive value of the quadratic form; i.e. $\mathbf{K}$ is not positive-definite, and the structure is unstable. □

If the signs of the prestresses are reversed, the self-equilibrium equations with respect to the prestresses in Eq. (2.36) obviously do also hold. However, if the structure is kinematically indeterminate, then the structure with reversed signs of prestresses becomes unstable, although it is still in a state of self-equilibrium.

Lemma 3.7 *If signs of all prestresses are reversed for a stable structure that is kinematically indeterminate, then the structure becomes unstable.*

Proof. Because the structure is kinematically indeterminate, the set $\mathbf{\Psi}_i^E$ $(i \in \mathcal{J}_0^E)$ of mechanisms is not empty.

Since the original structure is stable, the quadratic form Q is positive for $\mathbf{\Psi}_i^E$ $(i \in \mathcal{J}_0^E)$; i.e.

$$Q = \mathbf{\Psi}_i^{E\top} \mathbf{K} \mathbf{\Psi}_i^E = \mathbf{\Psi}_i^{E\top} \mathbf{K}_G \mathbf{\Psi}_i^E > 0$$

As the signs of the prestresses are reversed, the signs of all elements of $\mathbf{K}_G$ are reversed. Therefore, it turns out to be

$$\mathbf{\Psi}_i^{E\top} \mathbf{K} \mathbf{\Psi}_i^E < 0$$

and the structure becomes unstable, because there is a vector that results in negative value of the quadratic form. □

We have mentioned that the structures with positive semi-definite force density can be super stable, which is irrelevant to the materials and level of prestresses. We did also explain the axial stiffness of the members are considered to be infinite in the prestress stability. However, the stability of the tensegrity structure that are made of practical materials and not super stable (the force density matrix has negative eigenvalues) depends on the relative relationship between the axial stiffness of members and level of prestresses. This is illustrated by the following lemma.

Lemma 3.8 *Let* $\lambda^E_{\min} = \min_{i\in\mathcal{J}^E_+} \lambda^E_i$ *and* $\lambda^G_{\min} = \min_j \lambda^G_j$. *The structure is stable if the following assumptions are satisfied:*

[L1] The prestresses are small enough such that $\lambda^E_{\min} + \lambda^G_{\min} > 0$.

[L2] Any eigenvector $\boldsymbol{\Psi}^E_i$ $(i \in \mathcal{J}^E_0)$ *of* $\mathbf{K}_E$ *can be expressed as a linear combination of the eigenvectors* $\boldsymbol{\Psi}^G_j$ $(j \notin \mathcal{J}^G_-)$ *of* $\mathbf{K}_G$, *and at least one coefficient* κ_j $(j \in \mathcal{J}^G_+)$ *has a nonzero value.*

Proof. A nontrivial vector $\mathbf{d}$ is divided into two parts as

$$\mathbf{d} = \mathbf{d}_0 + \mathbf{d}_+$$

where

$$\mathbf{d}_0 = \sum_{i\in\mathcal{J}^E_0} \alpha_i \boldsymbol{\Psi}^E_i, \quad \mathbf{d}_+ = \sum_{i\in\mathcal{J}^E_+} \alpha_i \boldsymbol{\Psi}^E_i$$

The quadratic form Q^E of $\mathbf{K}_E$ is written as

$$\begin{aligned} Q^E = \mathbf{d}^\top \mathbf{K}_E \mathbf{d} &= \mathbf{d}_0^\top \mathbf{K}_E \mathbf{d}_0 + \mathbf{d}_+^\top \mathbf{K}_E \mathbf{d}_+ \\ &= \mathbf{d}_+^\top \mathbf{K}_E \mathbf{d}_+ \\ &= \sum_{i\in\mathcal{J}^E_+} \alpha_i^2 \lambda^E_i \\ &\geq \sum_{i\in\mathcal{J}^E_+} \alpha_i^2 \lambda^E_{\min} \end{aligned} \tag{3.27}$$

where the equality is satisfied if $\mathbf{d}$ is in the direction of $\mathbf{\Psi}_i^E$ corresponding to the lowest positive eigenvalue of $\mathbf{K}_E$, or in the null-space of $\mathbf{K}_E$.

Using the second assumption, $\mathbf{d}_0$ and $\mathbf{d}_+$ can be also written in terms of $\mathbf{\Psi}_j^G$ as

$$\mathbf{d}_0 = \sum_{j \notin \mathcal{J}_-^G} \kappa_{0j} \mathbf{\Psi}_j^G, \quad \mathbf{d}_+ = \sum_{j \in \mathcal{J}_-^G} \kappa_{+j} \mathbf{\Psi}_j^G + \sum_{j \notin \mathcal{J}_-^G} \kappa_{+j} \mathbf{\Psi}_j^G$$

which leads to

$$\begin{aligned} \mathbf{d} &= \mathbf{d}_0 + \mathbf{d}_+ \\ &= \sum_{j \in \mathcal{J}_-^G} \kappa_{+j} \mathbf{\Psi}_j^G + \sum_{j \notin \mathcal{J}_-^G} (\kappa_{0j} + \kappa_{+j}) \mathbf{\Psi}_j^G \end{aligned}$$

The quadratic form Q^G of $\mathbf{K}_G$ is written as

$$\begin{aligned} Q^G = \mathbf{d}^\top \mathbf{K}_G \mathbf{d} &= \sum_{j \in \mathcal{J}_-^G} \kappa_{+j}^2 \lambda_j^G + \sum_{j \notin \mathcal{J}_-^G} (\kappa_{0j} + \kappa_{+j})^2 \lambda_j^G \\ &\geq \sum_{j \in \mathcal{J}_-^G} \kappa_{+j}^2 \lambda_j^G \\ &\geq \sum_{j \in \mathcal{J}_-^G} \kappa_{+j}^2 \lambda_{\min}^G \end{aligned} \tag{3.28}$$

Note from the second assumption that the first inequality of Eq. (3.28) is not satisfied in equality if $\mathbf{d}$ is in the null-space of $\mathbf{K}_E$. From Eqs. (3.27), (3.28), the first assumption $\lambda_{\min}^E + \lambda_{\min}^G > 0$, and the relation

$$\sqrt{\mathbf{d}_+^\top \mathbf{d}_+} = \sum_{i \in \mathcal{J}_+^E} \alpha_i^2 \geq \sum_{j \in \mathcal{J}_-^G} \kappa_{+j}^2 \geq 0$$

the following relation is obtained

$$\begin{aligned} \mathbf{d}^\top \mathbf{K}_E \mathbf{d} + \mathbf{d}^\top \mathbf{K}_G \mathbf{d} &\geq \sum_{i \in \mathcal{J}_+^E} \alpha_i^2 \lambda_{\min}^E + \sum_{j \in \mathcal{J}_-^G} \kappa_{+j}^2 \lambda_{\min}^G \\ &\geq 0 \end{aligned} \tag{3.29}$$

where the second inequality is satisfied in equality only if $\mathbf{d}$ is in the null-space of $\mathbf{K}_E$. Hence, the equalities in Eqs. (3.28) and (3.29) are not satisfied simultaneously, and the relation

$$Q = \mathbf{d}^\top \mathbf{K} \mathbf{d} > 0 \tag{3.30}$$

is obtained and the structure is stable. □

It is not necessarily true that a stable structure satisfies the assumptions in Lemma 3.8. Therefore, Lemma 3.8 is not the necessary but the sufficient conditions for the stability of a tensegrity structure.

If the structure is stable, then the external work corresponding to any mode of infinitesimal mechanism ($\boldsymbol{\Psi}_i^E$ $(i \in \mathcal{J}_0^E)$ in our notation) is positive.

Let $\mathbf{M}$ denote the mechanism matrix of which the ith column is $\boldsymbol{\Psi}_i^E$ $(i \in \mathcal{J}_0^E)$, and consider a nontrivial vector $\mathbf{d}$ in the null-space of $\mathbf{K}_E$ as $\mathbf{d} = \sum_{i \in \mathcal{J}_0^E} \alpha_i \boldsymbol{\Psi}_i^E = \mathbf{M}\boldsymbol{\alpha}$. The quadratic form of $\mathbf{K}$ can be written as

$$\mathbf{d}^\top \mathbf{K} \mathbf{d} = \boldsymbol{\alpha}^\top \mathbf{M}^\top \mathbf{K}_G \mathbf{M} \boldsymbol{\alpha} \tag{3.31}$$

Guest (2006) commented that the matrix used for stability test by Calladine and Pellegrino (1991, 1992) is equivalent to $\mathbf{M}^\top \mathbf{K}_G \mathbf{M}$ in Eq. (3.31) that can be considered as a *reduced form* of $\mathbf{K}_G$.

If a structure is stable, it is certainly true that $\mathbf{M}^\top \mathbf{K}_G \mathbf{M}$ is positive definite. So this is a necessary condition for stability. However, because the matrix is a reduced form of $\mathbf{K}_G$, only the mechanisms are considered as deformation modes. Therefore, positive-definiteness of $\mathbf{M}^\top \mathbf{K}_G \mathbf{M}$ may not necessarily lead to positive-definiteness of $\mathbf{K}$, especially when the structure is not super stable with negative eigenvalues in $\mathbf{K}_G$. So their condition (in stability test) is not a sufficient condition for the stability of the tensegrity structures that are kinematically indeterminate.

In fact, their stability test agrees with the definition of prestress stability introduced in Chapter 2, where the influence of the materials or level of prestresses are implicitly ignored, because the axial stiffness of the members are assumed to be infinite (or large enough) so that the level of prestresses can not dominate the positive definiteness of the quadratic form of the tangent stiffness matrix with respect to the mechanisms.

A numerical example of symmetric prismatic tensegrity structure in Chapter 7 will show how the materials or level of prestresses can affect the stability of the tensegrity structures with negative eigenvalues in the force density matrix, so that the material is also considered to be one of the critical parameters for the stability of the tensegrity structures.

3.4 Discussions and Conclusions

A necessary condition, in which the geometry matrix should be full-rank, for stability of tensegrity structures is firstly presented based on investigation of affine motions of the structures. This necessary condition is proved to be equivalent to that derived in the theory of structural rigidity in mathematics, and is considered to be more comprehensible and easy to implement. Together with this necessary condition, it is further proved that a tensegrity structure is guaranteed to be super stable if two more conditions are satisfied: the force density matrix is positive semi-definite and it has minimum rank deficiency for non-degeneracy condition. Super stable structures have many superior advantages compared to the structures that are not super stable: any stretched versions of them are also super stable. This property could be useful for a practical structure, because imperfections in construction will not hurt stability of the structure if it is super stable.

Full-rank of the geometry matrix and positive semi-definiteness of the force density matrix are also necessary conditions for super stability of a tensegrity structure. In Chapter 4, we will present an efficient method, called *adaptive force density method*, for the form-finding problem of tensegrity structures. In this method, positive semi-definiteness of the force density method could be ensured such that it can lead to a (super) stable structure without much additional computation cost.

Stability of tensegrity structures can be studied in another way. That is to investigate linear dependence of the eigenvectors of the linear and geometrical stiffness matrices. A sufficient condition is presented showing that a tensegrity structure is stable if level of prestresses is small enough compared to member stiffness. And it is proved that kinematically indeterminate structures will become unstable if signs of prestresses are reversed, although they are still in self-equilibrium. Moreover, prestress stability is demonstrated to be the necessary but not sufficient condition for stability of tensegrity structures.

Chapter 4

ADAPTIVE FORCE DENSITY METHOD

This chapter is to present an efficient numerical method, called *adaptive force density method*, for the form-finding problem of tensegrity structures.

We have discussed in Chapter 3 that positive semi-definiteness of the force density matrix is a necessary condition and one of the sufficient conditions for super stability of a tensegrity structure. A super stable structure is always preferable in the design, since any stretched versions of it are still super stable. Hence, imperfection in construction will not alter super stability of the structures, which is considered to be a very important point for practical structures since uncertainties in manufacture and construction are unavoidable. Moreover, the force density method has great advantage in transforming non-linear equilibrium equations into linear forms by introduction of the concept of force densities.

These backgrounds motivate our study on an efficient form-finding method that can ensure a stable structure and have good control over its configuration as well. The proposed method is an extension of the basic idea of the force density method, and hence, has its advantages in dealing with non-linear equations in linear manner and providing insight into structural properties of the structures. Satisfying the non-degeneracy condition presented in Chapter 2 is the key to this method.

4.1 Introduction

Among the existing methods for the form-finding problem of tensegrity structures, the methods extended from the idea of the force density method, which is originally proposed for cable nets by Schek (1974), are considered to be very effective. The concept of force density is introduced to transform the non-linear equations with respect to the nodal coordinates into linear equations, as discussed in Chapter 2. Hence, only linear equations need to be solved for the determination of their configurations. Basically, we are concerned with two methods in the family of the force density method – the symmetry approach in Chapter 7 and 8, and the adaptive force density method discussed in this chapter.

Based on the symmetry properties of the structure, where every node can be transformed to any other by a proper symmetry operation of a specific group, Connelly and Back (1998) presented a catalogue of tensegrity structures with spherical shapes. The term 'stress' used in their literature is actually the force density used in our study. We will use the similar methods to investigate the self-equilibrium and stability of the symmetric prismatic and star-shaped tensegrity structures in Chapter 7 and 8, respectively.

Remind the non-degeneracy condition for the tensegrity structures presented in Chapter 2. The force density matrix should have rank deficiency of at least $d+1$ for a non-degenerate tensegrity structure in d-dimensional space. Notice that the force density matrix is determined by the connectivity of the structure and the force densities of its members. Hence, for a non-degenerate tensegrity structure, there must exist some sets of force densities that satisfy the non-degeneracy condition, while the topology of the structure is assumed to be given. This gives us a clear clue to find these feasible force densities, and then to determine the configuration of the structure.

Vassart and Motro (1999) proposed an analytical technique based on the strategy discussed above. The force densities are denoted by symbols or semi-symbols. The force density matrix is then calculated in symbolic form to find out the conditions to derive the necessary rank deficiency. This method can have insight of the structures in some extents by investigating the symbolic non-degeneracy condition. However, for the structures with relatively large number of members,

it may not be efficient enough. And it cannot ensure a symmetric structure even though it has the symmetry form for the force densities. Moreover, the relations between the force densities may turn out to be less meaningful while there are too many, since the force density is the ratio of prestress to length, which has no explicit mechanical nor geometrical meanings.

Thus, an effective numerical method that can have some controls on the configurations of the structure is strongly desired. This motivates us to propose a new numerical method to conquer the problems in the analytical methods.

In the proposed method, the required rank deficiency of the force density matrix is achieved relying on the efficient algorithm that can be easily implemented in the computers. The proposed method is called *adaptive force density method* because (a) it is an extension of the basic formulation and initial idea of the force density method proposed, and (b) the method is based on eigenvalue analysis of the force density matrix, and can automatically adjust the values of the force densities to adapt to the requirement on rank deficiency.

4.2 Constraints

This section presents the constraints, including those introduced by the definition of the force density matrix, and constraints on the symmetry properties and the elevation of the structure, in the linear forms of force densities and nodal coordinates.

The form-finding process is divided into two design stages. The constraints with respect to the force densities are incorporated into the first design stage of the proposed form-finding process introduced in the next section to find the feasible force densities that satisfy the non-degeneracy condition.

And the constraints with respect to the nodal coordinates are incorporated into the second design stage to determine the configuration.

4.2.1 Force Density Matrix

The force density matrix can be directly formulated from the force densities as defined in Eq. (2.16), if the connectivity of the structure is known. Hence, we

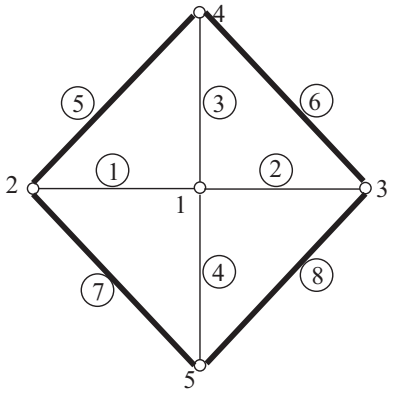

Figure 4.1: A two-dimensional tensegrity structure.

can establish the linear equation between the force density matrix and the force densities.

Let $\mathcal{I}$ denote the set of members connected to node i. From the direct definition of force density matrix $\mathbf{E}$, the ith column $\mathbf{E}_i$ of $\mathbf{E}$ can be written in terms of the force density vector $\mathbf{q}$ by a matrix $\bar{\mathbf{B}}^i \in \Re^{n\times m}$ as

$$\bar{\mathbf{B}}^i\mathbf{q} = \mathbf{E}_i$$

where (j,k)- component $\bar{\mathbf{B}}^i_{(j,k)}$ $(k = 1, 2, \ldots, m)$ of $\bar{\mathbf{B}}^i$ is defined as

$$\bar{\mathbf{B}}^i_{(j,k)} = \begin{cases} 1 & \text{if } i = j \text{ and } k \in \mathcal{I} \\ -1 & \text{if nodes } i \text{ and } j \text{ are connected by member } k \\ 0 & \text{for other cases} \end{cases} \tag{4.1}$$

For example, the matrix $\bar{\mathbf{B}}^1$ corresponding to node 1 of the two-dimensional tensegrity structure as shown in Fig. 4.1 can be written as

$$\bar{\mathbf{B}}^1 = \begin{pmatrix} 1 & 1 & 1 & 1 & 0 & 0 & 0 & 0 \\ -1 & 0 & 0 & 0 & 0 & 0 & 0 & 0 \\ 0 & -1 & 0 & 0 & 0 & 0 & 0 & 0 \\ 0 & 0 & -1 & 0 & 0 & 0 & 0 & 0 \\ 0 & 0 & 0 & -1 & 0 & 0 & 0 & 0 \end{pmatrix}$$

By letting $\bar{\mathbf{B}}^\top = (\bar{\mathbf{B}}^{1\top}, \ldots, \bar{\mathbf{B}}^{i\top}, \ldots, \bar{\mathbf{B}}^{n\top})$ and $\bar{\mathbf{g}}^\top = (\mathbf{E}_1^\top, \ldots, \mathbf{E}_i^\top, \ldots, \mathbf{E}_n^\top)$, the following relation between the force density matrix and force density vector

can be written in a linear form as follows

$$\bar{\mathbf{B}}\mathbf{q} = \bar{\mathbf{g}} \tag{4.2}$$

From the definition of $\bar{\mathbf{B}}$, we can see that there exists a row of which the kth component ($k = 1, 2, \ldots, m$) is -1 while the others are zero. So the rank of $\bar{\mathbf{B}}$ is m; i.e. $\bar{\mathbf{B}}$ is full-rank.

Eq. (4.2) can be regarded as a linear constraint on the force densities due to the force density matrix. Note that this linear constraint has to be exactly satisfied, while the constraints presented in the following are optional according to the requirements by the designers.

4.2.2 Specific Force Densities

In some cases, we may expect that some specific force densities can have the assigned values according to our preference, or we may expect some force densities to have definite relations on their values. These requirements on the force densities can also be formulated in a linear form so as to be incorporated into the first design stage for finding the feasible force densities.

The linear constraints on the values and relations of some specific force densities can be formulated as follows by using constant matrix $\hat{\mathbf{B}}$ and vector $\hat{\mathbf{g}}$

$$\hat{\mathbf{B}}\mathbf{q} = \hat{\mathbf{g}} \tag{4.3}$$

For example, if we have four force densities q_1, q_2, q_3 and q_4 for a structure, and we want that q_2 is twice of q_1, and q_3 has the values 0.5, then the linear constraints Eq. (4.3) on the force densities can be written as

$$\begin{pmatrix} 1 & -2 & 0 & 0 \\ 0 & 0 & 1 & 0 \end{pmatrix} \begin{pmatrix} q_1 \\ q_2 \\ q_3 \\ q_4 \end{pmatrix} = \begin{pmatrix} 0 \\ 0.5 \end{pmatrix}$$

4.2.3 Symmetry Properties

Here, we consider the rotational symmetry about the z-axis of the structure as an example to show how to formulate the symmetry properties in linear equations.

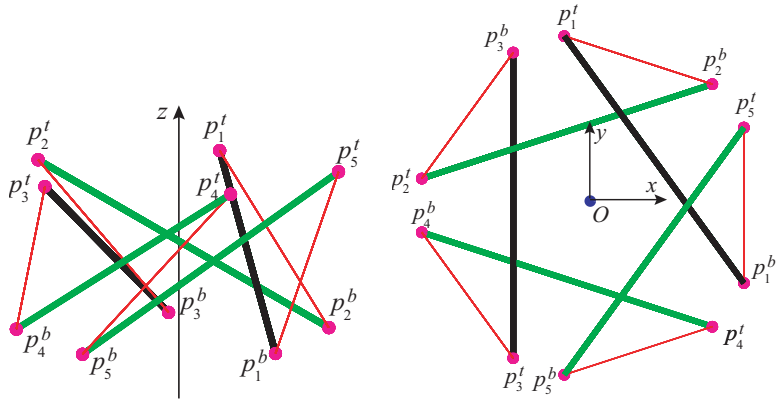

(a) perspective view (b) top view

Figure 4.2: An example of rotational symmetry of five struts.

The linear equations need to be in two different forms: the one with respect to the force densities, and the one with respect to the nodal coordinates, which are incorporated into the first and the second design stages, respectively.

4.2.3.1 Symmetry of Force Densities

n^b-fold symmetry of a structure refers to the fact that a member among a set of n^b members can be moved to any other member in the set by the rotation about the z-axis by $2i\pi/n^b$, where i is an appropriate integer value. These n^b members are said to be in the same *orbit* and have the same lengths and forces, and the same force densities as well. There are usually more than one orbit of struts in a symmetric structure.

For example, the five struts shown in thick lines in Fig. 4.2 belong to the same orbit. Any one of the strut can be moved to another in the same orbit by the rotation about the z-axis through a proper angle $2i\pi/5$ ($i \in \{1, 2, 3, 4\}$). Note that the cables in thin lines belong to a different orbit.

Since the force densities of the members in the same orbit of a symmetric structure have the same values, the symmetry of the structure with respect to the force density vector can be written as

$$\mathbf{Fq} = \mathbf{0} \tag{4.4}$$

There are only two non-zero elements $+1$ and -1 in each row of $\mathbf{F}$.

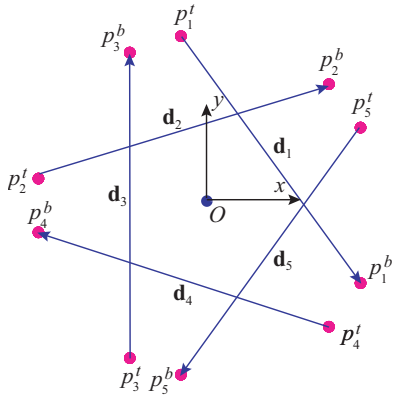

Figure 4.3: Directed graph of the five struts in Fig. 4.2.

For example, if members i and j $(i < j)$ are in the same orbit, there must be one row k of $\mathbf{F}$ consisting of $+1$ and -1 at ith and jth elements, respectively, and the remaining elements in the row are 0 as

$$\mathbf{F}_{(k,p)} = \begin{cases} 1 & \text{for } p = i \\ -1 & \text{for } p = j \\ 0 & \text{for other cases} \end{cases}$$

The linear constraint (8.11) on the symmetry properties with respect to the force densities will be incorporated in the first design stage of the proposed method in the next section.

4.2.3.2 Symmetry of Nodal Coordinates

Since every node of a tensegrity structure must be connected by at leat one strut so as to maintain its self-equilibrium in the usual cases, it is sufficient to consider only the struts while describing the symmetry properties of the structure. Moreover, since the struts in different orbits are geometrically independent in view of symmetry, the symmetry properties are formulated only for the struts in one orbit. The formulation can be simply extended to the whole structure.

Consider one of the orbits, in which there are n^b struts. Denote the higher and lower nodes of the strut i by p_i^t and p_i^b, respectively. The x- and y-coordinates of the nodes p_i^t and p_i^b are denoted by the vectors $\mathbf{x}_i^t = (x_i^t, y_i^t)^\top$ and $\mathbf{x}_i^b = (x_i^b, y_i^b)^\top$, respectively.

The directed member vector $\mathbf{d}_i \in \Re^2$ $(i = 1, \ldots, n^b)$ of the struts on xy-plane is defined as

$$\mathbf{d}_i = \mathbf{x}_i^b - \mathbf{x}_i^t$$

which corresponds to the edges of a directed graph Harary (1969). The edges are directing from the nodes with smaller labels to the ones with larger labels. For example, Fig. 4.3 shows the directed graph of the five struts in Fig. 4.2.

The directed members $\mathbf{d}_i$ in the kth orbit of struts are combined to $\mathbf{d}^k \in \Re^{2n^b}$ as

$$\mathbf{d}^k = (\mathbf{d}_1^\top, \ldots, \mathbf{d}_{n^b}^\top)^\top$$

$\mathbf{x}_i^b$ and $\mathbf{x}_i^t$ in the orbit are also combined to $\mathbf{x}^k \in \Re^{4n^b}$ as

$$\mathbf{x}^k = \left((\mathbf{x}_1^b)^\top, \ldots, (\mathbf{x}_{n^b}^b)^\top, (\mathbf{x}_1^t)^\top, \ldots, (\mathbf{x}_{n^b}^t)^\top\right)^\top$$

The relationship between $\mathbf{d}^k$ and $\mathbf{x}^k$ in orbit k can be written as follows by a matrix $\mathbf{T}^k \in \Re^{2n^b \times 4n^b}$:

$$\mathbf{d}^k = \mathbf{T}^k \mathbf{x}^k \tag{4.5}$$

where the matrix $\mathbf{T}^k$ is constructed by the $2n^b$-by-$2n^b$ identity matrix $\mathbf{I}^{2n^b}$ as

$$\mathbf{T}^k = \begin{pmatrix} \mathbf{I}^{2n^b} & -\mathbf{I}^{2n^b} \end{pmatrix}$$

The symmetry properties of a structure can be easily described by the group representation theory. The n^b struts in an orbit constitute a cyclic group of order n^b. Details of cyclic group and its representation theory can be found in many mathematics or chemistry textbooks, e.g., Bishop (1973). However, knowledge on group representation theory is not necessary here, because the two-dimensional E_1 irreducible representation matrix $\mathbf{R}_i$ of the cyclic group defined as follows is identical to the transformation matrix of counter-clockwise rotation about the z-axis by $2(i-1)\pi/n^b$, which might be more familiar to the designers:

$$\mathbf{R}_i = \begin{pmatrix} C_i & -S_i \\ S_i & C_i \end{pmatrix}$$

where $C_i = \cos(2(i-1)\pi/n^b)$ and $S_i = \sin(2(i-1)\pi/n^b)$.

If $\mathbf{d}_1$ coincides with $\mathbf{d}_i$ by the counter-clockwise rotation about z-axis by the angle $2(i-1)\pi/n^b$, the following relation holds:

$$\mathbf{d}_i = \mathbf{R}_i \mathbf{d}_1$$

which can be rewritten with respect to $\mathbf{d}^k$ as follows by using the 2-by-2 identity matrix $\mathbf{I}^2$:

$$\begin{pmatrix} \mathbf{R}_i & \dots & -\mathbf{I}^2 & \dots \end{pmatrix} \mathbf{d}^k = \mathbf{0} \tag{4.6}$$

Combining all the relations of $\mathbf{d}_i$ $(i \neq 1)$ and $\mathbf{d}_1$ similar to Eq. (4.6) by using the matrix $\mathbf{S}^k \in \Re^{2(n^b-1)\times 2n^b}$, we obtain

$$\mathbf{S}^k \mathbf{d}^k = \mathbf{0} \tag{4.7}$$

By substituting Eq. (4.5) into Eq. (4.7) and letting $\bar{\mathbf{S}} = \mathbf{S}^k \mathbf{T}^k \in \Re^{2(n^b-1)\times 4n^b}$, the rotational symmetry of the struts in orbit k can be expressed in a linear form with respect to the nodal coordinates in xy-plane as

$$\bar{\mathbf{S}} \mathbf{x}^k = \mathbf{0}$$

Because the rotational symmetry of the struts in different orbits can be formulated independently, the rotational symmetry of the whole structure in terms of the generalized coordinate vector $\mathbf{X} = \left((\mathbf{x}^1)^\top, \dots, (\mathbf{x}^{n^l})^\top \right)^\top \in \Re^{2n}$ in xy-plane can then be combined as

$$\mathbf{S}\mathbf{X} = \mathbf{0} \tag{4.8}$$

where the elements of $\bar{\mathbf{S}}$ for each orbit have been incorporated into the matrix $\mathbf{S}$.

If the structure has n^l similar orbits of struts, with n^b struts in each orbit, the matrix $\mathbf{S}(\in \Re^{2n^l(n^b-1)\times 4n^l n^b})$ can be calculated by the tensor product of the n^l-by-n^l identity matrix $\mathbf{I}^{n^l}$ and the matrix $\bar{\mathbf{S}}$; i.e., $\mathbf{S} = \mathbf{I}^{n^l} \otimes \bar{\mathbf{S}}$.

This way, the symmetry properties of the whole structure can be formulated as a set of linear equations with respect to the generalized nodal coordinate vector $\mathbf{X}$ in xy-plane. The constraints Eq. (4.8) will be incorporated in the second design stage to ensure a rotationally symmetry of the structure.

4.2.4 Elevation

From the self-equilibrium equation with respect to the nodal coordinates in z-direction, we can also formulate the linear constraint on elevation of the structure with respect to the force densities.

Suppose that the elevation of the structure is assigned by the designer. Thus, z-coordinates of all the nodes are determined.

Since the following relation always holds

$$\mathbf{QCz} = \mathrm{diag}(\mathbf{Cz})\mathbf{q} = \mathbf{Wq}$$

the self-equilibrium equation in z-direction can be rewritten with respect to the force density vector $\mathbf{q}$ as

$$\mathbf{C}^\top\mathbf{Wq} = \mathbf{0}$$

By letting $\mathbf{N} = \mathbf{C}^\top\mathbf{W}$, the linear constraint on the elevation of a tensegrity structure with respect to the force densities can then be written as

$$\mathbf{Nq} = \mathbf{0} \tag{4.9}$$

which is incorporated in the first design stage in the next section for finding the feasible set of force densities. This way, we can have exact control over the elevation of the structure.

4.2.5 Summary of Constraints

So far, we have formulated the linear constraints on the force density matrix, specific force densities, symmetry properties and elevation with respect to the force densities. Only the constraint on the force density matrix is compulsory and the other two are optional.

The vectors on the right hand side of the linear constraints on the force density matrix in Eq. (4.2) and some specific force densities in Eq. (4.3) are usually not trivial. They are combined as

$$\mathbf{Bq} = \begin{pmatrix} \bar{\mathbf{B}} \\ \hat{\mathbf{B}} \end{pmatrix} \mathbf{q} = \begin{pmatrix} \bar{\mathbf{g}} \\ \hat{\mathbf{g}} \end{pmatrix} = \mathbf{g} \tag{4.10}$$

The optional constraints on symmetry in Eq. (8.11) and elevation in Eq. (8.4) with respect to the force density are combined as

$$\begin{pmatrix} \mathbf{F} \\ \mathbf{N} \end{pmatrix} \mathbf{q} = \mathbf{0} \tag{4.11}$$

Since the matrix in the linear equation (8.5) with respect to $\mathbf{q}$ is usually rank deficient, the solution of (8.5) can be written as

$$\mathbf{q} = \boldsymbol{\Psi}\boldsymbol{\alpha} \tag{4.12}$$

where $\boldsymbol{\alpha}$ is the coefficient vector, and the columns of the matrix $\boldsymbol{\Psi}$ span the solution space of Eq. (8.5). Note that $\boldsymbol{\Psi}$ is also a constant matrix when the constraints are given.

Since the force density matrix $\mathbf{E}$ has to satisfy the non-degeneracy condition and the force densities $\mathbf{q}$ are related to $\mathbf{E}$ through Eq. (4.10), the coefficient vector $\boldsymbol{\alpha}$ cannot be selected arbitrarily.

4.3 Form-finding Process

This section demonstrates how the constraints are incorporated into the adaptive force density method to uniquely determine the configuration of a tensegrity structure.

The form-finding process is divided into two design stages: the first stage is to find the feasible force densities that satisfy the non-degeneracy condition and the constraints, and the second stage is to uniquely determine the configuration of the structure satisfying the constraints.

4.3.1 Spectral Decomposition

By decomposing the force density matrix by the spectral decomposition and setting the necessary number of eigenvalues of the force density matrix to zero, the updated force density matrix can then achieve the required rank deficiency.

Because the force density matrix is symmetric, it can be written as follows by applying spectral decomposition (Lay, 1996):

$$\mathbf{E} = \boldsymbol{\Phi}\boldsymbol{\Lambda}\boldsymbol{\Phi}^{\top}$$

where the diagonal elements $\{\lambda_1, \lambda_2, \ldots, \lambda_n\}$ of the diagonal matrix $\mathbf{\Lambda}$ are the eigenvalues of $\mathbf{E}$, and they are numbered in non-decreasing order as

$$\lambda_1 \leq \lambda_2 \leq \ldots \leq \lambda_n$$

The ith column $\mathbf{\Phi}_i$ of $\mathbf{\Phi}$ is the eigenvector corresponding to λ_i. It is clear that the number of nonzero eigenvalues of $\mathbf{E}$ is equal to its rank.

Let r denote the number of non-positive eigenvalues of $\mathbf{E}$, and $h^\star (\leq d+1)$ denote the required rank deficiency of the force density matrix. We have the following two cases for the structure in d-dimensional space:

CASE 1: $r \leq h^\star$

CASE 2: $r > h^\star$

For CASE 1, we can simply assign 0 to the first $h^\star$ eigenvalues of $\mathbf{E}$ with smallest values to zero as

$$\lambda_i = 0, \quad (i = 1, 2, \ldots, h^\star) \tag{4.13}$$

to obtain $\bar{\mathbf{\Lambda}}$ with the modified eigenvalues. The force density matrix is modified by $\bar{\mathbf{\Lambda}}$ as

$$\bar{\mathbf{E}} = \mathbf{\Phi} \bar{\mathbf{\Lambda}} \mathbf{\Phi}^\top \tag{4.14}$$

This way, $\bar{\mathbf{E}}$ will have the required rank deficiency $h^\star$, and, it is positive semi-definite without negative eigenvalues.

However, for CASE 2 where $r > h^\star$, the rank deficiency will be larger than the required number, if the same operation as CASE 1 is applied. For this case, we may have several strategies; e.g., (a) assign positive values to some of the negative eigenvalues, or (b) specify more than $h^\star$ independent coordinates in the form-finding process presented later, etc. Since arbitrary chosen initial force densities usually result in $r \leq h^\star$, we will focus on only CASE 1.

Instead of assigning 0 to the $h^\star$ smallest eigenvalues zero, we can also assign 0 to eigenvalues with the $h^\star$ smallest absolute values. In some cases, the latter strategy may show stronger ability of searching new self-equilibrium configurations.

4.3.2 First Design Stage: Feasible Force Densities

As the first design stage of the form-finding process, an iterative algorithm is presented to find the feasible force densities satisfying the non-degeneracy condition and the linear constraints (4.10) and (8.5).

Suppose that we have obtained the force density vector $\mathbf{q}^i$ at the ith step of the iterative algorithm, the corresponding force density matrix $\mathbf{E}^i$ of which has the necessary rank deficiency. Substituting Eq. (8.6) into Eq. (4.10), we have

$$\mathbf{g}^i = \mathbf{B}\boldsymbol{\Psi}\boldsymbol{\alpha}^i \tag{4.15}$$

Since $\mathbf{B}\boldsymbol{\Psi}$ in Eq. (8.9) is usually full-rank and not square, the coefficient vector can be computed as follows by using the least square method

$$\boldsymbol{\alpha}^i = (\mathbf{B}\boldsymbol{\Psi})^{-}\mathbf{g}^i$$

where $(\ )^{-}$ denotes the generalized inverse of a matrix. The force density vector $\mathbf{q}^i$ can be updated to $\mathbf{q}^{i+1}$ by Eq. (8.6) as

$$\mathbf{q}^{i+1} = \boldsymbol{\Psi}(\mathbf{B}\boldsymbol{\Psi})^{-}\mathbf{g}^i \tag{4.16}$$

Note that $\mathbf{q}^{i+1}$ may not be equal to $\mathbf{q}^i$, so the new force density matrix $\mathbf{E}^{i+1}$ corresponding to $\mathbf{q}^{i+1}$ may not have the necessary rank deficiency and has to be recomputed based on the eigenvalue analysis and spectral decomposition. Spectral decomposition of the force density matrix presented previously needs to be applied again until the difference between the new and old force densities is small enough.

By iteratively applying Eqs. (4.13) and (8.12), we can adaptively find the feasible force density vector $\hat{\mathbf{q}}$, which can be summarized as follows:

Algorithm 4.1: Feasible force densities

Step 0: Give an initial $\mathbf{q}^0$ to obtain $\mathbf{E}^0$ by Eq. (2.15). Set $i := 0$.

Step 1: Assign 0 to the $h^\star$ smallest (absolute) eigenvalues of $\mathbf{E}^i$ and reconstruct $\bar{\mathbf{E}}^i$ by Eq. (4.14).

Step 2: Obtain $\mathbf{g}^{i+1}$, calculate $\mathbf{q}^{i+1}$ from Eq. (8.12) and update $\mathbf{E}^{i+1}$ by Eq. (2.15).

Step 3: If the updated force density matrix has the required rank deficiency $h^\star$, then let $\hat{\mathbf{q}} = \mathbf{q}^{i+1}$, compute $\hat{\mathbf{E}}$ and terminate the algorithm; otherwise, set $i \leftarrow i+1$ and return to Step 1.

This way, we can adaptively derive the force densities that satisfy the non-degeneracy condition for the tensegrity structures and the linear constraints on them. The next step is to uniquely determine the configuration of the structure.

4.3.3 Second Design Stage: Configuration

Let $\mathbf{H} \in \Re^{dn \times dn}$ ($d = 2$ or 3) denote the tensor product of the identity matrix $\mathbf{I}(\in \Re^{d\times d})$ and the force density matrix constructed by the feasible force densities $\mathbf{E} = \hat{\mathbf{E}}$ as

$$\mathbf{H} = \mathbf{I} \otimes \mathbf{E} \tag{4.17}$$

The equilibrium equations in all directions and the linear constraints on symmetry can be combined as follows by using $\mathbf{H}$ and the generalized coordinate vector $\mathbf{X}$

$$\begin{pmatrix} \mathbf{H} \\ \mathbf{S} \end{pmatrix} \mathbf{X} = \mathbf{0} \tag{4.18}$$

Note that if the elevation of the structure has been assigned, then the nodal coordinates in z-direction have been determined. Hence, the identity matrix in Eq. (4.17) becomes $\mathbf{I}(\in \Re^{2\times 2})$ for the three-dimensional structures, and the generalized coordinate vector $\mathbf{X}$ is $\mathbf{X}^\top = (\mathbf{x}^\top, \mathbf{y}^\top)$.

It should be noticed that there are $h^\star$ components of nodal coordinates in each direction that can be specified, because the rank deficiency of $\mathbf{E}$ is equal to $h^\star$. Therefore, the rank deficiency of $\mathbf{H}$ is $dh^\star$, and $dh^\star$ independent nodal coordinates can be specified if no symmetry is considered.

The solution of Eq. (4.18) can be written as

$$\mathbf{X} = \mathbf{G}\boldsymbol{\beta}$$

where $\boldsymbol{\beta}$ is the coefficient vector. Denote the rank of $\mathbf{G}$ by $r^G(\leq dh^\star)$. Hence, the number of independent nodal coordinate components that can be specified is r^G.

If we specify an independent set of nodal coordinates $\bar{\mathbf{X}} \in \Re^{r^G}$ and obtain the corresponding components $\bar{\mathbf{G}} \in \Re^{r^G \times dh^\star}$ in $\mathbf{G}$, where rank($\bar{\mathbf{G}}$)=r^G, the configuration of the structure in terms of nodal coordinates $\mathbf{X}$ can be determined by

$$\mathbf{X} = \mathbf{G}\bar{\mathbf{G}}^{-1}\bar{\mathbf{X}} \tag{4.19}$$

$\bar{\mathbf{G}}$ can be obtained by using the algorithm presented in the Chapter 5, where the Reduced Row-Echelon Form (RREF) of $\mathbf{G}^\top$ is extensively used to specify the independent set of nodal coordinates consecutively.

Since tensegrity structure should satisfy the self-equilibrium conditions, the vector of unbalanced loads $\boldsymbol{\epsilon} \in \Re^{dn}$ defined as follows can be used for evaluating the accuracy of the results:

$$\boldsymbol{\epsilon} = \mathbf{H}\mathbf{X}$$

The Euclidean norm of $\boldsymbol{\epsilon}$ is used to define the design error ξ as

$$\xi = \sqrt{\boldsymbol{\epsilon}^\top \boldsymbol{\epsilon}} \tag{4.20}$$

As a simple example for demonstrating how to determine the independent set of nodal coordinates to be specified based on the RREF of the transpose form $\mathbf{G}^\top$ of $\mathbf{G}$, the two-dimensional tensegrity structure consisting of (n =) 5 nodes and (m =) 8 members as shown in Fig. 4.1 is considered.

The force densities of members 1–4 and 5–8 can be 1.0 and −0.5, respectively, so that the structure is in a state of self-equilibrium. The force density matrix $\mathbf{E}$ is written as follows

$$\mathbf{E} = \begin{pmatrix} 4.0 & -1.0 & -1.0 & -1.0 & -1.0 \\ -1.0 & 0.0 & 0.0 & 0.5 & 0.5 \\ -1.0 & 0.0 & 0.0 & 0.5 & 0.5 \\ -1.0 & 0.5 & 0.5 & 0.0 & 0.0 \\ -1.0 & 0.5 & 0.5 & 0.0 & 0.0 \end{pmatrix}$$

where the no optional constraints are considered.

Since $\mathbf{H}$ is defined by $\mathbf{E}$ as Eq. (4.17), it is sufficient to investigate only the null-space $\mathbf{G}$ of $\mathbf{E}$, which can be written as

$$\mathbf{G} = \begin{pmatrix} 0.0 & 1.0 & 0.0 \\ 1.0 & 1.0 & 0.0 \\ -1.0 & 1.0 & 0.0 \\ 0.0 & 1.0 & -1.0 \\ 0.0 & 1.0 & 1.0 \end{pmatrix} \tag{4.21}$$

It can be seen from Eq. (4.21) that the rank of $\mathbf{G}$ is 3. Therefore, the rank deficiency r^E of $\mathbf{E}$ is 3, which satisfies the non-degeneracy condition for a two-dimensional structure. The RREF of $\mathbf{G}^\top$ is

$$\mathrm{RREF}(\mathbf{G}^\top) = \begin{pmatrix} 1.0 & 0.0 & 2.0 & 0.0 & 2.0 \\ 0.0 & 1.0 & -1.0 & 0.0 & 0.0 \\ 0.0 & 0.0 & 0.0 & 1.0 & -1.0 \end{pmatrix} \tag{4.22}$$

From Eq. (4.22), we know that the columns corresponding to the node groups $\{1, 2, 4\}$, $\{1, 2, 5\}$, $\{1, 3, 4\}$ and $\{1, 3, 5\}$ are linearly independent, respectively. Therefore, we can specify the coordinates of three nodes in one of these four node groups to obtain a unique and non-degenerate configuration.

4.3.4 Summary of Form-finding Process

The process of finding the configuration of a tensegrity structure with linear constraints on geometrical and mechanical properties of the structure can be summarized as follows:

Algorithm 4.2 – Form-finding Process

First Stage: *Feasible Force Densities*

[L1] Specify the topology.

[L2] Formulate the geometrical constraints with respect to the force densities.

[L3] Assign an initial set of force densities.

[L4] Find the feasible force densities by Algorithm 4.1.

Second Stage: *Determination of Configuration*

[L5] Formulate the geometrical constraints with respect to the nodal coordinates.

[L6] Specify an independent set of nodal coordinates to uniquely determine the configuration.

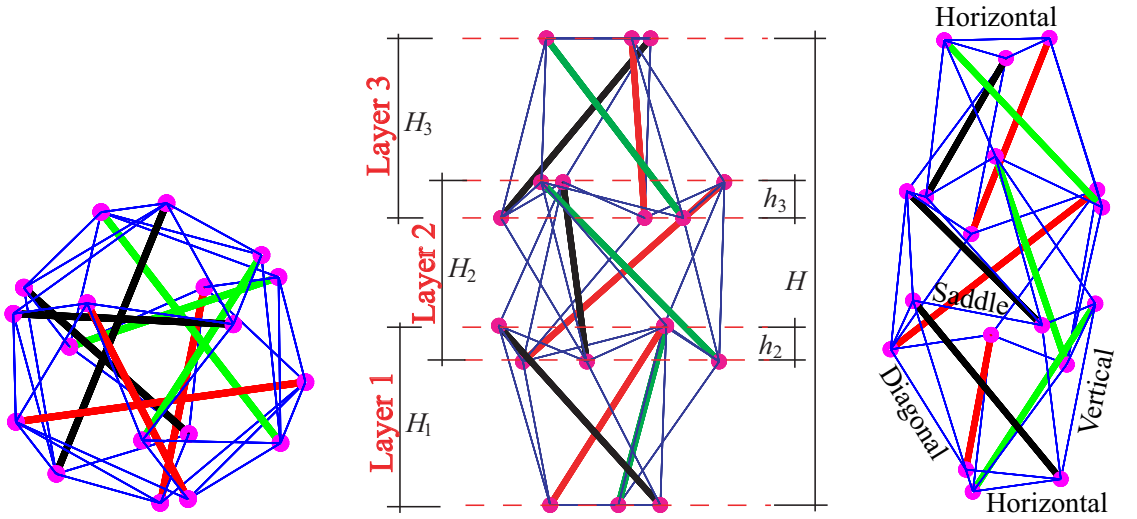

(a) Top view (b) Side view (c) Perspective view

Figure 4.4: A symmetric three-layer tensegrity tower with three struts in each layer.

As will be demonstrated in the numerical examples, designers can control the configuration of a tensegrity structure by changing the values of the parameters in Steps (1), (2), (3) and (6). Symmetry of the structure is ensured by the constraints in Steps (2) and (5).

4.4 Tensegrity Tower

Tensegrity tower, as shown in Fig. 4.4, is a special kind of tensegrity structures. It has one or more layers and at least three struts in each layer. The needle tower invented and built by Kenneth Snelson in Bryant Park in New York may be one of the best-known tensegrity towers in the world.

In this section, we give a detailed description of the geometrical properties and topology of the tensegrity towers, and use them as examples in the next section to demonstrate the capability of finding the desired configurations satisfying the geometrical constraints of the proposed method.

4.4.1 Configuration

Suppose that a tensegrity tower has n^l layers (orbits of struts) and n^b struts in each layer. The struts in each layer belong to the same orbit.

The nodes that have the same z-coordinate are said to be in the same plane. Thus, each layer has two different planes – the bottom and the top planes.

Since no strut physically contacts any other strut, the number n of nodes of a tensegrity tower is

$$n = 2n^l n^b$$

The cables of a tensegrity tower are classified into the following four types as shown in Fig. 4.4.(c), based on the connectivity, similar to the classification by Sultan *et al.* (2002):

- *Horizontal cables* that connect the nodes in the same plane. They can only exist in the bottom plane of the lowest layer and the top plane of the highest layer.
- *Vertical cables* that are connected by the nodes in the top and bottom planes of the same layer.
- *Saddle cables* that connect the nodes in different planes of the adjacent layers, e.g., the top plane of layer k and the bottom plane of layer $k + 1$.
- *Diagonal cables* that connect the nodes in the same top (or bottom) planes of the adjacent layers, e.g., the top (or bottom) plane of layer k and the top (or bottom) plane of the layer $k + 1$.

4.4.2 Elevation

Denote the height of the ith layer by H_i $(i = 1, \ldots, n^l)$, and the overlap between two adjacent layers i and $i - 1$ by h_i $(i = 1, \ldots, n^l)$ where $h_1 = 0$. Designers are free to design the elevation of the structure by assigning H_i and h_i. The total height H of the structure can be computed by

$$H = \sum_{i=1}^{n^l} (H_i - h_i)$$

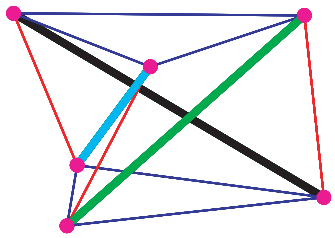

Figure 4.5: The one-layer tensegrity tower (also called the prismatic tensegrity tower with $\mathbf{D}_3$ symmetry in Chapter 7.

The z-coordinates z_k^t of the nodes in the top plane of layer k ($k = 1, \ldots, n^l$) can be determined as

$$z_k^t = \sum_{i=1}^{k} (H_i - h_i)$$

And the coordinates z_k^b of the nodes in the bottom plane of layer k can be computed by

$$z_k^b = z_k^t - H_k$$

This way, the vector $\mathbf{z}$ of the z-coordinates of the tensegrity tower can be determined.

4.4.3 Topology

In order to formulate the connectivity matrix $\mathbf{C}$ in a simple manner for a tensegrity tower with any number of layers ($n^l \geq 1$) and any number of struts ($n^b \geq 3$) in each layer, topology of a general tensegrity tower is defined in this subsection.

The nodes in the bottom and top planes of layer k are labelled by $p_{k,j}^b$ and $p_{k,j}^t$, respectively, as

$$\begin{aligned} p_{k,j}^b &= 2(k-1)n^b + j \\ p_{k,j}^t &= (2k-1)n^b + j \end{aligned} \quad (j = 1, \ldots, n^b) \tag{4.23}$$

4.4.3.1 Struts

The jth strut $P_{k,j}^B$ in layer k is connected by nodes $p_{k,j}^b$ and $p_{k,j}^t$ in different planes:

$$P_{k,j}^B = [p_{k,j}^b, p_{k,j}^t]$$

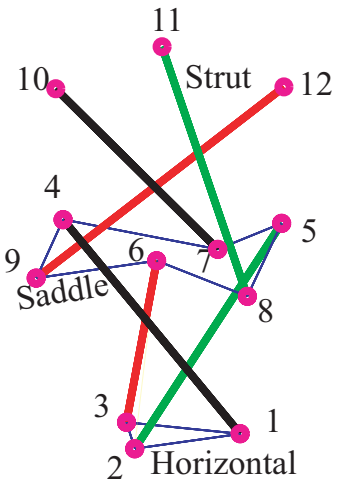

Figure 4.6: An example of connectivity of struts, horizontal cables and saddle cables.

where $[i, j]$ indicates that nodes i and j are connected to construct a member. A simple example with $n^b = 3$ is illustrated in Fig. 4.6, where the vertical and diagonal cables are removed for clarity.

4.4.3.2 Horizontal and Saddle Cables

For the one-layer tensegrity towers ($n^l = 1$) as shown in Fig. 7.3, it has been proved that the structure is not super stable if the horizontal cables are not connected with the adjacent nodes Connelly and Terrell (1995). Although this is not always true for the prestress stability as will be discussed in Chapter 7, the horizontal and saddle cables are assumed to connect the adjacent nodes as shown in Fig. 4.6, in order to avoid the risk of achieving an unstable structure in view of either super or prestress stability. Thus the connectivity of horizontal and saddle cables are given as follows:

- *horizontal cables* $P^H_{1,j}$ and $P^H_{n^l,j}$ are connected by the adjacent nodes in the bottom and top planes of the lowest and highest layers, respectively, as

$$\begin{aligned} P^H_{1,j} &= [p^b_{1,j}, p^b_{1,j+1}] \\ P^H_{n^l,j} &= [p^t_{n^l,j}, p^t_{n^l,j+1}] \end{aligned} \quad (j = 1, \ldots, n^b) \tag{4.24}$$

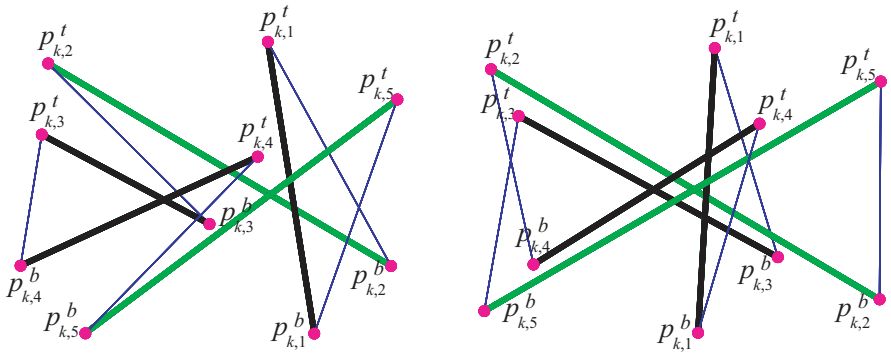

(a) $c^v = 1$ (b) $c^v = 2$

Figure 4.7: An example of connectivity of vertical cables in layer k.

- *saddle cables* are connected by the nodes in the top plane of layer k and the bottom plane of layer $k+1$ as

$$\begin{aligned} P^S_{k,2j-1} &= [p^t_{k,j}, p^b_{k+1,j}] \\ P^S_{k,2j} &= [p^b_{k+1,j}, p^t_{k,j+1}] \end{aligned} \tag{4.25}$$

  where $j = 1, \ldots, n^b$ and $k = 1, \ldots, n^l - 1$.

The following relations have been used in Eqs. (4.24) and (4.25) for brevity.

$$p^b_{k,n^b+1} = p^b_{k,1}, \quad p^t_{k,n^b+1} = p^t_{k,1}$$

4.4.3.3 Vertical and Diagonal Cables

Connectivity of vertical and diagonal cables is not unique. For example, it may be noticed in Figs. 4.7.(a) and (b) that $p^t_{k,1}$ is connected to $p^t_{k,2}$ and $p^t_{k,3}$ by the vertical cables, respectively, leading to different topology. To illuminate this difference, we introduce the parameters c^v and c^d to define the connectivity of vertical and diagonal cables as follows:

- *vertical cable*: The connectivity of the vertical cables are defined by using an integer $c^v \in \{1, \ldots, n^b\}$ as

$$P^V_{k,j} = [p^t_{k,j}, p^b_{k,j+c^v}]$$

  where $j = 1, \ldots, n^b$, $k = 1, \ldots, n^l$, and $j + c^v = j + c^v - n^b$ if $j + c^v > n^b$.

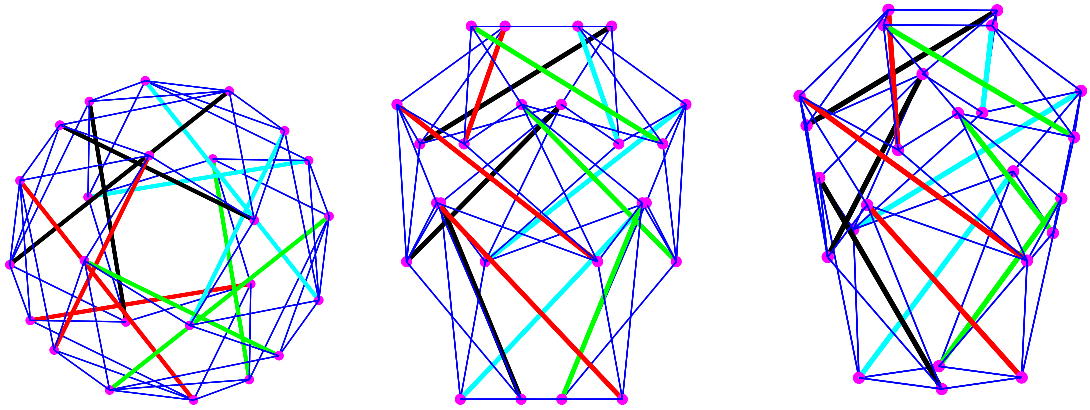

(a) Top view (b) Side view Perspective view

Figure 4.8: A three-layer tensegrity tower with four struts in each layer.

- *diagonal cable*: The connectivity of the diagonal cables are defined by using an integer $c^d \in \{0, \ldots, n^b - 1\}$ as

$$P_{k,j}^{D_b} = [p_{k,j}^b, p_{k+1,j+c^d}^b]$$
$$P_{k,j}^{D_t} = [p_{k,j}^t, p_{k+1,j+c^d}^t]$$

  where $j = 1, \ldots, n^b,\ k = 1, \ldots, n^l - 1$, and $j + c^d = j + c^d - n^b$ if $j + c^d > n^b$.

From the connectivity of the members and nodes for a general n^l-layer tensegrity tower, with n^b struts in each layer, the numbers of struts m^b, horizontal cables m^h, vertical cables m^v, saddle cables m^s and diagonal cables m^d can be written as

$$\begin{array}{ll} m^b = n^l n^b, & m^h = 2n^b, \\ m^s = 2(n^l - 1)n^b, & m^v = n^l n^b, \\ m^d = 2(n^l - 1)n^b, & \end{array} \tag{4.26}$$

and the number m of all members of the structure is

$$m = 6n^l n^b - 2n^b \tag{4.27}$$

Following the definition of connectivity of each type of members and the numbering in Eq. (4.23), the connectivity matrix $\mathbf{C} \in \Re^{m \times n}$ can be easily constructed.

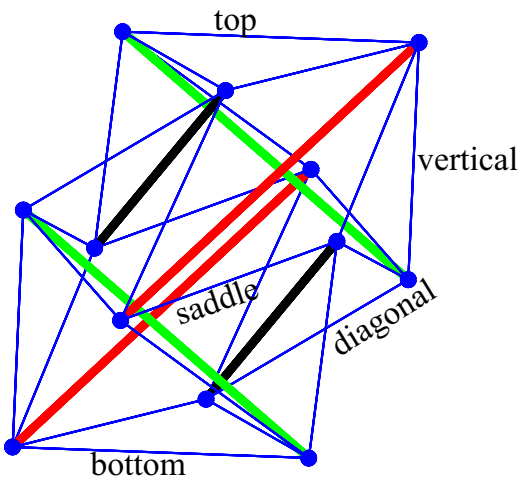

Figure 4.9: A two-layer tensegrity structure.

4.5 Numerical Examples

Some numerical examples are given in this section to show how to use the proposed method for the form-finding problem of the tensegrity structures, and to investigate the efficiency of the method.

4.5.1 Two-layer Tensegrity Structures

The proposed adaptive force density method is first applied to a two-layer tensegrity structure as shown in Fig. 4.9. The structure is composed of 12 nodes and 30 members; i.e. $n = 12$, $m = 30$. Its six struts are divided into two groups: (1) struts of the upper stage, and (2) struts of the lower stage. The 24 cables are divided into: (3) top and bottom bases, (4) saddle, (5) vertical, and (6) diagonal, as indicated in Fig. 4.9.

Linear constraints on the symmetry properties and elevation are not engaged in this two-layer tensegrity structure. The required rand deficiency of the force density matrix is set to the minimum one; i.e., $h^\star = 4$ for the three-dimensional structures considered here.

Example 1:

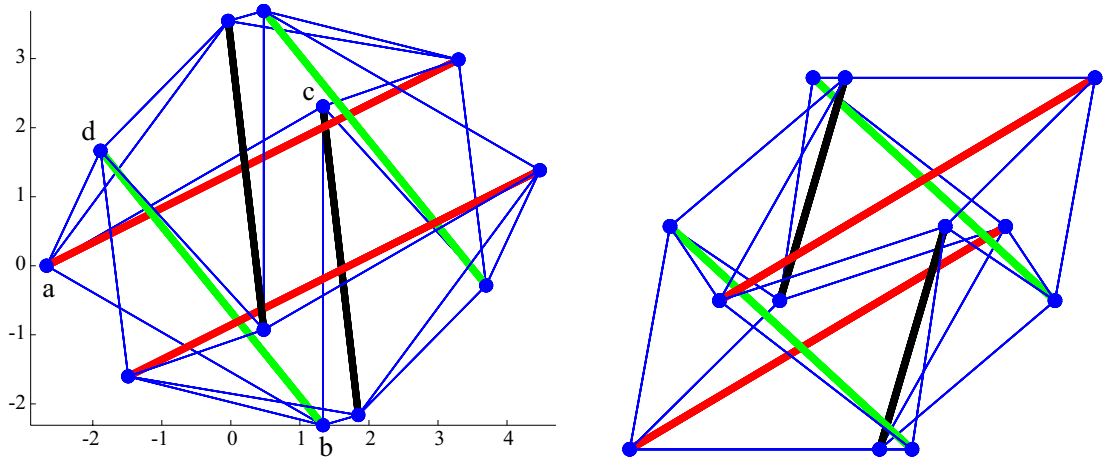

(a) top view (b) side view

Figure 4.10: Example 1: a two-layer tensegrity structure.

By specifying an initial set of force densities as $\{-1.5, -1.5, 1.0, 2.0, 1.0, 1.0\}$ for the six groups, Algorithm 4.1 finds the feasible set of force densities $\{-1.8376, -1.8376, 0.9281, 1.9918, 1.1737, 0.9958\}$ with 158 iterations.

The relative error of force density vector at each iteration, defined as the Euclidean norm of the difference of $\mathbf{q}^i$ to the final value $\hat{\mathbf{q}}$, is plotted in Fig. 4.11. Termination condition of Algorithm 4.1 is that the force density matrix $\hat{\mathbf{E}}$ has the required rank deficiency $h^\star$ $(=n-\text{rank}(\hat{\mathbf{E}})=4)$ where $|\lambda_{h^\star}| < 10^{-5}$ and $|\lambda_{h^\star+1}| > 10^{-5}$. A very good convergence of Algorithm 4.1 can be seen from Fig. 4.11, where the relative error comes very close to zero with only 20 iterations.

If we specify the coordinates of nodes a, b and c, which are defined in Fig. 4.10(a), as $\{(-2.6667, 0.0, 0.0), (1.3333, -2.3094, 0.0), (1.3334, 2.3094, 0.0)\}$ to make the bottom base located on the xy-plane, and node d in the lower stage as $(-1.8867, 1.6666, 3.3333)$, we can then achieve the final configuration of the structure as shown in Figs. 4.9 and 4.10.

Example 2:

Since the initial force densities and independent nodal coordinates can be arbitrarily given by the designers, we can have some controls over the geometrical and mechanical properties of the structure. Furthermore, new configurations can be easily found by changing the values of initial force densities and nodal

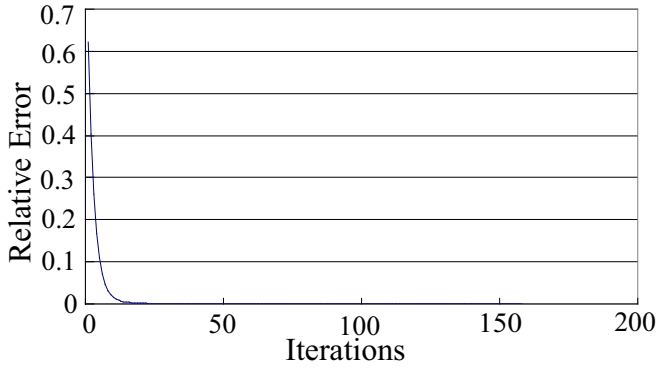

Figure 4.11: Convergence of the algorithm for feasible force densities.

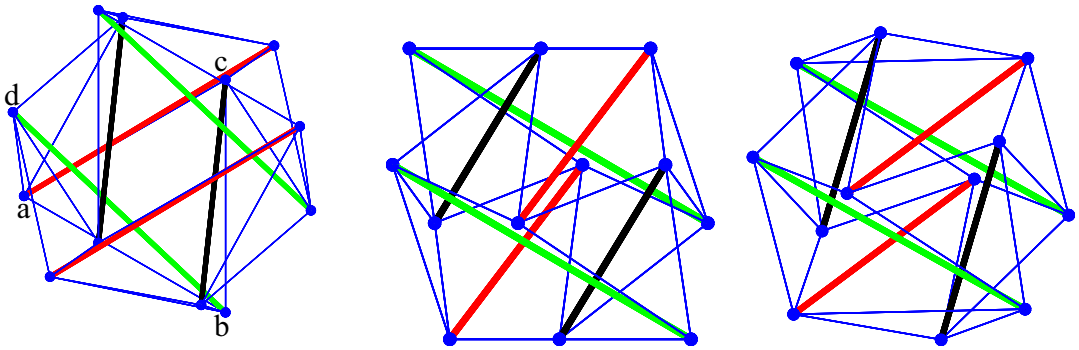

(a) top view (b) side view (c) perspective view

Figure 4.12: Example 2: a two-layer tensegrity structure.

coordinates.

If x-coordinate of node d is modified to -2.8867 from -1.8867 as Example 2 without changing any other parameter, a new configuration of the two-layer tensegrity structure as shown in Fig. 4.12 is obtained. We can also change the initial force densities at the first step of Algorithm 4.1 to search for new configurations.

The design errors ξ defined in Eq. (4.20) are less than 10^{-13} for Examples 1 and 2. Both the structures obtained here have only one infinitesimal mechanism and one prestress mode; i.e. they are kinematically and statically indeterminate. In the meantime, the force density matrices for both cases are positive semi-definite with rank deficiency of four, and the structures are super stable from Lemma

Table 4.1: Elevation of the three-layer tensegrity tower.

H_1	H_2	H_3	h_1	h_2	h_3	H
10.0	8.0	6.0	0.0	3.0	2.0	19.0

Table 4.2: Feasible force densities of each group of members.

q^{b_1}	q^{b_2}	q^{b_3}	q^{h_1}	q^{h_2}	q^{v_1}	q^{v_2}	q^{v_3}
−1.1656	−1.1226	−1.2366	1.2758	1.2652	0.5718		
q^{s_1}	q^{s_2}		q^{d_1}	q^{d_2}	q^{d_3}	q^{d_4}	
1.4572	1.4547		0.8484	0.8262	0.5609	0.4190	

4.5. So, it is clear in these examples that introduction of prestresses stiffens the infinitesimal mechanism to make the structures stable.

4.5.2 Three-layer tensegrity tower

Consider a tensegrity tower as shown in Fig. 4.8, which consists of three layers and four struts in each layer; i.e., $n^l = 3$ and $n^b = 4$. The structure is composed of 24 nodes and 64 members, including 12 struts, 8 horizontal cables, 12 vertical cables, 16 saddle cables and 16 diagonal cables. The saddle cables that are continuously connected and the members of other types in the same obit are classified into different groups. Therefore, there exist 14 groups in total, and the members in the same group have the same force densities.

As an example, we assign the elevation of the structure as listed in Table 4.1. Note that the heights of every layer and the overlaps are not uniform. The total height H is 19.0.

To start Algorithm 4.1, the initial force densities of all struts and all cables are assigned as -1 and $+1$, respectively. Algorithm 4.1 runs 394 iterative steps for finding the feasible force densities as listed in Table 4.2, where q^{b_i}, q^{h_i}, q^{v_i}, q^{s_i} and q^{d_i} denote the force densities of the groups of struts, horizontal cables, vertical cables, saddle cables and diagonal cables, respectively.

The final force density matrix $\hat{\mathbf{E}}$ has four zero eigenvalues and 20 positive eigenvalues, the minimum and maximum values of which are 0.1803 and 7.1592, respectively. Therefore, the structure satisfies the non-degeneracy condition.

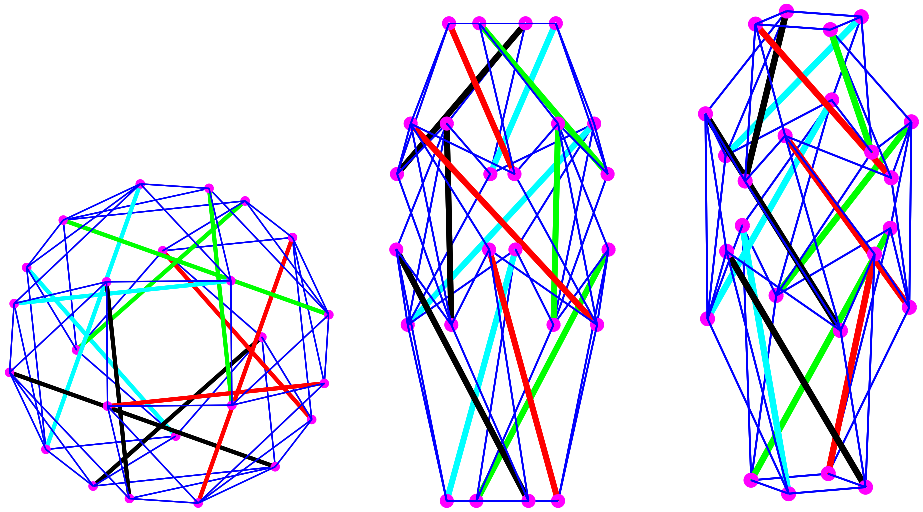

(a) Top view (b) Side view Perspective view

Figure 4.13: New configuration of the symmetric three-layer tensegrity tower with the same force densities and coordinates in z-direction but different coordinates in xy-plane.

In the second design stage, there are up to four independent coordinates in xy-plane that can be arbitrarily specified by the designers, while the constraint on symmetry is considered.

Based on the algorithm of consecutively specifying the independent set of nodal coordinates described in Chapter 5, the xy-coordinates of the nodes $p^b_{1,1}$ and $p^t_{1,1}$ connected by the strut $P^B_{1,1}$ in the lowest layer are selected to be specified. Note that this is not the only independent set of coordinates. If the xy-coordinates of these two nodes are specified as $(10.0, 0)$ and $(2.5, 4.0)$, then the configuration of the structure is uniquely determined as shown in Fig. 4.8. It is easy to observe from the top view of the structure that the struts in the same layer (orbit) are rotationally symmetric by the angle $\pi/2$.

If the same nodal coordinates in xy-plane are specified to the strut $P^B_{2,1}$ in layer 2, the configuration is then uniquely determined as shown in Fig. 4.13. As can be easily observed, the new configuration of the structure becomes slightly slender compared with the configuration in Fig. 4.8. Note that only the nodal coordinates in xy-plane have been changed in the second stage of the form-finding

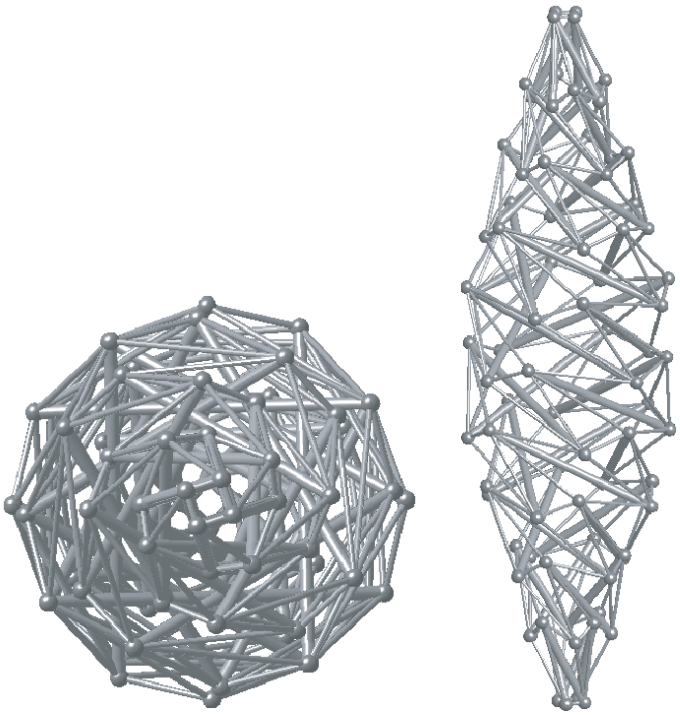

(a) Top view (b) Side view

Figure 4.14: A ten-layer tensegrity tower with four struts in each layer. The structure is rotationally symmetric about z-axis as specified, and is precisely control in z-coordinates.

process. Therefore, Algorithm 4.1 need not be applied again to find the feasible force densities.

Both of these two structures are confirmed to be super stable by the sufficient conditions listed in Lemma 3.5.

4.5.3 Ten-layer Tensegrity Tower

As a more complex example, a ten-layer tensegrity tower as shown in Fig. 4.14 with four struts in each layer; i.e., $n^l = 10$ and $n^b = 4$, is considered. The structure is composed of 80 nodes and 232 members.

For simplicity, the heights and overlaps are uniformly assigned as $H_i = 10.0$ and $h_i = 2.0$ except for $h_1 = 0.0$, respectively. The total height H is 82.0. Constraint on symmetry is also incorporated for this structure. The initial force

densities of all struts and cables are given as -1 and $+1$, respectively.

After 511 iterative steps in Algorithm 4.1 for finding the feasible force density vector, four independent nodal coordinates in xy-plane need to be specified for this symmetric ten-layer tensegrity tower. If the xy-coordinates of the nodes $p^b_{2,1}$ and $p^t_{2,1}$ connected by the strut $P^B_{2,1}$ in layer 2 are specified as $(10.0, 0)$ and $(2.5, 4.0)$, its configuration is obtained as shown in Fig. 4.14, where the top view and the side view have been drawn in different scales.

The structure is super stable, and the necessary condition for a non-degenerate tensegrity structure is also satisfied.

By modifying the values of the initial force densities and the independent nodal coordinates, more new and interesting configurations can be systematically found. Hence, it can be concluded that the proposed method is applicable to a tensegrity tower with any number of layers ($n^l \geq 1$) and any number of struts in each layers ($n^b \geq 3$), although other examples of more complex structures are not presented.

4.6 Discussions and Conclusions

In this chapter, we have presented an efficient numerical method, called adaptive force density method, for the form-finding problem of tensegrity structures. The method is extended from the basic idea of the force density method originally developed for the problem of cable nets, and hence, it also has the advantage of the force density method in dealing with non-linear equations in a linear manner. The proposed method is efficient enough to deal with complex structures with a large number of nodes and members. By introducing geometrical constraints into it form-finding process, the method shows a strong capability in controlling mechanical and geometrical properties of the structures, which was thought to be a common disadvantage of the family of the force density method. More importantly, the proposed method can ensure a super stable during the process of searching for feasible force densities.

The form-finding process is divided into two interrelated design stages: finding the feasible force densities, and determining the configuration. To control configuration of a structure, the constraints, such as the force density matrix, some

specific force densities, symmetry properties, and elevation, are formulated as linear forms with respect to the force densities and nodal coordinates, respectively. Among these, the constraints with respect to the force densities are incorporated into the first design stage to constrain the direction of finding the feasible force densities from the initially given values. And the linear constraints on the nodal coordinates are incorporated into the second design stage to uniquely determine the configuration of the structure.

The following parameters are needed as inputs in the form-finding process of the proposed method:

[L1] topology;

[L2] geometrical constraints;

[L3] an initial set of force densities;

[L4] an independent set of nodal coordinates.

Among these, the geometrical constraints are optional, while the others are necessary for the method.

The tensegrity towers are used as numerical examples to illustrate the capability of the proposed method in finding proper configurations subjected to the specified geometrical constraints. Moreover, designers can avoid the tedious job of modelling the topology, and can concentrate only on the design aspect according to their preferences, based on the detailed description of the geometry of the tensegrity towers.

The proposed method is a general, and hence is applicable to any kind of tensegrity structures, if the necessary inputs listed above are available. Generality of the method comes from that fact that any tensegrity structures that are free-standing have to satisfy the non-degeneracy condition and self-equilibrium equations presented in Chapter 2.

However, the proposed method is unlikely to control all aspects of a tensegrity structure, although it is shown to do an excellent job in some of them. For example, it is not easy to exactly assign the lengths of all members. This is due to the variables that are dealt with in the form-finding process are force densities,

which do not have explicit physical meanings. To have controls over some other geometrical properties of a structure, a direct approach that makes use of directed graphs in graph theory will be presented in the next chapter.

Chapter 5

DIRECT APPROACH

This chapter is to present the direct approach for form-finding problem of tensegrity structures. The method has capability of precisely controlling directions of some members of the structures, which might be important to designers in the shape design.

The adaptive force density method presented in Chapter 4 was shown to have good convergence properties, and have some controls over the mechanical and geometrical properties of the structures by introducing linear constraints. But it is still a tough task for it to have controls over some geometrical properties of a structure in precision, for example, directions of some members. This comes from that the force densities involved in the method are the ratios of self-stresses to member lengths, which do not have explicit physical meaning in reality. In this chapter, we are to show that the direct approach making use of directed graph in graph theory has such capability.

The final configuration of the structure may end up in a degenerate one, such that some nodes may contact and/or some members intersect with each other. To ensure a non-degenerate configuration, an algorithm for calculating the necessary number of independent coordinate components is presented. It should be noticed that this non-degeneracy condition for the structures modeled as directed graphs is different from that presented in Chapter 2 in terms of rank deficiency of the force density matrix.

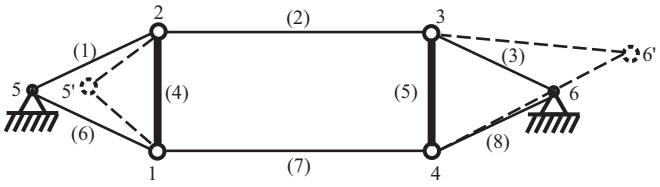

Figure 5.1: A two-dimensional tensegrity structure with fixed nodes. The fixed nodes cannot be considered in self-equilibrium equations of the structure, and hence, the final solution of the form-finding process may end up in an undesirable configuration, as indicated by the dotted lines.

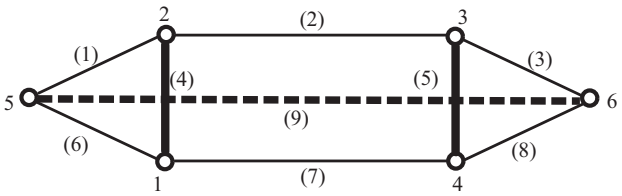

Figure 5.2: The two-dimensional tensegrity structure with fixed member. The structure with fixed nodes in Fig. 5.1 is transformed to a free-standing structure by the introduction of the fixed (auxiliary) member (9).

5.1 Equilibrium Analysis

This section introduces the auxiliary member, which connects the supports, to transform the tensegrity structures with supports into free-standing structures.

The self-equilibrium equations with respect to the prestresses in each direction are formulated.

5.1.1 Auxiliary Member

In designing tensegrity structures with supports, the locations of the supports should be taken into consideration, because the final configuration derived from the direct approach presented later may end up with undesirable configuration.

For example, suppose that we want to design a two-dimensional tensegrity structure as shown in Fig. 5.1. The structure consists of $n = 6$ nodes and $m = 8$ members. Nodes 5 and 6 are the supports.

If we specify a set of prestresses arbitrarily by the method presented later,

it may end up with an undesirable configuration, e.g., as shown in the dotted lines in Fig. 5.1; i.e. nodes 5 and 6 are located unfavorably. This is because that the equilibrium of the fixed nodes has not been included in the self-equilibrium equations.

To present a unified approach to the form-finding problem of tensegrity structures with and without supports, we introduce auxiliary members called *fixed members* to connect the supports. For the structure shown in Fig. 5.1, we connect nodes 5 and 6 by the auxiliary member 9 as shown in Fig. 5.2.

5.1.2 Self-equilibrium

Consider a structure consisting of m members and n nodes including the fixed members and fixed nodes. The numbers of fixed members and nodes are denoted by m_f and n_f, respectively.

The free members and nodes are numbered such that the nodes $\{1, \ldots, n-n_f\}$ and members $\{1, \ldots, m-m_f\}$, respectively, which are preceding the fixed ones.

By using the connectivity matrix $\mathbf{C}$ defined in Eq. (2.1), the enlarged connectivity matrix $\mathbf{B}$ of the d-dimensional structure is defined as

$$\mathbf{B} = \mathbf{C} \otimes \mathbf{I}^d$$

where $\otimes$ and $\mathbf{I}^d \in \Re^{d\times d}$ denote tensor product and identity matrix, respectively.

For example, the enlarged connectivity matrix $\mathbf{B} \in \Re^{18\times 12}$ of the two-dimensional

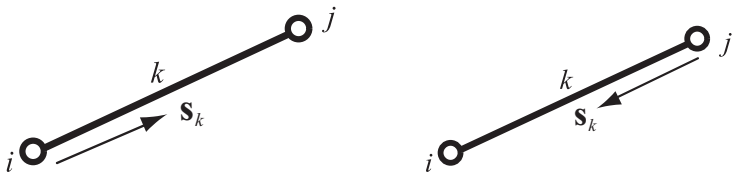

(a) positive (in tension) (b) negative (in compression)

Figure 5.3: Definition of prestress vector $\mathbf{s}_k$ $(i < j)$. A cable that is in tension is defined to have positive direction pointing from one of its node bearing smaller number to the other node with larger number, and a strut that is in compression has negative direction.

structure in Fig. 5.2 is

$$\mathbf{B} = \left(\begin{array}{c|c} \mathbf{B}^a & \mathbf{B}^b \\ \hline \mathbf{O} & \mathbf{B}^f \end{array}\right) =$$

	n_1^x	n_1^y	n_2^x	n_2^y	n_3^x	n_3^y	n_4^x	n_4^y	n_5^x	n_5^y	n_6^x	n_6^y
m_1^x	0	0	1	0	0	0	0	0	−1	0	0	0
m_1^y	0	0	0	1	0	0	0	0	0	−1	0	0
m_2^x	0	0	1	0	−1	0	0	0	0	0	0	0
m_2^y	0	0	0	1	0	−1	0	0	0	0	0	0
m_3^x	0	0	0	0	1	0	0	0	0	0	−1	0
m_3^y	0	0	0	0	0	1	0	0	0	0	0	−1
m_4^x	1	0	−1	0	0	0	0	0	0	0	0	0
m_4^y	0	1	0	−1	0	0	0	0	0	0	0	0
m_5^x	0	0	0	0	1	0	−1	0	0	0	0	0
m_5^y	0	0	0	0	0	1	0	−1	0	0	0	0
m_6^x	1	0	0	0	0	0	0	0	−1	0	0	0
m_6^y	0	1	0	0	0	0	0	0	0	−1	0	0
m_7^x	1	0	0	0	0	0	−1	0	0	0	0	0
m_7^y	0	1	0	0	0	0	0	−1	0	0	0	0
m_8^x	0	0	0	0	0	0	1	0	0	0	−1	0
m_8^y	0	0	0	0	0	0	0	1	0	0	0	−1
m_9^x	0	0	0	0	0	0	0	0	1	0	−1	0
m_9^y	0	0	0	0	0	0	0	0	0	1	0	−1

where $\mathbf{B}^a$ corresponds to the free members and free nodes, while $\mathbf{B}^f$ corresponds to fixed members and fixed nodes. Note that n_i^x and n_i^y denote the columns corresponding to the equilibrium in x- and y-directions, respectively, at node i. m_k^x and m_k^y denote the rows corresponding to the x- and y-components, respectively, of member k.

Let $\mathbf{s}_k \in \Re^d$ denote the prestress vector of member k that is connected to nodes i and j $(i < j)$. Note that the prestress vector $\mathbf{s}_k$ of member k is different from the prestress s_k used so far, which is a value but not vector denoting the magnitude of the prestress.

The positive direction, i.e., tensile state, of $\mathbf{s}_k$ as shown in Fig. 5.3(a) is defined as a vector starting from i and directing to j $(i < j)$. Fig. 5.3(b) shows the negative direction of $\mathbf{s}_k$, which means that member k is in compression.

For member k of a two-dimensional structure, its force components of $\mathbf{s}_k$ are written as $\mathbf{s}_k = (s_k^x, s_k^y)^\top$. In three-dimensional space, $\mathbf{s}_k = (s_k^x, s_k^y, s_k^z)^\top$. The prestress (prestress) vector of all members, called *generalized force vector*, is defined as $\mathbf{s} = (\mathbf{s}_1^\top, \cdots, \mathbf{s}_m^\top)^\top \in \Re^{sm}$

Consider the two-dimensional structure in Fig. 5.2 again for example. Since all the free nodes are in self-equilibrium state, the equilibrium equations of a free node, e.g. node 4, are written as

$$\begin{aligned} -s_5^x - s_7^x + s_8^x = 0 \\ -s_5^y - s_7^y + s_8^y = 0 \end{aligned}$$

which can be rewritten by using the enlarged connectivity matrix as

$$\begin{aligned} (\mathbf{B}^\top)_7 \mathbf{s} = 0 \\ (\mathbf{B}^\top)_8 \mathbf{s} = 0 \end{aligned}$$

where $(\mathbf{B}^\top)_i$ denotes the ith row of $\mathbf{B}^\top$. $(\mathbf{B}^\top)_7$ and $(\mathbf{B}^\top)_8$ correspond to the x- and y-directions, respectively, of node 4.

Hence, the self-equilibrium equation for the whole structure can be written as

$$\mathbf{B}^\top \mathbf{s} = \mathbf{0} \tag{5.1}$$

5.2 Geometrical Constraints

This section formulates the geometrical constraints of the structure as linear equations with respect to the prestresses and nodal coordinates, which will be incorporated in the form-finding process presented in the next section.

5.2.1 Member Directions

In the design process of tensegrity structures, it is usually desirable that the directions of some members can be directly specified by the designers. The direction of a member, however, should coincide with that of its force vector, because members of the tensegrity structures can transmit only prestresss.

Consider a tensegrity structure in three-dimensional space. Let $\mathbf{d}_k = (d_k^x, d_k^y, d_k^z)^\top$ denote a vector in the direction of member k, where the vector $\mathbf{d}_k$ of some members are given according to designer's preference.

The direction vector $\mathbf{d}_k$ and the prestress vector $\mathbf{s}_k$ of member k should satisfy the relation $\mathbf{d}_k \times \mathbf{s}_k = \mathbf{0}$ which can be explicitly written as

$$\begin{aligned} d_k^x s_k^y &= d_k^y s_k^x \\ d_k^y s_k^z &= d_k^z s_k^y \\ d_k^z s_k^x &= d_k^x s_k^z \end{aligned} \tag{5.2}$$

Define $\bar{\mathbf{T}}$ as

$$\bar{\mathbf{T}} = \begin{pmatrix} 0 & 1 & 0 \\ 0 & 0 & 1 \\ 1 & 0 & 0 \end{pmatrix}$$

Eq. (5.2) can be written in a linear form as follows

$$\mathrm{diag}(\mathbf{d}_k)\bar{\mathbf{T}}\mathbf{s}_k - \mathrm{diag}(\bar{\mathbf{T}}\mathbf{d}_k)\mathbf{s}_k = \mathbf{0} \tag{5.3}$$

where $\mathrm{diag}(\mathbf{x})$ is the diagonal version of $\mathbf{x}$, the ith diagonal component of it is the ith component x_i of $\mathbf{x}$. By letting

$$\bar{\mathbf{N}}_k = \mathrm{diag}(\mathbf{d}_k)\bar{\mathbf{T}} - \mathrm{diag}(\bar{\mathbf{T}}\mathbf{d}_k)$$

Eq. (5.3) can be rewritten as

$$\bar{\mathbf{N}}_k \mathbf{s}_k = \mathbf{0} \tag{5.4}$$

By assembling Eq. (5.4) through all members for which the directions are specified, the following linear relation is derived for $\mathbf{s}$:

$$\bar{\mathbf{N}}\mathbf{s} = \mathbf{0} \tag{5.5}$$

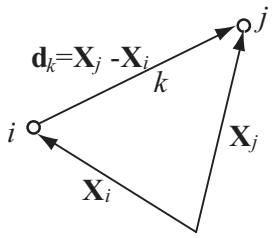

Figure 5.4: Coordinate difference vector $\mathbf{d}_k$ of member k $(i < j)$.

5.2.2 Directions of Fixed Members

In order to consider the fixed nodes (supports) in a similar manner as free nodes (internal nodes) in the self-equilibrium equation, we have introduced the concept of auxiliary fixed members, of which the directions are to be specified.

For a three-dimensional structure, let $\mathbf{X}_i = (x_i, y_i, z_i)^\top$ denote the coordinate vector of node i. The coordinate difference vector $\mathbf{d}_k = (d_k^x, d_k^y, d_k^z)^\top$ of member k that connects nodes i and j $(i < j)$ is defined as

$$\mathbf{d}_k = \mathbf{X}_j - \mathbf{X}_i \tag{5.6}$$

which is illustrated in Fig. 5.4.

Using the relation between the direction of a member and its prestress vector, $\mathbf{d}_k \times \mathbf{s}_k = \mathbf{0}$ should be satisfied; i.e.

$$\begin{aligned} d_k^x v_k^y &= d_k^y v_k^x \\ d_k^y v_k^z &= d_k^z v_k^y \\ d_k^z v_k^x &= d_k^x v_k^z \end{aligned} \tag{5.7}$$

Since Eq. (5.7) has the same form as Eq. (5.2), the relation similar to Eq. (5.3) can be easily obtained as

$$\mathrm{diag}(\mathbf{d}_k)\bar{\mathbf{T}}\mathbf{s}_k - \mathrm{diag}(\bar{\mathbf{T}}\mathbf{d}_k)\mathbf{s}_k = \mathbf{0} \tag{5.8}$$

$\mathbf{d}_k$ can be expressed as follows using Eq. (5.6):

$$\mathbf{d}_k = -\mathbf{B}_k\mathbf{X} \tag{5.9}$$

where the rows of $\mathbf{B}_k \in \Re^{3\times 3n}$ consist of the $(3k-2)$th, $(3k-1)$th, and $(3k)$th rows of $\mathbf{B}$ for a three-dimensional structure.

Let $\mathbf{d}^f \in \Re^{3n^f}$ denote the vector consisting of the coordinate difference vectors of the fixed members. The relation between $\mathbf{d}^f$ and $\mathbf{X}^f$ is written as

$$\mathbf{d}^f = -\mathbf{B}^f\mathbf{X}^f$$

The vector consisting of force vectors of the fixed members is denoted by $\mathbf{s}^f \in \Re^{3m^f}$. Let $\mathbf{I}^f \in \Re^{m^f \times m^f}$ denote the identity matrix. By using $\mathbf{T}^f = \mathbf{I}^f \otimes \bar{\mathbf{T}}$, Eq. (5.8) for fixed members is assembled as

$$\mathrm{diag}(\mathbf{d}^f)\mathbf{T}^f\mathbf{s}^f - \mathrm{diag}(\mathbf{T}^f\mathbf{d}^f)\mathbf{s}^f = \mathbf{0} \tag{5.10}$$

In Eq. (5.10), $\mathbf{d}^f$ is determined because the coordinates $\mathbf{X}^f$ of the fixed nodes are known a priori, and $\mathbf{T}^f$ is a constant matrix. Since $\mathbf{s}^f$ is the selected components of $\mathbf{s}$, it is easy to see that Eq. (5.10) can be rewritten by using a known matrix $\hat{\mathbf{N}}$ as

$$\hat{\mathbf{N}}\mathbf{s} = \mathbf{0} \tag{5.11}$$

5.2.3 Symmetry Properties

The configuration of a tensegrity structure usually has symmetry properties; i.e. invariance conditions to reflection with respect to some planes and/or rotation around some axes. Therefore, the member direction vectors should be specified to satisfy such symmetry conditions. The same prestresss should be assigned to the symmetrically located members.

For example, consider a part of a two-dimensional structure as shown in Fig. 5.5(a), whose members are rotationally arranged by θ ($= \pi/3$). Select two adjacent members k and k' as shown in Fig. 5.5(b) to illustrate the process of formulating their rotational symmetry properties. Members k and k' connect pairs of nodes (i, j) and (i', j'), respectively. The rotation matrix is defined as

$$\mathbf{M}_l = \begin{pmatrix} \cos\theta & \sin\theta & 0 \\ -\sin\theta & \cos\theta & 0 \\ 0 & 0 & 1 \end{pmatrix}$$

The relation between the coordinate difference vectors of members k and k' is written as

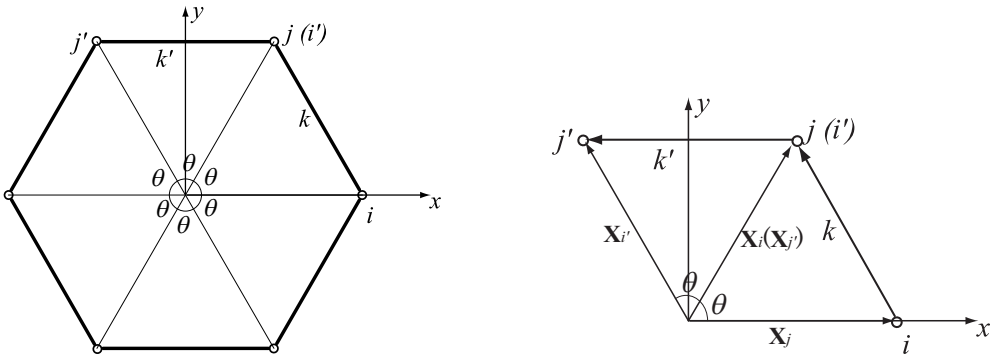

(a) Configuration of a two-dimensional structure.

(b) Rotational symmetry of members k and k'.

Figure 5.5: Rotational symmetry of a two-dimensional structure ($i < j$ and $i' < j'$).

$$\mathbf{d}_{k'} = \mathbf{M}_l \mathbf{d}_k$$

From Figs. 5.3 and 5.4, we know that the direction of $\mathbf{d}_k$ is the same as the positive direction of $\mathbf{s}_k$. So the symmetry property of the prestresses of members k and k' can be written as

$$\mathbf{s}_{k'} = \mathbf{M}_l \mathbf{s}_k \tag{5.12}$$

By letting $\mathbf{S}_l = \begin{pmatrix} \mathbf{0} & \cdots & \mathbf{M}_l & \cdots & -\mathbf{I} & \cdots & \mathbf{0} \end{pmatrix}$, Eq. (5.12) can be rewritten as

$$\mathbf{S}_l \mathbf{s} = \mathbf{0} \tag{5.13}$$

The rotational symmetry of other members of the structure can be formulated in a similar way. Reflectional symmetry can be also written in a similar form as Eq. (5.13). By combining Eq. (5.13) through all the symmetry conditions, the following linear equation is obtained as

$$\mathbf{S}\mathbf{s} = \mathbf{0} \tag{5.14}$$

5.3 Form-finding Process

In this section, we introduce an algorithm for directly specifying the prestresses and nodal coordinates consecutively. Linear equations are formulated based on

the equilibrium equations and geometrical constraints in terms of prestresses and nodal coordinates.

5.3.1 Prestresses

From the equilibrium equation (5.1) and the geometrical constraints (5.5), (5.11) and (5.14), we obtain

$$\begin{pmatrix} \mathbf{B}^\top \\ \bar{\mathbf{N}} \\ \hat{\mathbf{N}} \\ \mathbf{S} \end{pmatrix} \mathbf{s} = \mathbf{0} \tag{5.15}$$

By letting $\mathbf{H}^\top = (\mathbf{B}, \bar{\mathbf{N}}^\top, \hat{\mathbf{N}}^\top, \mathbf{S}^\top)$, Eq. (5.15) can be rewritten as

$$\mathbf{H}\mathbf{s} = \mathbf{0} \tag{5.16}$$

Our task is to find a set of non-trivial prestresses ($\mathbf{s} \neq \mathbf{0}$) that satisfy Eq. (5.16).

Let $r^H = 3m - \text{rank}(\mathbf{H})$ for a three dimensional structure. If $r^H = 0$, then there exists only trivial solution $\mathbf{s} = \mathbf{0}$. If $r^H > 0$, then the static relation (5.16) is underdetermined. Tensegrity structures often fall into this category. So we will focus only on the underdetermined case here.

The solution of Eq. (5.16) can be written by using a matrix $\mathbf{G} \in \Re^{dm \times r^H}$ as

$$\mathbf{s} = \mathbf{G}\boldsymbol{\alpha} \tag{5.17}$$

where the columns of $\mathbf{G}$ are self-equilibrium modes and $\boldsymbol{\alpha} \in \Re^{r^H}$ is the coefficient vector. Since $\boldsymbol{\alpha}$ has no explicit mechanical meaning, we will determine it by specifying a independent set of prestresses $\bar{\mathbf{s}}$ instead of specifying the coefficients directly.

Let $\mathcal{I} \subseteq \{1, \ldots, dm\}$ denote the set of indices of components of $\mathbf{s}$ to be specified. $\bar{\mathbf{s}}$ is defined as the vector consisting of the component s_j ($j \in \mathcal{I}$) of $\mathbf{s}$. By assembling the corresponding rows of $\mathbf{G}$ to generate a sub-matrix $\bar{\mathbf{G}}$, the relation between $\bar{\mathbf{s}}$ and $\boldsymbol{\alpha}$ can be written as

$$\bar{\mathbf{s}} = \bar{\mathbf{G}}\boldsymbol{\alpha} \tag{5.18}$$

If $\bar{\mathbf{G}} \in \Re^{r^H \times r^H}$ is full-rank, Eq. (5.18) can be solved as

$$\boldsymbol{\alpha} = \bar{\mathbf{G}}^{-1}\bar{\mathbf{s}}$$

By substituting $\boldsymbol{\alpha}$ back to Eq. (5.17), the force vector $\mathbf{s}$ of all members is obtained as

$$\mathbf{s} = \mathbf{G}\bar{\mathbf{G}}^{-1}\bar{\mathbf{s}} \tag{5.19}$$

Let $(\mathbf{G})_k$ denote the kth row of $\mathbf{G}$. $\Pi = \{\pi(l)|l = 1, 2, \ldots, dm\}$ denotes a permutation of dm indices $1, 2, \ldots, dm$, where $\pi(l)$ stands for the location of index l in Π. The following algorithm generates $\mathfrak{I}$ and $\bar{\mathbf{G}}$, where the Reduced Row-Echelon Form (RREF) (Borse, 1997) summarized in Appendix A is effectively used:

Algorithm 5.1:

Step 0 Let $\mathfrak{I} = \emptyset$, feasible set $\mathcal{A} = \{1, 2, \ldots, dm\}$, $\Pi^0 = \{\pi^0(l)|l = 1, 2, \ldots, dm\}$ and $\pi^0(l) = l$ $(l = 1, \ldots, dm)$. Set $i := 0$.

Step 1 If $i = h$, then $\bar{\mathbf{G}} := \hat{\mathbf{G}}$, and STOP. Otherwise, set $i \leftarrow i + 1$.

Step 2 Choose $j \in \mathcal{A}$. Update $\mathfrak{I} := \mathfrak{I} \cup j$. Define $\Pi^i = \{\pi^i(l)|l = 1, 2, \ldots, dm\}$ by

$$\pi^i(l) = \begin{cases} \pi^{i-1}(l) & (l < j) \\ dm & (l = j) \\ \pi^{i-1}(l) - 1 & (l > j) \end{cases}$$

Step 3 Generate $\mathbf{Q}$ by eliminating $(\mathbf{G})_k$ $(\forall k \in \mathfrak{I})$ from $\mathbf{G}$. Let $\hat{\mathbf{G}}$ be the matrix consisting of $(\mathbf{G})_k$ $(\forall k \in \mathfrak{I})$.

Step 4 Compute the RREF of the matrix $(\hat{\mathbf{G}}^\top, \mathbf{Q}^\top)$ in a form of

$$\mathbf{W} = \begin{pmatrix} \mathbf{I} & \mathbf{W}^{\mathrm{U}} \\ \mathbf{O} & \mathbf{W}^{\mathrm{L}} \end{pmatrix}$$

where $\mathbf{W}^{\mathrm{U}} \in \Re^{i \times (dm-i)}$ and $\mathbf{W}^{\mathrm{L}} \in \Re^{(h-i)\times(dm-i)}$.

Step 5 Update $\mathcal{A}$ as

$$\mathcal{A} = \left\{ l | (\mathbf{W}^{\mathrm{L}})_{\pi^i(l)} \neq \mathbf{0} \quad (\pi^i(l) = 1, \ldots, dm - i) \right\}$$

and go to Step 1.

5.3.2 Nodal Coordinates

Knowing only the prestresses, we are still unable to uniquely determine the configuration of the structure. Since $\mathbf{s}_k$ for all members are known by using the procedure presented previously, Eq. (5.8) is rewritten as

$$\text{diag}(\bar{\mathbf{T}}\mathbf{s}_k)\mathbf{d}_k - \text{diag}(\mathbf{s}_k)\bar{\mathbf{T}}\mathbf{d}_k = \mathbf{0} \tag{5.20}$$

Let $\mathbf{I}^m \in \Re^{m\times m}$ denote the identity matrix. By using $\mathbf{T} = \mathbf{I}^m \otimes \bar{\mathbf{T}}$, Eq. (5.20) is assembled through all members as

$$\text{diag}(\mathbf{T}\mathbf{s})\mathbf{d} - \text{diag}(\mathbf{s})\mathbf{T}\mathbf{d} = \mathbf{0} \tag{5.21}$$

where $\mathbf{d} = (\mathbf{d}_1^\top, \ldots, \mathbf{d}_m^\top)^\top$.

Incorporating Eq. (5.9) into Eq. (5.21), the constraints on $\mathbf{X}$ can be written in the following form:

$$\mathbf{F}\mathbf{X} = \mathbf{0} \tag{5.22}$$

where

$$\mathbf{F} = \text{diag}(\mathbf{T}\mathbf{s})\mathbf{B} - \text{diag}(\mathbf{s})\mathbf{T}\mathbf{B}$$

is a known matrix. Note that the symmetry conditions have been implicitly included in Eq. (5.22).

Let $r^F = 3n - \text{rank}(\mathbf{F})$ and suppose an underdetermined case $r^H > 0$. The solution of Eq. (5.22) can be written as

$$\mathbf{X} = \mathbf{P}\boldsymbol{\beta} \tag{5.23}$$

where $\boldsymbol{\beta} \in \Re^{r^F}$ is the coefficient vector and $\mathbf{P} \in \Re^{dn\times r^F}$.

The nodal coordinates can be divided into the unknown components $\mathbf{X}^c \in \Re^{dn^c}$ of the free nodes and the specified components $\mathbf{X}^f \in \Re^{dn^f}$ of the fixed nodes (supports). The matrix $\mathbf{P}$ can then be divided into $\mathbf{P}^c$ and $\mathbf{P}^f$, accordingly. Hence, Eq. (5.23) is rewritten as

$$\begin{pmatrix} \mathbf{X}^c \\ \mathbf{X}^f \end{pmatrix} = \begin{pmatrix} \mathbf{P}^c \\ \mathbf{P}^f \end{pmatrix} \boldsymbol{\beta} \tag{5.24}$$

Let $r^f = \text{rank}(\mathbf{P}^f)$. Select r^f independent rows from $\mathbf{P}^f$ to obtain matrix $\bar{\mathbf{P}}$ by utilizing its RREF form. The vector $\bar{\mathbf{X}}$ of independent nodal coordinates

are selected from $\mathbf{X}^f$ correspondingly. If $r^f = r^F$, the nodal coordinates of the structure can then be uniquely determined as follows

$$\mathbf{X} = \mathbf{P}\bar{\mathbf{P}}^{-1}\bar{\mathbf{X}} \tag{5.25}$$

Otherwise, we are able to specify $(r^F - r^f)$ independent nodal coordinates to obtain $\bar{\mathbf{X}}$ by using the same procedure described in Algorithm 5.1.

5.3.3 Stress States

For a tensegrity structure, it is important to know whether each member is in tension or in compression. From Figs. 5.3 and 5.4, we can see that the direction of $\mathbf{d}_k$ is the same as that of the member in tension. So the inner product g_k of $\mathbf{d}_k$ and $\mathbf{s}_k$ has the following properties

$$g_k = \mathbf{s}_k^\top \mathbf{d}_k \quad \begin{cases} > 0 & \text{tension} \\ < 0 & \text{compression} \\ = 0 & \text{member } k \text{ is removable} \end{cases} \tag{5.26}$$

For the case of $g_k = 0$, member k can be removed because

[L1] If $\mathbf{s}_k = \mathbf{0}$, then there exists no force in member k, and its existence is unnecessary.

[L2] If $\mathbf{d}_k = \mathbf{0}$, then nodes i and j coincide. So member k and node i or j can be removed.

5.3.4 Evaluation of Design

By using Eq. (5.16) and Eq. (5.22), the errors ξ^s and ξ^x of the prestresses and nodal coordinates, respectively, for a d-dimensional structure are defined as

$$\xi^s = \sqrt{(\mathbf{Hs})^\top \mathbf{Hs}/(dm)} \tag{5.27}$$

$$\xi^x = \sqrt{(\mathbf{FX})^\top \mathbf{FX}/(dn)} \tag{5.28}$$

5.3.5 Design Procedure

So far, we have presented the procedure and algorithm for designing a tensegrity structure, which is modelled by a directed graph. The designer procedure can be summarized as follows:

Algorithm 5.2: Design procedure

Step 1: Generate the self-equilibrium system by replacing the supports with the auxiliary fixed members.

Step 2: Give the topology.

Step 3: Assign the directions of some members, and coordinates of supports so as to define $\bar{\mathbf{N}}$ and $\hat{\mathbf{N}}$, respectively. Give the symmetry properties by the matrix $\mathbf{S}$.

Step 4: Specify $\bar{\mathbf{s}}$ and obtain $\bar{\mathbf{G}}$ by using Algorithm 5.1. Compute $\mathbf{s}$ from Eq. (5.19).

Step 5: Specify $\bar{\mathbf{X}}$ and obtain $\bar{\mathbf{P}}$. Compute $\mathbf{X}$ from Eq. (5.25).

Step 6: Determine the stress states of the members. Remove member k satisfying $\mathbf{s}_k^\top \mathbf{d}_k = 0$. Convert the auxiliary fixed members back to supports.

5.4 Non-degeneracy Condition

The configurations found by using Algorithm 5.2 may be degenerate – the structures turn out to lie in the space with lower dimensions than the interested one. This section presents an algorithm for obtaining the non-degeneracy condition, in terms of the number of independent nodal coordinates that can be specified, for the tensegrity structures modelled as directed graphs.

In order to do that, we suppose that

[L1] directions of all members have been known;

[L2] no member has zero prestress.

5.4.1 Geometrical Interpretation

Before considering the whole structure, it might be helpful to consider firstly the conditions for the determination of one node and one member in the interested d-dimensional space. This node and member are called the *reference node* and *reference member*, respectively.

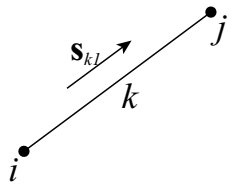

Figure 5.6: Member k, directed from i to j ($i < j$).

a. Reference node:

It is easy to learn that we need to specify d coordinates to determine the location of the reference node in a d-dimensional space, if no other information is available.

b. Reference member:

Consider the (reference) member k as shown in Fig. 5.6 that is connected to the reference node i. Since its direction is known from the presumption and the reference node i has been determined by specifying the d coordinates, it might be easy to learn that only *one* parameter is needed to determine the other node j of the member. This parameter can be length of the member or projection of the member in any direction as long as it is not equal to zero. This is clear from the following equation for the nodal coordinates of node j:

$$\begin{pmatrix} x_j \\ y_j \\ z_j \end{pmatrix} = \begin{pmatrix} x_i \\ y_i \\ z_i \end{pmatrix} + \alpha \mathbf{d}_k$$

where α is an unknown coefficient that can be considered as the distance from node i to node j along the direction $\mathbf{d}_k$ of member k.

c. The nodes connected to the reference member:

Now, we can have determined the location of one member by specifying $d+1$ coordinate components. Consider any other node p, which is connected to the

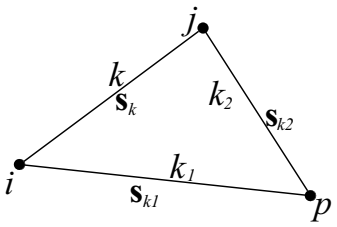

Figure 5.7: The node p connected to the reference member k. Location of p can be uniquely determined by the coordinate difference vectors $\mathbf{s}_{k1}$ and $\mathbf{s}_{k2}$ if it is not lying on the extension line of member k.

determined member k as shown in Fig. 5.7. $\mathbf{d}_{k1}$ and $\mathbf{d}_{k2}$ denote the directions of member k_1 and k_2, respectively. To determine the location of the unknown node p, a little more complexity may arise:

- CASE 1: Node p is connected by only two nodes in the structure, or the members connected to it lie in the same line.
- CASE 2: Node p is connected by more than two nodes.

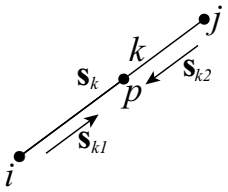

Figure 5.8: Node p is connected by only two other nodes i and j. Location of p cannot uniquely determined because it is lying in (extension line of) member k, and one more variable is needed to locate it.

Since the structure is in a state of self-equilibrium and no member has zero prestress from the preassumption, we may know immediately that if the node is connected by only other two nodes; i.e. two members, then the two members have to lie on the same line, e.g. Fig. 5.8. Thus, the relation $\mathbf{d}_{k_1} = \pm\mathbf{d}_{k_2}$ between the directions of member k_1 and k_2 has to be satisfied for CASE 1. In this case, one more parameter has to be specified to determine the location of node p.

For CASE 2 that we do not need any further information about node p to locate it since it can be easily determined by run along the (negative) directions of members k_1 and k_2 and then find their intersection, e.g. in Fig. 5.7. The intersection is where the node p is located.

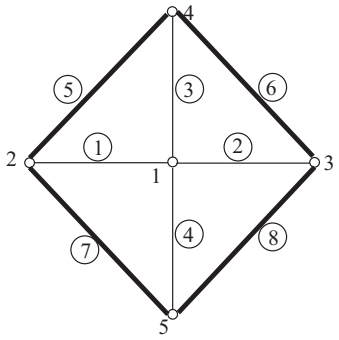

Figure 5.9: A two-dimensional tensegrity structure that can be determined by only 3 coordinate components.

For example, Fig. 5.9 shows a two-dimensional tensegrity structure. Since each node of the structure connected by more than two nodes, where no member of the same triangle is parallel to each other, only 3 independent coordinate components are needed to identify the configuration of the structure, no matter which node (member) is selected as reference node (member) to start off the counting.

5.4.2 Necessary Condition

Let $\mathcal{I}$ and $\mathcal{J}$ denote the sets of determined nodes and undetermined nodes, respectively.

By applying the operations mentioned above starting from the reference node and reference member with d+1 independent coordinate components, it is possible to determine all the locations of other nodes of the structure. However, as will be seen in an example later, these operations may not be sufficient. In the follows, we will see how to systematically apply these operations following a simple example.

Consider a structure consisting of n nodes. Let i and j denote two nodes of the structure. The (i, j) component $\bar{\mathbf{C}}(i, j)$ of the connectivity matrix $\bar{\mathbf{C}} \in \Re^{n \times n}$

is defined as

$$\bar{\mathbf{C}}(i,j) = \bar{\mathbf{C}}(j,i) = \begin{cases} 2 & \text{for } i = j \text{ and the location of node } i \text{ has been determined} \\ 1 & \text{if nodes } i \text{ and } j \text{ are connected} \\ 0 & \text{others} \end{cases} \tag{5.29}$$

Note that the connectivity matrix $\bar{\mathbf{C}}$ defined here is different from the usual one defined in Eq. (2.1).

From the definition of connectivity matrix $\bar{\mathbf{C}}$ of the structure, we can have the following lemma.

Lemma 5.1 *If the trace of the connectivity matrix is equal to (trace($\bar{\mathbf{C}}$)=)$2n$, locations of all nodes can have been uniquely determined.*

5.4.3 Algorithm Description

In the following, the two-dimensional structure as shown in Fig. 5.2 is used to illustrate how the connectivity matrix is utilized to determine the number r of independent nodal coordinate components for a unique non-degenerate structure.

Step 0:

The initial connectivity matrix of this structure is

	1	2	3	4	5	6
1	0	1	0	1	1	0
2	1	0	1	0	1	0
3	0	1	0	1	0	1
4	1	0	1	0	0	1
5	1	1	0	0	0	1
6	0	0	1	1	1	0
$\mathbf{c}=$	3	3	3	3	3	3

where all the diagonal elements are zero since no node is determined at the first stage. The i element $\mathbf{c}(i)$ is the sum of the i-th column of the connectivity matrix $\bar{\mathbf{C}}$. Obviously, the value tells how many nodes are connected to the node i. Accordingly, we may know that all nodes are connected by other three nodes in the structure, and therefore, every node belongs to the CASE 2 for this structure.

Step 1:

We can arbitrarily select a member, e.g. member (6) connecting nodes 1 and 5, as the reference member by specifying ($r = d + 1 =$)3 independent nodal coordinate components of them. The components of the connectivity matrix $\bar{\mathbf{C}} \in \Re^{6\times 6}$ corresponding to the determined nodes 1 and 5 can be written as

	①	2	3	4	⑤	6
①	2	1	0	1	1	0
⑤	1	1	0	0	2	1
$\mathbf{r} =$		2	0	1		0
$\mathbf{c} =$		3	3	3		3

(5.30)

where ⓘ indicates that the location of node i has been determined. Therefore, the determined set $\mathcal{I}$ of nodes becomes $\mathcal{I} = \{1, 5\}$ and the undetermined set $\mathcal{J} = \{2, 3, 4, 6\}$ at the current stage. And the (1,1) and (5,5) elements of the connectivity matrix become 2.

Nodes 1 and 5 are connected by the reference member (6), and the undetermined node 2 is connected by more than two members; i.e., members 1, 2 and 4. Thus, node 2 can be uniquely determined without specifying any additional coordinate component.

These facts can also be told by observing only the reduced form of the connectivity matrix $\bar{\mathbf{C}}$ in Eq. (5.30), where the rows corresponding to undetermined nodes have been excluded. Sum of the corresponding rows in the connectivity matrix $\bar{\mathbf{C}}$ of all undetermined nodes ($\mathcal{J} = \{2, 3, 4, 6\}$) is denoted as $\mathbf{r}$ in Eq. (5.30). It can be easily observed that the value of $\mathbf{r}_i$ corresponding to an undetermined node i is the number of determined nodes that it is connected to. Therefore, if we have $\mathbf{r}_i \geq 2$ and $\mathbf{c}_i > 2$ where $i \in \mathcal{J}$, the location of node i can then be determined.

Step 2:

Thus, node 2 can be uniquely determined without adding additional components. Hence, we can obtain $r = 3$ at this stage where $\mathcal{I} = \{1, 2, 5\}$ and

$\mathcal{J} = \{3, 4, 6\}$. The reduced form of connectivity matrix becomes

	①	②	3	4	⑤	6
①	2	1	0	1	1	0
②	0	2	1	0	1	0
⑤	1	1	0	0	2	1
r =			1	1		1
c =			3	3		3

(5.31)

There is one problem in this step: as indicated by the values of the corresponding elements of **r** to the undetermined nodes, all of which are equal to 1 in this case, we cannot determine any node from the determined set $\mathcal{I}$, since all nodes in $\mathcal{J}$ are connected by only one determined node while we need two or more to locate them.

In order to make the process progress, some more information is needed. Suppose that we specify one more parameter to locate node 3. The number of the independent nodal coordinate components r becomes 4 and the reduced form of the connectivity matrix in Eq. (5.31) becomes

	①	②	③	4	⑤	6
①	2	1	0	1	1	0
②	0	2	1	0	1	0
③	0	1	2	1	0	1
⑤	1	1	0	0	2	1
r =				2		1
c =				3		3

(5.32)

Hence, we have $r = 4$, $\mathcal{I} = \{1, 2, 3, 5\}$ and $\mathcal{J} = \{4, 6\}$ for this step.

Step 3:

Easily, we know that node 4 can be located by nodes 1 and 3 from Eq. (5.32), so the reduced form of the connectivity matrix becomes

	①	②	③	④	⑤	6
①	2	1	0	1	1	0
②	0	2	1	0	1	0
③	0	1	2	1	0	1
④	1	0	1	2	0	1
⑤	1	1	0	0	2	1
r =						3
c =						3

(5.33)

At this step, $r = 4$, $\mathcal{I} = \{1, 2, 3, 4, 5\}$ and $\mathcal{J} = \{6\}$. And from Eq. (5.33), it is obvious that the location node 6 can also be uniquely determined without any further information. And therefore, all the nodes have been located.

Starting from any member as reference member and selecting any undetermined nodes in $\mathcal{J}$ to be located by giving further information in Step 2 will give us the same answer – in order to determine this non-degenerate two-dimensional tensegrity structure, four ($r = 4$) independent nodal coordinate components are needed.

5.4.4 Algorithm Summarization

Following the process stated above, we can now summarize the algorithm for finding the necessary number of independent coordinate components for a tensegrity structure as follows:

Algorithm 5.3:

STEP 0: Define the connectivity matrix $\bar{\mathbf{C}}$. Select the reference member with $r = d + 1$, and obtain $\mathcal{I}^0$ and $\mathcal{J}^0$. Let i :=0.

STEP 1: If $\mathbf{r}_k^i < 2$ $(\forall k \in \mathcal{J}^i)$, consider STEP 1b; otherwise, consider STEP 1a for all $k(\in \mathcal{J}^i)$ where $\mathbf{r}_k^i \geq 2$.

STEP 1a: Consider the following two case:

CASE 1: if $\mathbf{c}_k^i > 2$ $(k \in \mathcal{J}^i)$, let $r := r$, update $\mathcal{J}^{i+1} := \mathcal{J}^i + k$ and $\mathcal{I}^{i+1} := \mathcal{I}^i - k$;

CASE 2: if $\mathbf{c}_k^i = 2$ $(k \in \mathcal{J}^i)$, let $r := r + 1$, update $\mathcal{J}^{i+1} := \mathcal{J}^i + k$ and $\mathcal{I}^{i+1} := \mathcal{I}^i - k$.

STEP 1b: Arbitrarily select one node k where $\mathbf{r}_k^i = 1$ and $\mathbf{c}_k^i > 2$. Update $\mathcal{J}^{i+1} := \mathcal{J}^i + k$ and $\mathcal{I}^{i+1} := \mathcal{I}^i - k$.

Let $\bar{\mathbf{C}}(k, k) = 2$ $(\forall k \in \mathcal{J}^{i+1} - \mathcal{J}^i)$.

STEP 2: If trace($\bar{\mathbf{C}}$)=$2n$, terminate; otherwise, let $i =: i + 1$ and return to STEP 1.

This way, we can find out the necessary number r of independent coordinate components by using only the connectivity relation (topology) of the structure.

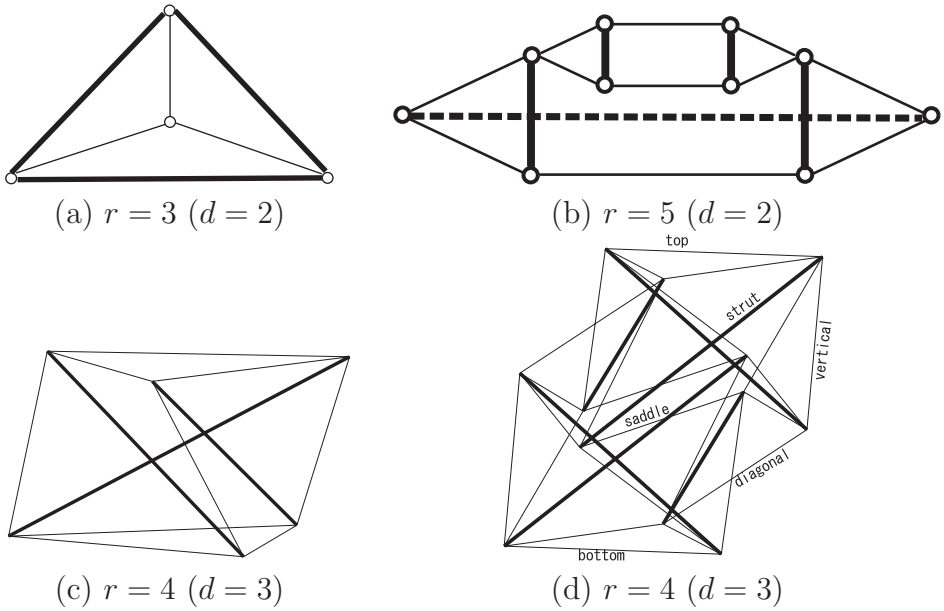

(a) $r = 3$ $(d = 2)$ (b) $r = 5$ $(d = 2)$

(c) $r = 4$ $(d = 3)$ (d) $r = 4$ $(d = 3)$

Figure 5.10: Examples of the necessary number r of the independent coordinate components for the non-degenerate tensegrity structures in d-dimensional space.

5.4.5 Non-degenerate Structures

Besides the simple two-dimensional structure presented in detail previously, the necessary number of independent coordinate components of several other two- and three-dimensional tensegrity structures are shown in Fig. 5.10.

5.5 Numerical Examples

In this section, a rotationally symmetric three-dimensional tensegrity dome and a diamond-shaped tensegrity structure are investigated to demonstrate the capability of the proposed method for generating various shapes.

5.5.1 Diamond-shaped Structure

Consider a tensegrity structure that consists of 6 nodes and 13 members as shown in Fig. 5.11.

Consider firstly Example 1 without any explicit geometrical constraint. The rank of matrix $\mathbf{H}$ has been computed to find $r^H = 22$; i.e. there are 22 prestress

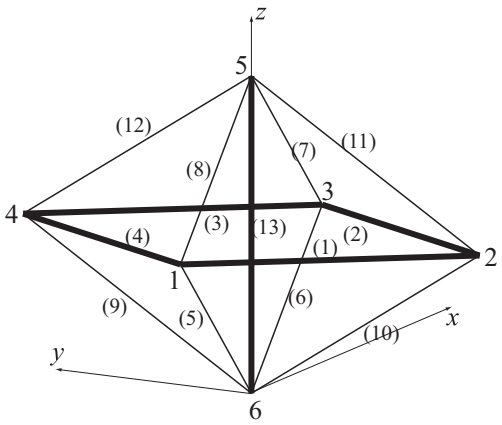

Figure 5.11: Example 1 of diamond-shaped tensegrity.

Table 5.1: Prestresses of Example 1 of the diamond-shaped tensegrity structure.

	Variables $\mathbf{s}_k$								Results $\mathbf{s}_k$					
k	1	2	5	6	7	8	9	10	3	4	10	11	12	13
x	1	1	-1	1	1	-1	0		-1	1	0	0	0	0
y	-1	1	0	0	0	0	1		1	1	-1	-1	1	0
z	0	0	1	1	-1	-1	1	1	0	0		-1	-1	-4

components needed to be specified. By using the Algorithm 5.1, we consecutively specify the prestresses $(\mathbf{s}_1, \mathbf{s}_2, \mathbf{s}_3, \mathbf{s}_4, \mathbf{s}_9, \mathbf{s}_{10}, \mathbf{s}_{11}, \mathbf{s}_{12}, v_{13}^z)$ listed as *Variables* in Table 5.1. Then the results computed by Eq. (5.19) are shown in *Results*.

The rank of matrix $\mathbf{F}$ has been computed to find $r^F = 4$; i.e. there exist 4 nodal coordinates needed to be specified. This agrees with the necessary number of independent nodal coordinate components for the non-degenerate tensegrity structure in three-dimensional space, computed by Algorithm 5.3.

The specified 4 nodal coordinates and the results using a method similar to Algorithm 5.1 for specifying prestresses are shown in Table 5.2. The obtained configuration is as shown in Fig. 5.11. Note that the locations and force vectors of members 1–4 have been obtained to be rotationally symmetric around z-axis by $\pi/2$, although only the prestresses of members 1 and 2 have been specified.

If we specify $v_{10}^z = 3$, which is different from $v_{10}^z = 1$ in the previous example,

Table 5.2: Nodal coordinate of Example 1 of the diamond-shaped tensegrity structure.

	Variables $\mathbf{X}_i$		Results $\mathbf{X}_i$				
i	5	6	1	2	3	4	5
x		0	-2	0	2	0	0
y		0	0	-2	0	2	0
z	4	0	2	2	2	2	

then all nodes will be degenerated into one node with only three nodal coordinates that can be specified; i.e. $r^H = 3$. It means that we cannot obtain the desirable configuration although the generalized force vector $\mathbf{s}$ satisfies the equilibrium conditions and all geometrical constraints.

In the following examples of the diamond-shaped tensegrity structure, we will show how to search new configurations practically by changing the values of some variables to be specified. To reduce the number of independent variables or to assign geometrical characteristics, we introduce some explicit geometrical constraints such that members 1–4 are symmetrically located around z-axis by $\pi/2$, and member 13 is chosen as a fixed member; i.e. the nodal coordinates of nodes 5 and 6 are given as (0, 0, 4) and (0, 0, 0), respectively. In this case, there are only 13 components of prestresses needed to be specified; i.e. $r^H = 13$, and no nodal coordinate can be given because $r^f = r^F = 4$.

Consider Example 2 with the symmetric geometrical constraints as described above. In this example, we specify $(\mathbf{s}_1)_{e2} = 2(\mathbf{s}_1)_{e1}$, where $(\mathbf{s}_1)_{ei}$ denote the prestress vector of member 1 in Example i. The prestresses of members 5, 6, 9 and 10 are the same as those in Example 1. The specified variables and computed results of the prestresses are shown in Table 5.3. The results of nodal coordinates are listed in Table 5.4.

We can see from Fig. 5.12 that the compressive element consisting of symmetrically arranged members 1–4 is located at a higher place than in Example 1, because larger values have been given for the force components of member 1.

If we let $(\mathbf{s}_1)_{e3} = 0.2(\mathbf{s}_1)_{e2}$ and the other variables of prestresses remain the same as those in Example 2, then we obtain a new configuration as shown in Fig. 5.13 as Example 3.

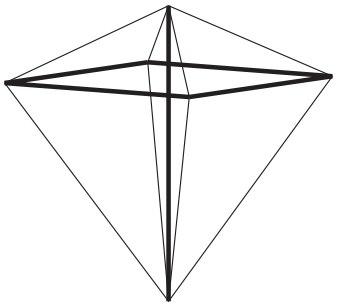

Figure 5.12: Example 2 of diamond-shaped tensegrity structure. Components of prestresses in member (1) are specified as two times to those in Example 1 in Fig. 5.11, while other specified components are untouched.

Table 5.3: Prestresses of Example 2 of the diamond-shaped tensegrity structure.

	Variables $\mathbf{s}_k$					Results $\mathbf{s}_k$								
k	1	5	6	9	10	2	3	4	7	8	10	11	12	13
x	2	-1	1	0		2	-2	2	3	-3	0	0	0	0
y	-2	0	0	1		2	2	2	0	0	-1	-3	3	0
z	0	1	1	1	1	0	0	0	-1	-1		-1	-1	-4

5.5.2 Tensegrity Dome

The three-dimensional tensegrity dome (also called cable dome) as shown in Fig. 5.14(a) consists of 24 free nodes, 8 fixed nodes and 60 members. Its fixed nodes are located on a circle, the radius of which is 15 m. The auxiliary fixed members, which are shown in dashed lines in Fig. 5.14(b), are utilized to substitute the fixed nodes to free nodes, and to transform the original structure into a free-standing structure. Therefore, there are 66 members but no fixed node in the substituted model.

Without introducing any geometrical or mechanical constraints, there are totally (r^H=)99 independent components of the prestresses that can be specified arbitrarily. This may be a burden rather than benefit since a large number of prestresses have to be specified by designers.

Since the structure used as an architecture usually has symmetric properties, we classify its cables into 8 groups; six cables in each group. The cables in each

Table 5.4: Nodal coordinates of Example 2 of the diamond-shaped tensegrity structure.

	Variables $\mathbf{X}_i$		Results $\mathbf{X}_i$			
i	5	6	1	2	3	4
x	0	0	-3	0	3	0
y	0	0	0	-3	0	3
z	4	0	3	3	3	3

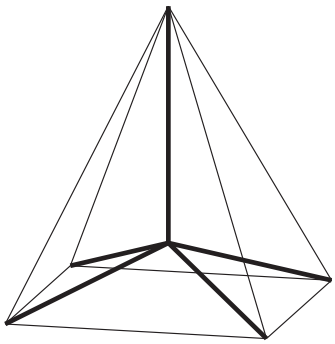

Figure 5.13: Example 3 of diamond-shaped tensegrity. The members have reversed signs of prestresses compared to those in Examples 1 and 2.

group are rotationally symmetric around z-axis by $\pi/3$. This way, there are only $(r^H=)15$ independent components of prestresses needed to be specified.

As Example 1, we specify 15 independent prestress components as listed in Table 5.5.2. The necessary number of independent nodal coordinates of the structure is $r = 4$, and the number that can be specified is $r^F - r^f = 2$ since the nodal coordinates of the fixed nodes have been determined.

If we specify the x-coordinates of nodes 2 and 8 as -5 and -10, respectively, we can obtain configuration of the structure as shown in Fig. 5.14.(a).

Table 5.5: Prestress components specified for the tensegrity dome.

	1	7	13	19	25	31
x	-1	-1	-1	-3	-1	-3
y	1.7321	1.7321	0		-1.7321	-5.1963
z	0	0			0.5	-1.5

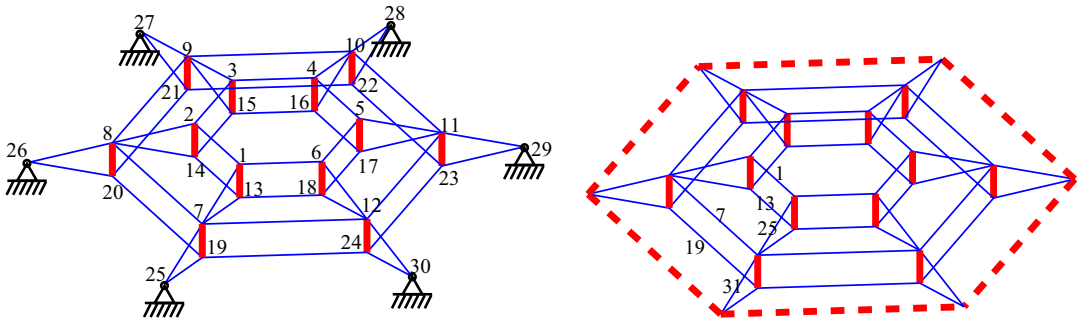

(a) initial model (b) substituted model

Figure 5.14: Perspective view of a three-dimensional cable dome (Example 1). The structure with fixed nodes in (a) is transformed to the free-standing structure in (b), so as to take all nodes into consideration of self-equilibrium of the structure.

Consider Example 2, where we change the values of s_{31}^x and s_{31}^y in Example 1 to -2 and 3.4642, respectively, without changing the values of other parameters, we can achieve a configuration as shown in Fig. 5.15.

The calculation errors of prestresses and nodal coordinates of the examples considered in this section are within 10^{-15} and 10^{-14}, respectively, by using Eq. (5.27) and Eq. (5.28), which confirms the accuracy of the proposed method.

5.6 Discussions and Conclusions

A general method has been presented for direct design of the member directions, internal forces (prestresses) and nodal locations of tensegrity structures with given topology, where the structures are modeled as directed graphs. The self-equilibrium equations are written in terms of the components of the prestresses using the incidence matrix in graph theory.

A concept of auxiliary (fixed) members is introduced to present a unified approach for a general tensegrity structures, that do or do not consist of fixed nodes (supports). A non-degenerate structure investigated in terms of directed graphs should have enough number of independent nodal coordinate components, after the determination of components of prestresses. An efficient algorithm using a special form of incidence matrix is proposed to determine this necessary number

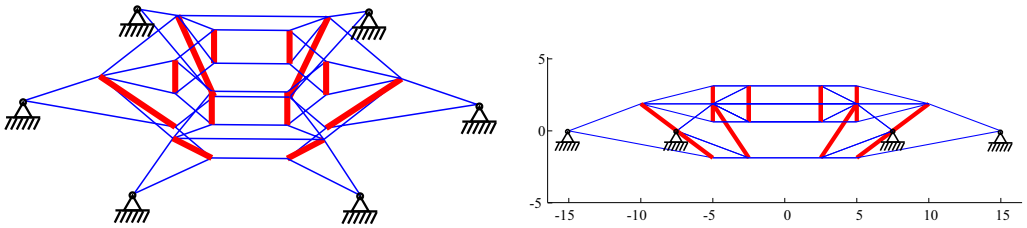

(a) perspective view (b) side view

Figure 5.15: Example 2 of the three-dimensional prestressed tensegrity structure. Directions of the struts in the outer circle are specified not to parallel to those in the inner circle.

for a non-degenerate structure.

In the proposed method, directions of members and symmetry properties are first assigned as geometrical constraints, and the member force vectors are computed from the constrained equilibrium equations. The locations of some nodes including the supports are then assigned to obtain the locations of all nodes. The solution obtained by this method satisfies the equilibrium conditions and the geometrical constraints exactly. Designers are enabled to have direct control over prestresses and the configuration of the structure simultaneously, which is considered to be a major advantage of the method. New configurations can also be obtained by changing the forces and geometrical constraints.

The proposed method is efficient since only linear equations need to be solved. A general algorithm has been presented to find the independent variables consecutively. Unfortunately, it is not an easy task to specify the members to be in tension or compression because the equilibrium shape is not known a priori.

Chapter 6

SYMMETRY-ADAPTED FORMULATIONS

This chapter is to present analytical formulations for the symmetry-adapted matrices, based on group representation theory. The formulations will be used in Chapters 7 and 8 to demonstrate that the self-equilibrated configuration and stability can be effectively studied making use of the high level of symmetry properties of the structures.

Symmetry properties of some structures have attracted attentions for a long time for simplification of structural analysis. Many researchers have been trying to obtain symmetry-adapted (block-diagonal) forms of relevant matrices, such as the equilibrium matrix, the force density matrix and the stiffness matrices. Computational costs can be significantly reduced by considering the blocks in symmetry-adapted forms, which have much smaller dimensions than the original matrices. Among the existing studies, those based on group representation theory are more powerful than the others, and provide a more systematical way to make use of symmetry properties of the structures. However, transformation matrices that transform initial coordinate systems into symmetry-adapted coordinate systems are usually necessary in these conventional methods. These numerical methods may lose the opportunity to derive analytical symmetry-adapted forms, especially for complex structures, since analytical calculations turn out to be impossible for them.

To have more insight into structural properties and to derive stability conditions for a whole class of structures, it would be more helpful to have the *analytical*

symmetry-adapted forms of the matrices. In this chapter, we present the direct strategy to these analytical forms, for the force density matrix, geometrical stiffness matrix as well as the equilibrium matrix. Self-equilibrated configuration of a structure with high level of symmetry can also be determined by considering singularity of specific blocks of the symmetry-adapted force density matrix.

The analytical formulations presented in this chapter makes it possible to derive the super stability and (prestress) stability conditions as will be discussed in Chapter 7, and to prove in Chapter 8 that star-shaped structures are guaranteed to be super stable if and only if the structures have odd number of struts, which are closest to each other.

6.1 Introduction

It has been discussed in Chapter 3 that positive semi-definiteness of the geometrical stiffness matrix $\mathbf{K}_G$ is the necessary condition for super stability. Since $\mathbf{K}_G$ can be written as the Kronecher tensor product ($\otimes$) of a d-by-d identity matrix $\mathbf{I}$ and the force density matrix $\mathbf{E}$ for a d-dimensional structure:

$$\mathbf{K}_G = \underset{d\times d}{\mathbf{I}} \otimes \mathbf{E} \text{ or } \mathbf{K}_G = \mathbf{E} \otimes \underset{d\times d}{\mathbf{I}}, \tag{6.1}$$

it is sufficient to consider positive semi-definiteness of $\mathbf{E}$ instead of that of $\mathbf{K}_G$ in super stability investigation of a structure.

Sizes of the stiffness matrices will increase in proportion to the number of nodes. Hence, computational cost for stability investigation may greatly increase for the complex structures with large numbers of nodes and members. One good way to deal with this situation is to rewrite the matrices in block-diagonal (symmetry-adapted) forms taking advantage of their symmetry properties, where the current coordinate system is transformed into a symmetry-adapted coordinate system. Since eigenvalues of the matrices will not be changed after the transformation coordinate system, positive definiteness of a matrix can be verified by that of the independent blocks in the leading diagonal of its symmetry-adapted form. Computational costs as well as memory needed for storing the entries of the matrix can then be significantly reduced, because sizes of these blocks are much smaller compared to the original matrix.

In the conventional approaches to the derivation of the symmetry-adapted matrices, transformation matrices are necessary to be applied on both side of the matrices. Kangwai *et al.* (1999) presented an introduction and review of these conventional methods. However, this kind of numerical approaches can only deal with every specific structure but not the whole class in one calculation; for example, super stability of the prismatic structure $\mathbf{D}_{1001}^{1,2}$ can be easily verified using the symmetry-adapted forms of its stiffness matrices, however, new computations are necessary for the structures with similar properties, e.g., the structure $\mathbf{D}_{1001}^{1,5}$ or $\mathbf{D}_{1002}^{1,2}$. Furthermore, it might take a lot of computation time in deriving the symmetry-adapted forms, especially for complicated structures, even though the total time for structural analysis and stability investigation is still much smaller than those in the original coordinate systems. To present a direct strategy for the *analytical* formulations of the stiffness matrices and the related matrices, so as to provide the opportunity for further insight into the stability properties of the whole class of structures with similar symmetry, is the major subject of the chapter. It is notable in the proposed strategy that transformation matrices, and therefore, the matrix computations with them, turn out to be unnecessary. As a result, computational costs are further reduced, although it is not the major motivation in the development of the methodology. These formulations are mainly based on group representation theory.

In the chapter, we mainly deal with the structures with dihedral symmetry, and the strategy is expected to be applicable to the structures belong to other point group. And because the nodes of prismatic structures have one-to-one correspondence to the symmetry operations of the dihedral group, they are used as example structures representing the structures with dihedral symmetry for simplicity. Another class of structures with dihedral symmetry—star-shaped structures—will be discussed in Chapter 8.

Following this introduction section, the chapter is organized as follows: Section 2 gives a brief introduction to the group representation theory and dihedral symmetry, which will be used for presenting the symmetry-adapted formulations. Section 3 presents the formulation of the symmetry-adapted force density matrix, based on which self-equilibrated configurations and conditions for super stability of prismatic structures will be presented in Chapter 7 and those for star-shaped

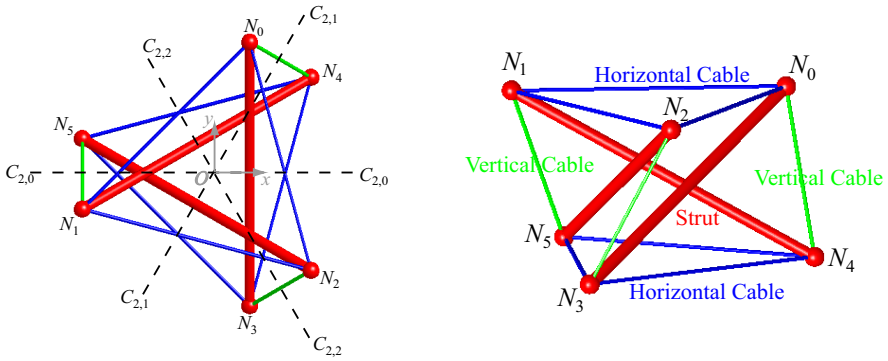

(a) top view (b) side view

Figure 6.1: Prismatic tensegrity structure with symmetry of dihedral group $\mathbf{D}_3$. The group $\mathbf{D}_3$ has six symmetry operations. The structure consists of six nodes and six horizontal cables having one-to-one correspondence to symmetry operations, and three vertical cables and struts having one-to-two correspondence to symmetry operations.

structures in Chapter 8. Section 4 and Section 5 formulate symmetry-adapted forms of the geometrical stiffness matrix and the equilibrium matrix. Symmetry-adapted mechanisms are derived from the transpose of the symmetry-adapted equilibrium matrix. Section 6 briefly discusses and concludes this chapter.

6.2 Group and Matrix Representation

Symmetry of a structure can be systematically dealt with using group representation theory. To prepare for the symmetry-adapted formulations in the coming sections, some basic concepts of group and its matrix representation are briefly introduced in this section. For more details, see Appendix B or refer to the textbooks, e.g., those by Bishop (1973); Kettle (1995).

6.2.1 Group

A group is defined by a set of elements and combination rules between these elements. The elements in a group should satisfy four general criteria—closure, associativity, identity and inverse. The number of elements in a group is called *order* of it. In description of symmetry property of a structure, the elements are

called *symmetry operations*. A symmetry operation is an operation, which moves the structure in such a way that its final position is physically indistinguishable from its initial position. If there is at least one point in the structure that does not change its position by any symmetry operations of a group, that group is called *point group*. There are in total five different types of symmetry operations in a point group: (1) identity operation, (2) rotation operation about the principal axis, (3) reflection operation, (4) rotation operation about an improper axis (rotation-reflection operation), and (5) inversion operation.

Prismatic tensegrity structures, e.g., the simplest structure in three-dimensional space as shown in Fig. 6.1, are of dihedral symmetry: they are physically indistinguishable by the symmetry operations of dihedral group $\mathbf{D}_n$. Dihedral group is a point group, and consists of (1) identity operation, (2) (cyclic) rotation operations, and (3) rotation-reflection operations (two-fold rotations). For convenience, we take z-axis of the Cartesian coordinate system as the principal axis, and regard the point (0,0,0) as the origin. The origin does not change its position by any symmetry operations of the group. A dihedral group $\mathbf{D}_n$ is of order $2n$: it consists of n-fold rotations C_n^i ($i \in \{0, \ldots, n-1\}$) about z-axis, and n two-fold rotations $C_{2,i}$ ($i \in \{0, \ldots, n-1\}$) about the axes through the origin and perpendicular to z-axis.

A prismatic tensegrity structure with $\mathbf{D}_n$ symmetry consists of $2n$ nodes, $2n$ horizontal cables, n vertical cables and n struts. We assign that cables carry tension and struts carry compression. Nodes of a prismatic structure lie in two parallel planes; horizontal cables connect the nodes in the same plane, and vertical cables and struts connect those in different planes. The nodes and horizontal cables have one-to-one correspondence to the symmetry operations of the group, while struts and vertical cables have one-to-two correspondence.

6.2.2 Matrix Representation

Group multiplication table describes combinations of two operations (elements) of a group. If a set of matrices obeys the group multiplication table of a group, these matrices are said to form a *matrix representation* of that group. A matrix representation that can be reduced to a linear combination (direct sum) of several

Table 6.1: Irreducible matrix representations $\mathbf{R}_i^\mu$ of dihedral group $\mathbf{D}_n$. The first column denotes representations μ of the group, the first row denotes its symmetry operations with i running from 0 to $n-1$. C_{ik} and S_{ik} respectively denote $\cos(2ik\pi/n)$ and $\sin(2ik\pi/n)$. x, y, z and R_x, R_y, R_z respectively stand for symmetry operations of the corresponding coordinates and rotations about those axes.

$\mathbf{D}_n$	C_n^i	$C_{2,i}$		
A_1	1	1		
A_2	1	-1	$z,\ R_z$	
(B_1)	$(-1)^i$	$(-1)^i$		n even
(B_2)	$(-1)^i$	$(-1)^{(i+1)}$		n even
E_1	$\begin{pmatrix} C_i & -S_i \\ S_i & C_i \end{pmatrix}$	$\begin{pmatrix} C_i & S_i \\ S_i & -C_i \end{pmatrix}$	$(x,y)\ (R_x,R_y)$	
E_k	$\begin{pmatrix} C_{ik} & -S_{ik} \\ S_{ik} & C_{ik} \end{pmatrix}$	$\begin{pmatrix} C_{ik} & S_{ik} \\ S_{ik} & -C_{ik} \end{pmatrix}$		$k \in \{2,\ldots,p\}$
	$\mathbf{R}_i^\mu$	$\mathbf{R}_{n+i}^\mu$		$i \in \{0,\ldots,n-1\}$

matrix representations is called *reducible matrix representation*, otherwise, they form an *irreducible matrix representation*. *Characters* are defined as traces of the irreducible representation matrices. They will be shown to be important in identifying the block structures of the symmetry-adapted matrices.

A dihedral group $\mathbf{D}_n$ consists of two one-dimensional irreducible matrix representations A_1 and A_2 for n odd, or four with B_1 and B_2 in addition for n even, and p two-dimensional irreducible matrix representations E_k $(k = 1,\ldots,p)$ where

$$p = \begin{cases} (n-1)/2, & n \text{ odd} \\ (n-2)/2, & n \text{ even} \end{cases} . \tag{6.2}$$

The irreducible matrix representations of a dihedral group $\mathbf{D}_n$ are listed in Table 6.1. The one-dimensional matrix representations are unique, and their characters are the representation matrices themselves; characters of the two-dimensional representation matrices are also unique—character of the cyclic rotation C_n^i for E_k is $2C_{ik}$, and that of the two-fold rotation $C_{2,i}$ for any E_k is zero, but we may have some limited choices for their representation matrices. In Table 6.1, we chose the positive z-direction as the positive direction of rotations to formulate the two-dimensional representation matrices. The symbols x, y and z in the fourth column of the table respectively stand for x-, y- and z-coordinates, and

R_x, R_y and R_z stand for rotations about these axes (Atkins *et al.*, 1970). We will show in the next chapter that the blocks of the symmetry-adapted force density matrix corresponding to the representations that stand for coordinates—A_2 and E_1 representations in the case of dihedral group—should be singular to ensure a non-degenerate configuration; and we will point out in Section 5 that the rigid-body motions exist in the blocks of the stiffness matrices corresponding to these representations.

6.3 Symmetry-adapted Force Density Matrix

This section presents the direct strategy for the symmetry-adapted force density matrix, of which the blocks are written as sums of the products of the force densities with their associated irreducible representation matrices. Since the nodes of prismatic structures form a regular representation—they have one-to-one correspondence to the symmetry operation of the dihedral group, they are taken as example structures for the presentation of the symmetry-adapted force density matrix.

6.3.1 Force Density Matrix

Every node of a prismatic tensegrity structure is connected by three different types of members: two horizontal cables, one vertical cable and one strut; and each type of members has the same self-stress and length. The nodes in the top plane of the structure are numbered from 0 to $n-1$, and those in the bottom are n to $2n-1$. We use the notation $\mathbf{D}_n^{h,v}$ to describe the connectivity of a prismatic tensegrity with $\mathbf{D}_n$ symmetry: h and v respectively describe the connectivity of the horizontal and vertical cables, while that of struts is fixed. We describe the connectivity of a reference node N_0 as follows — all other connections are then defined by the symmetry.

[L1] Without loss of generality, we assume that a strut connects node N_0 in the top plane to node N_n in the bottom plane.

[L2] A horizontal cable connects node N_0 to node N_h: symmetry also implies that a horizontal cable must also connect node N_0 to node N_{n-h}. We restrict $1 \leq h \leq n/2$.

[L3] A vertical cable connects node N_0 in the top plane to node N_{n+v} in the bottom plane. We restrict $1 \leq v \leq n/2$ (choosing $n/2 \leq v \leq n$ would give essentially the same set of structures, but in left-handed versions).

For example, the structure in Fig. 6.1 is denoted as $\mathbf{D}_3^{1,1}$.

Let q_h, q_v and q_s denote the force densities (self-stress to length ratios) of horizontal cables, vertical cables and struts, respectively. Let $\mathcal{I}$ denote the set of members connected to node i. The (i,j)-component $E_{(i,j)}$ of the force density matrix $\mathbf{E} \in \Re^{2n \times 2n}$ is given as

$$E_{(i,j)} = \begin{cases} \sum_{k \in \mathcal{I}} q_k & \text{for } i = j, \\ -q_k & \text{if nodes } i \text{ and } j \text{ are connected by member } k, \\ 0 & \text{for other cases.} \end{cases} \tag{6.3}$$

From the numbering and connectivity of nodes, $\mathbf{E}$ can be written as

$$\mathbf{E} = \begin{pmatrix} \mathbf{E}_1 & \mathbf{E}_2 \\ \mathbf{E}_2^{\mathrm{T}} & \mathbf{E}_1 \end{pmatrix}. \tag{6.4}$$

Denote $q = 2q_h + q_s + q_v$, and let $\mathbf{I}^m \in \Re^{n \times n}$ be a matrix with only one non-zero element $I_{(i,i+m)} = 1$ ($i \in \{1, 2, \ldots, n\}$ and $i+m = i+m-n$ if $i+m > n$) in each row and column, $\mathbf{E}_1$ and $\mathbf{E}_2$ ($\in \Re^{n \times n}$) are

$$\mathbf{E}_1 = q\mathbf{I}^0 - q_h\mathbf{I}^h - q_h\mathbf{I}^{n-h} \text{ and } \mathbf{E}_2 = -q_s\mathbf{I}^0 - q_v\mathbf{I}^v. \tag{6.5}$$

Note that $\mathbf{I}^0$ is an n-by-n identity matrix.

Consider the structure $\mathbf{D}_4^{1,2}$ for example. It has $\mathbf{D}_4$ symmetry, and its connectivity is $h = 1, v = 2$. From the definition of the force density matrix, we have

$$\mathbf{E}_1 = q\mathbf{I}^0 - q_h\mathbf{I}^1 - q_h\mathbf{I}^3 = \begin{pmatrix} q & -q_h & 0 & 0 \\ -q_h & q & -q_h & 0 \\ 0 & -q_h & q & -q_h \\ -q_h & 0 & -q_h & q \end{pmatrix}$$

$$\mathbf{E}_2 = -q_s\mathbf{I}^0 - q_v\mathbf{I}^2 = \begin{pmatrix} -q_s & -q_v & 0 & 0 \\ 0 & -q_s & -q_v & 0 \\ 0 & 0 & -q_s & -q_v \\ -q_v & 0 & 0 & -q_s \end{pmatrix},$$

where

$$\mathbf{I}^h = \mathbf{I}^1 = \begin{pmatrix} 0 & 1 & 0 & 0 \\ 0 & 0 & 1 & 0 \\ 0 & 0 & 0 & 1 \\ 1 & 0 & 0 & 0 \end{pmatrix}, \mathbf{I}^{n-h} = \mathbf{I}^3 = \begin{pmatrix} 0 & 0 & 0 & 1 \\ 1 & 0 & 0 & 0 \\ 0 & 1 & 0 & 0 \\ 0 & 0 & 1 & 0 \end{pmatrix},$$

$$\text{and} \quad \mathbf{I}^v = \mathbf{I}^2 = \begin{pmatrix} 0 & 1 & 0 & 0 \\ 0 & 0 & 1 & 0 \\ 0 & 0 & 0 & 1 \\ 1 & 0 & 0 & 0 \end{pmatrix}.$$

6.3.2 Symmetry-adapted Formulation

In this subsection, we present the direct formulation of the symmetry-adapted force density matrix, structure of which can be identified using the linear combination of representations of the nodes (Fowler and Guest, 2000; Kettle, 1995).

Linear combination of representations for transformation of nodes (members) are helpful in identifying structure of the symmetry-adapted force density matrix. For this purpose, every node (member) is considered to be physically distinct, unlike the case where all nodes and all members of the same type are regarded to be physically indistinguishable when we described symmetry of the structure in Section 2. To consider transformation of nodes under symmetry operations, we use the structure with $\mathbf{D}_3$ symmetry in Fig. 6.1 as an example structure. Rotation C_3^1 exchanges positions of nodes as

$$N_0 \to N_1 \to N_2 \to N_0 \text{ and } N_3 \to N_4 \to N_5 \to N_3.$$

Moreover, transformations of the nodes under each symmetry operation of $\mathbf{D}_3$

can be written in matrix form $\mathbf{R}_N$ as

operations	C_3^0	C_3^1	C_3^2
$\mathbf{R}_N$	$\begin{pmatrix} 1 & & & & & \\ & 1 & & & & \\ & & 1 & & & \\ & & & 1 & & \\ & & & & 1 & \\ & & & & & 1 \end{pmatrix}$	$\begin{pmatrix} 0 & 1 & & & & \\ & 0 & 1 & & & \\ & & 0 & 1 & & \\ & & & 0 & 1 & \\ & & & & 0 & 1 \\ 1 & & & & & 0 \end{pmatrix}$	$\begin{pmatrix} 0 & & 1 & & & \\ & 0 & & 1 & & \\ & & 0 & & 1 & \\ & & & 0 & & 1 \\ 1 & & & & 0 & \\ & 1 & & & & 0 \end{pmatrix}$
trace($\mathbf{R}_N$)	6	0	0

operations	$C_{2,0}$	$C_{2,1}$	$C_{2,2}$
$\mathbf{R}_N$	$\begin{pmatrix} 0 & & 1 & & & \\ & 0 & & & & 1 \\ & & 0 & & 1 & \\ 1 & & & 0 & & \\ & & 1 & & 0 & \\ & 1 & & & & 0 \end{pmatrix}$	$\begin{pmatrix} 0 & & & & 1 & \\ & 0 & & 1 & & \\ & & 0 & & & 1 \\ & 1 & & 0 & & \\ 1 & & & & 0 & \\ & & 1 & & & 0 \end{pmatrix}$	$\begin{pmatrix} 0 & & & & & 1 \\ & 0 & & & 1 & \\ & & 0 & 1 & & \\ & & 1 & 0 & & \\ & 1 & & & 0 & \\ 1 & & & & & 0 \end{pmatrix}$
trace($\mathbf{R}_N$)	0	0	0

Trace of $\mathbf{R}_N$ is equal to the number of nodes that remain unchanged under a specific symmetry operation. The matrices $\mathbf{R}_N$ indeed form a *reducible* matrix representation of the group $\mathbf{D}_3$, since they satisfy its multiplication table. This reducible matrix representation can be rewritten as a linear combination (direct sum) of its irreducible matrix representations, making use of the important property that a change in coordinate system will not change the trace, or character, of a representation matrix. For the structure with $\mathbf{D}_3$ symmetry for example, traces of the representation matrices can be summarized as

operations		C_3^0	C_3^1	C_3^2	$C_{2,0}$	$C_{2,1}$	$C_{2,2}$	
$\Gamma(N)$	$\{$	6,	0,	0;	0,	0,	0	$\}$

To identify how many copies of each irreducible representation are present in their linear combination $\Gamma(N)$, such that trace of the reducible representation matrix under a symmetry operation is equal to the sum of those of irreducible matrices under that operation, we consider

$\Gamma(N)$	$\{6,$	$0,$	$0;$	$0,$	$0,$	$0\}$
$= A_1$	$= \{1,$	$1,$	$1;$	$1,$	$1,$	$1\}$
$+A_2$	$+\{1,$	$1,$	$1;$	$-1,$	$-1,$	$-1\}$
$+2E_1$	$+2\{2,$	$2 \times (-\frac{1}{2}),$	$2 \times (-\frac{1}{2});$	$0,$	$0,$	$0\}$

From which, we learn that the reducible matrix representation of the nodes is direct sum of one copy of each one-dimensional irreducible matrix representation and two copies of each two-dimensional; i.e., $\Gamma(N) = A_1 + A_2 + 2E_1$, for the structure with $\mathbf{D}_3$ symmetry.

In general, any node of a prismatic tensegrity structure with $\mathbf{D}_n$ symmetry is transformed to a different node by any symmetry operation except for the identity operation: all nodes, in total $2n$, remain unchanged under the identity operation such that the trace of $\mathbf{R}_N$ corresponding to it is $2n$, and $\mathbf{R}_N$ have zero traces under all other symmetry operations of the group. Hence, we have $\Gamma(N) = \{2n, 0, \ldots, 0;\ 0, \ldots, 0\}$. From characters of the irreducible matrices of dihedral group, the reducible matrix representation of the nodes can be written as a linear combination $\Gamma(N)$ of the irreducible representations in a general form as follows

$$\begin{aligned}
\Gamma(N) &= A_1 + A_2 + (B_1 + B_2) + 2\sum_{k=1}^{p} E_k \\
&= \{1, \ldots, 1;\ 1, \ldots, 1\} && A_1 \\
&+ \{1, \ldots, 1;\ -1, \ldots - 1\} && A_2 \\
&+ (\{1, \ldots, (-1)^i, \ldots, (-1)^n;\ 1, \ldots, (-1)^i, \ldots, (-1)^n\}) && (B_1) \\
&+ (\{1, \ldots, (-1)^i, \ldots, (-1)^n;\ -1, \ldots, (-1)^{i+1}, \ldots, (-1)^{n+1}\}) && (B_2) \\
&+ 2\sum_{k=1}^{p} \{2C_{0k}, \ldots, 2C_{ik}, \ldots, 2C_{(n-1)k};\ 0, \ldots, 0\} && 2E_k \\
&= \{2n, 0, \ldots, 0;\ 0, \ldots, 0\}.
\end{aligned} \tag{6.6}$$

We use $\tilde{(\cdot)}$ to denote the symmetry-adapted form of a matrix. $\Gamma(N)$ characterizes structure of the symmetry-adapted force density matrix $\tilde{\mathbf{E}}$.

[L1] The number of the representation μ in $\Gamma(N)$ indicates dimensions of $\tilde{\mathbf{E}}^{\mu}$. Hence, we learn from Eq. (6.6) that the blocks corresponding to the one-dimensional representations are 1-by-1 matrices, and those of two-dimensional representations are 2-by-2 matrices.

[L2] Dimensions of a representation indicate times of its corresponding block appearing in the symmetry-adapted form; thus, each one-dimensional representation has only one copy, and each two-dimensional representation has two copies of blocks lying in the leading diagonal of $\tilde{\mathbf{E}}$.

Thus, the block structure of $\tilde{\mathbf{E}}$ can be written in a general form as follows according to the linear combination $\Gamma(N)$ of representations for transformation of nodes in Eq. (6.6)

$$\underset{2n\times 2n}{\tilde{\mathbf{E}}} = \begin{pmatrix} \underset{1\times 1}{\tilde{\mathbf{E}}^{A_1}} & & & & & & & & \\ & \underset{1\times 1}{\tilde{\mathbf{E}}^{A_2}} & & & & & & & \\ & & (\underset{1\times 1}{\tilde{\mathbf{E}}^{B_1}}) & & & & & & \\ & & & (\underset{1\times 1}{\tilde{\mathbf{E}}^{B_2}}) & & & & & \\ & & & & \underset{2\times 2}{\tilde{\mathbf{E}}^{E_1}} & & & & \\ & & & & & \underset{2\times 2}{\tilde{\mathbf{E}}^{E_1}} & & & \\ & & & & & & \ddots & & \\ & & & & & & & \underset{2\times 2}{\tilde{\mathbf{E}}^{E_p}} & \\ & & & & & & & & \underset{2\times 2}{\tilde{\mathbf{E}}^{E_p}} \end{pmatrix}, \tag{6.7}$$

where the blocks $\tilde{\mathbf{E}}^{B_1}$ and $\tilde{\mathbf{E}}^{B_2}$ corresponding to representations B_1 and B_2 exist only if n is even.

In conventional methods, $\tilde{\mathbf{E}}$ is usually obtained using the unitary transformation matrix $\mathbf{T} \in \Re^{2n\times 2n}$:

$$\tilde{\mathbf{E}} = \mathbf{T}\mathbf{E}\mathbf{T}^{\mathrm{T}}, \tag{6.8}$$

where $\mathbf{T}\mathbf{T}^{\mathrm{T}}$ is an identity matrix:

$$\mathbf{T}\mathbf{T}^{\mathrm{T}} = \underset{2n\times 2n}{\mathbf{I}}. \tag{6.9}$$

Although the transformation matrix is not needed to derive the blocks $\tilde{\mathbf{E}}^{\mu}$ in our direct strategy as presented later in Eq. (6.12), it is necessary for the proof of its formulation. Hence, we introduce the details of $\mathbf{T}$ for obtaining $\tilde{\mathbf{E}}$ as in Eq. (6.8) before presenting its direct formulation in Lemma 1. Because nodes of a symmetric prismatic tensegrity structure have one-to-one correspondence to the symmetry operations; i.e., any node can be transformed to another by only one symmetry operation of that group, $\mathbf{T}$ can be easily obtained from the irreducible matrix representations: for one-dimensional representation μ, the row $\mathbf{T}^{\mu} \in \Re^{1\times 2n}$ of $\mathbf{T}$ corresponding to μ is

$$\mathbf{T}^{\mu} = \frac{1}{\sqrt{2n}} \left(\mathbf{R}_0^{\mu}, \mathbf{R}_1^{\mu}, \ldots, \mathbf{R}_j^{\mu}, \ldots, \mathbf{R}_{2n-1}^{\mu} \right), \tag{6.10}$$

where $\mathbf{R}_j^{\mu}$ is the character of the one-dimensional representation μ, and $\mathbf{T}^{\mu}$ is normalized as $\mathbf{T}^{\mu}(\mathbf{T}^{\mu})^{\top} = 1$ by dividing $\sqrt{2n}$. For example, $\mathbf{T}^{A_2}$ for representation A_2 of the structure with $\mathbf{D}_3$ symmetry is

$$\mathbf{T}^{A_2} = \frac{1}{\sqrt{6}}\left(1, 1, 1, -1, -1, -1\right).$$

For a two-dimensional representation E_k, there are four rows in $\mathbf{T}^{E_k} \in \Re^{4\times 2n}$. The irreducible representation matrix $\mathbf{R}_j^{E_k}$ of the jth symmetry operation corresponding to representation E_k is

$$\mathbf{R}_j^{E_k} = \begin{pmatrix} R_j^{E_k}(1,1) & R_j^{E_k}(1,2) \\ R_j^{E_k}(2,1) & R_j^{E_k}(2,2) \end{pmatrix}$$

The four elements of $\mathbf{R}_j^{E_k}$ are located in the jth column of $\mathbf{T}^{E_k}$ as follows to construct the transformation matrix

$$\mathbf{T}^{\mu} = \frac{1}{\sqrt{n}}\begin{pmatrix} R_0^{\mu}(1,1), & \ldots, & R_j^{\mu}(1,1), & \ldots, & R_{2n-1}^{\mu}(1,1) \\ R_0^{\mu}(1,2), & \ldots, & R_j^{\mu}(1,2), & \ldots, & R_{2n-1}^{\mu}(1,2) \\ R_0^{\mu}(2,1), & \ldots, & R_j^{\mu}(2,1), & \ldots, & R_{2n-1}^{\mu}(2,1) \\ R_0^{\mu}(2,2), & \ldots, & R_j^{\mu}(2,2), & \ldots, & R_{2n-1}^{\mu}(2,2) \end{pmatrix} = \frac{1}{\sqrt{n}}\begin{pmatrix} (C_{jk}), & (C_{jk}) \\ -(S_{jk}), & (S_{jk}) \\ (S_{jk}), & (S_{jk}) \\ (C_{jk}), & -(C_{jk}) \end{pmatrix}, \tag{6.11}$$

where $[C_{jk}]$ and $[S_{jk}]$ ($\in \Re^n$) are row vectors:

$$\begin{aligned} (C_{jk}) &= \left(C_0, C_k, \ldots, C_{jk}, \ldots, C_{(n-1)k}\right) \\ (S_{jk}) &= \left(S_0, S_k, \ldots, S_{jk}, \ldots, S_{(n-1)k}\right), \text{ for } j = 0, \ldots, n-1. \end{aligned}$$

For example, $\mathbf{T}^{E_1}$ for the structure with $\mathbf{D}_3$ symmetry is

$$\begin{aligned} \mathbf{T}^{E_1} &= \frac{1}{\sqrt{3}}\begin{pmatrix} C_0 & C_1 & C_2 & C_0 & C_1 & C_2 \\ -S_0 & -S_1 & -S_2 & S_0 & S_1 & S_2 \\ S_0 & S_1 & S_2 & S_0 & S_1 & S_2 \\ C_0 & C_1 & C_2 & -C_0 & -C_1 & -C_2 \end{pmatrix} \\ &= \frac{1}{\sqrt{3}}\begin{pmatrix} 1 & -\frac{1}{2} & -\frac{1}{2} & 1 & -\frac{1}{2} & -\frac{1}{2} \\ 0 & -\frac{\sqrt{3}}{2} & \frac{\sqrt{3}}{2} & 0 & \frac{\sqrt{3}}{2} & -\frac{\sqrt{3}}{2} \\ 0 & \frac{\sqrt{3}}{2} & -\frac{\sqrt{3}}{2} & 0 & \frac{\sqrt{3}}{2} & -\frac{\sqrt{3}}{2} \\ 1 & -\frac{1}{2} & -\frac{1}{2} & -1 & \frac{1}{2} & \frac{1}{2} \end{pmatrix}. \end{aligned}$$

Combining $\mathbf{T}^{\mu}$ for all representations to $\mathbf{T}$, it is easy to verify that $\mathbf{T}$ is a unitary transformation matrix satisfying Eq. (6.9) from the great orthogonality theorem (Kettle, 1995). Substituting $\mathbf{T}$ into Eq. (6.8), the force density matrix can be

Table 6.2: Selected irreducible representation matrices corresponding to the nodes connecting to node 0.

	identity	horizontal cable		strut	vertical
μ	$\mathbf{R}_0^\mu$	$\mathbf{R}_h^\mu$	$\mathbf{R}_{n-h}^\mu$	$\mathbf{R}_n^\mu$	$\mathbf{R}_{n+v}^\mu$
A_1	1	1	1	1	1
A_2	1	1	1	-1	-1
B_1	1	$(-1)^h$	$(-1)^{n-h}$	1	$(-1)^v$
B_2	1	$(-1)^h$	$(-1)^{n-h}$	-1	$(-1)^{v+1}$
E_k	$\begin{pmatrix} 1 & 0 \\ 0 & 1 \end{pmatrix}$	$\begin{pmatrix} C_{hk} & -S_{hk} \\ S_{hk} & C_{hk} \end{pmatrix}$	$\begin{pmatrix} C_{hk} & S_{hk} \\ -S_{hk} & C_{hk} \end{pmatrix}$	$\begin{pmatrix} 1 & 0 \\ 0 & -1 \end{pmatrix}$	$\begin{pmatrix} C_{vk} & S_{vk} \\ S_{vk} & -C_{vk} \end{pmatrix}$

block-diagonalized with the structure as in Eq. (11.9). Super stability investigation and self-equilibrium analysis are then significantly simplified by dealing with these blocks, dimensions of which are only one or two no matter how complicated the structure is. However, it is difficult to derive analytical symmetry-adapted force density matrix for complicated structure that has a large number of nodes in this way, since size of the transformation matrix $\mathbf{T}$ increases in proportion to the number of its nodes. Moreover, the symmetry-adapted formulation by Eq. (6.8) can only deal with each specific structure, but not all structures with similar symmetry properties. To have more systematic solution, Lemma 1 below presents a direct way for deriving the symmetry-adapted force density matrix of the structures with dihedral symmetry.

In Lemma 1, only a representative node, e.g., node 0, is sufficient to present the blocks $\tilde{\mathbf{E}}^\mu$ of $\tilde{\mathbf{E}}$ corresponding to representation μ. Consider the structure $\mathbf{D}_n^{h,v}$ in general. Irreducible representation matrices corresponding to the nodes connected to it as members are $\mathbf{R}_0^\mu$, $\mathbf{R}_h^\mu$, $\mathbf{R}_{n-h}^\mu$, $\mathbf{R}_n^\mu$ and $\mathbf{R}_{n+v}^\mu$, which are listed in Table 6.2. In the following lemma, we show that blocks $\tilde{\mathbf{E}}^\mu$ of each representation μ can be directly written as sum of products of the force densities and their corresponding irreducible representation matrices.

Lemma 6.1 *The block $\tilde{\mathbf{E}}^\mu$ corresponding to representation μ of the symmetry-adapted force density matrix $\tilde{\mathbf{E}}$ can be written in a general form as*

$$\tilde{\mathbf{E}}^\mu = q\mathbf{R}_0^\mu - q_h\mathbf{R}_h^\mu - q_h\mathbf{R}_{n-h}^\mu - q_s\mathbf{R}_n^\mu - q_v\mathbf{R}_{n+v}^\mu \tag{6.12}$$

Proof. Using components $\mathbf{T}^\mu$ of $\mathbf{T}$ corresponding to representation μ, the block $\tilde{\mathbf{E}}^\mu$ can be computed as

$$\tilde{\mathbf{E}}^\mu = \mathbf{T}^\mu \mathbf{E} (\mathbf{T}^\mu)^{\mathrm{T}} \tag{6.13}$$

[L1] *One-dimensional representations*

For the one-dimensional representations, $\mathbf{T}^\mu$ is a vector denoted as $\mathbf{T}^\mu = [\boldsymbol{\alpha}_1, \boldsymbol{\alpha}_2]$. From Eq. (11.5), Eq. (6.13) becomes

$$\tilde{\mathbf{E}}^\mu = \boldsymbol{\alpha}_1 \mathbf{E}_1 \boldsymbol{\alpha}_1^{\mathrm{T}} + \boldsymbol{\alpha}_2 \mathbf{E}_1 \boldsymbol{\alpha}_2^{\mathrm{T}} + 2\boldsymbol{\alpha}_1 \mathbf{E}_2 \boldsymbol{\alpha}_2^{\mathrm{T}}. \tag{6.14}$$

Consider representation A_1 for example. All irreducible representation matrices (equal to their characters) are equal to 1, hence, all the elements in $\mathbf{T}^{A_1}$ (also in $\boldsymbol{\alpha}_1$ and $\boldsymbol{\alpha}_2$) are $\frac{1}{\sqrt{2n}}$. Therefore, we have

$$\boldsymbol{\alpha}_1 \mathbf{I}^a \boldsymbol{\alpha}_1^{\mathrm{T}} + \boldsymbol{\alpha}_2 \mathbf{I}^a \boldsymbol{\alpha}_2^{\mathrm{T}} = \frac{2n}{2n} = 1 = \mathbf{R}_a^{A_1}, \quad a \in \{0, h, n-h\}. \tag{6.15}$$

In a similar manner, we can also have

$$2\boldsymbol{\alpha}_1 \mathbf{I}^b \boldsymbol{\alpha}_2^{\mathrm{T}} = 2\frac{n}{2n} = 1 = \mathbf{R}_{n+b}^{A_1}, \quad b \in \{0, v\}. \tag{6.16}$$

From Eqs. (11.6), (6.14), (6.15) and (6.16), we have

$$\begin{aligned}
\tilde{\mathbf{E}}^{A_1} &= \boldsymbol{\alpha}_1 \mathbf{E}_1 \boldsymbol{\alpha}_1^{\mathrm{T}} + \boldsymbol{\alpha}_2 \mathbf{E}_1 \boldsymbol{\alpha}_2^{\mathrm{T}} + 2\boldsymbol{\alpha}_1 \mathbf{E}_2 \boldsymbol{\alpha}_2^{\mathrm{T}} \\
&= \boldsymbol{\alpha}_1 (q\mathbf{I}^0 - q_h \mathbf{I}^h - q_h \mathbf{I}^{n-h}) \boldsymbol{\alpha}_1^{\mathrm{T}} + \boldsymbol{\alpha}_2 (q\mathbf{I}^0 - q_h \mathbf{I}^h - q_h \mathbf{I}^{n-h}) \boldsymbol{\alpha}_2^{\mathrm{T}} \\
&\quad + 2\boldsymbol{\alpha}_1 (-q_s \mathbf{I}^0 - q_v \mathbf{I}^v) \boldsymbol{\alpha}_2^{\mathrm{T}} \\
&= q(\boldsymbol{\alpha}_1 \mathbf{I}^0 \boldsymbol{\alpha}_1^{\mathrm{T}} + \boldsymbol{\alpha}_2 \mathbf{I}^0 \boldsymbol{\alpha}_2^{\mathrm{T}}) - q_h (\boldsymbol{\alpha}_1 \mathbf{I}^h \boldsymbol{\alpha}_1^{\mathrm{T}} + \boldsymbol{\alpha}_2 \mathbf{I}^h \boldsymbol{\alpha}_2^{\mathrm{T}}) \\
&\quad - q_h (\boldsymbol{\alpha}_1 \mathbf{I}^{n-h} \boldsymbol{\alpha}_1^{\mathrm{T}} + \boldsymbol{\alpha}_2 \mathbf{I}^{n-h} \boldsymbol{\alpha}_2^{\mathrm{T}}) - q_s (2\boldsymbol{\alpha}_1 \mathbf{I}^0 \boldsymbol{\alpha}_2^{\mathrm{T}}) - q_v (2\boldsymbol{\alpha}_1 \mathbf{I}^v \boldsymbol{\alpha}_2^{\mathrm{T}}) \\
&= q\mathbf{R}_0^{A_1} - q_h \mathbf{R}_h^{A_1} - q_h \mathbf{R}_{n-h}^{A_1} - q_s \mathbf{R}_n^{A_1} - q_v \mathbf{R}_{n+v}^{A_1},
\end{aligned}$$

where $a \in \{0, h, n-h\}$ and $b \in \{0, v\}$. hence, Eq. (6.12) holds for representation A_1.

For other one-dimensional representations A_2, B_1 and B_2, the proof is summarized as follows

$$\begin{aligned}
A_2: \quad & \boldsymbol{\alpha}_1\mathbf{I}^a\boldsymbol{\alpha}_1^{\mathrm{T}} + \boldsymbol{\alpha}_2\mathbf{I}^a\boldsymbol{\alpha}_2^{\mathrm{T}} = \tfrac{1}{2n}\sum_{i=0}^{n-1}[1+(-1)(-1)] = 1 = \mathbf{R}_a^{A_2} \\
& 2\boldsymbol{\alpha}_1\mathbf{I}^b\boldsymbol{\alpha}_2^{\mathrm{T}} = \tfrac{2}{2n}\sum_{i=0}^{n-1}[1\times(-1)] = -1 = \mathbf{R}_{n+b}^{A_2} \\
B_1: \quad & \boldsymbol{\alpha}_1\mathbf{I}^a\boldsymbol{\alpha}_1^{\mathrm{T}} + \boldsymbol{\alpha}_2\mathbf{I}^a\boldsymbol{\alpha}_2^{\mathrm{T}} = \tfrac{2}{2n}\sum_{i=0}^{n-1}(-1)^{i+(i+a)} = (-1)^a = \mathbf{R}_a^{B_1} \\
& 2\boldsymbol{\alpha}_1\mathbf{I}^b\boldsymbol{\alpha}_2^{\mathrm{T}} = \tfrac{2}{2n}\sum_{i=0}^{n-1}(-1)^{i+(i+b)} = (-1)^b = \mathbf{R}_{n+b}^{B_1} \\
B_2: \quad & \boldsymbol{\alpha}_1\mathbf{I}^a\boldsymbol{\alpha}_1^{\mathrm{T}} + \boldsymbol{\alpha}_2\mathbf{I}^a\boldsymbol{\alpha}_2^{\mathrm{T}} = \tfrac{2}{2n}\sum_{i=0}^{n-1}[(-1)^{i+(i+a)} + (-1)^{(i+1)+(i+1+a)}] = (-1)^a = \mathbf{R}_a^{B_2} \\
& 2\boldsymbol{\alpha}_1\mathbf{I}^b\boldsymbol{\alpha}_2^{\mathrm{T}} = \tfrac{2}{2n}\sum_{i=0}^{n-1}(-1)^{i+(i+1+b)} = (-1)^{b+1} = \mathbf{R}_{n+b}^{B_2}.
\end{aligned} \tag{6.17}$$

Therefore, the lemma is true for the blocks $\tilde{\mathbf{E}}^{\mu}$ corresponding one-dimensional representations.

[L2] *Two-dimensional blocks*

Let $\mathbf{T}_r^{E_k}$ and $\mathbf{T}_s^{E_k}$ $(r,s \in \{1,2,3,4\})$ respectively denote the rth and sth rows of $\mathbf{T}^{E_k} \in \Re^{4\times 4}$. Denoting $\mathbf{T}_r^{E_k} = [\boldsymbol{\alpha}_1, \boldsymbol{\alpha}_2]$ and $\mathbf{T}_s^{E_k} = [\boldsymbol{\beta}_1, \boldsymbol{\beta}_2]$, the (r,s)th element $\tilde{E}_{(r,s)}^{E_k}$ of $\tilde{\mathbf{E}}^{E_k}$ can be computed as follows from Eq. (11.5)

$$\begin{aligned}
\tilde{E}_{(r,s)}^{E_k} &= \mathbf{T}_r^{E_k}\mathbf{E}(\mathbf{T}_s^{E_k})^{\mathrm{T}} \\
&= (\boldsymbol{\alpha}_1\mathbf{E}_1\boldsymbol{\beta}_1^{\mathrm{T}} + \boldsymbol{\alpha}_2\mathbf{E}_1\boldsymbol{\beta}_2^{\mathrm{T}}) + (\boldsymbol{\alpha}_1\mathbf{E}_2\boldsymbol{\beta}_2^{\mathrm{T}} + \boldsymbol{\beta}_1\mathbf{E}_2\boldsymbol{\alpha}_2^{\mathrm{T}}) \\
&= (q\sigma_{(r,s)}^0 - q_h\sigma_{(r,s)}^h - q_h\sigma_{(r,s)}^{n-h}) + (-q_s\tau_{(r,s)}^0 - q_v\tau_{(r,s)}^v),
\end{aligned} \tag{6.18}$$

where $\boldsymbol{\alpha}_2\mathbf{E}_2^{\mathrm{T}}\boldsymbol{\beta}_1^{\mathrm{T}} = \boldsymbol{\beta}_1\mathbf{E}_2\boldsymbol{\alpha}_2^{\mathrm{T}}$ has been applied.

From Eq. (11.6), we have

$$\begin{aligned}
\sigma_{(r,s)}^a &= \boldsymbol{\alpha}_1\mathbf{I}^a\boldsymbol{\beta}_1^{\mathrm{T}} + \boldsymbol{\alpha}_2\mathbf{I}^a\boldsymbol{\beta}_2^{\mathrm{T}} \quad \text{with } a \in \{0, h, n-h\} \\
\tau_{(r,s)}^b &= \boldsymbol{\alpha}_1\mathbf{I}^b\boldsymbol{\beta}_2^{\mathrm{T}} + \boldsymbol{\beta}_1\mathbf{I}^b\boldsymbol{\alpha}_2^{\mathrm{T}} \quad \text{with } b \in \{0, v\}.
\end{aligned} \tag{6.19}$$

Consider the case of $(r,s) = (1,1)$ for example. From Eq. (6.19), we have following equations for $a \in \{0, h, n-h\}$ and $b \in \{0, v\}$ since $\boldsymbol{\alpha}_1 = \boldsymbol{\alpha}_2 =$

$$\boldsymbol{\beta}_1 = \boldsymbol{\beta}_2 = \big(C_0, C_k, \ldots, C_{jk}, \ldots, C_{(n-1)k}\big)$$

$$\begin{aligned}
\sigma^a_{(1,1)} &= 2\boldsymbol{\alpha}_1 \mathbf{I}^a \boldsymbol{\alpha}_1^{\mathrm{T}} = 2\sum_{i=0}^{n-1} \frac{C_{ik}}{\sqrt{n}} \frac{C_{(i+a)k}}{\sqrt{n}} = \frac{2}{n}\sum_{i=0}^{n-1} C_{ik}(C_{ik}C_{ak} - S_{ik}S_{ak}) \\
&= \frac{C_{ak}}{n}\sum_{i=0}^{n-1}(1 + C_{2ik}) - \frac{S_{ak}}{n}\sum_{i=0}^{n-1} S_{2ik} = C_{ak} \\
\tau^b_{(1,1)} &= 2\boldsymbol{\alpha}_1 \mathbf{I}^b \boldsymbol{\alpha}_1^{\mathrm{T}} = 2\frac{1}{n}\sum_{i=0}^{n-1} C_{ik}C_{(i+b)k} = \frac{2}{n}\sum_{i=0}^{n-1} C_{ik}(C_{ik}C_{bk} - S_{ik}S_{bk}) = C_{bk},
\end{aligned}$$

where $\sum_{i=0}^{n-1} S_{2ik} = \sum_{i=0}^{n-1} C_{2ik} = 0$ has been applied.

In a similar way, we have the following table for $\sigma^a_{(r,s)}$ $(a \in \{0, h, n-h\})$

$r \backslash s$	1	2	3	4
1	C_{ak}	0	S_{ak}	0
2	0	C_{ak}	0	$-S_{ak}$
3	S_{ak}	0	C_{ak}	0
4	0	$-S_{ak}$	0	C_{ak}

(6.20)

and for $\tau^b_{(r,s)}$ $(b \in \{0, v\})$, we have

$r \backslash s$	1	2	3	4
1	C_{bk}	S_{bk}	0	0
2	S_{bk}	$-C_{bk}$	0	0
3	0	0	C_{bk}	S_{bk}
4	0	0	S_{bk}	$-C_{bk}$

(6.21)

Therefore, we have

$$\begin{aligned}
\begin{pmatrix} \tilde{\mathbf{E}}^{E_k} & \\ & \tilde{\mathbf{E}}^{E_k} \end{pmatrix} &= q \begin{pmatrix} 1 & 0 & 0 & 0 \\ 0 & 1 & 0 & 0 \\ 0 & 0 & 1 & 0 \\ 0 & 0 & 0 & 1 \end{pmatrix} - q_h \begin{pmatrix} C_{hk} & 0 & S_{hk} & 0 \\ 0 & C_{hk} & 0 & -S_{hk} \\ S_{hk} & 0 & C_{hk} & 0 \\ 0 & -S_{hk} & 0 & C_{hk} \end{pmatrix} \\
&\quad - q_h \begin{pmatrix} C_{(n-h)k} & 0 & S_{(n-h)k} & 0 \\ 0 & C_{(n-h)k} & 0 & -S_{(n-h)k} \\ S_{(n-h)k} & 0 & C_{(n-h)k} & 0 \\ 0 & -S_{(n-h)k} & 0 & C_{(n-h)k} \end{pmatrix} \\
&\quad - q_s \begin{pmatrix} 1 & 0 & 0 & 0 \\ 0 & -1 & 0 & 0 \\ 0 & 0 & -1 & 0 \\ 0 & 0 & 0 & -1 \end{pmatrix} - q_v \begin{pmatrix} C_{vk} & S_{vk} & 0 & 0 \\ S_{vk} & -C_{vk} & 0 & 0 \\ 0 & 0 & C_{vk} & S_{vk} \\ 0 & 0 & S_{vk} & -C_{vk} \end{pmatrix}.
\end{aligned}$$

Therefore, the following equation holds

$$\tilde{\mathbf{E}}^{E_k} = q\mathbf{R}_0^{E_k} - q_h\mathbf{R}_h^{E_k} - q_h\mathbf{R}_{n-h}^{E_k} - q_s\mathbf{R}_n^{E_k} - q_v\mathbf{R}_{n+v}^{E_k}, \tag{6.22}$$

since $C_h + C_{n-h} = 2C_h$, $S_h + S_{n-h} = 0$ and

$$\mathbf{R}_0^{E_k} = \begin{pmatrix} 1 & 0 \\ 0 & 1 \end{pmatrix}, \quad \mathbf{R}_h^{E_k} + \mathbf{R}_{n-h}^{E_k} = 2\begin{pmatrix} C_{hk} & 0 \\ 0 & C_{hk} \end{pmatrix},$$
$$\mathbf{R}_n^{E_k} = \begin{pmatrix} 1 & 0 \\ 0 & -1 \end{pmatrix}, \quad \mathbf{R}_{n+v}^{E_k} = \begin{pmatrix} C_{vk} & S_{vk} \\ S_{vk} & -C_{vk} \end{pmatrix},$$

Thus, the lemma also holds for the two-dimensional representations.

In summary, the lemma is proved.

□

Using the following force densities for each type of members that will be derived in the next chapter

$$q_v = -q_s, \quad t = \frac{q_h}{q_v} = +\frac{\sqrt{2-2C_v}}{2(1-C_h)}, \tag{6.23}$$

Eq. (6.12) can be rewritten as follows

$$\frac{1}{q_v}\tilde{\mathbf{E}}^{\mu} = 2t\mathbf{R}_0^{\mu} - t\mathbf{R}_h^{\mu} - t\mathbf{R}_{n-h}^{\mu} + \mathbf{R}_n^{\mu} - \mathbf{R}_{n+v}^{\mu}. \tag{6.24}$$

6.4 Symmetry-adapted Geometrical Stiffness Matrix

In this section, we present the direct strategy for the symmetry-adapted geometrical stiffness matrix, which will be used in the next chapter for the investigation of prestress stability of prismatic tensegrity structures based on the reduced stiffness matrix (quadratic form of the geometrical stiffness matrix with respect to the mechanisms).

From Table 6.1, we can see that the representations E_1 and A_2 respectively stand for symmetry operations on xy- and z-coordinates. Hence, direct sum of them, $E_1 + A_2$, stands for coordinates a node in three-dimensional external

Table 6.3: Reducible representation matrices for external coordinate system.

$$\mathbf{N}_0 = \begin{pmatrix} 1 & 0 & 0 \\ 0 & 1 & 0 \\ 0 & 0 & 1 \end{pmatrix}, \quad \mathbf{N}_h = \begin{pmatrix} C_h & -S_h & 0 \\ S_h & C_h & 0 \\ 0 & 0 & 1 \end{pmatrix} \quad \mathbf{N}_{n-h} = \begin{pmatrix} C_h & S_h & 0 \\ -S_h & C_h & 0 \\ 0 & 0 & 1 \end{pmatrix}$$

$$\mathbf{N}_n = \begin{pmatrix} 1 & 0 & 0 \\ 0 & -1 & 0 \\ 0 & 0 & -1 \end{pmatrix}, \quad \mathbf{N}_{n+v} = \begin{pmatrix} C_v & S_v & 0 \\ S_v & -C_v & 0 \\ 0 & 0 & -1 \end{pmatrix}$$

(Cartesian) coordinate system. External coordinates of the whole structure can be constructed by attaching E_1+A_2 to each node, such that the linear combination of representations of nodal displacements $\Gamma(D)$ can be defined as follows using that of the nodes $\Gamma(N)$

$$\begin{aligned} \Gamma(D) &= \Gamma(N) \times (E_1 + A_2) \\ &= (A_1 + A_2 + (B_1 + B_2) + 2\sum_{k=1}^{p} E_k) \times (E_1 + A_2) \\ &= 3A_1 + 3A_2 + (3B_1 + 3B_2) + 6\sum_{k=1}^{p} E_k, \end{aligned} \tag{6.25}$$

where $\times$ denotes direct product (table of direct product of two representations of dihedral group can be found in many textbooks on group representation theory, e.g., the concise book by Altmann and Herzig (1994)). Similar to $\Gamma(N)$, Eq. (6.25) characterizes structure of the symmetry-adapted geometrical stiffness matrix $\tilde{\mathbf{K}}_G$: the blocks corresponding to the one- and two-dimensional representations are 3-by-3 and 6-by-6 matrices, respectively.

From Eq. (6.25), (reducible) representation matrix $\bar{\mathbf{R}}_m^\mu$ of the mth operation of nodal displacements can be formulated as follows using the direct sum of irreducible matrices of E_1 and A_2:

$$\bar{\mathbf{R}}_m^\mu = \mathbf{R}_m^\mu \otimes \begin{pmatrix} \mathbf{R}_m^{E_1} & 0 \\ \mathbf{O} & \mathbf{R}_m^{A_2} \end{pmatrix} = \mathbf{R}_m^\mu \otimes \mathbf{N}_m \tag{6.26}$$

$$\text{or} \quad \bar{\mathbf{R}}_m^\mu = \mathbf{N}_m \otimes \mathbf{R}^\mu, \tag{6.27}$$

where $\mathbf{N}_m$ for $m \in \{0, h, n-h, n, n+v\}$ are listed in Table 6.3. These two formulations are equivalent, and we will consider only Eq. (6.26) in the following.

Similarly to the symmetry-adapted force density matrix, we have the following lemma for the symmetry-adapted geometrical stiffness matrix $\tilde{\mathbf{K}}_G$.

Lemma 6.2 *The blocks $\tilde{\mathbf{K}}_G^{\mu}$ of the symmetry-adapted geometrical stiffness matrix $\tilde{\mathbf{K}}_G$ can be written in a general form as*

$$\frac{1}{q_v}\tilde{\mathbf{K}}_G^{\mu} = 2t\bar{\mathbf{R}}_0^{\mu} - t\bar{\mathbf{R}}_h^{\mu} - t\bar{\mathbf{R}}_{n-h}^{\mu} + \bar{\mathbf{R}}_n^{\mu} - \bar{\mathbf{R}}_{n+v}^{\mu}. \tag{6.28}$$

Proof. Lemma 2 can be proved in a similar manner as Lemma 1 using the transformation matrix, which is constructed from the reducible matrix representations as in Eq. (6.26). And the detailed proof is skipped here. □

From Eq. (6.28), the blocks $\tilde{\mathbf{K}}_G^{A_1}$ and $\tilde{\mathbf{K}}_G^{A_2}$ can be written as

$$\begin{aligned}
\frac{1}{q_v}\tilde{\mathbf{K}}_G^{A_1} &= \begin{pmatrix} 2t(1-C_h)+1-C_v & -S_v & 0 \\ -S_v & 2t(1-C_h)-1+C_v & 0 \\ 0 & 0 & 0 \end{pmatrix} \\
\frac{1}{q_v}\tilde{\mathbf{K}}_G^{A_2} &= \begin{pmatrix} 2t(1-C_h)-1+C_v & S_v & 0 \\ S_v & 2t(1-C_h)+1-C_v & 0 \\ 0 & 0 & 0 \end{pmatrix}.
\end{aligned} \tag{6.29}$$

It is easy to verify that the eigenvalues of $\tilde{\mathbf{K}}_G^{A_1}$ are the same as those of $\tilde{\mathbf{E}}^{E_1}$ and $\tilde{\mathbf{E}}^{A_2}$; similar relationship between the eigenvalues of $\tilde{\mathbf{K}}_G^{A_2}$ and $\tilde{\mathbf{E}}^{E_1}$, $\tilde{\mathbf{E}}^{A_1}$ also holds. This can also be interpreted using the direct product of representation A_1 (or A_2) of the force density matrix and the representation $(E_1 + A_2)$ of the attached Cartesian coordinate system as

$$\begin{aligned}
A_1 \times (E_1 + A_2) &= E_1 + A_2 \\
A_2 \times (E_1 + A_2) &= E_1 + A_1.
\end{aligned} \tag{6.30}$$

In a similar way, relationships between the eigenvalues of symmetry-adapted forms of the force density matrix and the geometrical stiffness matrices are summarized in Table 6.4.

Blocks $\tilde{\mathbf{K}}_G^{B_1}$ and $\tilde{\mathbf{K}}_G^{B_2}$, when they exist for n even, are

$$\begin{aligned}
\frac{1}{q_v}\tilde{\mathbf{K}}_G^{B_1} &= \begin{pmatrix} \phi_1 & (-1)^{v+1}S_v & 0 \\ (-1)^{v+1} & \phi_2 & 0 \\ 0 & 0 & \phi_3 \end{pmatrix} \\
\frac{1}{q_v}\tilde{\mathbf{K}}_G^{B_2} &= \begin{pmatrix} \phi_4 & (-1)^{v}S_v & 0 \\ (-1)^{v} & \phi_5 & 0 \\ 0 & 0 & \phi_6 \end{pmatrix},
\end{aligned} \tag{6.31}$$

Table 6.4: Relationships between eigenvalues of symmetry-adapted forms of the geometrical stiffness matrix and the force density matrix.

$\tilde{\mathbf{K}}_G^{\mu}$	$\tilde{\mathbf{E}}^{\mu}$						n
$3A_1$		A_2			E_1			
$3A_2$	A_1				E_1			
$3B_1$				B_2			E_p	even
$3B_2$			B_1				E_p	even
$6E_1$	A_1	A_2			E_1	E_2		
$6E_k$					E_{k-1}	E_k	E_{k+1}	
$6E_p$						E_{p-1}	$2E_p$	odd
$6E_p$			B_1	B_2		E_{p-1}	E_p	even

where

$$\begin{array}{ll} \phi_1 = 2t(1-(-1)^h C_h) + 1 - (-1)^v C_v & \phi_2 = 2t(1-(-1)^h C_h) - 1 + (-1)^v C_v \\ \phi_3 = 2t(1-(-1)^h) - 1 + (-1)^v & \phi_4 = 2t(1-(-1)^h C_h) + 1 + (-1)^v C_v \\ \phi_5 = 2t(1-(-1)^h C_h) - 1 - (-1)^v C_v & \phi_6 = 2t(1-(-1)^h) - 1 - (-1)^v \end{array} . \tag{6.32}$$

And blocks $\tilde{\mathbf{K}}_G^{E_k}$ of the two-dimensional representations E_k are

$$\frac{1}{q_v}\tilde{\mathbf{K}}_G^{E_k} = \begin{pmatrix} \varphi_1+\varphi_2 & -\varphi_3 & 0 & -\varphi_4 & -\varphi_5-\varphi_6 & 0 \\ -\varphi_3 & \varphi_1-\varphi_2 & 0 & \varphi_5-\varphi_6 & \varphi_4 & 0 \\ 0 & 0 & \varphi_7-\varphi_8 & & 0 & \varphi_9 \\ -\varphi_4 & \varphi_5-\varphi_6 & 0 & \varphi_1-\varphi_2 & \varphi_3 & 0 \\ -\varphi_5-\varphi_6 & \varphi_4 & 0 & \varphi_3 & \varphi_1+\varphi_2 & 0 \\ 0 & & \varphi_9 & 0 & 0 & \varphi_7+\varphi_8 \end{pmatrix}, \tag{6.33}$$

where

$$\begin{array}{lll} \varphi_1 = 2t(1-C_hC_{hk}) & \varphi_2 = 1 - C_vC_{vk} & \varphi_3 = S_vC_{vk} \\ \varphi_4 = C_vS_{vk} & \varphi_5 = 2tS_hS_{hk} & \varphi_6 = S_vS_{vk} \\ \varphi_7 = 2t(1-C_{hk}) & \varphi_8 = 1 - C_{vk} & \varphi_9 = S_{vk}. \end{array} \tag{6.34}$$

6.5 Symmetry-adapted Equilibrium Matrix

This section presents the symmetry-adapted equilibrium matrix $\tilde{\mathbf{D}}$ and the mechanisms $\tilde{\mathbf{M}}$ lying in the null-space of its transpose $\tilde{\mathbf{D}}^{\mathrm{T}}$.

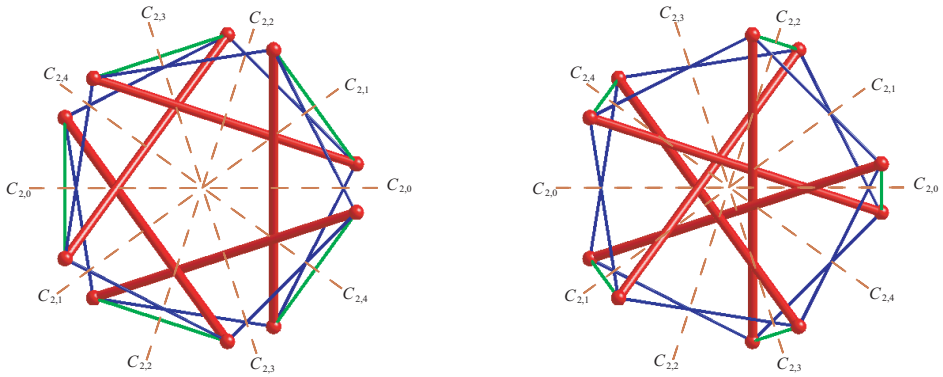

(a) $h = 1, v = 1$ (b) $h = 1, v = 2$

Figure 6.2: Structures $\mathbf{D}_n^{h,v}$ with $n(= 5)$ odd. One strut and one vertical cable remain unchanged by any two-fold rotations, and all of them are transformed to different struts by n-fold rotations except for identity operation.

6.5.1 Block Structure

Unlike the force density matrix $\mathbf{E}$ or the geometrical stiffness matrix $\mathbf{K}_G$, the equilibrium matrix $\mathbf{D} \in \Re^{6n \times 4n}$ of a prismatic tensegrity structure is not square. In conventional methods, the symmetry-adapted equilibrium matrix $\tilde{\mathbf{D}}$ can be computed as follows using the transformation matrices $\mathbf{T}_D$ and $\mathbf{T}_M$ respectively for external and internal coordinate systems (see, for example, Kangwai and Guest (2000) or Kawaguchi and Suzuki (2005))

$$\underset{6n\times 4n}{\tilde{\mathbf{D}}} = \underset{6n\times 6n}{\mathbf{T}_D}\ \mathbf{D}\big(\underset{4n\times 4n}{\mathbf{T}_M}\big)^{\mathrm{T}} \tag{6.35}$$

To make clear the structure of $\tilde{\mathbf{D}}$, we firstly investigate linear combination of representations of its members (internal coordinates). It should be noted that different types of members cannot be transformed to each other by any symmetry operation. Thus, the horizontal cables, struts and vertical cables should be considered separately.

6.5.1.1 Horizontal Cables

Because horizontal cables have one-to-one correspondence to symmetry operations as the nodes, the linear combination $\Gamma(M_h)$ of the representations of them

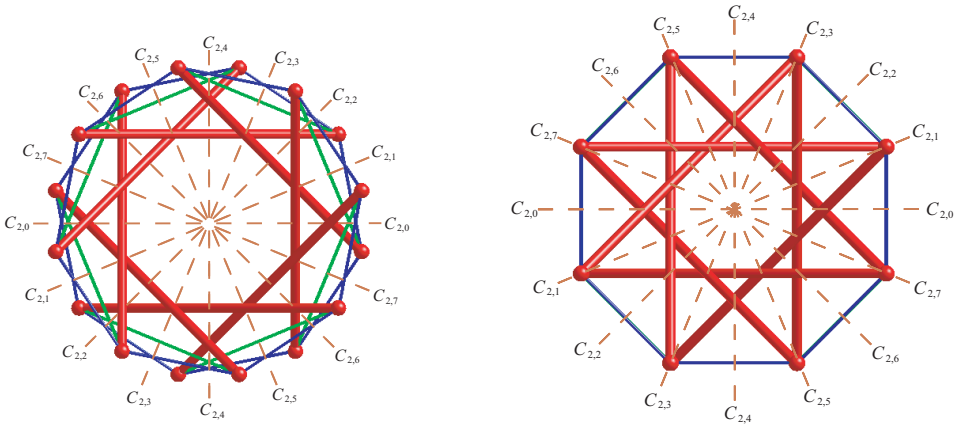

(a) $h = 1, v = 1$ (b) $h = 1, v = 2$

Figure 6.3: Structures $\mathbf{D}_n^{h,v}$ with $n(=8)$ even. Two struts remain unchanged by a two-fold rotation $C_{2,2i}$, and all struts are transformed to other struts by $C_{2,2i+1}$. All vertical cables are changed by $C_{2,2i}$, and two are unchanged by $C_{2,2i+1}$ for v odd; Two vertical cables are unchanged by $C_{2,2i}$, and all are changed by $C_{2,2i+1}$ for v even.

is the same as that of the nodes, which is

$$\Gamma(M_h) = A_1 + A_2 + (B_1 + B_2) + 2\sum_{k=1}^{p} E_k \tag{6.36}$$

6.5.1.2 Struts and Vertical Cables

Struts or vertical cables have one-to-two correspondence to symmetry operations; i.e., there are in total two symmetry operations that can transform a member to itself. To derive the linear combinations of their representations, we need to consider the following cases.

[L1] *n odd*

When n is odd, there are always one strut and one vertical cable remain unchanged by any two-fold rotation (see the structures with $\mathbf{D}_5$ symmetry shown in Fig. 6.2 as an example). Hence, we have

$$\Gamma(M_s) = \Gamma(M_v) = \{n, 0, 0, \ldots, 0;\ 1, 1, \ldots, 1\} = A_1 + \sum_{k=1}^{p} E_k \tag{6.37}$$

[L2] *n even*

For any two-fold rotation about $C_{2,2i}$ $(i = 0, 1, \ldots, n-1)$ axis, there are always two struts remain unchanged while all struts change their positions by the two-fold rotations about $C_{2,2i+1}$ axes. Therefore

$$\Gamma(M_s) = \{n, 0, 0, \ldots, 0;\ 2, 0, 2, 0, \ldots, 2, 0\} = A_1 + B_1 + \sum_{k=1}^{p} E_k \qquad (6.38)$$

For the linear combination of vertical cables, we need to consider the following two cases dependent on their connectivity v

(a) *v odd:* e.g., Fig. 6.3.(a)

For any two-fold rotation about $C_{2,2i}$ axis, all vertical cables change their positions, while there are always two vertical cables remain unchanged for any two-fold rotation about $C_{2,2i+1}$ axis, so we have

$$\Gamma(M_v) = \{n, 0, 0, \ldots, 0;\ 0, 2, 0, 2, \ldots, 0, 2\} = A_1 + B_2 + \sum_{k=1}^{p} E_k \quad (6.39)$$

(b) *v even:* e.g., Fig. 6.3.(b)

By applying any two-fold rotation about $C_{2,2i}$ axis, two vertical cables remain unchanged, while all are changed by applying any $C_{2,2i+1}$ rotation, thus

$$\Gamma(M_v) = \{n, 0, 0, \ldots, 0;\ 2, 0, 2, 0, \ldots, 2, 0\} = A_1 + B_1 + \sum_{k=1}^{p} E_k \quad (6.40)$$

The linear combinations of representations of the horizontal cables $\Gamma(M_h)$, struts $\Gamma(M_s)$ and vertical cables $\Gamma(M_v)$ are summarized as

	v odd	v even
$\Gamma(M_h)$	$A_1 + A_2 + (B_1 + B_2) + 2\sum_{k=1}^{p} E_k$	
$\Gamma(M_s)$	$A_1 + (B_1) + \sum_{k=1}^{p} E_k$	
$\Gamma(M_v)$	$A_1 + (B_2) + \sum_{k=1}^{p} E_k$	$A_1 + (B_1) + \sum_{k=1}^{p} E_k$
$\Gamma(M)$	$3A_1 + A_2 + (2B_1 + 2B_2) + 4\sum_{k=1}^{p} E_k$	$3A_1 + A_2 + (3B_1 + B_2) + 4\sum_{k=1}^{p} E_k$

(6.41)

Structure of $\tilde{\mathbf{D}}$ can be elucidated based on the linear combination $\Gamma(D)$ of representations of displacements in Eq. (6.25) and that $\Gamma(M)$ of members in Eq. (6.41). For example, the A_1 block $\tilde{\mathbf{D}}^{A_1}$ is a 3-by-3 matrix, because there are three A_1 representations in both of $\Gamma(D)$ and $\Gamma(M)$. Furthermore, columns of $\tilde{\mathbf{D}}^{A_1}$ come from the horizontal cables, struts and vertical cables separately, because all of $\Gamma(M_h)$, $\Gamma(M_s)$ and $\Gamma(M_v)$ have one representation A_1. Similarly, $\tilde{\mathbf{D}}^{A_2}$ is a 3-by-1 matrix (vector), and the only column comes from the horizontal cables because there is no representation A_2 exists for struts or vertical cables. The structure of other blocks can be identified based on $\Gamma(D)$ and $\Gamma(M)$ in a similar manner.

6.5.2 Unitary Member Direction

The concept of unitary member direction introduced in this subsection has a vital role in deriving the symmetry-adapted equilibrium matrix, and then, the mechanisms.

The equilibrium matrix $\mathbf{D}$ can be formulated as follows (see details in Chapter 2)

$$\mathbf{D} = \begin{pmatrix} \mathbf{D}^x \\ \mathbf{D}^y \\ \mathbf{D}^z \end{pmatrix} = \begin{pmatrix} \mathbf{C}^{\mathrm{T}}\mathbf{U}\mathbf{L}^{-1} \\ \mathbf{C}^{\mathrm{T}}\mathbf{V}\mathbf{L}^{-1} \\ \mathbf{C}^{\mathrm{T}}\mathbf{W}\mathbf{L}^{-1} \end{pmatrix}, \tag{6.42}$$

where $\mathbf{C} \in \Re^{4n\times 2n}$ describes connectivity of the structure; $\mathbf{U}$, $\mathbf{V}$ and $\mathbf{W}$ ($\in \Re^{4n\times 4n}$) are diagonal matrices, of which the diagonal entries are coordinate differences in each of directions x, y and z; and $\mathbf{L}\in \Re^{4n\times 4n}$ is a diagonal matrix, of which diagonal entries are member lengths. Hence, diagonal entries of $\mathbf{U}\mathbf{L}^{-1}$, $\mathbf{U}\mathbf{L}^{-1}$, and $\mathbf{U}\mathbf{L}^{-1}$ are components of the unitary member directions in each direction. When we apply transformation matrices to $\mathbf{D}$ to derive its symmetry-adapted form $\tilde{\mathbf{D}}$ as in Eq. (6.35), we are actually dealing with the unitary member directions. Hence, the symmetry-adapted equilibrium matrix can be directly derived using these unitary member directions.

Consider a unit cell of the structure as shown in Fig. 6.4. The coordinate of the reference node can be written in a general form as follows (details for them

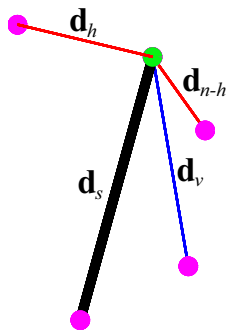

Figure 6.4: Unit cell of prismatic tensegrity structures with dihedral symmetry. Every node is connected by two horizontal cables, one vertical cable and one strut.

can be found in Chapter 7)

$$\mathbf{X}_0 = \begin{pmatrix} x_0 \\ y_0 \\ z_0 \end{pmatrix} = \begin{pmatrix} C_v - 1 + \sqrt{2(1-C_v)} \\ S_v \\ \frac{H}{2} \end{pmatrix} = \begin{pmatrix} 2S_{v/2}(1-S_{v/2}) \\ S_v \\ \frac{H}{2} \end{pmatrix} \tag{6.43}$$

where H denotes height(-to-radius ratio) of the structure. Other nodes of the structure can be determined using symmetry operations.

Denote the lengths of the strut, horizontal cable and vertical cable as l_s, l_h and l_v, respectively. The unitary directions $\mathbf{d}_h$ and $\mathbf{d}_{n-h}$ of the two horizontal cables connected to the reference node can be computed as

$$\begin{aligned} l_h\mathbf{d}_h &= \mathbf{X}_0 - \mathbf{N}_h\mathbf{X}_0 = \begin{pmatrix} x_0 - C_h x_0 + S_h y_0 \\ y_0 - C_h y_0 - S_h x_0 \\ 0 \end{pmatrix} = 4S_{\frac{h}{2}}S_{\frac{v}{2}} \begin{pmatrix} C_{\frac{h+v}{2}} + S_{\frac{h}{2}} \\ S_{\frac{h+v}{2}} - C_{\frac{h}{2}} \\ 0 \end{pmatrix}, \\ l_h\mathbf{d}_{n-h} &= \mathbf{X}_0 - \mathbf{N}_{n-h}\mathbf{X}_0 = \begin{pmatrix} x_0 - C_h x_0 - S_h y_0 \\ y_0 - C_h y_0 + S_h x_0 \\ 0 \end{pmatrix} = 4S_{\frac{h}{2}}S_{\frac{v}{2}} \begin{pmatrix} -C_{\frac{h-v}{2}} + S_{\frac{h}{2}} \\ S_{\frac{h-v}{2}} + C_{\frac{h}{2}} \\ 0 \end{pmatrix} \end{aligned} \tag{6.44}$$

(6.45)

Thus,

$$\mathbf{d}_h + \mathbf{d}_{n-h} = \frac{8S_{\frac{h}{2}}^2 S_{\frac{v}{2}}}{l_h} \begin{pmatrix} 1 - S_{\frac{v}{2}} \\ C_{\frac{v}{2}} \\ 0 \end{pmatrix}. \tag{6.46}$$

Unitary directions of the strut $\mathbf{d}_s$ and vertical cable $\mathbf{d}_v$ are

$$
\begin{aligned}
l_s\mathbf{d}_s &= \mathbf{X}_0 - \mathbf{N}_n\mathbf{X}_0 = \begin{pmatrix} 0 \\ 2y_0 \\ H \end{pmatrix} = \begin{pmatrix} 0 \\ 2S_v \\ H \end{pmatrix}, \\
l_v\mathbf{d}_v &= \mathbf{X}_0 - \mathbf{N}_{n+v}\mathbf{X}_0 = \begin{pmatrix} x_0 - C_v x_0 - S_v y_0 \\ y_0 + C_v y_0 - S_v x_0 \\ H \end{pmatrix} = 4S_{\frac{v}{2}}(1 - S_{\frac{v}{2}}) \begin{pmatrix} -S_{\frac{v}{2}} \\ C_{\frac{v}{2}} \\ \bar{H} \end{pmatrix}
\end{aligned} \tag{6.47}
$$

where $\bar{H} = H/[4S_{\frac{v}{2}}(1 - S_{\frac{v}{2}})]$.

6.5.3 Symmetry-adapted Formulation and its Mechanisms

It should be noticed again that there is only one symmetry operation of dihedral group that can take one horizontal cable to another, while there are two different symmetry operations for struts and vertical cables. Hence, rows of $\mathbf{T}_M$ corresponding to different members will have different norms, and this difference should be taken into account in the direct strategy for $\tilde{\mathbf{D}}$, because $\mathbf{T}_M$ is applied on only one side of $\mathbf{D}$ as in Eq. (6.35).

For a one-dimensional representation μ, the transformation matrix ${}_h\mathbf{T}^{\mu}_M$ for horizontal cables is the same as that for the nodes, since both of them have one-to-one correspondence with the symmetry operations:

$$
{}_h\mathbf{T}^{\mu}_M = \frac{1}{\sqrt{2n}} \left(\mathbf{R}^{\mu}_0, \ldots, \mathbf{R}^{\mu}_j, \ldots, \mathbf{R}^{\mu}_{2n-1} \right). \tag{6.48}
$$

Since the jth and $(n+j)$th ($j = \in \{0, \ldots, n-1\}$) symmetry operations take the strut connected by nodes N_j and N_{n+j} to itself, the transformation matrix ${}_s\mathbf{T}^{\mu}_M$ for struts can be written as

$$
{}_s\mathbf{T}^{\mu}_M = \frac{1}{\sqrt{4n}} \left(\mathbf{R}^{\mu}_0 + \mathbf{R}^{\mu}_n, \ldots, \mathbf{R}^{\mu}_j + \mathbf{R}^{\mu}_{n+j}, \ldots, \mathbf{R}^{\mu}_{n-1} + \mathbf{R}^{\mu}_{2n-1} \right); \tag{6.49}
$$

and similarly, ${}_v\mathbf{T}^{\mu}_M$ for vertical cables is

$$
\begin{aligned}
{}_v\mathbf{T}^{\mu}_M = \frac{1}{\sqrt{4n}} \quad & \left(\mathbf{R}^{\mu}_0 + \mathbf{R}^{\mu}_{n+v}, \ldots, \mathbf{R}^{\mu}_j + \mathbf{R}^{\mu}_{n+j+v}, \ldots, \mathbf{R}^{\mu}_{n-1-v} + \mathbf{R}^{\mu}_{2n-1}, \right. \\
& \left. \mathbf{R}^{\mu}_{n-v} + \mathbf{R}^{\mu}_n, \ldots, \mathbf{R}^{\mu}_{n-1} + \mathbf{R}^{\mu}_{n-1+v} \right).
\end{aligned} \tag{6.50}
$$

Note that there are $2n$ entries in ${}_h\mathbf{T}^{\mu}_M$ but only n entries in ${}_s\mathbf{T}^{\mu}_M$ and ${}_v\mathbf{T}^{\mu}_M$, which are identical to the number of these different types of members. Furthermore,

the linear combinations of representations for struts and vertical cables can also be identified considering entries of ${}_s\mathbf{T}_M^{\mu}$ and ${}_v\mathbf{T}_M^{\mu}$. Consider representation A_1 for example, $\mathbf{R}_j^{A_1} = 1$ holds for all operations ($\forall j \in \{1, \ldots, 2n-1\}$) such that $\mathbf{R}_j^{A_1} + \mathbf{R}_{n+j}^{A_1} = 2 \neq 0$ and $\mathbf{R}_j^{A_1} + \mathbf{R}_{n+j+v}^{A_1} = 2 \neq 0$, hence, both struts and vertical cables have A_1 representation. However, we have $\mathbf{R}_j^{A_2} + \mathbf{R}_{n+j}^{A_2} = 1 + (-1) = 0$ and $\mathbf{R}_j^{A_2} + \mathbf{R}_{n+j+v}^{A_2} = 1 + (-1) = 0$ for representation A_2, from which we learn that struts and vertical cables do not have representation A_2. In a similar way, we can identify that struts have representation B_1 for n even since $\mathbf{R}_j^{B_1} + \mathbf{R}_{n+j}^{B_1} = (-1)^{j+1} + (-1)^{n+j+1} \neq 0$, but do not have representation B_2 since $\mathbf{R}_j^{B_2} + \mathbf{R}_{n+j}^{B_2} = (-1)^{j+1} + (-1)^{n+j} = 0$. And it is easy to show that vertical cables have representation B_1 for v odd, and B_2 for v odd, when they exist for n even.

For a two-dimensional representation E_k, transformation matrix ${}_h\mathbf{T}_M^{E_k} \in \Re^{4\times 2n}$ for the horizontal cables is again the same as that for nodes given in Eq. (6.11). For the struts and vertical cables, the transformation matrices are respectively written as follows

$$
\begin{aligned}
{}_s\bar{\mathbf{T}}_M^{E_k} &= \begin{pmatrix} (C_{jk} + C_{jk}) \\ -(S_{jk} + S_{jk}) \\ (S_{jk} + S_{jk}) \\ (C_{jk} + (-C_{jk})) \end{pmatrix} = \begin{pmatrix} (2C_{jk}) \\ (0) \\ (2S_{jk}) \\ (0) \end{pmatrix}, \\
{}_v\bar{\mathbf{T}}_M^{E_k} &= \begin{pmatrix} (C_{jk} + C_{(j+v)k}) \\ -(S_{jk} + S_{(j+v)k}) \\ (S_{jk} + S_{(j+v)k}) \\ (C_{jk} + (-C_{(j+v)k})) \end{pmatrix} = 2 \begin{pmatrix} (C_{(j+\frac{1}{2}v)k} C_{\frac{vk}{2}}) \\ -(C_{(j+\frac{1}{2}v)k} S_{\frac{vk}{2}}) \\ (S_{(j+\frac{1}{2}v)k} C_{\frac{vk}{2}}) \\ (S_{(j+\frac{1}{2}v)k} S_{\frac{vk}{2}}) \end{pmatrix} \quad \text{for } j = 0, \ldots, n-1. \qquad (6.51)
\end{aligned}
$$

It is apparent that the first and the second rows, and the third and the fourth rows are dependent, hence, only the first and the third rows need to be contained in the transformation matrices ${}_s\mathbf{T}_M^{E_k}$ and ${}_h\mathbf{T}_M^{\mu}$ ($\in \Re^{2\times n}$), which are normalized as

$$
\begin{aligned}
{}_s\mathbf{T}_M^{E_k} &= \frac{1}{\sqrt{2n}} \begin{pmatrix} (2C_{jk}) \\ (2S_{jk}) \end{pmatrix}, \\
{}_v\mathbf{T}_M^{E_k} &= \frac{1}{\sqrt{n(1+C_{vk})}} \begin{pmatrix} (C_{jk} + C_{(j+v)k}) \\ (S_{jk} + S_{(j+v)k}) \end{pmatrix} \quad \text{for } j = 0, \ldots, n-1. \qquad (6.52)
\end{aligned}
$$

Transformation matrix $\mathbf{T}_M^{\mu}$ of the members for the representation μ can then

Table 6.5: Norms for transformation matrices in internal coordinate system for different types of members.

Representation\ Member	Horizontal	Strut	Vertical
One-dimensional	$\sqrt{2n}$	$\sqrt{4n}$	$\sqrt{4n}$
Two-dimensional	$\sqrt{n}$	$\sqrt{2n}$	$\sqrt{n(1+C_{vk})}$

be combined as

$$\mathbf{T}_M^{\mu} = \begin{pmatrix} {}_h\mathbf{T}_M^{\mu} & \mathbf{O} & \mathbf{O} \\ \mathbf{O} & {}_s\mathbf{T}_M^{\mu} & \mathbf{O} \\ \mathbf{O} & \mathbf{O} & {}_v\mathbf{T}_M^{\mu} \end{pmatrix}, \tag{6.53}$$

and that $\mathbf{T}_M \in \Re^{4n\times 4n}$ of the members for all representations can be further assembled as

$$\mathbf{T}_M = \begin{pmatrix} \mathbf{T}_M^{A_1} \\ \mathbf{T}_M^{A_2} \\ \vdots \\ \mathbf{T}_M^{E_p} \end{pmatrix} \tag{6.54}$$

Notice from the formulations of transformation matrices that, the transform matrix for horizontal cables, which is not normalized with the entries coming directly from the irreducible representation matrices, has different norms compared to those for vertical cables and struts. These norms are used to make the transformation matrices unitary, and are listed in Table 6.5 for different types of members as well as representations.

As indicated in the formulations of the equilibrium matrix $\mathbf{D}$ and its transformation matrices, components of its symmetry-adapted form $\tilde{\mathbf{D}}$ can be separately formulated for different types of members. Since horizontal cables have one-to-one correspondence with the symmetry operations, their symmetry-adapted components $\tilde{\mathbf{D}}_h^{\mu}$ for representation μ can be directly formulated as follows using its unitary member directions $\mathbf{d}_h$ and $\mathbf{d}_{n-h}$

$$\tilde{\mathbf{D}}_h^{\mu} = \mathbf{R}_0^{\mu} \otimes \mathbf{d}_h + \mathbf{R}_h^{\mu} \otimes \mathbf{d}_{n-h}, \tag{6.55}$$

in a similar way to the formulation of the symmetry-adapted geometrical stiffness matrix presented in Section 4.

The symmetry-adapted components $\tilde{\mathbf{D}}_s^\mu$ of struts and $\tilde{\mathbf{D}}_v^\mu$ of vertical cables can be formulated as follows similarly to that of horizontal cables in Eq. (6.56)

$$\tilde{\mathbf{D}}_s^\mu = \frac{1}{a_s^\mu}(\bar{\mathbf{R}}_0^\mu + \bar{\mathbf{R}}_n^\mu) \otimes \mathbf{d}_s \text{ and } \tilde{\mathbf{D}}_v^\mu = \frac{1}{a_v^\mu}(\bar{\mathbf{R}}_v^\mu + \bar{\mathbf{R}}_{n+v}^\mu) \otimes \mathbf{d}_v \tag{6.56}$$

where $a_s^\mu = a_v^\mu = \sqrt{2}$ for one-dimensional representation and $a_s^\mu = \sqrt{2}$, $a_v^\mu = \sqrt{1 + C_{vk}}$ for two-dimensional representation, taking into account of the difference between the norm of the horizontal cables and those of the vertical cables and struts as listed in Table 6.5. These coefficients are necessary because the vertical cables and struts have one-to-two correspondence with the symmetry operations. Moreover, $\bar{\mathbf{R}}_j^\mu = \mathbf{R}_j^\mu$ for one-dimensional representations, and

$$\bar{\mathbf{R}}_j^{E_k} = \begin{pmatrix} C_{jk} \\ S_{jk} \end{pmatrix} \tag{6.57}$$

for two-dimensional representations $\mu = E_k$, because of interdependence between some specific components of the irreducible representation matrices for vertical cables and struts as discussed in Eq. (6.51); this indeed agrees with the dimensions of the equilibrium matrix for the components of these two types of members.

For convenience, we write the symmetry-adapted components of all types of members corresponding to each representation μ together in a form as

$$\mathbf{D}^\mu = \begin{pmatrix} \mathbf{D}_h^\mu & \mathbf{D}_s^\mu & \mathbf{D}_v^\mu \end{pmatrix}. \tag{6.58}$$

Since all types of members consist of representation A_1, $\tilde{\mathbf{D}}^{A_1}$ can be formulated as

$$\underset{3\times3}{\tilde{\mathbf{D}}^{A_1}} = \begin{pmatrix} \mathbf{d}_h + \mathbf{d}_{n-h}, & \frac{1+1}{\sqrt{2}}\mathbf{d}_s, & \frac{1+1}{\sqrt{2}}\mathbf{d}_v \end{pmatrix} = \begin{pmatrix} \mathbf{d}_h + \mathbf{d}_{n-h}, & \sqrt{2}\mathbf{d}_s, & \sqrt{2}\mathbf{d}_v \end{pmatrix} \tag{6.59}$$

$\tilde{\mathbf{D}}^{A_1}$ is singular, because its three columns are linear independent. To verify the independency of these vectors, we need only to figure out whether there exists a non-zero coefficient a that satisfies the following equation considering the scaled versions of the three columns of $\tilde{\mathbf{D}}^{A_1}$ from Eqs. (6.46) and (6.47)

$$\begin{pmatrix} -4S_{\frac{v}{2}}^2(1 - S_{\frac{v}{2}}) \\ 2S_v(1 - S_{\frac{v}{2}}) \\ H \end{pmatrix} = a \begin{pmatrix} 1 - S_{\frac{v}{2}} \\ C_{\frac{v}{2}} \\ 0 \end{pmatrix} + \begin{pmatrix} 0 \\ 2S_v \\ H \end{pmatrix} \tag{6.60}$$

where the vector on the left-hand side of the equation is the scaled version of $\mathbf{d}_v$ by $\frac{1}{l_v}$ as $\frac{1}{l_v}\mathbf{d}_v$, and the first and second vectors on right-hand side are those of $\mathbf{d}_h + \mathbf{d}_{n-h}$ by $\frac{1}{S^2_{\frac{h}{2}} S_{\frac{v}{2}}}$ and $\mathbf{d}_s$ by $\frac{1}{l_s}$, respectively. The above equation holds for $a = -4S^2_{\frac{v}{2}} \neq 0$, such that the three columns in $\tilde{\mathbf{D}}^{A_1}$ are linear independent, and therefore, $\tilde{\mathbf{D}}^{A_1}$ is singular with rank deficiency of one.

Denote the numbers of self-stress modes and mechanisms, including rigid-body motions, as n^s and n^m, respectively. For a structure with $\mathbf{D}_n$ symmetry, the equilibrium matrix $\mathbf{D}$ of which is a $6n$-by-$4n$ matrix, we have (Calladine, 1978)

$$n^m - n^s = 6n - 4n = 2n. \tag{6.61}$$

We observe from the force densities obtained in Eq. (7.24) that, the structure consists only one possible relation between different types of members. Hence, it has only one mode of self-stresses, such that $n^s = 1$. Therefore, the number n^m of mechanisms of the structure including rigid-body motions is

$$n^m = n^s + 2n = 2n + 1. \tag{6.62}$$

To see which blocks these mechanisms are lying in, we consider the minimum rank deficiency of each block by calculating $\Gamma(D) - \Gamma(M)$ for v even

$$\begin{aligned}
\Gamma(D) - \Gamma(M) &= (3A_1 + 3A_2 + (3B_1 + 3B_2+)6\sum_{k=1}^{p} E_k) \\
&\quad -(3A_1 + A2 + (2B_1 + 2B_2+)4\sum_{k=1}^{p} E_k) \\
&= 2A_2 + (2B_2) + 2\sum_{k=1}^{p} E_k,
\end{aligned}$$

and for v odd

$$\begin{aligned}
\Gamma(D) - \Gamma(M) &= (3A_1 + 3A_2 + (3B_1 + 3B_2+)6\sum_{k=1}^{p} E_k) \\
&\quad -(3A_1 + A2 + (3B_1 + B_2+)4\sum_{k=1}^{p} E_k) \\
&= 2A_2 + (B_1 + B_2) + 2\sum_{k=1}^{p} E_k,
\end{aligned}$$

from which it is apparent that the block $\tilde{\mathbf{D}}^{A_2}$ has rank deficiency of at least two no matter v is even or odd, since it is a 3-by-1 matrix; and rank deficiencies of other blocks can be calculated in a similar way. To sum up, rank deficiency of the equilibrium matrix is at least $2n$ in total for all cases, because $2+(2+)2\sum_{k=1}^{p} 2 = 2+(1+1+)2\sum_{k=1}^{p} 2 = 2n$. Since at least $2n$ of the $2n+1$ mechanisms of the structure lie in the null-space of the blocks expect for $\tilde{\mathbf{D}}^{A_1}$ from $\Gamma(D)-\Gamma(M)$, and furthermore, $\tilde{\mathbf{D}}^{A_1}$ is singular with rank deficiency of at least one, all blocks in $\tilde{\mathbf{D}}$ except for $\tilde{\mathbf{D}}^{A_1}$ are full-rank; and the rank deficiencies of these blocks are characterized by the number of corresponding representations present in $\Gamma(D)-\Gamma(M)$.

Only horizontal cables have A_2 representation, thus

$$\tilde{\mathbf{D}}^{A_2} = \begin{pmatrix} \mathbf{d}_h + \mathbf{d}_{n-h} \end{pmatrix}. \tag{6.63}$$

The two mechanisms lying in the null-space of its transpose $(\tilde{\mathbf{D}}^{A_2})^{\mathrm{T}}$ are

$$\mathbf{d}_1^{A_2} = \begin{pmatrix} 1+S_{\frac{v}{2}} \\ -C_{\frac{v}{2}} \\ 0 \end{pmatrix} \text{ and } \mathbf{d}_2^{A_2} = \begin{pmatrix} 0 \\ 0 \\ 1 \end{pmatrix}. \tag{6.64}$$

When n is even, the struts have representation B_1; the horizontal cables have representation B_1 for v odd and B_2 for v even. Hence, for n even and v odd, we have

$$\tilde{\mathbf{D}}^{B_1} = \begin{pmatrix} \mathbf{d}_h + (-1)^h \mathbf{d}_{n-h}, & \sqrt{2}\mathbf{d}_s \end{pmatrix} \text{ and } \tilde{\mathbf{D}}^{B_2} = \begin{pmatrix} \mathbf{d}_h + (-1)^h \mathbf{d}_{n-h}, & \sqrt{2}\mathbf{d}_v \end{pmatrix}, \tag{6.65}$$

and when both n and v are even, we have

$$\tilde{\mathbf{D}}^{B1} = \begin{pmatrix} \mathbf{d}_h + (-1)^h \mathbf{d}_{n-h}, & \sqrt{2}\mathbf{d}_s & \sqrt{2}\mathbf{d}_v \end{pmatrix} \text{ and } \tilde{\mathbf{D}}^{B2} = \begin{pmatrix} \mathbf{d}_h + (-1)^h \mathbf{d}_{n-h} \end{pmatrix}. \tag{6.66}$$

$\tilde{\mathbf{D}}^{E_k}$ for a two-dimensional representation E_k is

$$\begin{aligned} \tilde{\mathbf{D}}^{E_k} &= \left(\mathbf{R}_0 \otimes \mathbf{d}_h + \mathbf{R}_h \otimes \mathbf{d}_{n-h},\ \tfrac{1}{\sqrt{2}} \begin{pmatrix} C_0 + C_n \\ S_0 + S_n \end{pmatrix} \otimes \mathbf{d}_s,\ \tfrac{1}{\sqrt{1+C_{vk}}} \begin{pmatrix} C_0 + C_{vk} \\ S_0 + S_{vk} \end{pmatrix} \otimes \mathbf{d}_v \right) \\ &= \left(\begin{pmatrix} 1 & 0 \\ 0 & 1 \end{pmatrix} \otimes \mathbf{d}_h + \begin{pmatrix} C_{hk} & -S_{hk} \\ S_{hk} & C_{hk} \end{pmatrix} \otimes \mathbf{d}_{n-h},\ \sqrt{2} \begin{pmatrix} C_0 \\ 0 \end{pmatrix} \otimes \mathbf{d}_s,\ \tfrac{1}{\sqrt{1+C_{vk}}} \begin{pmatrix} 1 + C_{vk} \\ S_{vk} \end{pmatrix} \otimes \mathbf{d}_v \right) \end{aligned} \tag{6.67}$$

which can be written in a symbolic form as

$$\tilde{\mathbf{D}}^{E_k} = \begin{pmatrix} \varepsilon_1 & -\varepsilon_3 & 0 & \eta_1 \\ \varepsilon_2 & -\varepsilon_4 & \zeta_1 & \eta_2 \\ 0 & 0 & \zeta_2 & \eta_3 \\ \varepsilon_3 & \varepsilon_1 & 0 & \eta_4 \\ \varepsilon_4 & \varepsilon_2 & 0 & \eta_5 \\ 0 & 0 & 0 & \eta_6 \end{pmatrix} \tag{6.68}$$

where

$$\begin{aligned} \varepsilon_1 &= C_{(h+v)/2} + S_{h/2} + C_{hk}(-C_{(h-v)/2} + S_{h/2}) \\ \varepsilon_2 &= S_{(h+v)/2} - C_{h/2} + C_{hk}(S_{(h-v)/2} + C_{h/2}) \\ \varepsilon_3 &= S_{hk}(C_{(h-v)/2} - S_{h/2}) \\ \varepsilon_4 &= -S_{hk}(S_{(h-v)/2} + C_{h/2}) \end{aligned} \tag{6.69}$$

$$\begin{array}{lll} \zeta_1 = 2S_v, & \zeta_2 = H, & \bar{H} = H/[4S_{v/2}(1 - S_{v/2})], \\ \eta_1 = -(1 + C_{vk})S_{v/2}, & \eta_2 = (1 + C_{vk})C_{v/2}, & \eta_3 = (1 + C_{vk})\bar{H}, \\ \eta_4 = -S_{vk}S_{v/2}, & \eta_5 = S_{vk}C_{v/2}, & \eta_6 = S_{vk}\bar{H}. \end{array} \tag{6.70}$$

Hence, the mechanisms lying in the null-space of $(\tilde{\mathbf{D}}^{E_k})^{\mathrm{T}}$ are

$$\tilde{\mathbf{d}}_1^{E_k} = \begin{pmatrix} \eta_6(\varepsilon_2\varepsilon_3 - \varepsilon_1\varepsilon_4) \\ 0 \\ 0 \\ -\eta_6(\varepsilon_1\varepsilon_2 + \varepsilon_3\varepsilon_4) \\ \eta_6(\varepsilon_1^2 + \varepsilon_3^2) \\ \eta_4(\varepsilon_1\varepsilon_2 + \varepsilon_3\varepsilon_4) - \eta_1(\varepsilon_2\varepsilon_3 - \varepsilon_1\varepsilon_4) - \eta_5(\varepsilon_1^2 + \varepsilon_3^2) \end{pmatrix} \tag{6.71}$$

and

$$\tilde{\mathbf{d}}_2^{E_k} = \begin{pmatrix} \zeta_2\eta_6(\varepsilon_1\varepsilon_2 + \varepsilon_3\varepsilon_4) \\ -\zeta_2\eta_6(\varepsilon_1^2 + \varepsilon_3^2) \\ \zeta_1\eta_6(\varepsilon_1^2 + \varepsilon_3^2) \\ \zeta_2\eta_6(-\varepsilon_1\varepsilon_4 + \varepsilon_2\varepsilon_3) \\ 0 \\ \zeta_2\eta_4(\varepsilon_1\varepsilon_4 - \varepsilon_2\varepsilon_3) - \zeta_2\eta_1(\varepsilon_1\varepsilon_2 + \varepsilon_3\varepsilon_4) + (\zeta_2\eta_2 - \zeta_1\eta_3)(\varepsilon_1^2 + \varepsilon_3^2) \end{pmatrix} \tag{6.72}$$

Some elements in the mechanisms can be computed as follows for convenience

$$\begin{aligned} \varepsilon_2\varepsilon_3 - \varepsilon_1\varepsilon_4 &= 2(S_{v/2} - 1)(-S_{hk}S_h) \\ \varepsilon_1\varepsilon_2 + \varepsilon_3\varepsilon_4 &= -2(S_{v/2} - 1)C_{v/2}(C_{hk} - C_h) \\ \varepsilon_1^2 + \varepsilon_3^2 &= 2(S_{v/2} - 1)[(C_{hk} - C_h)(S_{v/2} + C_h) - S_h^2] \end{aligned} \tag{6.73}$$

6.5.4 Rigid-body Motions

The rigid-body motions of a prismatic tensegrity structures are identified in this subsection to be present in A_2 and E_1 blocks of the stiffness matrices. Because the symmetry-adapted mechanisms come from the null-space of transpose of the equilibrium matrix, they must lead to trivial quadratic form of the linear stiffness matrix with them, hence, we only need to verify whether they also lead to trivial quadratic form $\tilde{\mathbf{Q}}^{\mu}$ of the geometrical stiffness matrix.

From Eqs. (6.31) and (6.64), we have the following equation for representation A_2

$$\begin{aligned}\tilde{\mathbf{K}}_G^{A_2}\tilde{\mathbf{d}}_1^{A_2} &= q_v \begin{pmatrix} \sqrt{2(1-C_v)}-(1-C_v) & S_v & 0 \\ S_v & \sqrt{2(1-C_v)}+(1-C_v) & 0 \\ 0 & 0 & 0 \end{pmatrix} \begin{pmatrix} 1+S_{v/2} \\ -C_{v/2} \\ 0 \end{pmatrix} \\ &= 2q_v S_{v/2} \begin{pmatrix} 1-S_{v/2} & C_{v/2} & 0 \\ C_{v/2} & 1+S_{v/2} & 0 \\ 0 & 0 & 0 \end{pmatrix} \begin{pmatrix} 1+S_{v/2} \\ -C_{v/2} \\ 0 \end{pmatrix} = \mathbf{0}, \end{aligned} \tag{6.74}$$

and

$$\tilde{\mathbf{K}}_G^{A_2}\tilde{\mathbf{d}}_2^{A_2} = q_v \begin{pmatrix} \sqrt{2(1-C_v)}-(1-C_v) & S_v & 0 \\ S_v & \sqrt{2(1-C_v)}+(1-C_v) & 0 \\ 0 & 0 & 0 \end{pmatrix} \begin{pmatrix} 0 \\ 0 \\ 1 \end{pmatrix} = \mathbf{0}. \tag{6.75}$$

Hence, the quadratic form $\tilde{\mathbf{Q}}^{A_2}$ of $\tilde{\mathbf{K}}_G^{A_2}$ with respect to the mechanisms $\tilde{\mathbf{d}}_1^{A_2}$ and $\tilde{\mathbf{d}}_2^{A_2}$ corresponding to the representation A_2 are zero:

$$\tilde{\mathbf{Q}}^{A_2} = \tilde{\mathbf{M}}^{A_2}\tilde{\mathbf{S}}^{A_2}(\tilde{\mathbf{M}}^{A_2})^{\mathrm{T}} = \mathbf{O}, \tag{6.76}$$

where

$$\tilde{\mathbf{M}}^{A_2} = \begin{pmatrix} \mathbf{d}_1^{A_2} & \mathbf{d}_2^{A_2} \end{pmatrix}, \tag{6.77}$$

from which, we know that the two mechanisms lying in $\tilde{\mathbf{D}}^{A_2}$ are the rigid-body motions.

From Eq. (6.28), $\tilde{\mathbf{K}}_G^{E_1}$ is

$$\tilde{\mathbf{K}}_G^{E_k} = q_v \begin{pmatrix} \varphi_1+\varphi_2 & -\varphi_3 & 0 & -\varphi_4 & -\varphi_5-\varphi_6 & 0 \\ -\varphi_3 & \varphi_1-\varphi_2 & 0 & \varphi_5-\varphi_6 & \varphi_4 & 0 \\ 0 & 0 & \varphi_7-\varphi_8 & & 0 & \varphi_9 \\ -\varphi_4 & \varphi_5-\varphi_6 & 0 & \varphi_1-\varphi_2 & \varphi_3 & 0 \\ -\varphi_5-\varphi_6 & \varphi_4 & 0 & \varphi_3 & \varphi_1+\varphi_2 & 0 \\ 0 & & \varphi_9 & 0 & 0 & \varphi_7+\varphi_8 \end{pmatrix}, \tag{6.78}$$

where

$$\begin{array}{lll} \varphi_1 = 2S_{v/2}(1+C_h) & \varphi_2 = S_v^2 & \varphi_3 = S_vC_v \\ \varphi_4 = \varphi_3 & \varphi_5 = \varphi_1 & \varphi_6 = \varphi_2 \\ \varphi_7 = 2S_{v/2} & \varphi_8 = 1-C_v & \varphi_9 = S_v. \end{array} \tag{6.79}$$

Because mechanisms denote direction of nodal displacements that do not change member lengths, magnitudes of them are not important. Hence, mechanisms $\tilde{\mathbf{d}}_1^{E_1}$ and $\tilde{\mathbf{d}}_2^{E_1}$ can be simplified as follows from Eqs. (6.71) and (6.72)

$$\tilde{\mathbf{d}}_1^{E_1} = \begin{pmatrix} 1 \\ 0 \\ 0 \\ 0 \\ 1 \\ 0 \end{pmatrix} \text{ and } \tilde{\mathbf{d}}_2^{E_1} = \begin{pmatrix} 0 \\ S_v\bar{H} \\ -2S_{v/2}(1+S_{v/2})H \\ -S_v\bar{H} \\ 0 \\ S_v \end{pmatrix}. \tag{6.80}$$

It is easy to verify that

$$\tilde{\mathbf{K}}_G^{E_1}\tilde{\mathbf{d}}_1^{E_1} = \mathbf{0} \text{ and } \tilde{\mathbf{K}}_G^{E_1}\tilde{\mathbf{d}}_2^{E_1} = \mathbf{0}, \tag{6.81}$$

from which, we have

$$\tilde{\mathbf{Q}}^{E_1} = \tilde{\mathbf{M}}^{E_1}\tilde{\mathbf{S}}^{E_1}(\tilde{\mathbf{M}}^{E_1})^{\mathrm{T}} = \mathbf{O}, \tag{6.82}$$

where

$$\tilde{\mathbf{M}}^{E_1} = \begin{pmatrix} \mathbf{d}_1^{E_1} & \mathbf{d}_2^{E_1} \end{pmatrix}. \tag{6.83}$$

Because there are two copies of blocks for each two-dimensional representation, the four mechanisms—two copies of $\tilde{\mathbf{d}}_1^{E_1}$ and $\tilde{\mathbf{d}}_2^{E_1}$—are the rigid-body motions of the structure.

In summary, we have identified all the six rigid-body motions of a prismatic tensegrity structure with dihedral symmetry—two in the A_2 block and four in the E_1 blocks.

6.6 Discussions and Conclusions

For the structures with dihedral symmetry, we have presented a direct strategy for the analytical derivation of their symmetry-adapted force density matrix, geometrical stiffness matrix as well as equilibrium matrix. Mechanisms in the symmetry-adapted coordinate system are derived from transpose of the symmetry-adapted equilibrium matrix. Moreover, the rigid-body motions are identified to be present in the blocks corresponding to the representations A_2 and E_1, as indicated in the character table.

The symmetry-adapted forms of these matrices can significantly simplify stability investigation and structural analysis, because sizes of the blocks in their leading diagonals become much smaller than those of the original matrices; and more importantly, they provide us the possibility to have further insight into the stability of the whole class of structures with similar symmetry properties based on the analytically formulated blocks as will be discussed in the next two chapters.

As have been discussed, the diagonal blocks of the force density matrix are only 1-by-1 or 2-by-2 matrices, such that positive semi-definiteness of them can be easily verified. Using the analytical symmetry-adapted force density matrix, Chapter 7 will discuss the condition of super stability for prismatic structures, showing that they are super stable if and only if their horizontal cables are connected to adjacent nodes. Furthermore, Chapter 8 will present the super stability condition for star-shaped structures: the structures are super stable if they have odd number of struts, and moreover, the struts are as close to each other as possible.

From the analytical formulations for the symmetry-adapted geometrical stiffness matrix and mechanisms, it will be demonstrated in Chapter 7 that prestress stability of prismatic structures can be verified by investigating positive definiteness of the reduced stiffness matrix in block-diagonal form, which is the quadratic form of the geometrical stiffness matrix with respect to the mechanisms lying in the null-space of transpose of the equilibrium matrix. Height(-to-radius ratio) of this class of structures is found to be involved in the symmetry-adapted mechanisms, which gives us a clear clue to investigate the influence of height(-to-radius

ratio) on their prestress stability as will be discussed in Chapter 7.

The formulations presented in this chapter are for the structures with dihedral symmetry, but the methodologies developed are considered to be applicable to the structures belonging to other point groups, which will be one of our future studies.

Chapter 7

PRISMATIC STRUCTURES

In this chapter, we study self-equilibrated configuration and stability of prismatic tensegrity structures, which have symmetry of dihedral group.

Prismatic structures, for example the simplest example as shown in Fig. 7.1, are one of the most well-known forms of tensegrity structures. Many researchers have used them as numerical examples to demonstrate the efficiency of their form-finding methods, however, few study has been carried out to investigate their stability, except for the super stability investigation of this class of structures by Connelly and Terrell (1995).

Using the analytical formulation of the symmetry-adapted force density matrix presented in Chapter 6, we will show that the blocks in its diagonal for the prismatic structures with dihedral symmetry agree with those derived by Connelly and Terrell (1995) in another way, so that this class of structures can be proved to be super stable if and only if their horizontal cables are connected to adjacent nodes.

Furthermore, it is shown that the structures that are not super stable may still be (prestress) stable under certain conditions; investigation of these conditions and classification of the stability of prismatic structures are the other main subjects of this chapter. The investigation of their prestress stability extensively makes use of the symmetry-adapted geometrical stiffness matrix and mechanisms analytically derived in Chapter 6.

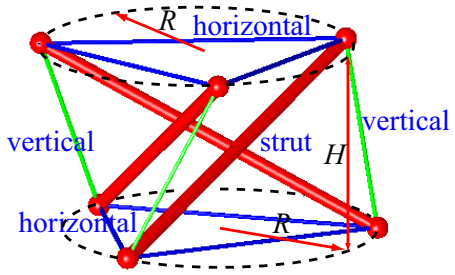

Figure 7.1: The simplest prismatic tensegrity structure in three-dimensional space. The thin and thick lines denote, respectively, cables that carry tension, and struts that carry compression. The nodes lie in two horizontal planes. This structure has $\mathbf{D}_3$ symmetry, and using the notation described at the end of Section 2.1, is denoted $\mathbf{D}_3^{1,1}$.

7.1 Introduction

After showing that some prismatic tensegrity structures are super stable, Connelly and Terrell (1995) listed the following three questions, where the terms 'rigid' and 'tensigrid' denote prestress stable and tensegrity structure in the questions, respectively:

[L1] Can other methods be applied to show that some of the other prismatic tensigrids are rigid?

[L2] Can it be shown that some of the other prismatic tensigrids are not rigid?

[L3] How "often" it is rigid?

In this chapter, we will demonstrate that stability of prismatic tensegrity structures is dependent on the connectivity of the members (horizontal cables and vertical cables), the height/radius ratio, and prestress to member stiffness ratio. It is shown that structures that are not super stable can still be stable in some cases. For example, the structure shown in Fig. 7.2(a) is not super stable, and it is prestress stable if it is assigned the right height/radius ratio as will be discussed later in this chapter.

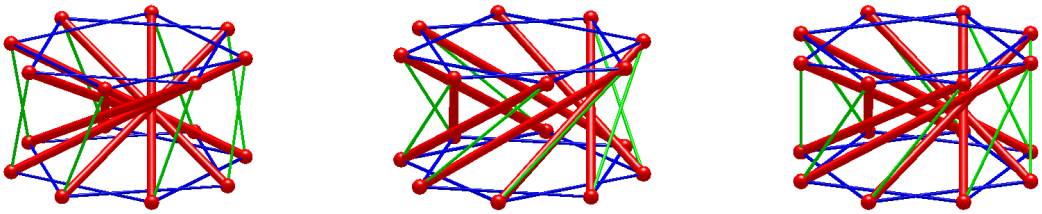

(a) prestress stable ($\mathbf{D}_8^{2,3}$) (b) unstable ($\mathbf{D}_8^{2,1}$) (c) divisible ($\mathbf{D}_8^{2,2}$)

Figure 7.2: Prismatic tensegrity structures with $\mathbf{D}_8$ symmetry. The structure $\mathbf{D}_8^{2,3}$ is prestress stable when its height/radius ratio is within the range of [0.4,3.1]; the structure $\mathbf{D}_8^{2,1}$ can never be stable, and the structure $\mathbf{D}_8^{2,2}$ can be physically divided into two identical substructures $\mathbf{D}_4^{1,1}$.

Following this introduction, the chapter is organized as follows. Section 2 discusses a simple method for the determination of self-equilibrated configurations of a general prismatic structure by considering the self-equilibrium of a reference node instead of the whole structure; presents another method for the self-equilibrated configuration by ensuring enough rank deficiency of the force density matrix using the symmetry-adapted formulation given in Chapter 6; and further gives out the condition of super stability for prismatic structures based on the symmetry-adapted force density matrix. Conditions for the divisible structures, which can be physically divided into several identical substructures, are given in Section 3. Section 4 discusses the critical parameters for the stability of prismatic tensegrity structures. Section 5 presents the catalogue of the stability of prismatic tensegrity structures with up to ten struts, and Section 6 concludes the paper.

7.2 Symmetry and Configuration

As shown in Fig. 7.1, we define the class of prismatic tensegrity structures as follows. The structures have $2n$ nodes, arranged in two horizontal circles of radius R around the vertical z-axis, which is an n-fold symmetry-axis. Within each circle, each node is connected by 'horizontal' cables to two other nodes. The two planes containing the nodes are at $z = \pm H/2$. Each node is connected by a strut and a 'vertical' cable to nodes in the other plane. The structure

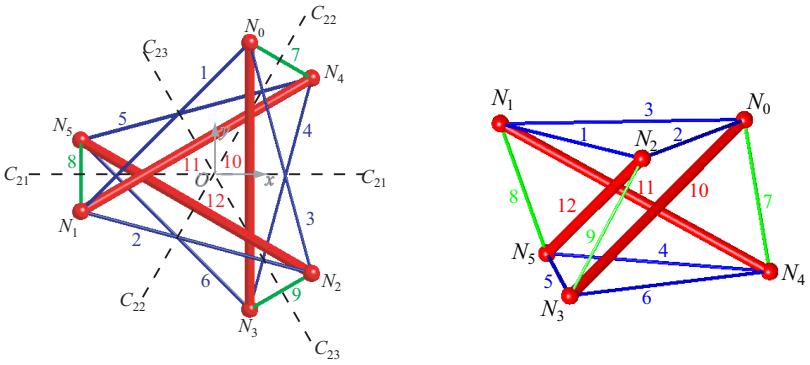

(a) top view (b) side view

Figure 7.3: The prismatic tensegrity structure $\mathbf{D}_3^{1,1}$.

has $\mathbf{D}_n$ symmetry, using the Schoenflies notation, and this symmetry allows us to calculate self-equilibrated configurations by considering the equilibrium equations of only one node.

7.2.1 Orbits

Consider a specific set of elements (nodes or members) of a structure with symmetry G. If one element in a set can be transformed to any other member of that set by a proper symmetry operation in G, then this set of elements are said to belong to the same *orbit*. A structure can have several different orbits of elements of the same type.

We are considering structures that have dihedral symmetry, denoted $\mathbf{D}_n$: there is a single major n-fold rotation (C_n^i) axis, which we assume is the vertical, z-axis, and n 2-fold rotation (C_{2j}) axes perpendicular to this axis (Kettle, 1995). In total there are $2n$ symmetry operations.

For a prismatic tensegrity structure, there is one orbit of nodes, and each symmetry operation transforms a reference node into one of the other nodes; there is a one-to-one correspondence between the nodes and the symmetry operations. (When there is a one-to-one correspondence between elements and symmetry operations, the orbit is called a *regular orbit*). There are in total $2n$ nodes, arranged in two horizontal planes, with n nodes in each. An example structure with $\mathbf{D}_3$ symmetry is shown in Fig. 7.3: nodes N_0, N_1, N_2, and nodes N_3, N_4,

Table 7.1: Transformation of nodes and members of the structure $\mathbf{D}_3^{1,1}$ in Fig. 7.3 corresponding to the symmetry operations of $\mathbf{D}_3$. The elements listed in the left-hand column are transformed to the elements shown in the table by the symmetry operations given in the top row.

	$E(C_3^0)$	C_3^1	C_3^2	C_{21}	C_{22}	C_{23}	
node N_0	N_0	N_1	N_2	N_3	N_4	N_5	
member 1	1	2	3	6	4	5	horizontal cables
member 7	7	8	9	9	7	8	vertical cables
member 10	10	11	12	10	11	12	struts

N_5 lie in the top and bottom horizontal planes, respectively. Any node, e.g., node N_0, can be transformed to any other node, including itself, by one of the symmetry operations of $\mathbf{D}_3$ as listed in Table 7.1.

There are three orbits of members: horizontal cables, vertical cables, and struts. Each node is connected by two horizontal cables lying in a horizontal plane, one vertical cable, and one strut: the vertical cable and strut connect nodes in different planes. The members in each orbit have the same length; we assume a symmetric internal prestress state, and hence the internal force, and the force density (internal force to length ratio) are also the same in each member of an orbit. There are $2n$ horizontal cables, and each symmetry operation transforms a reference cable into one of the other cables; there is a one-to-one correspondence between the horizontal cables and the symmetry operations (the horizontal cables form a regular orbit). There are, however, only n vertical cables, and n struts; there is a one-to-two correspondence between the vertical cables (or struts) and the symmetry operations. Each vertical cable and strut intersects one of the 2-fold horizontal rotation axes, and this 2-fold operation transforms the vertical cable (or strut) into itself. For example, transformations of the members of the structure with $\mathbf{D}_3$ symmetry by the symmetry operations are listed in Table 7.1. For some structures, the horizontal cables may cross one another; we neglect to consider any interference, essentially assuming that these cables can pass through one another.

7.2.2 Transformation Matrices

Let $\mathbf{x}_0$ and $\mathbf{x}_i$ ($\in \Re^3$) denote the coordinates of nodes N_0 and N_i in three-dimensional space, respectively. Suppose that node N_0 can be transformed to node N_i by a symmetry operation in the group $\mathbf{D}_n$. Then we have the following equation with the *transformation matrix* $\mathbf{R}_i \in \Re^{3\times 3}$

$$\mathbf{x}_i = \mathbf{R}_i \mathbf{x}_0. \tag{7.1}$$

Because the nodes form a regular orbit, there will be one matrix $\mathbf{R}_i$ for each symmetry operation in the group. These matrices are said to form a *representation* Γ_{xyz} of the group $\mathbf{D}_n$.

The matrices $\mathbf{R}_i$ form a *reducible* representation of $\mathbf{D}_n$. However, it is straightforward to write this reducible representation in terms of *irreducible representations*. The irreducible representations that make up Γ_{xyz} can be read off from a set of character tables, e.g., Altmann and Herzig (1994). For any $\mathbf{D}_n$, Γ_{xyz} is the direct sum of the irreducible representations A_2 and E_1 (the standard notation is E for $\mathbf{D}_3$ and $\mathbf{D}_4$, but we will use E_1 for these cases too). The irreducible representation A_2 is one-dimensional, and corresponds to the transformation of the z-coordinate. The irreducible representation E_1 is two-dimensional, and corresponds to the transformation of the x- and y-coordinates. Thus the transformation matrices $\mathbf{R}_i \in \Re^{3\times 3}$ can be written as

$$\mathbf{R}_i = \begin{pmatrix} \mathbf{R}_i^{E_1} & \\ & \mathbf{R}_i^{A_2} \end{pmatrix}, \tag{7.2}$$

where the matrices $\mathbf{R}_i^{E_1} \in \Re^{2\times 2}$ form the representation E_1, and the matrices $\mathbf{R}_i^{A_2} \in \Re^{1\times 1}$ form the representation A_2.

The one-dimensional matrices $\mathbf{R}_i^{A_2}$ are unique, but there is some limited choice for the two-dimensional matrices $\mathbf{R}_i^{E_1}$. By choosing a positive rotation around the z-axis for $\mathbf{R}_1$, the transformation matrix $\mathbf{R}_i$ for the cyclic rotation C_n^i through $2i\pi/n$ can be written as

$$\mathbf{R}_i = \begin{pmatrix} C_i & -S_i & 0 \\ S_i & C_i & 0 \\ 0 & 0 & 1 \end{pmatrix} \quad \text{for } 0 \le i \le n-1, \tag{7.3}$$

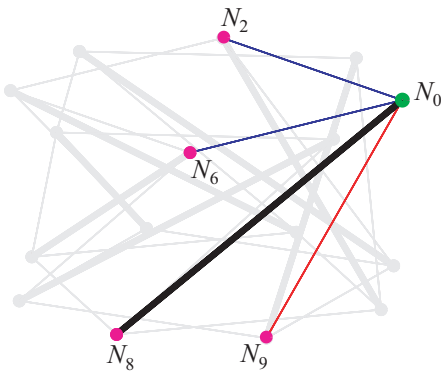

Figure 7.4: All nodes connected to a reference node N_0 of the structure $\mathbf{D}_8^{2,1}$.

where $C_i = \cos(2i\pi/n)$ and $S_i = \sin(2i\pi/n)$, and i is running from 0 to $n-1$. By choosing that a dihedral rotation about the x-axis transforms node N_0 to node N_n, the transformation matrices $\mathbf{R}_i$ for the 2-fold rotations can be written as

$$\mathbf{R}_i = \begin{pmatrix} C_i & S_i & 0 \\ S_i & -C_i & 0 \\ 0 & 0 & -1 \end{pmatrix} \quad \text{for } n \leq i \leq 2n-1. \tag{7.4}$$

7.2.3 Self-equilibrated Configuration by Symmetry

There is only one orbit of nodes, and hence to find a totally symmetric state of prestress, we only need to consider equilibrium of one node under zero external loading: equilibrium of any other node is identical, by symmetry (Connelly and Back, 1998).

Consider a single *reference node* N_0, and the members that are connected to it — an example is shown in Fig. 7.4. The coordinates $\mathbf{x}_h$ and $\mathbf{x}_{n-h}$ of the nodes N_h and N_{n-h} connected to the reference node as horizontal cables can be computed as follows by using Eq. (7.1)

$$\begin{aligned} \mathbf{x}_h &= \mathbf{R}_h \mathbf{x}_0, \\ \mathbf{x}_{n-h} &= \mathbf{R}_{n-h} \mathbf{x}_0, \end{aligned} \tag{7.5}$$

and the direction vectors $\mathbf{d}_h$ and $\mathbf{d}_{n-h}$ of the horizontal cables can be written as

$$\begin{aligned} \mathbf{d}_h &= \mathbf{x}_h - \mathbf{x}_0 = (\mathbf{R}_h - \mathbf{I}^3)\mathbf{x}_0, \\ \mathbf{d}_{n-h} &= \mathbf{x}_{n-h} - \mathbf{x}_0 = (\mathbf{R}_{n-h} - \mathbf{I}^3)\mathbf{x}_0, \end{aligned} \tag{7.6}$$

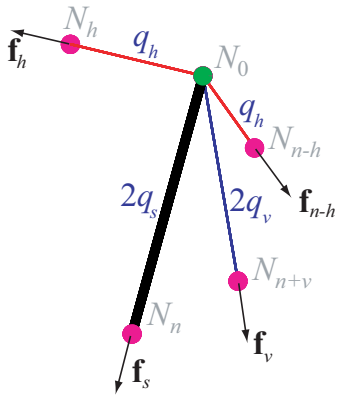

Figure 7.5: Self-equilibrium of the reference node of prismatic tensegrity structures. The three cable forces, $\mathbf{f}_h$, $\mathbf{f}_{n-h}$ and $\mathbf{f}_v$ are all tensile, and have a positive magnitude; the strut force $\mathbf{f}_s$ is compressive, and has a negative magnitude.

where $\mathbf{I}^3$ denotes the 3-by-3 identity matrix. Similarly, the coordinates $\mathbf{x}_s$ and $\mathbf{x}_v$ of the nodes N_n and N_{n+v} in the bottom plane that are connected to N_0 by a strut and a vertical cable, respectively, can be calculated by

$$\begin{aligned} \mathbf{x}_s &= \mathbf{R}_n \mathbf{x}_0, \\ \mathbf{x}_v &= \mathbf{R}_{n+v} \mathbf{x}_0, \end{aligned} \tag{7.7}$$

and their direction vectors $\mathbf{d}_s$ and $\mathbf{d}_v$ are

$$\begin{aligned} \mathbf{d}_s &= \mathbf{x}_s - \mathbf{x}_0 = (\mathbf{R}_n - \mathbf{I}^3)\mathbf{x}_0, \\ \mathbf{d}_v &= \mathbf{x}_v - \mathbf{x}_0 = (\mathbf{R}_{n+v} - \mathbf{I}^3)\mathbf{x}_0. \end{aligned} \tag{7.8}$$

Let q_h, q_s and q_v denote the force densities of the horizontal cables, strut and vertical cable, respectively, where the force density is the ratio of the axial force f_i to the length l_i; i.e., $q_i = f_i/l_i$. Because tensegrity structures are pin-jointed and carry only axial forces in the members, the direction of the axial force is identical to that of the member. Thus, the axial force vectors $\mathbf{f}_h$ and $\mathbf{f}_{n-h}$ of the horizontal cables can be written as

$$\begin{aligned} \mathbf{f}_h &= f_h \mathbf{d}_h / l_h = q_h \mathbf{d}_h = q_h (\mathbf{R}_h - \mathbf{I}^3)\mathbf{x}_0, \\ \mathbf{f}_{n-h} &= f_h \mathbf{d}_{n-h} / l_h = q_h \mathbf{d}_{n-h} = q_h (\mathbf{R}_{n-h} - \mathbf{I}^3)\mathbf{x}_0. \end{aligned} \tag{7.9}$$

Similarly, the axial force vectors $\mathbf{f}_s$ and $\mathbf{f}_v$ of the strut and vertical cable are

$$\begin{aligned} \mathbf{f}_s &= q_s (\mathbf{R}_{n+s} - \mathbf{I}^3)\mathbf{x}_0, \\ \mathbf{f}_v &= q_v (\mathbf{R}_{n+v} - \mathbf{I}^3)\mathbf{x}_0. \end{aligned} \tag{7.10}$$

When no external load is applied, the node N_0 should be in equilibrium, i.e.,

$$\mathbf{f}_h + \mathbf{f}_{n-h} + \mathbf{f}_s + \mathbf{f}_v = \mathbf{0}. \tag{7.11}$$

Substituting Eqs. (8.2) and (8.3) into Eq. (8.4), it gives

$$\tilde{\mathbf{E}}\mathbf{x}_0 = \mathbf{0}, \tag{7.12}$$

where

$$\begin{aligned}\tilde{\mathbf{E}} = \quad & 2q_h \begin{pmatrix} C_h - 1 & 0 & 0 \\ 0 & C_h - 1 & 0 \\ 0 & 0 & 0 \end{pmatrix} \\ & + q_s \begin{pmatrix} 0 & 0 & 0 \\ 0 & -2 & 0 \\ 0 & 0 & -2 \end{pmatrix} + q_v \begin{pmatrix} C_v - 1 & S_v & 0 \\ S_v & -C_v - 1 & 0 \\ 0 & 0 & -2 \end{pmatrix}. \end{aligned} \tag{7.13}$$

$\tilde{\mathbf{E}}$ is a block-diagonal matrix constructed from a 2-by-2 and a 1-by-1 sub-matrices on its leading diagonal. Both of these sub-matrices should be singular to allow the solution of Eq. (7.12) to give the position vector $\mathbf{x}_0$ of the reference node with non-trivial coordinates in three-dimensional space. For the singularity of the 1-by-1 sub-matrix, we have

$$0 - 2q_s - 2q_v = 0, \tag{7.14}$$

i.e.,

$$q_v = -q_s. \tag{7.15}$$

For the 2-by-2 sub-matrix, we can enforce singularity by ensuring that the determinant is equal to zero, i.e.,

$$[2q_h(C_h - 1) + 0 + q_v(C_v - 1)][2q_h(C_h - 1) - 2q_s - q_v(C_v + 1)] - q_v^2 S_v^2 = 0. \tag{7.16}$$

Using $q_v = -q_s$ from Eq. (7.15), and the trigonometric relationship $C_v^2 + S_v^2 = 1$, Eq. (7.16) reduces to

$$4\left(\frac{q_h}{q_v}\right)^2 (C_h - 1)^2 + 2C_v - 2 = 0. \tag{7.17}$$

Since both of q_h and q_v should have positive sign (they are both cables in tension), only the positive solution is adopted, i.e.,

$$t = \frac{q_h}{q_v} = +\frac{\sqrt{2-2C_v}}{2(1-C_h)}. \tag{7.18}$$

When both Eqs. (7.15) and (7.18) hold, $\tilde{\mathbf{E}}$ has a nullity of 2, and hence has a two-dimensional null-space. Any vector in that null-space can be the coordinate vector $\mathbf{x}_0$ of the reference node. In general, the coordinate vector can be written in terms of two parameters, R and H, as

$$\mathbf{x}_0 = \frac{R}{R_0}\begin{pmatrix} C_v - 1 + \sqrt{2-2C_v} \\ S_v \\ 0 \end{pmatrix} + \frac{H}{2}\begin{pmatrix} 0 \\ 0 \\ 1 \end{pmatrix}, \tag{7.19}$$

where R_0 is the norm of the first vector representing the coordinates in xy-plane, and then R and H denote the radius and height of the structure, which can have arbitrary real values. Connectivity of horizontal cables does not affect the self-equilibrated configuration of prismatic tensegrity structures, but, as we will see in Section 4, it affects the stability of the structures.

By the application of Eqs. (7.1), (7.3) and (7.4), the coordinates of all the other nodes N_i can be determined by running i from 1 to $2n-1$.

7.2.4 Force Densities by Non-degeneracy Condition

As another approach to derive the force densities for the prismatic structures, this section makes use of the non-degeneracy condition in terms of rank deficiency of the force density matrix in Chapter 2 and its analytical symmetry-adapted blocks corresponding to the A_2 and E_1 blocks. The symmetry-adapted force density matrix is derived from the formulation in Chapter 6, which agrees with the results by Connelly and Terrell (1995) so as to present the super stability condition for prismatic structures.

To ensure a non-degenerate tensegrity structure in three-dimensional space, the force density matrix $\mathbf{E}$, or equivalently $\tilde{\mathbf{E}}$, should have rank deficiency of at least four (see Chapter 2 for the non-degeneracy condition for free-standing structures). Rank deficiency of a symmetric matrix can be calculated by counting

the number of its zero eigenvalues. From Eq. (6.12), the block $\tilde{\mathbf{E}}^{A_1}$ is always equal to zero, since all representation matrices $\mathbf{R}_i^{A_1}$ of A_1 are equal to 1:

$$\begin{aligned}\tilde{\mathbf{E}}^{A_1} &= q\mathbf{R}_0^{\mu} - q_h\mathbf{R}_h^{\mu} - q_h\mathbf{R}_{n-h}^{\mu} - q_s\mathbf{R}_n^{\mu} - q_v\mathbf{R}_{n+v}^{\mu} \\ &= q - 2q_h - q_s - q_v = 0. \end{aligned} \tag{7.20}$$

The other three zero eigenvalues should come from $\tilde{\mathbf{E}}^{A_2}$ and the two copies of $\tilde{\mathbf{E}}^{E1}$, because representations A_2 and E_1 respectively stand for transformation of z- and xy-coordinates read off from Table 6.1. Hence,

$$\det(\tilde{\mathbf{E}}^{A_2}) = \det(\tilde{\mathbf{E}}^{E_1}) = 0, \tag{7.21}$$

where $\det(\cdot)$ denotes determinant of a matrix. From Eq. (6.12), we have

$$\tilde{\mathbf{E}}^{A_2} = q - q_h - q_h - q_s(-1) - q_v(-1) = 2(q_s + q_v) = 0, \tag{7.22}$$

$$\begin{aligned}\tilde{\mathbf{E}}^{E_1} = \; & q\begin{pmatrix} 1 & 0 \\ 0 & 1 \end{pmatrix} - q_h\begin{pmatrix} C_h & -S_h \\ S_h & C_h \end{pmatrix} - q_h\begin{pmatrix} C_{n-h} & -S_{n-h} \\ S_{n-h} & C_{n-h} \end{pmatrix} \\ & -q_s\begin{pmatrix} 1 & 0 \\ 0 & -1 \end{pmatrix} - q_v\begin{pmatrix} C_v & -S_v \\ S_v & C_v \end{pmatrix} \\ = \; & q_h\begin{pmatrix} 1-C_h & 0 \\ 0 & 1-C_h \end{pmatrix} + q_s\begin{pmatrix} 0 & 0 \\ 0 & 2 \end{pmatrix} + q_v\begin{pmatrix} 1-C_v & S_v \\ -S_v & 1+C_v \end{pmatrix} \end{aligned} \tag{7.23}$$

Relations between the force densities of different types of members from condition (7.21) as follows

$$q_v = -q_s, \quad t = \frac{q_h}{q_v} = +\frac{\sqrt{2-2C_v}}{2(1-C_h)}, \tag{7.24}$$

since q_v and q_h, and therefore, t, should be positive to let cables carry tension (positive prestress). This way, the force densities in a self-equilibrium state are derived by making the relevant blocks of the symmetry-adapted force density matrix to be singular so as to have enough rank deficiency for satisfying the non-degeneracy condition. It is apparent that they agree with those from the self-equilibrium equations of the representative node as shown in previous subsection.

7.3 Divisibility Conditions

Depending on the connectivity of members, a prismatic tensegrity structure may be completely separated into several identical substructures that have no mechanical relation with each other. The substructures are of lower symmetry compared

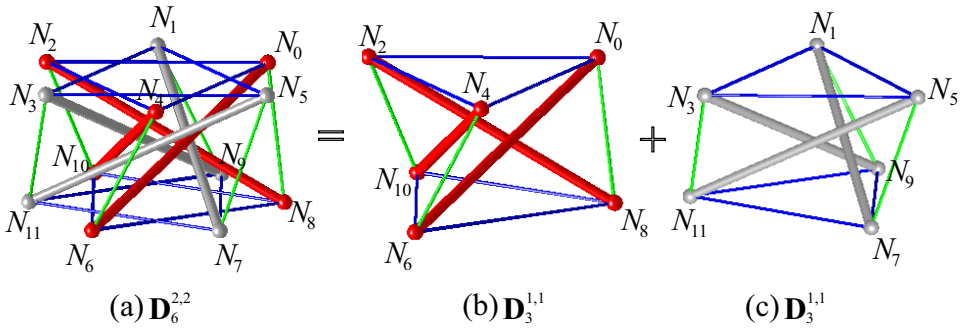

Figure 7.6: Divisible structure $\mathbf{D}_6^{2,2}$ and its substructures $\mathbf{D}_3^{1,1}$. The structure can be completely divided into two substructures, which have their own force mode and there is no physical relation between them such that they can have relative (finite) motions.

to the original structure. For example, the structure $\mathbf{D}_6^{2,2}$ in Fig. 7.6(a) can be divided into two identical substructures $\mathbf{D}_3^{1,1}$. We will exclude divisible structures from our stability investigation, because there is nothing to prevent the substructures moving relative to one another; the stability of the substructures themselves will be considered anyway for the lower symmetry case.

This section presents the necessary and sufficient divisibility conditions for prismatic tensegrity structures. It is demonstrated that divisibility of these structures depends on the connectivity of the horizontal and vertical cables.

7.3.1 Divisibility of Horizontal Cables

Suppose that we randomly select one node as the starting node, and travel to the next along the horizontal cables in the same horizontal plane. If we repeat this in a consistent direction, eventually, we must come back to the starting node. The nodes and horizontal cables that have been visited in the trip are said to belong to the same *circuit*. If there are more than one circuits in the plane, the horizontal cables are said to be *divisible*; otherwise, they are *indivisible*.

Denote the number of circuits of the horizontal cables in one plane by n^c, and the number of nodes in a circuit by n^s. Each time we travel along a horizontal cable of the circuit, we pass by h nodes, and hence by the time we return to the starting node, we have passed hn^s nodes. Suppose that, in this circuit, we have

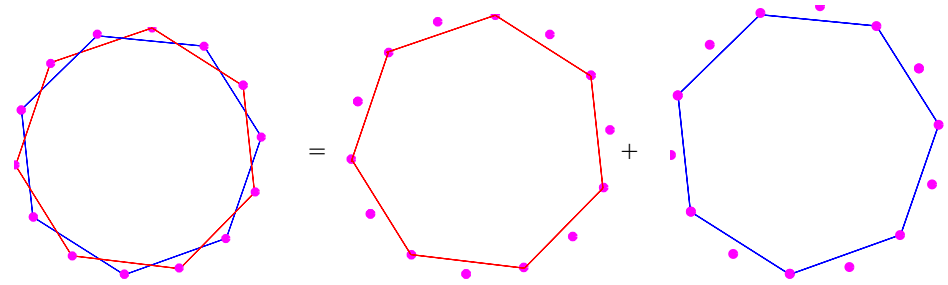

(a) $h = 2$, $n^s = 7$, $h^s = 1$, $n^c = 2$

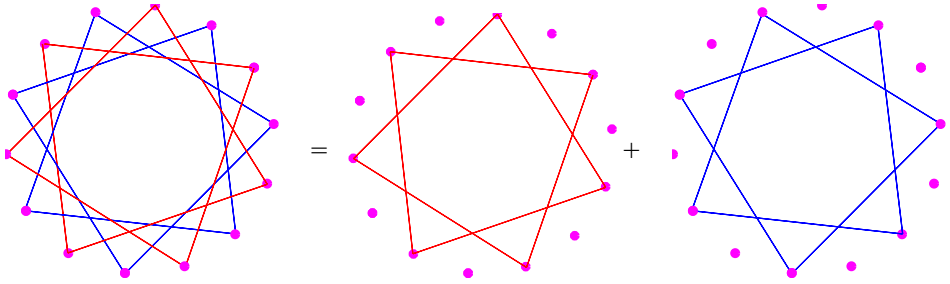

(b) $h = 4$, $n^s = 7$, $h^s = 2$, $n^c = 2$

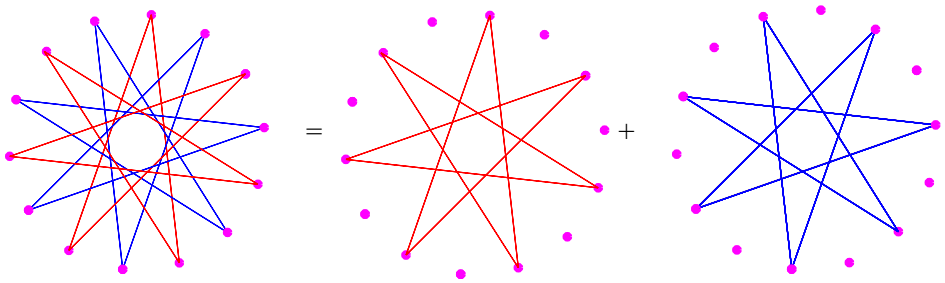

(c) $h = 6$, $n^s = 7$, $h^s = 3$, $n^c = 2$

Figure 7.7: An example of divisible horizontal cables ($n = 14$). The figures show the divisible cases of horizontal cables of the structure with $\mathbf{D}_{14}$ symmetry.

travelled around the plane h^s times, and have hence passed nh^s nodes. Thus,

$$n^s h = nh^s. \tag{7.25}$$

The number of circuits n^c in each horizontal plane is then given by

$$n^c = \frac{n}{n^s} = \frac{h}{h^s}. \tag{7.26}$$

The necessary and sufficient condition for the divisibility of horizontal cables in the same plane is that there is more than one circuit of nodes; i.e., $n^c \neq 1$. And hence, we have

$$h \neq h^s. \tag{7.27}$$

If the structure is divisible, the above parameters give useful information about the substructures. There will be n^c substructures, and they will have n^s nodes in each plane, with a connectivity of the horizontal cables of h^s.

Consider, for example, the divisible structure $\mathbf{D}_6^{2,2}$ shown in Fig. 7.6(a): node N_0 is connected to nodes N_2 and N_4 by the horizontal cables in the upper plane. It is easy to see that these three nodes form a circuit. This circuit does not have any mechanical relation with the other constituted by the nodes N_1, N_3 and N_5. The same situation occurs for the horizontal cables in the bottom plane. Therefore, the structure has in total four circuits, two in each plane:

Circuit	Nodes
1	N_0, N_2, N_4
2	N_1, N_3, N_5
3	N_6, N_8, N_{10}
4	N_7, N_9, N_{11}

(7.28)

In this case, travelling along one circuit takes us around the z-axis only once, but this is not always the case. For example, consider one of the planes of the structure with $\mathbf{D}_{14}$ symmetry as shown in Fig. 7.7; we can have the following cases where the horizontal cables are divisible.

[L1] In the case of $h = 2$, as shown in Fig. 7.7(a), the horizontal cables in the plane can be divided into two circuits ($n^c = 2$), seven nodes in each ($n^s = 7$). The horizontal cables connect each node to the adjacent node in the circuit ($h^s = 1$).

[L2] When $h = 4$, as shown in Fig. 7.7(b), the horizontal cables are divisible, with seven nodes in each circuit. For each circuit, the horizontal cables now connect a node to the second node away in that circuit, i.e., $h^s = 2$.

[L3] When $h = 6$, as shown in Fig. 7.7(c), the horizontal cables are again divisible. Now for each circuit, the horizontal cables connect a node to the third node away in that circuit, i.e., $h^s = 3$.

Note that Eq. (8.14) is only the divisibility condition for the horizontal cables but not for the whole structure. For example, the structure $\mathbf{D}_6^{2,1}$ in Fig. 7.8(a)

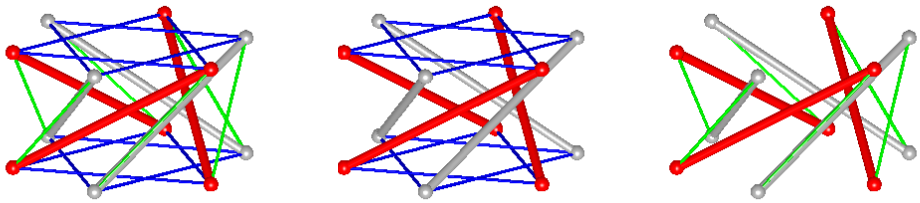

Figure 7.8: An example of indivisible structure, $\mathbf{D}_6^{2,1}$: (a) shows the entire structure; in (b), the vertical cables have been removed, and the remaining structure is divisible; in (c) the horizontal cables have been removed, showing that the vertical cables and the struts together connect all of the nodes, and the entire structure is therefore indivisible.

has two circuits of horizontal cables in each plane of nodes. However, those circuits are all connected by the struts and vertical cables, and the structure is indivisible. Hence, connectivity of vertical cables, which connect the circuits in different horizontal planes, should also be taken into consideration.

7.3.2 Divisibility of Vertical Cables

Suppose that the horizontal cables are divisible: the nodes in the circuits of horizontal cables containing N_0 and N_n are

$$\begin{array}{ll} \text{Circuit 1:} & N_0, N_h, N_{2h}, \ldots, N_{(n^s-1)h} \\ \text{Circuit 2:} & N_n, N_{n+h}, \ldots, N_{n+(n^s-1)h} \end{array} \tag{7.29}$$

Circuit 1 and Circuit 2 are connected by struts from our assumption for the connectivity of struts. If they are also connected by vertical cables, then the substructure constructed from these nodes can be completely separated from the original structure. Thus, the structure is divisible if the horizontal cables are divisible, and the following relationship holds

$$v = v^s h, \quad \text{with } v^s \text{ integer.} \tag{7.30}$$

As contrasting examples, consider $\mathbf{D}_6^{2,2}$ and $\mathbf{D}_6^{2,1}$, which both have the same arrangement of (divisible) horizontal cables. The structure $\mathbf{D}_6^{2,2}$ shown in Fig. 7.6(a)

satisfies Eq. (8.15) with $v^s = 1$ and hence is divisible. By contrast, the structure $\mathbf{D}_6^{2,1}$ in Fig. 7.8(a) has $v/h = 0.5$, does not satisfy Eq. (8.15), and is indivisible.

In summary, Eqs. (8.14) and (8.15) are the necessary and sufficient conditions for a divisible prismatic tensegrity structure. If both are satisfied, the original structure $\mathbf{D}_n^{h,v}$ can be divided into n^c identical substructures $\mathbf{D}_{n^s}^{h^s,v^s}$.

7.4 Stability

In this section we show the condition for super stability of prismatic structures, and investigate their (prestress) stability. In particular we will investigate the effect of a number of critical factors: the main one is the connectivity of the structure, but the height/radius ratio and the ratio of the stiffness to the force density of the members may also be important. All of the results are calculated using symmetry-adapted coordinates, and the common notation used in applied group representation theory is used to describe the results.

7.4.1 Super Stability

In Chapter 2, we have presented the sufficient conditions for super stability of tensegrity structures:

[L1] The member directions do not lie on same conic at infinity (Connelly, 1999), or equivalently, the geometry matrix of the structure has rank of six for three-dimensional structures;

[L2] The force density matrix $\mathbf{E}$, or equivalently, the geometrical stiffness matrix $\mathbf{K}_G$ is positive semi-definite;

[L3] $\mathbf{E}$ or $\mathbf{K}_G$ has maximal rank, which for prismatic tensegrity structures is $6n - 12$.

For prismatic tensegrity structures that are indivisible, the first condition is satisfied, and hence, only the last two conditions need to be considered for verifying super stability of the structures.

From the analytical formulation of each block in Eq. (6.24), the blocks $\tilde{\mathbf{E}}^{B_1}$ and $\tilde{\mathbf{E}}^{B_2}$ corresponding to the representations B_1 and B_2, when they exist for n even, are

$$\begin{aligned} \frac{1}{q_v}\tilde{\mathbf{E}}^{B_1} &= (2-(-1)^h-(-1)^{n-h})t+1-(-1)^v \\ \frac{1}{q_v}\tilde{\mathbf{E}}^{B_2} &= (2-(-1)^h-(-1)^{n-h})t-1+(-1)^v, \end{aligned} \tag{7.31}$$

and the two-dimensional blocks $\tilde{\mathbf{E}}^{E_k}$ $(k=1,\ldots,p)$ are

$$\frac{1}{q_v}\tilde{\mathbf{E}}^{E_k} = \begin{pmatrix} 2t(1-C_{hk})+1-C_{vk} & -S_{vk} \\ -S_{vk} & 2t(1-C_{hk})-(1-C_{vk}) \end{pmatrix}, \tag{7.32}$$

the two eigenvalues of which are easily computed as

$$\frac{\lambda_1^{E_k}}{q_v} = 2t(1-C_{hk})+\sqrt{2(1-C_{vk})}, \quad \frac{\lambda_2^{E_k}}{q_v} = 2t(1-C_{hk})-\sqrt{2(1-C_{vk})}. \tag{7.33}$$

$\lambda_1^{E_k}>0$ holds since $t>0$, $1-C_{hk}>0$ and $1-C_{vk}\geq 0$. For representation E_1, we know from Eq. (7.24) that $\lambda_2^{E_1}=0$. To satisfy positive semi-definiteness and minimum rank deficiency of the force density matrix, which are two of the sufficient conditions for super stability of tensegrity structures, $\lambda_2^{E_k}$ for $k>1$ should be positive. Connelly and Terrell (1995) obtained the same two-dimensional blocks making use of the special properties of the force density matrix as a circulant matrix, and further proved that all other two-dimensional blocks (for $k>1$) are positive definite if and only if $h=1$; i.e., horizontal cables are connected to adjacent nodes. Hence, the third sufficient condition is satisfied and the second is true for the two-dimensional blocks for the structures with $h=1$. Furthermore, from the divisibility condition (8.14), the structure is indivisible for $h=1$, so that the first sufficient condition is satisfied.

To verify whether $h=1$ is actually the super stability condition for prismatic structures, we also need to investigate the one-dimensional blocks: $\tilde{\mathbf{E}}^{A_1}=\tilde{\mathbf{E}}^{A_2}=0$ always holds as discussed previously; and $\tilde{\mathbf{E}}^{B_1}$ and $\tilde{\mathbf{E}}^{B_2}$ exist only when n is even,

for which we have the following relation from Eq. (7.31) for $h = 1$

$$\begin{aligned}
\frac{1}{q_v}\tilde{\mathbf{E}}^{B_1} &= (2-(-1)^h-(-1)^{n-h})t+1-(-1)^v = 4t+1-(-1)^v \geq 4t > 0 \\
\frac{1}{q_v}\tilde{\mathbf{E}}^{B_2} &= (2-(-1)^h-(-1)^{n-h})t-1+(-1)^v = 4t-1-(-1)^v \\
&= 2\frac{\sqrt{2-2C_v}}{1-C_1}-1-(-1)^v \geq 2\frac{\sqrt{2-2C_1}}{1-C_1}-1-(-1)^1 = \frac{2\sqrt{2}}{\sqrt{1-C_1}}-2>0
\end{aligned}$$

In summary, $h = 1$ guarantees two of the sufficient conditions for super stability of a prismatic tensegrity structure: its force density matrix has rank deficiency of four (one in $\tilde{\mathbf{E}}^{A_1}$, one in $\tilde{\mathbf{E}}^{A_2}$ and two in two copies of $\tilde{\mathbf{E}}^{E_1}$), which is the minimum value for non-degeneracy of a structure in three-dimensional space; and the force density matrix is positive semi-definite with rand deficiency of four.

7.4.2 Prestress Stability

When a prismatic structure is divisible, the reduced stiffness matrix $\mathbf{Q}$, quadratic form of the geometrical stiffness matrix with respect to the mechanisms, must have at least one zero eigenvalue, corresponding to the relative motion of the substructures.

When the structure is indivisible, and satisfies the third condition, but $\mathbf{K}_G$ is not positive semi-definite, then the structure may, or may not, be prestress stable. $\mathbf{K}_G$ has at least one negative eigenvalue, but whether or not this leads to a negative eigenvalue of $\mathbf{Q}$ depends upon a subtle interplay of the stress matrix and the mechanisms, which themselves depend upon the geometric realization of the structure.

7.4.2.1 Symmetry-adapted Forms

Symmetry can be used to simplify calculations and clarify the presentation of the results (Kangwai *et al.*, 1999; Kangwai and Guest, 2000). By using a symmetry-adapted coordinate system, the matrices in a structural calculation can be block-diagonalized. Here, we eventually block-diagonalize the reduced stiffness matrix $\mathbf{Q}$. The block-diagonalization is simply an orthogonal change of basis, and does

not affect the eigenvalues — thus the eigenvalues of $\mathbf{Q}$ are the assembly of the eigenvalues of the individual blocks of the symmetry-adapted $\tilde{\mathbf{Q}}$.

To block-diagonalize the matrices, we consider symmetry subspaces. Each symmetry subspace corresponds to one of the irreducible representations μ of the group. For the dihedral symmetry group $\mathbf{D}_n$, the irreducible representations are, $A_1, A_2, B_1, B_2, E_1, \ldots, E_{n/2-1}$ for n even, and $A_1, A_2, E_1, \ldots, E_{(n-1)/2}$ for n odd (Bishop, 1973).

The blocks of the symmetry-adapted stress matrix $\tilde{\mathbf{K}}_G$ and equilibrium matrix $\tilde{\mathbf{A}}$ corresponding to μ are denoted by $\tilde{\mathbf{K}}_G^\mu$ and $\tilde{\mathbf{A}}^\mu$, respectively. The symmetry-adapted mechanisms lying in the null-space of the transpose of $\tilde{\mathbf{A}}^\mu$ are written as columns of $\tilde{\mathbf{M}}^\mu$. Then, the block $\tilde{\mathbf{Q}}^\mu$ corresponding to the representation μ of the symmetry-adapted quadratic form $\tilde{\mathbf{Q}}$ is

$$\tilde{\mathbf{Q}}^\mu = (\tilde{\mathbf{M}}^\mu)^{\mathrm{T}} \tilde{\mathbf{K}}_G^\mu \tilde{\mathbf{M}}^\mu. \tag{7.34}$$

The matrices $\tilde{\mathbf{Q}}^\mu$ have dimensions of only one or two for prismatic tensegrity structures as discussed in Chapter 6. And the structure is prestress stable if and only if $\tilde{\mathbf{Q}}^\mu$ are positive definite for all representations μ. Note that we have excluded from $\tilde{\mathbf{Q}}^\mu$ the rigid-body motions, which in these cases would correspond to zero eigenvalues of $\tilde{\mathbf{Q}}^{A_2}$ and $\tilde{\mathbf{Q}}^{E_1}$.

In the follows, we show that the prestress stability of a prismatic tensegrity structure is not only influenced by the connectivity of horizontal cables but also that of the vertical cables, and furthermore, is sensitive to the height/radius ratio. We also show that the selection of materials and level of prestress is one of the critical factors for the stability of prestress stable structures.

7.4.2.2 Height/Radius Ratio

Consider the indivisible structure $\mathbf{D}_7^{3,2}$ in Fig. 7.9 as an example. The relationship between the minimum eigenvalues of each block $\tilde{\mathbf{Q}}^\mu$ and the height/radius ratio is plotted in Fig. 7.10.

The matrix $\tilde{\mathbf{Q}}^{A_1}$ is always positive definite, while positive definiteness of $\tilde{\mathbf{Q}}^{E_2}$ and $\tilde{\mathbf{Q}}^{E_3}$ vary depending on the height/radius ratio. The structure is prestress stable only when the height/radius ratio falls into the small region $[0.75, 1.05]$, which is shown as a shaded area in the figure.

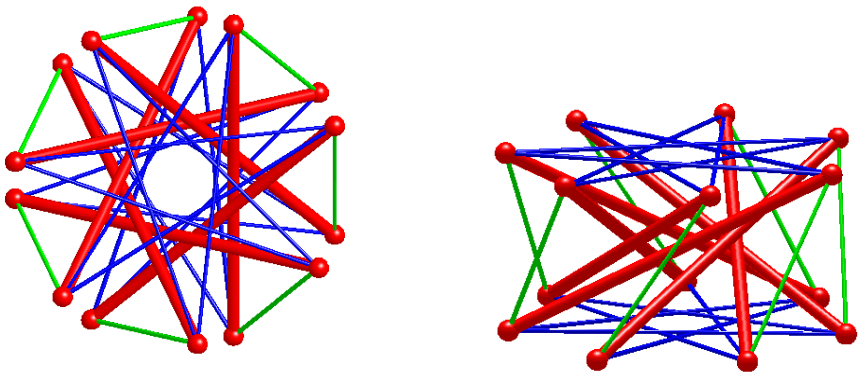

(a) top view (b) side view

Figure 7.9: The indivisible structure $\mathbf{D}_7^{3,2}$.

Consider another indivisible structure $\mathbf{D}_8^{2,3}$ with 16 nodes and 32 members as shown in Fig. 7.11. The dihedral group $\mathbf{D}_8$ has four one-dimensional and three two-dimensional representations. The relationship of the minimum eigenvalues of $\tilde{\mathbf{Q}}^{\mu}$ and the height/radius ratio is plotted in Fig. 7.11. The prestress stability region of the structure ranges from 0.4 to 3.1, which is much wider than that of the structure $\mathbf{D}_7^{3,2}$.

These examples have shown that the height/radius ratio of the structure can be a critical factor in the prestress stability of prismatic tensegrity structures.

7.4.2.3 Connectivity

As a prismatic tensegrity structure is super stable only if $h = 1$, it is clear that stability of this class of structures is directly related to the connectivity of horizontal cables. It has also been illustrated previously that in some special cases with the right height/radius ratio, the structure can still be prestress stable although it is not super stable. However, this is dependent upon the connectivity of both the horizontal and the vertical cables.

As an example, consider the structures $\mathbf{D}_8^{2,1}$ and $\mathbf{D}_8^{2,3}$, neither of which is super stable, and which only differ in the connectivity of their vertical cables. As we

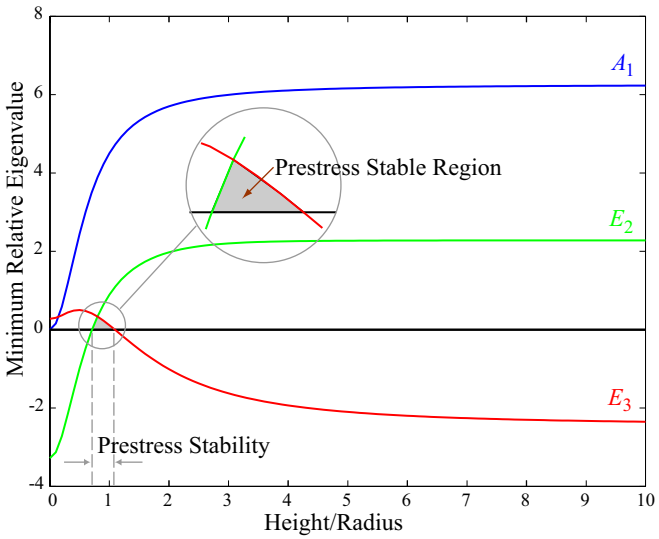

Figure 7.10: Influence of the height/radius ratio on the prestress stability of the structure $\mathbf{D}_7^{3,2}$. The structure is prestress stable when the ratio is in the range $[0.75, 1.05]$. In order to non-dimensionalize the results, the eigenvalues of $\mathbf{Q}$ are plotted relative to the force density in the vertical cables.

have seen in Fig. 7.11, $\mathbf{D}_8^{2,3}$ is prestress stable for a limited range of height/radius ratio. By contrast, the structure $\mathbf{D}_8^{2,1}$ in Fig. 7.12 is never prestress stable, because the minimum eigenvalue of $\tilde{\mathbf{Q}}^{E_3}$ is always negative.

7.4.2.4 Materials and Prestresses

So far, the prestress stability is investigated based on the positive definiteness of the quadratic form $\mathbf{Q}$ of the stress matrix with respect to the mechanisms, where the members are assumed to be made of materials with infinite stiffness. Here we show that selection of materials and level of prestresses does also affect the stability of the structures when they are not super stable.

We make the simplification that all of the struts and cables have the same axial stiffness. The key parameter is then the ratio of the axial stiffness to the prestress in the structure. Suppose that the cables and struts have axial stiffness AE/l, and that the vertical cables carry a force density of q_v. In the following example, we consider the stiffness for different values of $k = AE/(lq_v)$, where k is dimensionless. If the structure is linear-elastic, the strain due to a particular

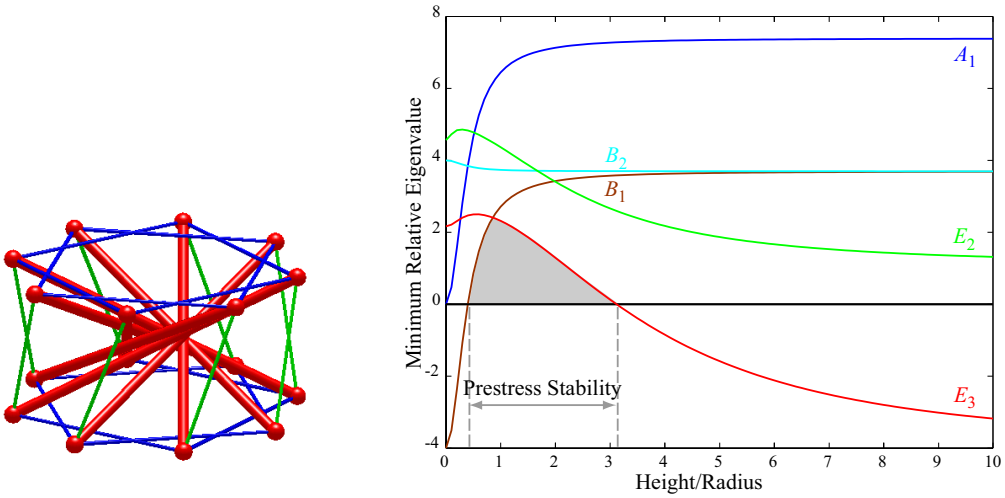

Figure 7.11: Influence of the height/radius ratio on the prestress stability of the structure $\mathbf{D}_8^{2,3}$. The structure is prestress stable when the ratio is in the range $[0.40, 3.10]$. The eigenvalues of $\mathbf{Q}$ are plotted relative to the force density in the vertical cables.

prestress will be $1/k$, and thus even values of $k = 100$ are too small to be realistic for conventional structures.

Fig. 7.13 shows the smallest eigenvalues of the tangent stiffness matrix for the structure $\mathbf{D}_7^{3,2}$, which is prestress stable with the height/radius ratio of 1.0. Results are plotted for $k = 10, 100, 1000$, and for the infinite stiffness case. As k reduces, the structure becomes less stable, and eventually loses stability altogether. Thus, the selection of materials and level of prestress is also a critical factor to the stability of tensegrity structures.

7.5 Catalogue of Symmetric Prismatic Structures

After the stability investigation, we are now in the position to present a catalogue describing the stability of prismatic tensegrity structures for small n:

- $h = 1$: The structures are super stable, and therefore are prestress stable.
- $h \neq 1$: There are two cases:

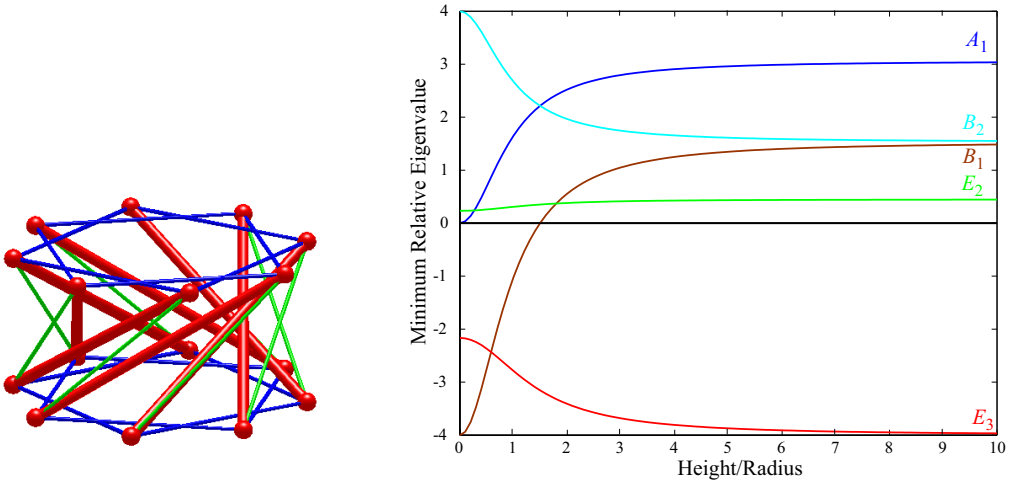

Figure 7.12: Influence of the height/radius ratio on the prestress stability of the structure $\mathbf{D}_8^{2,1}$. The structure is never stable. The eigenvalues of $\mathbf{Q}$ are plotted relative to the force density in the vertical cables.

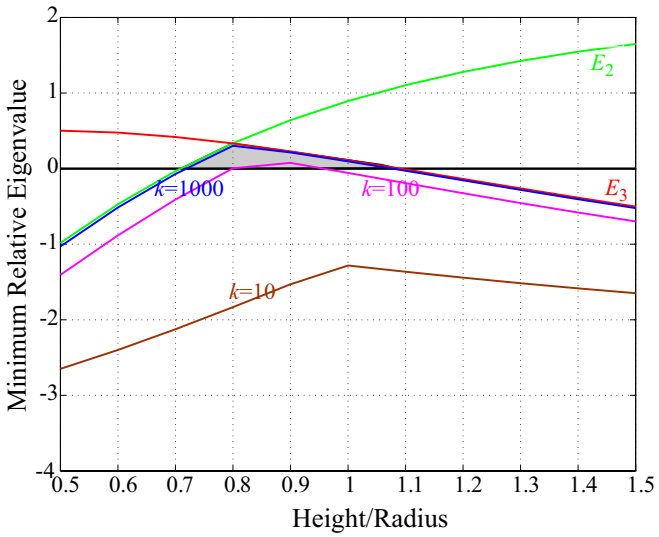

Figure 7.13: The influence of the stiffness/prestress ratio k on the stability of the structure $\mathbf{D}_7^{3,2}$. When k reduces, the structure becomes less stable. The eigenvalues of $\mathbf{K}$ are plotted relative to the force density in the vertical cables.

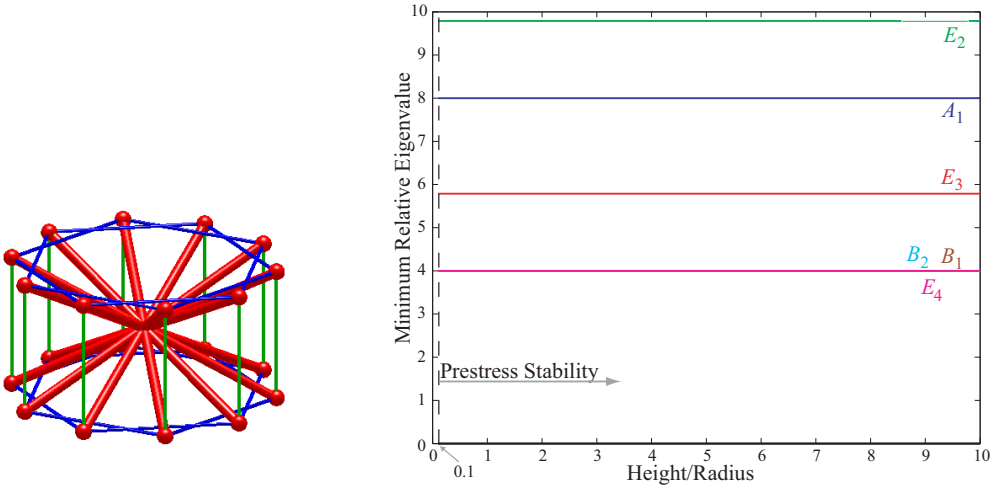

Figure 7.14: The structure $\mathbf{D}_{10}^{2,5}$ that is not super stable but is always prestress stable.

– *divisible*:

  The structures are divisible, and hence, unstable, if both of the conditions (8.14) and (8.15) are satisfied.

– *indivisible*:

  Prestress stability can be verified based on the symmetry-adapted form $\tilde{\mathbf{Q}}$ of reduced stiffness matrix, defined in Eq. (7.34).

We present in Table 7.2 a complete catalogue of prismatic tensegrity structures with symmetry $\mathbf{D}_n$ for $n \leq 10$.

From Table 7.2, it is easy to tell the stability of prismatic tensegrity structures. For example, the structure $\mathbf{D}_6^{2,2}$ can be divided into two identical substructures $\mathbf{D}_3^{1,1}$. Another example: for the structures with $n = 10$ and $h = 2$, the structure $\mathbf{D}_{10}^{2,3}$ is prestress stable in the region [0.70,1.35], and the structure $\mathbf{D}_{10}^{2,5}$ in Fig. 7.14 is always prestress stable. Note that all struts of the structure $\mathbf{D}_{10}^{2,5}$ run across the central (origin) point.

7.6 Discussions and Conclusions

A simple symmetry method has been presented to determine the self-equilibrated configuration of a prismatic tensegrity structure with dihedral symmetry. Rather than considering the whole structure, consideration of only one representative node is sufficient to find the force densities and the possible configurations in the state of self-equilibrium.

The symmetry-adapted formulation of the force density matrix presented in Chapter 6 has been used to derive the force densities of a general prismatic structure by ensuring the rank deficiency of four, which comes from the blocks corresponding to the representation A_2 and E_1. Using the analytical formulation and the force densities, it is shown that the blocks are identical to those by Connelly and Terrell (1995) in another way, and it is then further proved that prismatic structures are super stable if and only if their horizontal cables are connected to adjacent nodes.

The necessary and sufficient conditions for the divisibility of prismatic structures have been presented based on the connectivity of horizontal and vertical cables. Divisible structures have their own states of prestresses and rigid-body motions so that they can be physically separated into several identical substructures.

The prestress stability of prismatic structures is demonstrated to be related to the connectivity of the cables, and is also sensitive to the height/radius ratio. It is also shown that stability of a tensegrity structure that is not super stable is influenced by the selection of materials and level of prestress.

A complete catalogue of the prismatic tensegrity structures with relative small number of members has been presented. We have also developed a Java program to enable designers to interactively design the prismatic structures. The program is published online: *http://tensegrity.AIStructure.com/prismatic/*, where the latest version of JAVA Runtime and JAVA3D Runtime might be needed and can be freely downloaded from *http://java.sun.com*

Table 7.2: The stability of prismatic tensegrity structures $\mathbf{D}_n^{h,v}$. 's' denotes super stable, 'u' denotes unstable, and 'p' indicates that the structure is not super stable but is always prestress stable with arbitrary height/radius ratio. If the structure is prestress stable only in a specific region of height/radius ratio from h_1 to h_2, then this region is given by $[h_1, h_2]$; and if the structure can be divided, its substructures are given.

$n=3$	h
	1
v 1	s

$n=4$	h	
	1	2
v 1	s	u
2	s	$2\mathbf{D}_2^{1,1}$

$n=5$	h	
	1	2
v 1	s	u
2	s	u

$n=6$	h		
	1	2	3
v 1	s	u	u
2	s	$2\mathbf{D}_3^{1,1}$	u
3	s	p	$3\mathbf{D}_2^{1,1}$

$n=7$	h		
	1	2	3
v 1	s	u	u
2	s	u	[0.75,1.05]
3	s	u	u

$n=8$	h			
	1	2	3	4
v 1	s	u	u	u
2	s	$2\mathbf{D}_4^{1,1}$	u	$2\mathbf{D}_4^{2,1}$
3	s	[0.40,3.10]	u	u
4	s	$2\mathbf{D}_4^{1,2}$	[0.35,2.35]	$4\mathbf{D}_2^{1,1}$

$n=9$	h			
	1	2	3	4
v 1	s	u	u	u
2	s	u	u	u
3	s	u	$3\mathbf{D}_3^{1,1}$	u
4	s	u	[0.20,1.60]	u

$n=10$	h				
	1	2	3	4	
v 1	s	u	u	u	u
2	s	$2\mathbf{D}_5^{1,1}$	u	$2\mathbf{D}_5^{2,1}$	u
3	s	[0.70,1.35]	u	[0.75,1.25]	u
4	s	$2\mathbf{D}_5^{1,2}$	u	$2\mathbf{D}_5^{2,2}$	u
5	s	p	p	p	$5\mathbf{D}_2^{1,1}$

Chapter 8

STAR-SHAPED STRUCTURES

This chapter is to present self-equilibrated configuration, and more importantly, super stability condition of star-shaped tensegrity structures.

Star-shaped tensegrity structures have similar configuration to the prismatic structures studied in Chapter 7—both of them are of dihedral symmetry. However, as will be demonstrated in this chapter, they have very different stability properties, because the two additional nodes in star-shaped structures introduce more mechanisms.

Using the symmetry-adapted formulations presented in Chapter 6 for the structures with dihedral symmetry, we are to present the necessary and sufficient conditions for super stability of star-shaped structures in this chapter, and then to investigate their prestress stability. Moreover, some structures that are not super stable will be shown to have more than one stable configurations.

8.1 Introduction

Prismatic and star-shaped structures have similar symmetric configurations, but they are slightly different in connectivity. As shown in Fig. 8.1, the star-shaped structure has two more nodes lying on the (z-)axis going through the centers of the two circles on which other nodes are located. These two nodes are called *center nodes*, and other nodes are *boundary nodes*. Boundary nodes of a star-shaped structure are connected to center nodes by *radial cables*, unlike the prismatic structure where the (boundary) nodes are connected to each other by (horizontal) cables. Moreover, the center nodes of a star-shaped structure may have no

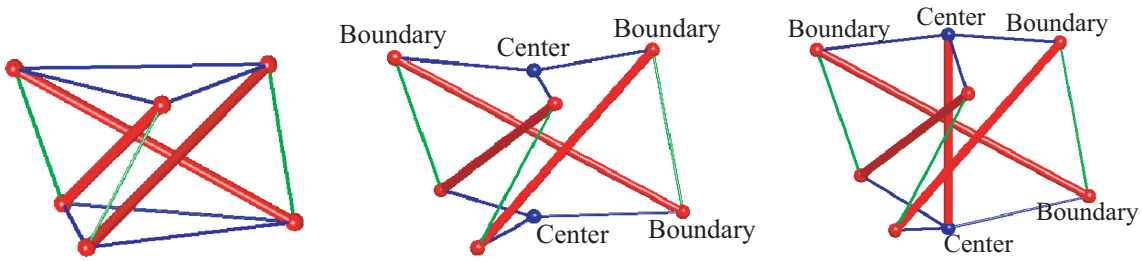

(a) (b) (c)

Figure 8.1: Tensegrity structures with dihedral symmetry $\mathbf{D}_3$. (a): prismatic tensegrity structure; (b), (c): star-shaped tensegrity structures. The star-shaped structures have two more (center) nodes than the prismatic structure. All of these structures are super stable.

physical connection as in Fig. 8.1(b), or they can be connected by an additional member (strut or cable) as in Fig. 8.1(c). All of these structures are of dihedral symmetry $\mathbf{D}_3$—the structures are indistinguishable under any of the six symmetry operations of dihedral group $\mathbf{D}_3$.

The prismatic structure has only one type (orbit) of nodes, such that any node of the structure can be moved to any other by a proper symmetry operation of the dihedral group. However, center and boundary nodes of a star-shaped structure are two different types of nodes, since there exists no such a symmetry operation in dihedral group that can move one node of a type to another node of the other.

The additional center nodes in star-shaped structures introduce more mechanisms than prismatic structures with the same symmetry. For example, numbers of mechanisms in the structures in Fig. 8.1(a), (b) and (c) are 1, 7 and 6, respectively, since all of these structures have only one mode of self-stress. Every boundary node of star-shaped structures has one mechanism in three-dimensional space, perpendicular to the plane in which the three members connecting it are lying. Hence, the star-shaped structure shown in Fig. 8.1.(b) has seven mechanisms, and the structure in Fig. 8.1.(c) has six mechanisms. Interestingly, both of these two star-shaped structures are super stable, although they consist of so many mechanisms. In this chapter, we will prove that there are some certain ways to verify super stability of star-shaped structures, making use of the symmetry-adapted formulations presented in Chapter 6.

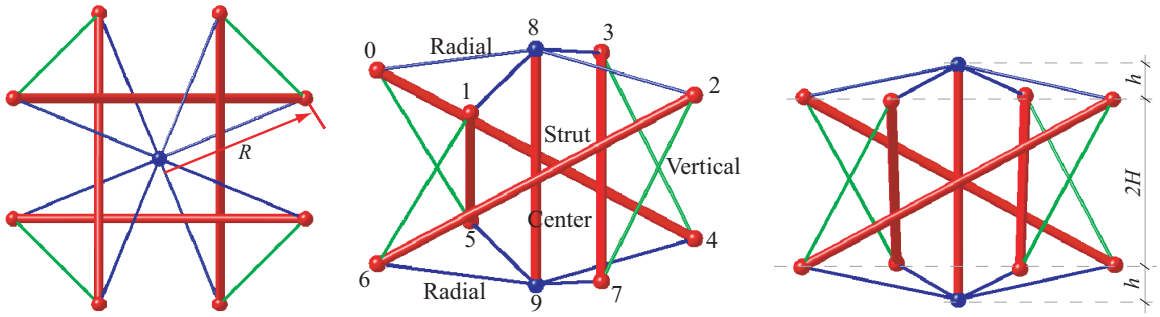

(a) top (b) perspective (c) side

Figure 8.2: Star-shaped tensegrity structure $\bar{\mathbf{D}}_4^1$ with center member. Configuration of the structure can be described by the parameters r, H and h.

8.2 Self-equilibrated Configuration

In this section, we firstly introduce the connectivity of nodes and members of a general star-shaped tensegrity structure, and then derive the force densities and configuration, making use of their symmetry properties as discussed in Chapter 7 for prismatic structures.

8.2.1 Connectivity and Symmetry

A star-shaped structure consists of two types of nodes—center nodes and boundary nodes, and three (or four) types of members—radial cables, vertical cables, struts (and a center member). The nodes (or members) of each type are of dihedral symmetry, since one of them can be taken to any others of the same type by proper symmetry operations of the dihedral group they belong to. Accordingly, we say that the structure has symmetry of dihedral group $\mathbf{D}_n$, where z-axis is taken as the principal axis. However, it is noticeable that nodes (or members) of different types can not be taken to each other by any symmetry operation of the group. Hence, each type of nodes (or members) forms an *orbit*, and different types of nodes (or members) belong to different orbits.

A star-shaped structure that is of dihedral symmetry $\mathbf{D}_n$ has $2n + 2$ nodes: $2n$ boundary nodes and two center nodes. We number the boundary nodes in the higher and lower circles as $\{0, \ldots, n-1\}$ and $\{n, \ldots, 2n-1\}$, respectively, and number the two center nodes $2n$ and $2n+1$, respectively. For example,

the numbering of the nodes of the structure $\bar{\mathbf{D}}_4^1$ is shown in Fig. 8.2.(b). The boundary nodes of the star-shaped structures are located on two parallel circles; and the center nodes are located on the (z-)axis, which goes through the centers of these two circles.

The members that connect the boundary nodes and the center nodes are called *radial cables*, and the *struts* and *vertical cables* connect the boundary nodes in different circles. Denoting the member that connects nodes i and j as $[i, j]$, members of a star-shaped structure can be defined as follows

$$\begin{array}{cc} \text{Radial cable :} & [2n, i] \text{ and } [2n+1, n+i] \\ \text{Vertical cable :} & [i, n+i+v] \\ \text{Strut :} & [i, n+i] \\ \text{Center member :} & [2n, 2n+1] \end{array} \quad , \text{ for } i \in \{0, \ldots, n-1\}, \tag{8.1}$$

where $n+i+v = i+v$ if $n+i+v \geq 2n$. Note that parameter v defines connectivity of vertical cables, and it can be assigned in the region of $1 \leq v < \frac{n}{2}$, as in that of the prismatic structures. Since only the connectivity of vertical cables in a star-shaped structure varies by v, while that of other types of members are fixed, its connectivity as well as symmetry can be denoted as $\mathbf{D}_n^v$. Moreover, for the structures with center members connecting their center members, we use the notation $\bar{\mathbf{D}}_n^v$. For example, the structure in Fig. 8.2 is denoted as $\bar{\mathbf{D}}_4^1$. Hence, a star-shaped structure $\mathbf{D}_n^v$ ($\bar{\mathbf{D}}_n^v$) has $4n$ (or $4n+1$) members—$2n$ radial cables, n struts, n vertical cables (and a center member).

To describe configuration of a star-shaped structure, we use the parameter r to denote radius of the circles of the boundary nodes lying on, $2H$ for distance between the two parallel circles, and h for the distance between the center node and the closes circle to it. Fig. 8.2 shows these notations for description of configuration of the structure $\bar{\mathbf{D}}_4^1$. It can be observed that the structure is convex if $h > 0$, and is concave if $h < 0$.

8.2.2 Self-equilibrium Analysis

Because the nodes of the same type have the same connectivity—every boundary node is connected by one radial cable, one vertical cable and one strut, and every center node is connected by n radial cables (and the center member)—and

moreover, a node with the members connected to it can be indistinguishably transformed to any other node, self-equilibrium analysis of the whole structure can be reduced to that of the representative nodes, a boundary node and a center node for star-shaped structures, to calculate the force density of each type of members in the state of self-equilibrium. Note that it is slightly different from the prismatic structures in Chapter 7, for the self-equilibrium analysis of which there is only one representative node.

Consider self-equilibrium of the boundary nodes first. Take a boundary in the upper plane as the *reference node*. Let $\mathbf{x}_0 \in \Re^3$ denote its coordinate vector in three-dimensional space. The coordinates of the other two boundary nodes in the lower plane, which are connected to the reference node by the strut and vertical cable, respectively, are denoted by $\mathbf{x}_s$ and $\mathbf{x}_v$; and that of the center node in the upper plane by the radial cable is $\mathbf{x}_c$.

Take z-axis as the principle axis and the original point $(0, 0, 0)$ as the invariant point against the symmetry operations. Because the boundary nodes are in the same orbit, the reference node $\mathbf{x}_0$ can be transformed to the other boundary nodes $\mathbf{x}_s$ and $\mathbf{x}_v$ connected to it by the proper two-fold rotations, which can be written as follows

$$\begin{aligned} \mathbf{x}_s &= \mathbf{R}_s \mathbf{x}_0 \\ \mathbf{x}_v &= \mathbf{R}_v \mathbf{x}_0 \end{aligned} \tag{8.2}$$

where the transformation matrices $\mathbf{R}_s$ and $\mathbf{R}_v$ are

$$\mathbf{R}_s = \begin{pmatrix} 1 & 0 & 0 \\ 0 & -1 & 0 \\ 0 & 0 & -1 \end{pmatrix}, \quad \mathbf{R}_v = \begin{pmatrix} C_v & S_v & 0 \\ S_v & -C_v & 0 \\ 0 & 0 & -1 \end{pmatrix} \tag{8.3}$$

by denoting $\cos(2v\pi/n)$ and $\sin(2v\pi/n)$ as C_v and S_v, respectively, for clarity.

The coordinate $\mathbf{x}_c$ of the center node in the upper plane is

$$\mathbf{x}_c = \begin{pmatrix} 0 \\ 0 \\ H + h \end{pmatrix} \tag{8.4}$$

Denote the force densities of the strut, vertical cable and radial cable as q_s, q_v and q_r, respectively. From Eqs. (8.3) and (8.4), the self-equilibrium equation of the reference node can be written as follows

$$q_s(\mathbf{x}_s - \mathbf{x}_0) + q_v(\mathbf{x}_v - \mathbf{x}_0) + q_r(\mathbf{x}_c - \mathbf{x}_0) = \mathbf{H}\mathbf{x}_0 + q_r\mathbf{x}_c = \mathbf{0} \tag{8.5}$$

where

$$\mathbf{H} = \begin{pmatrix} \mathbf{H}_1 & \\ & \mathbf{H}_2 \end{pmatrix} = -\begin{pmatrix} q_v(1-C_v)+q_r & -q_vS_v & \\ -q_vS_v & 2q_s+q_v(C_v+1)+q_r & \\ & & 2q_s+2q_v+q_r \end{pmatrix} \tag{8.6}$$

Since the self-equilibrium and prestress (super) stability of the tensegrity structures do not rely on the magnitude of the self-stresses in the members, we assume $q_s = -1$ for the strut without any loss of generality.

Since $\mathbf{H}_1$ and $\mathbf{H}_2$ are the two diagonal blocks of $\mathbf{H}$, Eq. (8.5) can be separated into the following two independent equations

$$\mathbf{H}_1\bar{\mathbf{x}}_0 = \mathbf{0} \tag{8.7}$$

where the vector $\bar{\mathbf{x}}_0 \in \Re^2$ denotes the coordinates of the reference node in xy-plane, and

$$\mathbf{H}_2 H + q_r(H+h) = (-2q_s - 2q_v - q_r)H + q_r(H+h) = 0 \tag{8.8}$$

In order to have non-trivial coordinates ($\bar{\mathbf{x}}_0 \neq \mathbf{0}$) in xy-plane, $\mathbf{H}_1$ should be singular. Hence, we have

$$(H+h)q_r^2 + h(C_v-1)q_r + 2H(C_v-1) = aq_r^2 + bq_r + c = 0 \tag{8.9}$$

The force density q_r of the radial cable can be solved as

$$q_r = \frac{-b+\sqrt{b^2-4ac}}{2a} \tag{8.10}$$

where the negative solution $q_r = \frac{-b-\sqrt{b^2-4ac}}{2a}$ has been ignored because we want only the positive value for the radial cables.

From Eq. (8.8), we have

$$q_v = 1 + q_r h/2H \tag{8.11}$$

The coordinate $\bar{\mathbf{x}}_0$ of the reference node in xy-plane lie in the null-space of $\mathbf{H}_1$ and its coordinate in z-direction is H. By applying the symmetry operations of the dihedral group $\mathbf{D}_n$, coordinates of all the other boundary nodes can then be uniquely determined.

The center node is connected by n radius cables and the center member if it exists. Because the center member lies on the z-axis, it is sufficient to consider the self-equilibrium of the center nodes only in z-direction, which can be written as

$$nq_r[(H+h)-H]+q_c[(H+h)-(-H-h)]=0 \tag{8.12}$$

Hence, we obtain

$$q_c=-nq_rh/(2H+2h) \tag{8.13}$$

So far, we have derived the force densities q_r, q_v, and q_c of the radial cables, vertical cables, and center member in Eqs. (8.10), (8.11), and (8.13), respectively, while the force density q_s of the strut is assumed to be -1.

8.3 Stability

In the stability investigation, the divisible structures that can be separated into several identical substructures should be excluded, because they should have been considered in the cases with lower symmetry. The conditions for identifying the divisible structures are presented in this section.

The sufficient and necessary conditions for the super stability of the structures without center member is presented. For the structures that are not divisible nor super stable, the prestress stability of them are shown to be dependent on the height/radius ratio.

8.3.1 Divisibility

A structure is said to be *divisible* if the members and nodes can be separated into several identical substructures. The substructures are pinned to the common center nodes and the center member if it exists. Rotation of one substructure about z-axis has no mechanical influence on the other substructures. Hence, the structure has finite mechanisms, and therefore, cannot be stable.

For example, the structure $\mathbf{D}_8^2$ with center member as shown in Fig. 8.3.(a) can be separated into two identical structures $\mathbf{D}_4^1$ as shown in Figs. 8.3.(b) and (c). The struts and vertical cables in each substructure connect one to another to form a closed circuit, so that the substructures are indivisible. It is obvious that

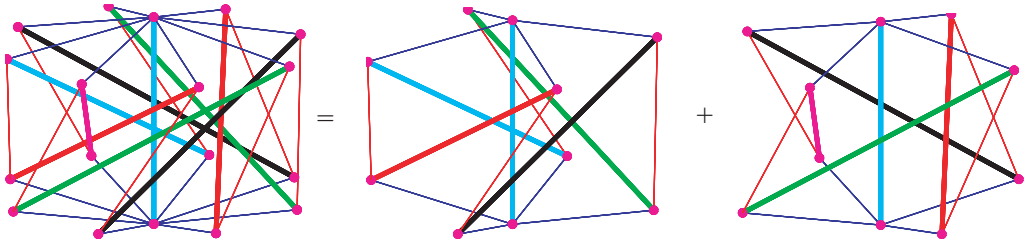

(a) original structure (b) substructure 1 (c) substructure 2

Figure 8.3: Divisible star-shaped tensegrity structure $\mathbf{D}_8^2$ with center member. The structure (a) can be 'divided' into two identical substructures (b) and (c). Note that the center member is also 'divided' into two halves, each one going to a substructure.

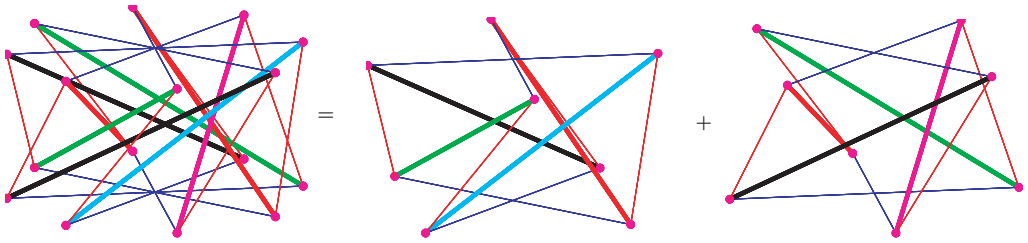

(a) original structure (b) substructure $\mathbf{D}_4^1$ (c) substructure $\mathbf{D}_4^1$

Figure 8.4: Divisible star-shaped tensegrity structure $\mathbf{D}_8^2$ without center member. The structure (a) can be divided into two identical substructures (b) and (c), without mechanical influence on the structure.

every substructure is in the state of self-equilibrium with the same force densities except for the center member, the force density of which is half of that of the original structure $\mathbf{D}_8^2$.

Similarly, the structures $\mathbf{D}_8^2$ without center member as shown in Fig. 8.4 is also divisible.

Because the boundary nodes are connected to the center nodes as radial cables, the structure is originally divisible if the struts and vertical cables are not considered. Thus, the divisibility of the structures is only related to the connectivities of struts and vertical cables.

Label the boundary nodes in the upper plane of the structure $\mathbf{D}_n^v$ from 0 to $n-1$, and the ones in the lower plane from n to $2n-1$. Node n is connected to node 0 as a strut. Hence, node i in the upper plane is connected by node $n+i$ in the lower plane as a strut. The center nodes in the upper and lower planes are

labelled as $2n$ and $2n+1$, respectively. And node $i(0 \leq i < n)$ connects node $n+i+v$ as a vertical cable.

Based on the connectivities of the struts and vertical cables mentioned above, we know that node i in the upper plane connects node $n+i+v$ as a strut, node $n+i+v$ connects node $i+v$ as a vertical cable, node $i+v$ connects $n+i+2v$ as a strut, and so on. Eventually, we must return back to the starting node i through this linkage. If we stop when the linkage returns back to the starting node i for the first time, the boundary nodes in the upper plane in the linkage can be listed as follows

$$i \rightarrow i+v \rightarrow i+2v \rightarrow \cdots \rightarrow i+jv-kn(=i) \tag{8.14}$$

where j and k are the minimum integers that they can be to ensure $0 \leq i+jv-kn \leq n-1$. The numbers j and k indicate the number of boundary nodes in the upper plane that have been visited and the number of rounds about z-axis, respectively.

From $i+jv-kn=i$ for returning to the starting node i, we have

$$jv = mn \tag{8.15}$$

If the structure is indivisible, we should have visited n boundary nodes in the upper node. Thus, we have $j=n$, and therefore, $v=m$, which can happen if and only if v and n have no common divisor except 1.

Hence, we can have the following lemma for the divisibility of star-shaped structures:

Lemma 8.1 *The necessary and sufficient indivisibility condition for a star-shaped tensegrity structure is that v and n have no common divisor except 1.*

Proof. The lemma has been proved based on the above discussions. □

8.3.2 Symmetry-adapted Force Density Matrix

The force density matrix $\mathbf{E} \in \Re^{(2n+2)\times(2n+2)}$ of a star-shaped tensegrity structure can be obtained going through the connectivity matrix and force densities as in Eq. (2.15) or the direct definition as in Eq. (2.16).

For example, the force density matrix $\mathbf{E} \in \Re^{8\times 8}$ of the structure $\mathbf{D}_3^1$ as shown in Fig. 8.1.(c) is

$$\mathbf{E} = \left(\begin{array}{ccc|ccc|cc} q & 0 & 0 & 1 & -q_v & 0 & -q_r & 0 \\ 0 & q & 0 & 0 & 1 & -q_v & -q_r & 0 \\ 0 & 0 & q & -q_v & 0 & 1 & -q_r & 0 \\ \hline 1 & 0 & -q_v & q & 0 & 0 & 0 & -q_r \\ -q_v & 1 & 0 & 0 & q & 0 & 0 & -q_r \\ 0 & -q_v & 1 & 0 & 0 & q & 0 & -q_r \\ \hline -q_r & -q_r & -q_r & 0 & 0 & 0 & 3q_r+q_c & -q_c \\ 0 & 0 & 0 & -q_r & -q_r & -q_r & -q_c & 3q_r+q_c \end{array}\right) \tag{8.16}$$

where the force densities of the struts are fixed as -1, and q is the sum of the force densities of the members connected to a boundary node; i.e., $q = -1 + q_v + q_r$. From the labels for the nodes defined previously, we know that the last two columns and rows of the force density matrix are corresponding to the center nodes.

Because the boundary nodes belong to the same orbit and form the *regular* dihedral group, we know that the linear combination of them can be written as follows from the discussion in Chapter 5

$$\Gamma(N^b) = A_1 + A_2 + (B_1 + B_2+)\sum_{k=1}^{p} 2E_k \tag{8.17}$$

And the two center nodes belong to the other orbit constituting a regular reflection group, so the linear combination of them is

$$\Gamma(N^c) = A_1 + A_2 \tag{8.18}$$

Because of the symmetry properties of the nodes, the force density matrix $\mathbf{E}$ can be block-diagonalized by using the unitary transformation matrix $\mathbf{T}$ such that

$$\tilde{\mathbf{E}} = \mathbf{T}\mathbf{E}\mathbf{T}^\top \tag{8.19}$$

where $\tilde{\mathbf{E}}$ denotes the symmetry-adapted version of $\mathbf{E}$.

Note that both of the boundary nodes and center nodes have the one-dimensional representations A_1 and A_2. Based on the irreducible representation matrices (characters as well for the one-dimensional representations), the non-normalized

transformation matrix corresponding to these two representations can then be written as follows

$$\begin{pmatrix} \mathbf{T}_b^{A_1} \\ \mathbf{T}_c^{A_1} \\ \mathbf{T}_b^{A_2} \\ \mathbf{T}_c^{A_2} \end{pmatrix} = \left(\begin{array}{cccc|cccc|cc} 1 & 1 & \dots & 1 & 1 & 1 & \dots & 1 & 0 & 0 \\ 0 & 0 & \dots & 0 & 0 & 0 & \dots & 0 & 1 & 1 \\ 1 & 1 & \dots & 1 & -1 & -1 & \dots & -1 & 0 & 0 \\ 0 & 0 & \dots & 0 & 0 & 0 & \dots & 0 & 1 & -1 \end{array}\right) \tag{8.20}$$

where the first n columns of the transformation matrix correspond to the n cyclic rotations of the boundary nodes about z-axis, the next n columns corresponds to the two-fold rotations, and the last two columns correspond to the reflection of the center nodes.

Applying the normalized version of the transformation matrix defined in Eq. (8.20) to the force density matrix as in Eq. (8.19), we derive the A_1 and A_2 blocks $\tilde{\mathbf{E}}^{A_1}$ and $\tilde{\mathbf{E}}^{A_2}$ of the symmetry-adapted force density matrix $\tilde{\mathbf{E}}$ as

$$\tilde{\mathbf{E}}^{A_1} = \begin{pmatrix} q_r & -\sqrt{n}q_r \\ -\sqrt{n}q_r & nq_r \end{pmatrix}, \quad \tilde{\mathbf{E}}^{A_2} = \begin{pmatrix} 2(q_v-1)+q_r & -\sqrt{n}q_r \\ -\sqrt{n}q_r & nq_r+2q_c \end{pmatrix} \tag{8.21}$$

$\tilde{\mathbf{E}}^{A_1}$ and $\tilde{\mathbf{E}}^{A_2}$ are positive semi-definite because their eigenvalues are

$$\begin{array}{ll} \lambda_1^{A_1} = 0, & \lambda_2^{A_1} = (n+1)q_r > 0 \\ \lambda_1^{A_2} = 0, & \lambda_2^{A_2} = q_r\frac{H+h}{H} + nq_r\frac{H}{H+h} > 0 \end{array} \tag{8.22}$$

from our assumption that $q_r > 0$ for the radial cables.

Since the center nodes have only A_1 and A_2 representations, we only need to derive the other blocks for the boundary nodes. And since the boundary nodes are of dihedral symmetry, the symmetry-adapted blocks corresponding the representation μ can be directly obtained as follows by using force densities and the irreducible representation matrices similar to the symmetry-adapted formulation of the force density matrix in Eq. (6.12)

$$\tilde{\mathbf{E}}^{\mu} = (q_v + q_r - 1)\mathbf{R}_0^{\mu} - (-1)\mathbf{R}_n^{\mu} - q_v\mathbf{R}_{n+v}^{\mu} \tag{8.23}$$

where $\mathbf{R}_0^{\mu}$, $\mathbf{R}_n^{\mu}$ and $\mathbf{R}_{n+v}^{\mu}$ are the irreducible representation matrices corresponding to the identity, struts and vertical cables for the representation μ, respectively.

When n is even, the one-dimensional representations B_1 and B_2 exist, and the irreducible representation matrices (characters) of them are

$$\begin{array}{lllll} B_1: & \mathbf{R}_0^{B_1} = 1, & \mathbf{R}_n^{B_1} = 1, & \mathbf{R}_{n+v}^{B_1} = (-1)^v \\ B_2: & \mathbf{R}_0^{B_2} = 1, & \mathbf{R}_n^{B_2} = -1, & \mathbf{R}_{n+v}^{B_2} = (-1)^{v+1} \end{array} \tag{8.24}$$

the $\tilde{\mathbf{E}}^{B_1}$ and $\tilde{\mathbf{E}}^{B_2}$ blocks corresponding to these representations can be written as

$$\begin{aligned}\tilde{\mathbf{E}}^{B_1} &= \lambda^{B_1} = q_r + 1 + (-1)^{v+1} > 0 \\ \tilde{\mathbf{E}}^{B_2} &= \lambda^{B_2} = q_r - 1 + (-1)^{v}\end{aligned} \tag{8.25}$$

Because B_2 block exists only if n is even, v should not be even; otherwise, n and v have common divisor except 1 so that the structure is divisible. When v is odd, we have

$$\lambda^{B_2} = q_r + 2 > 2 (> 0) \tag{8.26}$$

The irreducible representation matrices $\mathbf{R}_0^{E_k}$, $\mathbf{R}_n^{E_k}$ and $\mathbf{R}_{n+v}^{E_k}$ for the two-dimensional representations $E_k (1 \leq k \leq (n-1)/2)$ of the dihedral group $\mathbf{D}_n$ are

$$\mathbf{R}_0^{E_k} = \begin{pmatrix} 1 & 0 \\ 0 & 1 \end{pmatrix}, \quad \mathbf{R}_n^{E_k} = \begin{pmatrix} 1 & 0 \\ 0 & -1 \end{pmatrix}, \quad \mathbf{R}_{n+v}^{E_k} = \begin{pmatrix} C_{vk} & S_{vk} \\ S_{vk} & -C_{vk} \end{pmatrix} \tag{8.27}$$

From Eq. (8.23), the $\tilde{\mathbf{E}}^{E_k}$ corresponding to the two-dimensional representations $\mathbf{E_k}$, which appears twice in the $\tilde{\mathbf{E}}$, can be written as

$$\tilde{\mathbf{E}}^{E_k} = \begin{pmatrix} q_r + q_v(1 - C_{kv}) & -q_v S_{kv} \\ -q_v S_{kv} & q_r - 2 + q_v(1 + C_{kv}) \end{pmatrix} \tag{8.28}$$

Determinacy of $\tilde{\mathbf{E}}^{E_k}$ is equal to zero if $C_{vk} = C_v$; i.e., $k = 1$. Hence, the force density matrix has at least four zero eigenvalues—two in the duplicated $\tilde{\mathbf{E}}^{E_1}$ blocks and additional two in the one-dimensional $\tilde{\mathbf{E}}^{A_1}$ and $\tilde{\mathbf{E}}^{A_2}$ blocks, which satisfies the non-degeneracy condition for a general tensegrity structure.

8.3.3 Super Stability

In Lemma 3.2, we have presented the sufficient and necessary conditions for the super stability of a tensegrity structure in three-dimensional space:

[L1] The force density matrix has the minimum rank deficiency of four;

[L2] The force density matrix is positive semi-definite;

[L3] The geometry matrix has rank of six.

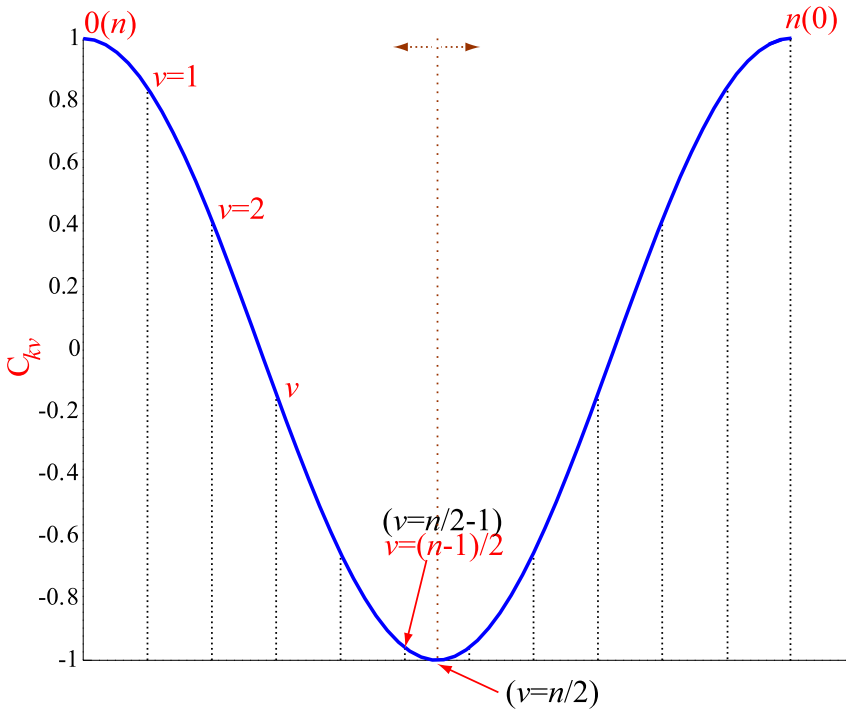

Figure 8.5: Cosine corresponding to the connectivity of vertical cables v ($n = 11$). It shows the idea, for super stability condition for the star-shaped tensegrity structures without center members, that $C_{kv} > C_v$ holds for any k only if n is odd.

In the following discussions on the stability, the third condition is assumed to be satisfied if the star-shaped tensegrity structure is indivisible.

We have known that the one-dimensional blocks are positive semi-definite if the structure is indivisible, with two zero eigenvalues in $\tilde{\mathbf{E}}^{A_1}$ and $\tilde{\mathbf{E}}^{A_2}$. If all the two-dimensional blocks $\tilde{\mathbf{E}}^{E_k}$ $(k \neq 1)$ are positive definite, while $\tilde{\mathbf{E}}^{E_1}$ is positive semi-definite, the first two conditions are also satisfied, and therefore, the structure is super stable. Thus, the problem of finding the super stable structures becomes that of finding the conditions for $\tilde{\mathbf{E}}^{E_k}(k \neq 1)$ being positive definite and $\tilde{\mathbf{E}}^{E_1}$ being positive semi-definite.

However, the positive definiteness of $\tilde{\mathbf{E}}^{E_k}$ in Eq. (8.28) is not so clear for the structures with center member, because the force densities are non-linear with respect o the h/H ratio. In the follows, we concentrate only on the simpler case where the center member is removed.

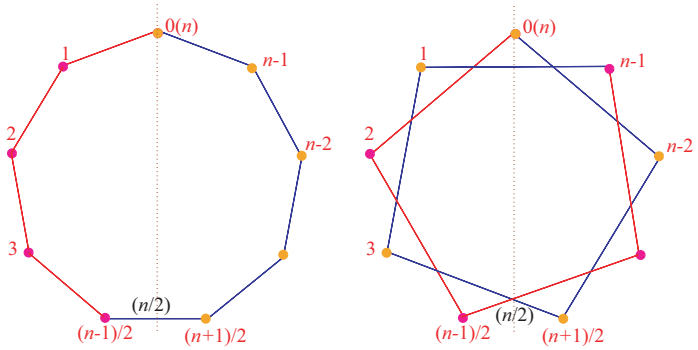

(a) $v = 1$ (indivisible) (b) $v = 2$ (indivisible)

(c) $v = 3$ (divisible) (d) $v = 4$ (indivisible)

Figure 8.6: Connectivity of boundary nodes in one plane through struts and vertical cables ($n = 9$). It shows the idea, for super stability condition for the star-shaped tensegrity structures without center members, that $C_{kv} > C_v$ holds for any k only if $v = (n-1)/2$.

When the center member is absent, we have $h = 0$ and the force densities of the vertical and radial cables become

$$\begin{aligned} q_v &= -q_s = 1 \\ q_r &= \sqrt{2(1-C_v)} \end{aligned} \tag{8.29}$$

The eigenvalues of the two-dimensional blocks $\tilde{\mathbf{E}}^{E_k}$ are

$$\begin{aligned} \lambda_1^{E_k} &= \sqrt{2(1-C_v)} + \sqrt{2(1-C_{kv})} > 0 \\ \lambda_2^{E_k} &= \sqrt{2(1-C_v)} - \sqrt{2(1-C_{kv})} \end{aligned} \tag{8.30}$$

In order to ensure that $\tilde{\mathbf{E}}^{E_k} (k \neq 1)$ is positive definite, we need

$$C_{kv} > C_v \tag{8.31}$$

To investigate in what cases can Eq. (8.31) be satisfied, consider the cosine for different v and kv as shown in Fig. 8.5. The cosine values are of reflection symmetry with respect to the center line running across $n/2$, and run as a cycle for kv.

Consider the boundary nodes in the upper plane. If the structure is indivisible, we will eventually stop at node 0 (or n as well) while starting from node v after n steps travelling along by kv, and every node in the plane will have been visited exactly once. For example, see the difference connectivities of the nine nodes in the upper plane of the indivisible structures with $\mathbf{D}_9$ symmetry as shown in Figs. 8.6.(a), (b) and (d). If the structure is divisible, at least one node is visited more than once within the n steps, e.g., three nodes of the divisible structure in Fig. 8.6.(c) have been visited in the trip.

We may notice that the cosine values in Fig. 8.5 corresponding to the labels of the nodes in Fig. 8.6 have the same reflection symmetry with respect to the plane running across $n/2$. This means that $C_i = C_{n-i}$. So, if k can run from 1 to n and the structure is indivisible, then C_{vk} can have the cosine values as in Fig. 8.5 exactly twice except for 1 and -1, because of the reflection symmetry.

If the structure is divisible, some nodes with $C_{kv} = C_v$ for their cosines are visited more than once. Hence, it will introduce additional zero eigenvalues in the force density matrix. The only exception is $\mathbf{D}_4^2$, because that it has 1 and -1 for the cosines only once because they are the maximum and minimum values that they can be. However, the geometry matrix of this structure is not full-rank, and therefore, the structure is not super stable.

Because the number of the two-dimensional representations of a dihedral group cannot exceed $n/2$, we can have the cosine values exactly once for C_{vk} if the structure is indivisible. Hence, in order to satisfy Eq. (8.31), the structure should be indivisible and C_v should have the minimum cosine value. $v = n/2$ (n is even) has the minimum cosine -1, but the structure is divisible. So, $v = (n-1)/2$ (n is odd) is the only possibility that Eq. (8.31) can be satisfied.

From the above discussions, we have the following lemma for super stability of star-shaped tensegrity structure without center member:

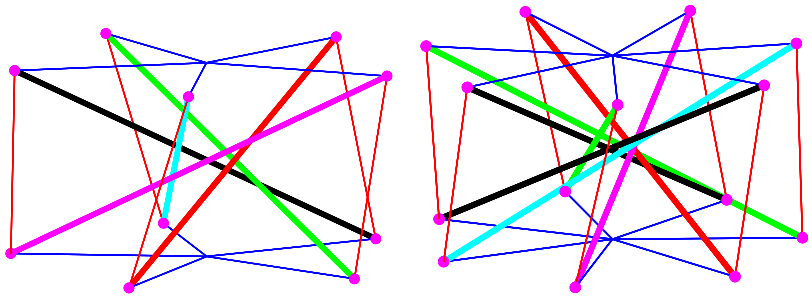

(a) $\mathbf{D}_5^2$ (b) $\mathbf{D}_7^3$

Figure 8.7: Star-shaped tensegrity structures that are super stable. All of them have odd number of struts, and the struts have minimum distances to each other.

Lemma 8.2 *A star-shaped tensegrity structure that is of dihedral symmetry and has no member connecting its center nodes is super stable if and only if the following two conditions are satisfied*

[L1] The structure has odd number of struts; i.e., n is odd.

[L2] The struts are as close to each other as possible, or in another term, the connectivity v of the vertical cables is $(n-1)/2$.

Proof. The lemma can be proved from the discussions for satisfying the relation in (8.31). □

When the structure is super stable, its struts come closest to but do not contact with each other. For example, the structure $\mathbf{D}_3^1$ in Fig. 8.1.(b) and the structures $\mathbf{D}_5^2$ and $\mathbf{D}_9^4$ in Fig. 8.7 are super stable.

8.3.4 Stability of the Structures without Center Member

Consider the star-shaped tensegrity structures without center member, the boundary nodes of which are of dihedral symmetry $\mathbf{D}_7$. In Figs. 8.8, 8.9 and 8.10, the minimum eigenvalue of the quadratic form of the geometrical stiffness with respect to the mechanisms against the ratio of the height and the radius of the structure are plotted.

It is obvious that $\mathbf{D}_7^3$ is always prestress stable because it is super stable. And we can observe that the structures $\mathbf{D}_7^1$ and $\mathbf{D}_7^2$ can be prestress stable if the height/radius ratio is large enough.

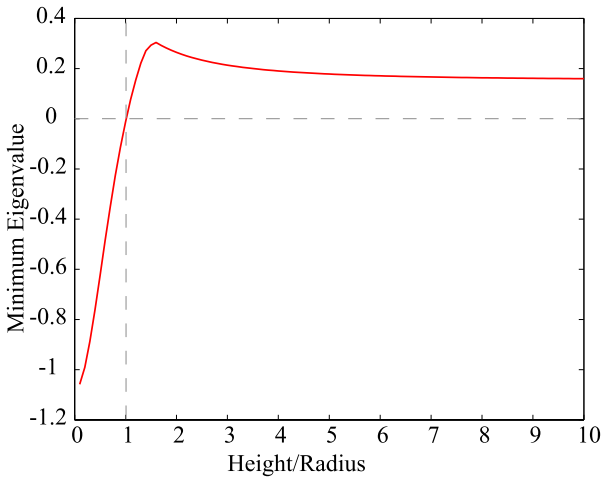

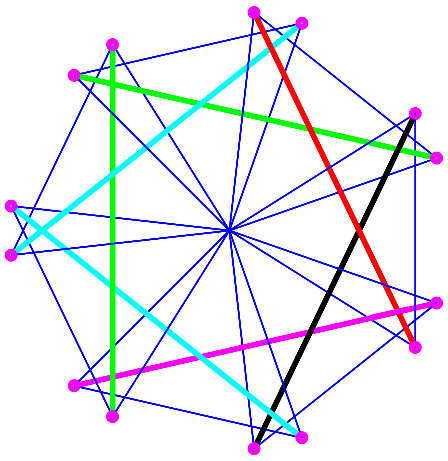

Figure 8.8: Star-shaped tensegrity structure $\mathbf{D}_7^1$ without center member. It is prestress stable when its height/radius ratio is large enough: $H/r > 1.0$ in this case.

Table 8.1: Prestress stable structures.

$v\backslash n$	3	4	5	6	7	8	9	10
1	S	P	P	P	P	P	P	P
2		D	S	D	P	D	P	D
3				D	S	P	N	P
4						D	S	D
5								D

Based on the numerical investigations of the stability of the star-shaped tensegrity structures without center member up to $n = 10$, we have the stability properties of the structures as listed in Table 8.1. Note that in Table 8.1, 'P', 'S' and 'D' denote prestress stable, super stable and divisible, respectively.

From the numerical investigations and Table 8.1, we may observe the following facts for the prestress stability of the indivisible structures without center member, which need to be carefully verified in the future work:

[L1] Prestress stability of the structures is sensitive to the height/radius ratio.

[L2] When the height/radius is large enough, the structures become prestress stable.

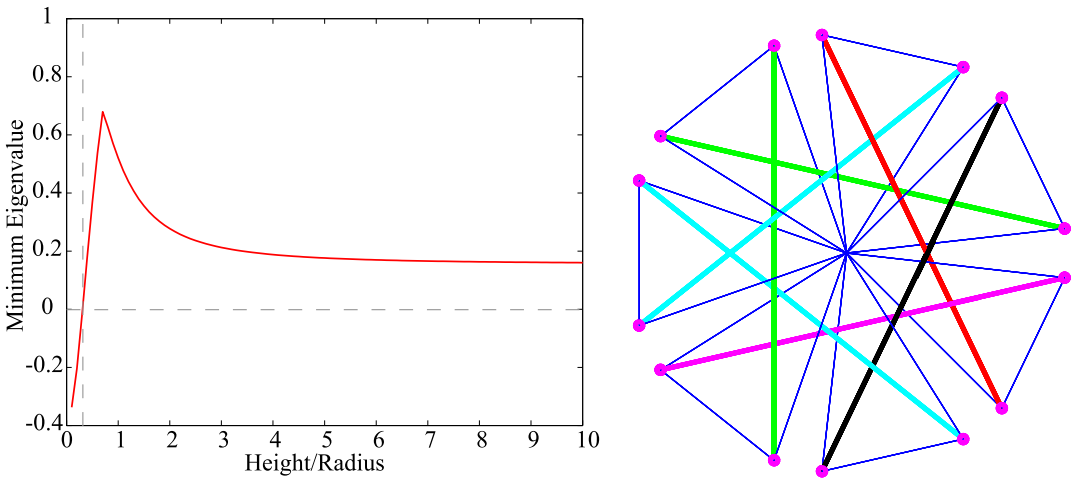

Figure 8.9: Star-shaped tensegrity structure $\mathbf{D}_7^2$ without center member. It is prestress stable when its height/radius ratio is large enough: $H/r > 0.3$ in this case.

However, it seems that it is apparent for us to draw the second conclusion as mentioned above, and it is a conjecture about the prestress stability of star-shaped structures at the moment. How to verify the above arguments might be considered in the future work, perhaps based on the symmetry-adapted form of the quadratic form of the geometrical stiffness matrix with respect to the mechanisms.

8.3.5 Stability of the Structures with Center Members

Some numerical examples of the star-shaped tensegrity structures with center member also show that they are super stable if the two sufficient and necessary conditions are satisfied as the structures without center member. For example, numerical investigation tells us that the structure in Fig. 8.1.(c) is super stable.

However, this is not guaranteed, because the distance h from the center node to the nearest horizontal plane can vary, and the force density matrix is non-linear with respect to the ratio h/H.

For the prestress stability of the star-shaped structures with center member, we consider the structure $\mathbf{D}_4^1$ as shown in Fig. 8.2. The similar structure to this without center member is shown in Table 8.1 to be prestress stable if the

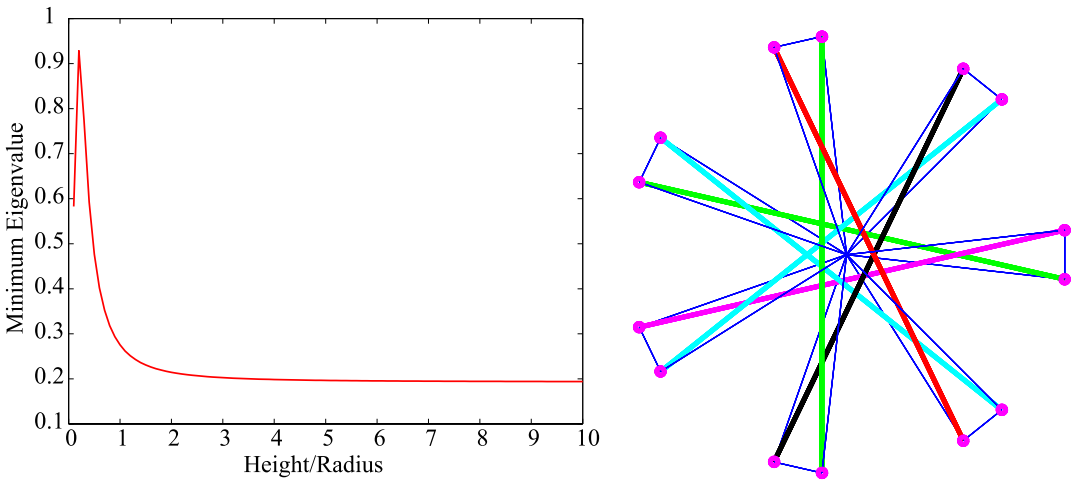

Figure 8.10: Star-shaped tensegrity structure $\mathbf{D}_7^3$ without center member. It is not super stable but always prestress stable.

height/radius ratio is large enough.

When $h = 0.0$, we can see from Fig. 8.11.(a) that the structure with center member (note that there exist no self-stress in the center member in this case) can be prestress stable if the height/radius ratio is large enough, which is larger than 0.5 in the case.

In order to investigate the influence of the value of h to the prestress stability of the structure, the ratio between the height and the radius of the structure is fixed as $H/r = 3.0$. By letting h run from -1.55 to 5.0, the relationship between the minimum eigenvalue of the quadratic form and h is plotted in Fig. 8.11.(b).

Remind that when $h < 0$, the center member is a cable or a strut when $h > 0$. From the Fig. 8.11.(b), it is implicit to tell the influence of h to the prestress stability of the structure when the center member is a cable. And it is apparent that the structure can become *more stable* with the increasing h when the center member is a strut.

From the above discussions on the prestress stability of the star-shaped structures with and without center member, we learn that it is sensitive to the height/radius ratio similar to the prismatic tensegrity structures. However, it is unlikely to tell explicitly in what circumstances the structures can be prestress stable.

And we have the conjecture for the star-shaped tensegrity structures that are

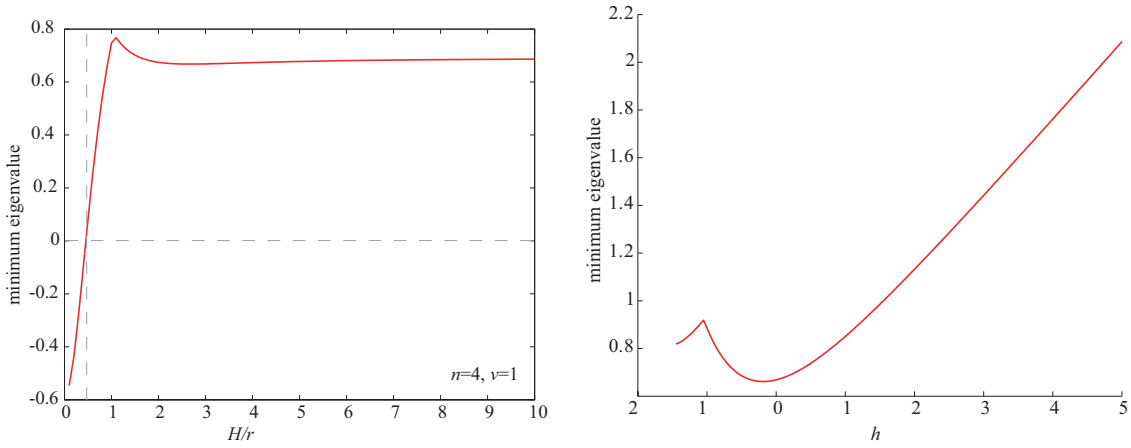

(a) $h = 0.0$ with varied H/r (b) $H/r = 3.0$ with varied h

Figure 8.11: The structure P_4^1 that is not super stable but can be prestress stable. It has a center member connecting its two center nodes.

not super stable: the structures are prestress stable if the height/radius ratio is large enough. The conjecture is promised to be proved based on the symmetry-adapted forms of the matrices.

8.4 Multi-stable Structure

From the super stability condition for a star-shaped tensegrity structure in Lemma 8.2, the structure $\mathbf{D}_4^1$ as shown in Fig. 8.12 is not super stable, and it can be prestress stable when the height/radius ratio is large enough from the numerical investigation.

Interestingly, the structure can have several stable configurations, which can be switched by proper external loads. For example, the photos of initial and another stable configurations of the physical model $\mathbf{D}_4^1$ are shown in Fig. 8.13.

To confirm the multi-stable behavior of this structure, structural analysis has been carried out. The ratio of hight to radius of the example structure is 1.0. The linear stiffness A_iE_i for struts and cables are set to 1.0×10^6 N and 1.0×10^2 N, respectively. The force densities of the struts, vertical cables and radial cables in the state of self-equilibrium are -1.0, 1.0, and $\sqrt{2}$, respectively. The displacements of node 10 in the bottom plane as in Fig. 8.14 in every direction

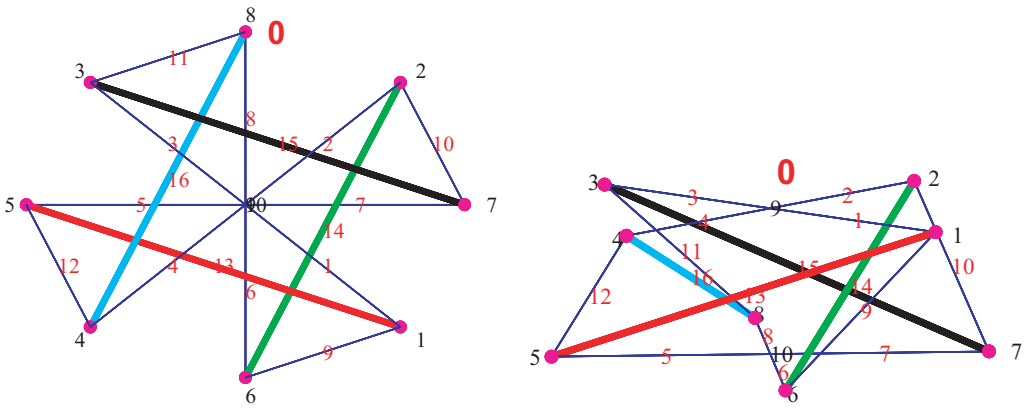

(a) top view (b) side view

Figure 8.12: The initial stable configuration of the star-shaped tensegrity structure $\mathbf{D}_4^1$. It is of dihedral symmetry.

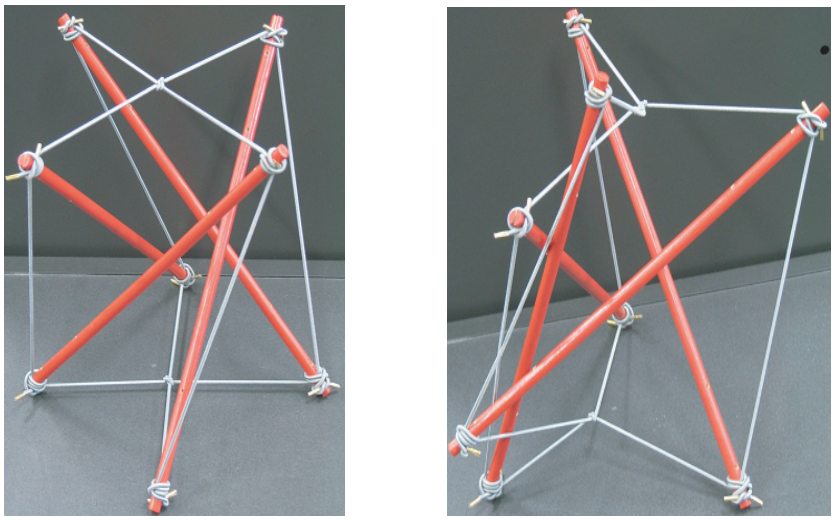

(a) initial stable configuration (b) the other stable configuration

Figure 8.13: The physical model of the initial stable configuration of the star-shaped tensegrity structure $\mathbf{D}_4^1$ with dihedral symmetry, and another stable configuration with lower symmetry. The two stable configurations can be switched to each other by proper external loads.

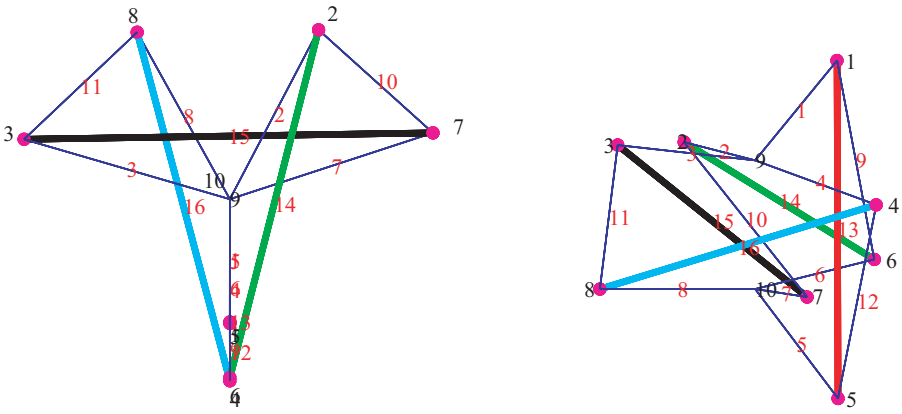

(a) top view (b) side view

Figure 8.14: The other stable configuration of the star-shaped tensegrity structure $\mathbf{D}_4^1$. External loads can be applied to exchange this configuration and the initial configuration as shown in Fig. 8.12. Note that dihedral symmetry of the initial structure is broken.

are constrained, while the displacements of node 6 in x-direction and node 9 in xy-plane are also constrained. This way, the rigid-body motions of the structure are constrained.

Enforced rotation of node 4 about z-axis is applied. It is moved counter-clockwise through $\pi/4$ by 20 steps, and finally arrives at the position as in Fig. 8.14 which is the other stable configuration of the structure. Displacement control has been used in the structural analysis. It can be observed from the figure that nodes 1, 4, 5 and 6 fall in the same line at the final stable configuration.

The strain energy stored in the structure can be calculated as the sum of those stored in each member:

$$\Pi = \sum q_i^2 l_i^3/(2A_i E_i)$$

The stain energy for each iteration step is plotted in Fig. 8.15, and the follows have been observed concerned about the enforced rotation θ of node 4

1. **At the initial position $\theta = 0^o$:**

   The strain energy is the local minima in the neighborhood, and therefore, it is in the state of self-equilibrium as well as stability.

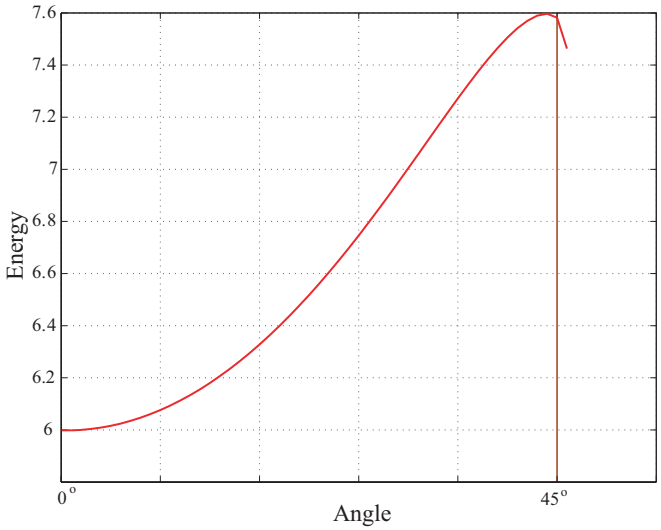

Figure 8.15: Strain energy of the structure $\mathbf{D}_4^1$ at every iteration step of the enforced rotation of node 4 about z-axis.

2. From $\theta = 0^o$ to the position with the maximum energy $\Pi_{\max}$:

The strain energy increases associated with the enforced rotation. It is equilibrated by the external loads, and is not in the state of self-equilibrium since the gradient of the energy Π against rotation θ is not equal to zero. Moreover, it would return to the initial configuration $\theta = 0^o$ if the external loads are removed at this stage.

3. At the position of $\Pi_{\max}$:

The structure is at the state of self-equilibrium since the gradient of Π to θ is zero, but it is not stable because the energy is the maximum. It will move back to the initial stable configuration, or move forward to next stable configuration, dependent on the infinitesimal disturbance of external loads.

4. Passing $\Pi_{\max}$:

This is not the stable nor the self-equilibrated configuration.

5. At the final position $\theta = 45^o$:

Although the structure is not at the state of stability nor self-equilibrium in the conventional meaning from the figure, further deformation is prevented

by the contact of three struts, and hence, it stops at this configuration and forms another 'stable' configuration.

The deformations of the structure at each step in the structural analysis are shown in Fig. 8.16.

8.5 Discussions and Conclusions

In this chapter, self-equilibrated configurations of star-shaped tensegrity structures have been analytically determined using the symmetry method presented in Chapter 7. The sufficient and necessary divisibility conditions for this class of structures have been derived based on the connectivity of vertical cables. Conditions for super stability of them have been further presented and proved using the analytical formulation of the symmetry-adapted force density matrix presented in Chapter 6.

Center nodes and boundary nodes of star-shaped structures belong to two different orbits, and hence, there are two representative nodes for this class of structures; self-equilibrated configurations are determined by considering self-equilibrium equations of these representative nodes, instead of the whole structure to give general solution of the whole class of structures. There are two kinds of star-shaped structures considered in this chapter: those with center members connecting the center nodes, and those without center members. Similarly to prismatic tensegrity structures, xy-coordinates are independent on z-coordinates for the structures without center members; while z-coordinates of the structures with center members also influence the xy-coordinates.

The divisible structures should be excluded from stability investigation, since the substructures should have been considered in the cases with lower symmetry. It has been proved that the structures are indivisible, only if the parameter n describing symmetry $\mathbf{D}_n$ of the structure and the parameter v describing connectivity of their vertical cables do not have common factors except 1. For the indivisible structures, numerical investigations shows that they can be prestress stable, if not super stable, when the height/radius ratios are large enough.

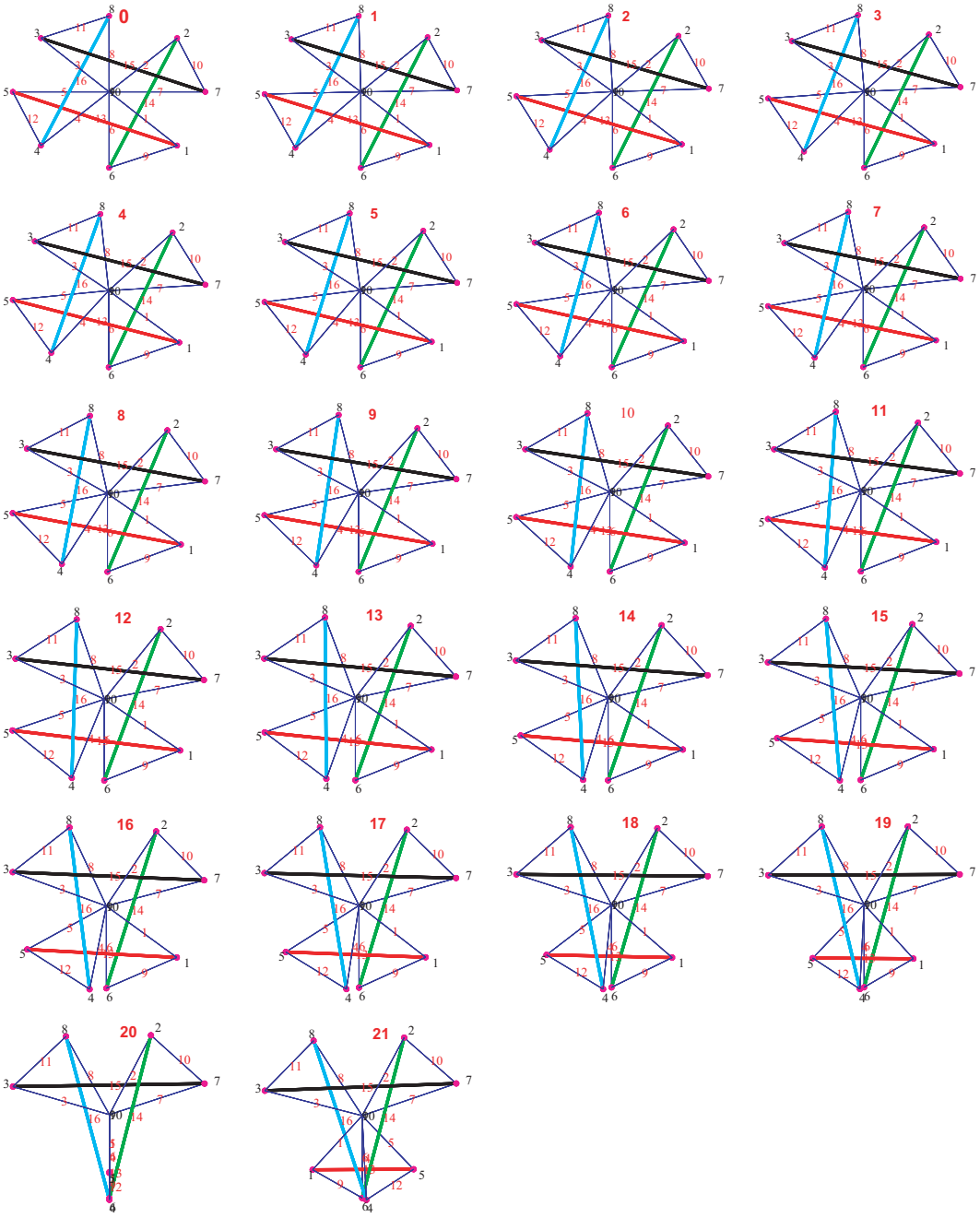

Figure 8.16: Multi-stable behavior of the star-shaped tensegrity structure $\mathbf{D}_4^1$. The two different stable configuration of the structure can be switched to each other by the proper external load, for example the enforced rotation of a boundary node in this numerical computation.

For the star-shaped structures without center members, the symmetry-adapted force density matrix formulated in Chapter 6 enables us the find the super stability condition for them: a structure is super stable if and only if the number of its struts is odd and the struts are closest to each other.

For the structures that are not super stable, numerical investigations indicate that they can be prestress stable if the ratio of hight to radius if high enough. Furthermore, some of the prestress stable structures, for example the structure $\mathbf{D}_4^1$ studied this chapter, might have several stable configurations with lower level of symmetry other than the initial configuration with dihedral symmetry. This multi-stable behavior has been successfully confirmed by numerical analysis and physical models.

Chapter 9

FORCE DESIGN

In this chapter, we present a bi-objective optimization approach for force design of tensegrity structures, which have more than one independent force modes.

From the self-equilibrium equation with respect to prestresses, the distribution of prestresses can be formulated as the linear combination of the independent modes of prestresses of the structure. Moreover, after the determination of configuration of a tensegrity structure by the designers, the only chance to influence its stiffness and stability is to determine the distribution of prestresses of the structure satisfying the self-equilibrium equation. Hence, we are provided the opportunity to design a structure as strong as possible (with the maximum stiffness) by carefully selecting the distribution of prestresses for the structures with multiple force modes. The process of determination of the prestresses for the structures with given configurations is called *force design*.

In this chapter, we are concerned about the force design of tensegrity structures through a bi-objective optimization problem. In the problem, the stiffness against external loads is to be maximized and the force deviation from their expected values. These two objectives will be demonstrated to be conflicting with each other such that there is no single optimal solution for both of them at the same time, and trade-off between them has to be determined in the force design. For this purpose, we present the curve of Pareto optimal solutions to assist decision making by the designers.

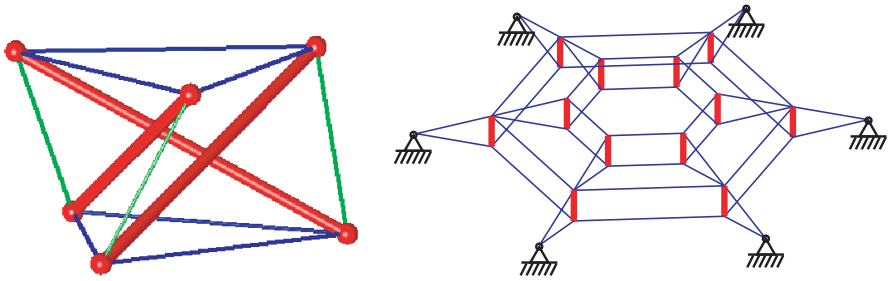

(a) prismatic structure $\mathbf{D}_3$ (b) cable dome

Figure 9.1: Example structures with different number of prestress modes. The structure (a) has only one prestress mode, and note from Lemma 3.7 that it becomes unstable if signs of prestresses are reversed. The structure (b) has two prestress modes, and hence, its stiffness is influenced by selecting a linear combination of these two modes.

9.1 Introduction

In Chapter 2, we discussed several stability criteria for tensegrity structures: a structure is stable when it has positive definite tangent stiffness matrix, and a structure is prestress stable if its reduced stiffness matrix is positive definite. In the definition of prestress stability, only stiffness of the structure in the directions of mechanisms are considered, while member stiffness is assumed to be infinite. As has been discussed, prestress stability is the necessary condition of stability, but not the sufficient condition. Moreover, if the structure has high enough ratio of stiffness to axial forces, e.g., the numerical example of the structure $\mathbf{D}_7^{3,2}$ in Chapter 7, then the prestress stable structure is guaranteed to be stable. Hence, for a kinematically indeterminate structure, it would be more convenient to investigate prestress stability of the structure, since the structure in practice usually has high enough member stiffness compared to level of prestresses.

The only possibility to influence stiffness of a kinematically indeterminate structure is to carefully select the distribution of prestresses in the case that its configuration is determined a priori, because the mechanisms come from configuration of the structure. Therefore, for the structures that have more than one modes of prestresses, e.g., the cable dome with two prestress modes in Fig. 9.1, we are provided the chance to select such a distribution; the optimization methods are considered to be particularly suitable for this purpose.

El-Lishani *et al.* (2005) presented a genetic algorithm (GA) to find out whether there exists any distribution that can stabilize the mechanisms—the reduced stiffness matrix is positive definite. Genetic algorithm is an excellent heuristic optimization method for discrete problems, but on the other hand, it has difficulties in dealing with continuous problems because continuous feasible region is not easy to be properly described by coding. Moreover, it is not stability but stiffness of a structure that mostly concerns the designers in the practical design, since stiffness describe capability of the structure in resisting external loads.

In this chapter, we formulate a multiobjective optimization problem for determination of distribution of prestresses of a tensegrity structure that has multiple prestress modes, and present a method for generating curve of the Pareto optimal solutions for the problem. There are two objectives considered in the problem: to increase the stiffness of tensegrity structures, and to have the prestresses as close as possible to the desired values. These objectives usually conflict with each other, so that there is no single optimal solution that simultaneously optimizes the two objectives. Presentation of the curve of Pareto optimal solutions may assist decision making of the designers, and enables they to select the most preferred solutions in view of the trade-off between the two objectives.

Following this introduction, the paper is organized as follows. Section 2 introduces the basic assumptions, and presents the formulas related to prestresses and stability criteria. Section 3 formulates the optimization problem with two objectives. An example of force design of a special kind of tensegrity structure, called tensegrity grid, is presented in Section 4. Brief conclusions and discussions are given in Section 5.

9.2 Multiobjective Optimization Problem

In addition to the three basic assumptions introduced for general pin-jointed structures in Chapter 2, configuration of a structure is assumed to be known so as to search for the optimal distribution of prestresses in this chapter. We formulate an optimization problem with two objectives: maximization of the stiffness, and minimization of deviation of prestresses from target values; signs of

the prestresses in some specific members and given strain energy for introduction of prestress into the structure are the constraints for the problem.

9.2.1 Objective Functions

Let r^D denote rank of the equilibrium matrix $\mathbf{D}$. For the structure with n nodes and m members, there exist $m-r^D$ independent modes $\mathbf{f}_i$ of prestress, and hence, distribution of prestress of the structure can be written as the linear combination of them as

$$\mathbf{s} = \sum_{i=1}^{m-r^D} \alpha_i \mathbf{f}_i = \mathbf{F}\boldsymbol{\alpha} \tag{9.1}$$

where $\mathbf{D}\mathbf{f}_i = \mathbf{0}$ and α_i is the coefficient of the i mode of prestress.

9.2.1.1 Maximum Stiffness

Prestress stability and stiffness of a tensegrity structure can verified by the smallest eigenvalue of the reduced stiffness matrix $\mathbf{Q}$, which is the quadratic form of the geometrical stiffness matrix $\mathbf{K}_G$ with respect to the mechanisms $\mathbf{M}$:

$$\mathbf{Q} = \mathbf{M}^{\mathrm{T}}\mathbf{K}_G\mathbf{M} \tag{9.2}$$

When the member stiffness is large enough compared to the level of prestresses. This is because that $\mathbf{Q}$ is also the smallest eigenvalue λ of $\mathbf{K}$ in this case. To simplify the problem, we assume that the stiffness of all members is infinite so that stability of the structure can be verified by the sign of λ: when λ is positive, the structure is stable; when it is negative, then the structure is unstable. Note that stability of the structure needs further investigation based on the higher-order terms of energy when $\lambda = 0$. Furthermore, the stiffness of the structure against external loads can be evaluated by the magnitude of λ: lager λ corresponds to higher stiffness of the structure. Hence, to increase the stiffness, a distribution of prestresses resulting in an increase of λ is to be found. For the given design conditions, such as material properties and loading conditions, the maximum deformation of the structure is usually expected to be minimized. Hence, we maximize the smallest eigenvalue λ of the quadratic form $\mathbf{Q}$ as one of the objective functions of the multiobjective optimization problem.

9.2.2 Uniform Prestresses

Uniform distribution of prestresses can have many advantages in design, construction and even in maintenance of tensegrity structures. For example, fabrication costs and complexity of construction process can be significantly reduced, if the member cross-sectional areas are same for the same type of members; moreover, we will have the same safety factor for the failure of members. The target prestresses are denoted by $\bar{\mathbf{s}}$, where the target values may be same for each type of members, or can be specified arbitrary by the designers. The difference $||\mathbf{s} - \bar{\mathbf{s}}||$ between $\mathbf{s}$ and $\bar{\mathbf{s}}$ is to be minimized as the other objective function. The least square method can simply give the optimal solution for this problem as follows

$$\mathbf{s} = \mathbf{F}\mathbf{F}^{-}\bar{\mathbf{s}} \tag{9.3}$$

where $\mathbf{F}^{-}$ denotes the generalized inverse of $\mathbf{F}$.

Note that both of the two objectives mentioned above are described in terms of member forces. However, they cannot have global optimal solutions at the same time. A trade-off between them is generally required in the force design of tensegrity structures.

9.2.3 Constraints

Suppose that the member force vector $\mathbf{s}$ is scaled to $k\mathbf{s}$ ($k > 0$). The equilibrium state of the structure is retained after scaling, and the stability does not depend on the value of k when the member stiffness is assumed to be infinite. However, λ is also modified to $k\lambda$. Therefore, the problem of maximizing the stiffness becomes that of searching the maximum scalar for the prestresses if we have no further constraints on the prestresses. To conquer this problem, a specific value of strain energy provided to pretension the structure is given in the study.

The strain energy Π of the structure can be written as

$$\Pi = \sum \frac{s_i^2 l_i}{2A_i E_i} \tag{9.4}$$

where l_i and $A_i E_i$ are the length and stiffness of member i. For simplicity, they are assumed to be same for all members, and therefore, the strain energy of the

structure is rewritten as

$$\Pi = a \sum s_i^2 l_i = a\mathbf{s}^\top \mathbf{s} \tag{9.5}$$

where a is a constant denoting $l_i/(2A_iE_i)$. The specified value of strain energy $\bar{\Pi}$ can be further simplified as follows by ignoring the constant a

$$\bar{\Pi} = \mathbf{s}^\top \mathbf{s} \tag{9.6}$$

Moreover, it is also expected that the prestresses conform to the types of the members; i.e. tension for cables and compression for struts, because cables have zero stiffness in compression. Let $\mathbf{s}^c$ and $\mathbf{s}^s$ denote the member force vectors of cables and struts. Then we will have $\mathbf{s}^c > \mathbf{0}$ and $\mathbf{s}^s < \mathbf{0}$ for the constraints on the signs of the prestresses.

9.2.4 Formulation

The multiobjective optimization problem is formulated as

$$\begin{array}{rl} \text{Minimize} & -\lambda \text{ and } ||\mathbf{s} - \bar{\mathbf{s}}|| \\ \text{S.T.} & \mathbf{s}^c > \mathbf{0} \\ & \mathbf{s}^s < \mathbf{0} \\ & \mathbf{s}^\top \mathbf{s} = \bar{\Pi} \end{array} \tag{9.7}$$

For a multiobjective optimization problem, we may have compromise solutions, called *Pareto optimal solutions*, in which it is impossible to improve all of the objectives at the same time. Many methods have been developed to solve the problem, among which we will adopt the constraint approach in the next section to list the Pareto optimal solutions as candidates for the assistance of decision making.

9.3 Examples

In this section, we consider the force design of a special tensegrity structure, called tensegrity grid, proposed by Motro (2003) as shown inFig. 9.2. It is constructed by assembling the unit cells as shown in Fig. 9.3 in x- and y-directions. Let r and c denote the numbers of rows and columns of the struts, respectively. Hence, there are $r + 1$ struts in each column and $c + 1$ struts in each row. Thus, the

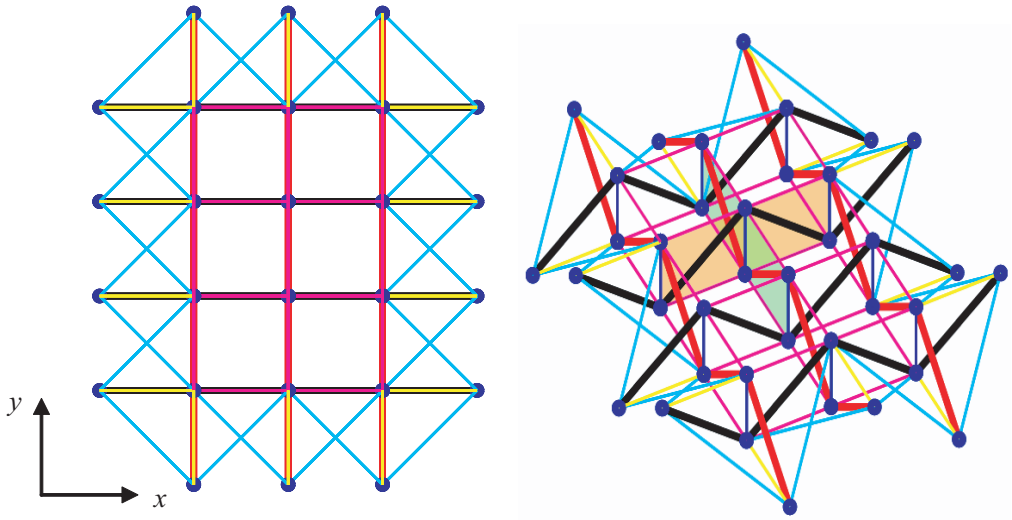

(a) Top view (b) Side view

Figure 9.2: An example of tensegrity grid. There are four rows (r=4) and three columns ($c = 3$) of struts, which are connected to each other at their ends in each row and column.

structure has $2rc + r + c$ struts and $n = 2(rc + r + c)$ nodes. The total number of members is $m = 7rc + 5r + 5c - 4$. The structure has only one infinitesimal mechanism irrespective of r and c. Thus, the quadratic form $\mathbf{Q}$ turns out to be a scalar, which is equal to λ. Moreover, there are at most $rc-r-c+3$ independent modes of prestresses. Note that the members, which are parallel to the xy-plane and connected to the boundary nodes, are bars carrying no force. The bars have both compressive and tensile stiffness so as to maintain stability of the structure.

The structure as shown in Fig. 9.2, which consists of 38 nodes and 115 members ($r = 5$ and $c = 4$) is used as a numerical example. Height of the structure is 5.0, and the projection of each strut on xy-plane has length of 5.0 as well. The prestresses are a linear combination of eight independent modes as in Eq. (9.1), where the coefficients are to be determined by solving the optimization problem (9.7).

In order to find the set of Pareto optimal solutions, we adopt the constraint approach where the second objective function $||\mathbf{s}-\bar{\mathbf{s}}||$ of the optimization problem (9.7) is incorporated in the constraints. Hence, problem (9.7) is transformed to

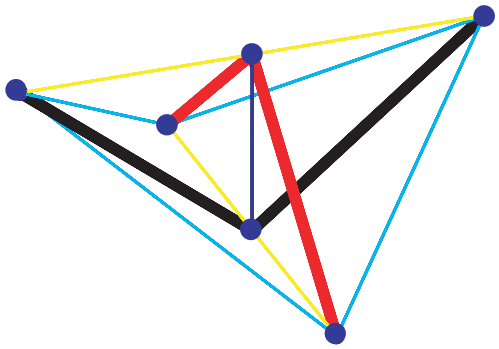

Figure 9.3: Unit cell of tensegrity grid. They are connected consecutively in x- and y-directions to form a tensegrity grid, e.g., the structure as shown in Fig. 9.2.

a single-objective optimization problem as

$$\begin{array}{rl} \text{Minimize} & -\lambda \\ \text{S.T.} & \mathbf{s}^c > \mathbf{0} \\ & \mathbf{s}^s < \mathbf{0} \\ & \mathbf{s}^\top \mathbf{s} = \bar{\Pi} \\ & ||\mathbf{s} - \bar{\mathbf{s}}|| < \epsilon \end{array} \tag{9.8}$$

where ϵ is the upper bound of the difference between the member forces from their target values. The set of Pareto optimal solutions for the original bi-objective optimization problem (9.7) can be derived by solving the revised single-objective optimization problem (9.8), where the upper bound ϵ for $||\mathbf{s} - \bar{\mathbf{s}}||$ is varied gradually and consecutively. The smallest value of ϵ can be determined by solving problem (9.7) ignoring the objective function $-\lambda$; it can also be easily found as the least square solution in Eq. (9.3). The largest value of ϵ can be derived by solving problem (9.7) to minimize $-\lambda$ only. We use the function *fmincon( )* in the Optimization Toolbox in MATLAB (Borse, 1997) for the single-objective problem (9.8). fmincon( ) is a nonlinear programming routine, which attempts to find a constrained minimum of a scalar function of several variables starting from an initial estimate.

The target prestresses of struts and cables are set to -1 and 1, respectively. If the prestresses exactly agree with the target values, the revised strain energy introduced to the structure is $\mathbf{s}^\top \mathbf{s} = 101$ because there are 101 struts and cables in addition to 14 bars carrying no force on the boundary. Hence, we set $\bar{\Pi} = 101$ for the problem. Note that these values are purely numerical without explicit

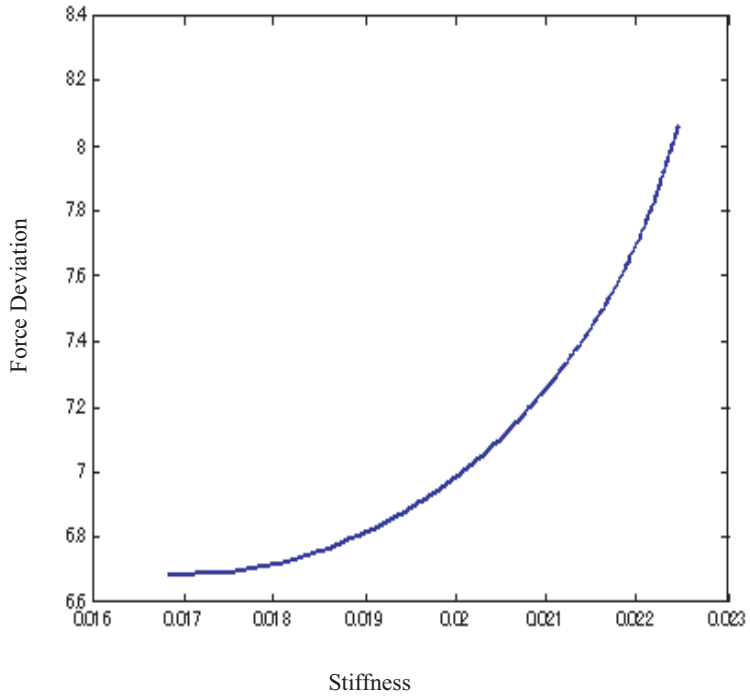

Figure 9.4: Pareto optimal solutions of problem (9.7) for maximizing stiffness and minimizing the deviation of prestresses from uniform distribution.

physical meaning, and are used to present the set of Pareto optimal solutions. The coefficients α_i of the force modes $\mathbf{f}_i$ are the variables in the optimization problem. The initial solution to start the fmincon( ) is determined by the least square method as in Eq. (9.3). The difference between the prestresses and the target values is distributed in the region [6.6849, 8.0662]. The upper bound ϵ is varied in this region to find λ by solving the problem (9.8). The generated Pareto optimal solutions are plotted in Fig. 4.

A trade-off relation between the two objective functions is clearly observed in Fig. 9.4, which conforms to the definition of the Pareto optimal solutions. Basically, larger difference between the prestresses and the target forces leads to higher stiffness, but they do not have linear relation. In the force design process, a compromise between the two objectives should be made. Curve of the Pareto optimal solutions can provide direct information to help designers in the further understanding of the structure and decision making in the force design.

9.4 Conclusions and Discussions

In the structural design, it is always desirable that the structure has the stiffness as high as possible, for the given design conditions, so as to let the structure be in good service against external loads. Moreover, uniform distribution of prestresses has many advantages, such as reduction of fabrication costs and complexity of construction process, and having the same safety factor for the failure of members.

Since tensegrity structures usually have multiple independent force modes, we have the freedom to choose the prestresses to have control over the mechanical properties of the structures. A bi-objective optimization problem has been presented to maximize the stiffness and to minimize the difference between the prestresses and their target values, subject to the constraints of given strain energy and types of members.

It is clear from the numerical example in Section 4 that distribution of prestresses has significant influence on the stiffness of the structure. Presentation of the curve of the Pareto optimal solutions enables designers to select a solution from the candidate solutions according to their preferences, although it is not possible to have maximum stiffness and uniform distribution of prestresses at the same time.

Chapter 10

FORCE IDENTIFICATION

This chapter is to use optimization methods to determine measurement positions of prestressed (pin-jointed) structures, for the purpose of identification of distribution of their prestresses.

Assessment and maintenance of member forces are of great importance for prestressed structures, which take advantages of prestress to enhance their stiffness. Therefore, the distribution of forces should be precisely identified and carefully adjusted in the construction process. The member forces should also be monitored and maintained after construction for the process of life-cycle management.

Our problem is to find out the optimal measurement positions such that the identification error is minimized when the number of measurement devices is determined a priori. This is a typical combinational discrete optimization problem that global optimal solution is hardly available, and heuristic methods are thought to be powerful for these problems. In this study, we focus on making improvement to Simulated Annealing (SA) method for searching (near) optimal solutions more efficiently and accurately.

10.1 Introduction

Based on the sensitivity analysis of the equilibrium equations, Zhang *et al.* (2004) have formulated the mean identification error (MIE) to reflect the accuracy of identification of the distribution of prestresses of the tension structures. However, only the measurement errors of prestresses have been taken into consider-

ation, while assuming that the configuration of the structure in terms of nodal coordinates is known a prior or measured without any error.

Four heuristic methods based on the basic idea of Stingy, Greedy methods and local search strategy were proposed by the authors to find the optimal set of measurement members with the minimal number, subjected to an upper-bound constraint on the MIE specified by the users.

In the view point of accuracy, the measurement errors of nodal coordinates should also be taken into account at the same time to reflect the identification error exactly, although the measurement errors of nodal coordinates may be small because of the high capability of advanced measurement devices nowadays.

On the other hand, the upper-bound constraint on mean identification error may be difficult to decide and needs experience on it, since the magnitude of it is dependent on the models or types of the structures. In some cases, a specified number of measurement devices, or a specified number of measurement members in other words, may be more comprehensible and easy to use to be deployed in the structure for the identification purpose with minimum error.

To this kind of combinational discrete optimization problem, the simulated annealing (SA), a heuristic method, has been proved to be a very powerful tool, because no sensitivity analysis of the objective function is needed.

However, there is no guarantee that the solutions derived by the heuristic methods are the global optimum, although they are convinced to be close to that.

In this chapter, we will make an improvement to the standard SA by starting from a better initial solution, determined by the Stingy method, to find the optimal solution. This solution derived by the improved SA is shown to be more robust than that by the standard SA by a numerical example.

10.2 Identification Error

This section is to present the formulation for the identification error, taking the measurement errors of prestresses as well as nodal coordinates into consideration.

10.2.1 Force Errors

The members are divided into two groups—the *measurement members*, of which the prestresses are to be measured, and the *estimation members*, of which the prestresses are to be estimated by those of the measurement members through self-equilibrium equations. Let $\mathbf{s}^m \in \Re^p$ denote the prestress vector of the p measurement members, and let $\mathbf{s}^e \in \Re^{m-p}$ denote the prestress vector of the $m-p$ estimation members.

The self-equilibrium equation Eq. (2.36) can be rewritten as follows by dividing the member forces into the measured set $\mathbf{s}^m$ and the estimated set $\mathbf{s}^e$ as

$$\mathbf{D}^m\mathbf{s}^m + \mathbf{D}^e\mathbf{s}^e = \mathbf{0} \tag{10.1}$$

where $\mathbf{D}^m \in \Re^{3n\times p}$ and $\mathbf{D}^e \in \Re^{3n\times(m-p)}$ are constructed by assembling the columns in $\mathbf{D}$ that correspond to the members in $\mathbf{s}^m$ and $\mathbf{s}^e$, respectively.

If $\mathbf{D}^e$ is full-rank; i.e., $\text{rank}(\mathbf{D}^e) = m-p$, then the least squares solution of $\mathbf{s}^e$ can be determined as follows

$$\mathbf{s}^e = -(\mathbf{D}^e)^-\mathbf{D}^m\mathbf{s}^m \tag{10.2}$$

Eq. (10.1) where $(\ )^-$ denotes the Moore-Penrose generalized matrix inverse. When $\mathbf{D}^e$ is rank deficient; i.e., $\text{rank}(\mathbf{D}^e) < m-p$, there exist $m-p-\text{rank}(\mathbf{D}^e)$ independent modes of $\mathbf{s}^e$ that satisfy Eq. (10.1), and Eq. (10.2) gives the solution that has the minimum norm among the possible solutions. Hence, $\mathbf{D}^e$ need be full-rank to have accurate estimation of the member forces. Furthermore, h or more members should be measured so as to exclude the h dependent columns in $\mathbf{D}$ from $\mathbf{D}^e$ to make it possible to be full-rank.

Combine the nodal coordinates as $\mathbf{X}^\top = (\mathbf{x}^\top, \mathbf{y}^\top, \mathbf{z}^\top)^\top$. Suppose that there exist measurement errors in $\mathbf{X}$ and $\mathbf{s}^m$. Total differential of Eq. (10.2) with respect to $\mathbf{X}$ and $\mathbf{s}^m$ leads to

$$\sum_{i=1}^{3n}\frac{\partial\mathbf{D}^m}{\partial X_i}\Delta X_i\mathbf{s}^m + \mathbf{D}^m\Delta\mathbf{s}^m + \sum_{i=1}^{3n}\frac{\partial\mathbf{D}^e}{\partial X_i}\Delta X_i\mathbf{s}^e + \mathbf{D}^e\Delta\mathbf{s}^e = \mathbf{0} \tag{10.3}$$

where Δx_i and $\Delta\mathbf{s}^m$, respectively, are the measurement errors of nodal coordinates and member forces to be measured, and $\Delta\mathbf{s}^e$ is the resulting estimation

error of the remaining members. $\frac{\partial \mathbf{D}^m}{\partial X_i}$ and $\frac{\partial \mathbf{D}^e}{\partial X_i}$ can be derived by assembling the corresponding entries in $\frac{\partial \mathbf{D}}{\partial X_i}$; see details in Section 4.

From Eqs. (10.2) and (10.3), $\Delta \mathbf{s}^e$ is written as

$$\Delta \mathbf{s}^e = -(\mathbf{D}^e)^- \left(\sum_{i=1}^{3n} \left[\frac{\partial \mathbf{D}^m}{\partial X_i} - \frac{\partial \mathbf{D}^e}{\partial X_i} (\mathbf{D}^e)^- \mathbf{D}^m \right] \mathbf{s}^m \Delta X_i + \mathbf{D}^m \Delta \mathbf{s}^m \right) \tag{10.4}$$

which is simplified as

$$\Delta \mathbf{s}^e = (\mathbf{H}, \mathbf{G}) \begin{pmatrix} \Delta \mathbf{x} \\ \Delta \mathbf{s}^m \end{pmatrix} \tag{10.5}$$

where

$$\begin{aligned} \mathbf{H}_i &= -(\mathbf{D}^e)^- \left[\frac{\partial \mathbf{D}^m}{\partial X_i} - \frac{\partial \mathbf{D}^e}{\partial X_i} (\mathbf{D}^e)^- \mathbf{D}^m \right] \mathbf{s}^m \\ \mathbf{H} &= (\mathbf{H}_1, \ldots, \mathbf{H}_i, \ldots, \mathbf{H}_{3n}) \\ \mathbf{G} &= -(\mathbf{D}^e)^- \mathbf{D}^m \end{aligned} \tag{10.6}$$

Combining the measurement errors $\Delta \mathbf{s}^m$ and estimation errors $\Delta \mathbf{s}^e$ of member forces as $\Delta \mathbf{s}$, we have the following equation from Eq. (10.5):

$$\Delta \mathbf{s} = \begin{pmatrix} \Delta \mathbf{s}^m \\ \Delta \mathbf{s}^e \end{pmatrix} = \begin{pmatrix} \mathbf{O} & \mathbf{I}_p \\ \mathbf{H} & \mathbf{G} \end{pmatrix} \begin{pmatrix} \Delta \mathbf{X} \\ \Delta \mathbf{s}^m \end{pmatrix} \tag{10.7}$$

where $\mathbf{I}_p \in \Re^{p \times p}$ is an identity matrix. In the following, the identity matrices are denoted by $\mathbf{I}$ with the size indicated by subscript. This way, the force error vector $\Delta \mathbf{s}$ of all members is formulated as a function of measurement errors of nodal coordinates $\Delta \mathbf{X}$ and member forces $\Delta \mathbf{s}^m$.

The partial differential of the equilibrium equation $\mathbf{D}$ formulated in Eq. (7.3) with respect to the parameter t can be written as

$$\frac{\partial \mathbf{D}}{\partial t} = \begin{pmatrix} \mathbf{C}^\top \frac{\partial \mathbf{U}}{\partial t} \mathbf{L}^{-1} + \mathbf{C}^\top \mathbf{U} \frac{\partial \mathbf{L}^{-1}}{\partial t} \\ \mathbf{C}^\top \frac{\partial \mathbf{V}}{\partial t} \mathbf{L}^{-1} + \mathbf{C}^\top \mathbf{V} \frac{\partial \mathbf{L}^{-1}}{\partial t} \\ \mathbf{C}^\top \frac{\partial \mathbf{W}}{\partial t} \mathbf{L}^{-1} + \mathbf{C}^\top \mathbf{W} \frac{\partial \mathbf{L}^{-1}}{\partial t} \end{pmatrix} \tag{10.8}$$

where t can be time or the coordinates of the free nodes in x-, y- or z-directions.

The components $\frac{\partial \mathbf{U}}{\partial t}$, $\frac{\partial \mathbf{V}}{\partial t}$, $\frac{\partial \mathbf{W}}{\partial t}$, and $\frac{\partial \mathbf{L}^{-1}}{\partial t}$ in Eq. (10.8) can be found in Eqs. (2.29) and (2.30) in Chapter 2.

10.2.2 Identification Error

Let e_c and e_f denote the upper bounds of measurement errors of nodal coordinates and member forces, respectively, which can be determined by using the ellipsoidal convex model proposed by Zhu *et al.* (1996) for example based on existing measurement data. The member forces and nodal coordinates with different dimensions are transformed into dimensionless variables by dividing them by e_c and e_f, respectively. Hence, their measurement errors are transformed into dimensionless variables, and Eq. (10.7) is rewritten as

$$\Delta \mathbf{s} = \mathbf{B}\Delta \mathbf{r} = \begin{pmatrix} \mathbf{O} & e_f \mathbf{I}_p \\ e_c \mathbf{H} & e_f \mathbf{G} \end{pmatrix} \begin{pmatrix} \Delta \mathbf{X}/e_c \\ \Delta \mathbf{s}^m/e_f \end{pmatrix} \tag{10.9}$$

where

$$\mathbf{B} = \begin{pmatrix} \mathbf{O} & e_f \mathbf{I}_p \\ e_c \mathbf{H} & e_f \mathbf{G} \end{pmatrix}, \quad \Delta \mathbf{r} = \begin{pmatrix} \Delta \mathbf{X}/e_c \\ \Delta \mathbf{s}^m/e_f \end{pmatrix} \tag{10.10}$$

When the sets of member forces to be estimated and measured are specified, $\mathbf{B}$ is a constant matrix from the definition of $\mathbf{H}$ and $\mathbf{G}$. Note that the force error depends on the patterns of the measurement errors. To incorporate the worst-case scenario, where $\Delta \mathbf{s}$ has the maximum Euclidean norm, the performance measure of the identification is defined as the *identification error* E as

$$E = \max \|\Delta \mathbf{s}\|_2 \tag{10.11}$$

which is equivalent to the 2-norm of the matrix $\mathbf{B}$ (Horn and Johnson, 1990):

$$E = \|\mathbf{B}\|_2 = \max ||\mathbf{B}\Delta \mathbf{r}||_2 \quad \text{subject to } ||\Delta \mathbf{r}||_2 = 1 \tag{10.12}$$

In Eq. (10.12), it is to find a vector $\Delta \mathbf{r}$ with unit norm leading to the maximum $\|\Delta \mathbf{s}\|_2$. Furthermore, the 2-norm of matrix $\mathbf{B}$ is equal to the square root of the largest eigenvalue λ_{max} of $\mathbf{B}^{\mathrm{H}}\mathbf{B}$, where $\mathbf{B}^{\mathrm{H}}$ is the conjugate transpose:

$$E = \sqrt{\lambda_{max}} \tag{10.13}$$

Since $\mathbf{B}$ is a real matrix, the conjugate transpose $\mathbf{B}^{\mathrm{H}}$ of $\mathbf{B}$ equals to its transpose $\mathbf{B}^{\top}$; i.e., $\mathbf{B}^{\mathrm{H}} = \mathbf{B}^{\top}$.

When all the members are to be measured; i.e., $p = m$, we have $E = e_f$, since

$$\mathbf{B} = (\mathbf{O},\ e_f \mathbf{I}_m), \quad \mathbf{B}^{\mathrm{H}}\mathbf{B} = \begin{pmatrix} \mathbf{O} & \mathbf{O} \\ \mathbf{O} & e_f^2 \mathbf{I}_m \end{pmatrix} \tag{10.14}$$

where $\mathbf{I}_m \in \mathbb{R}^{m \times m}$ is an identity matrix.

10.3 Optimal Placement of Measurement Devices

In this section, we formulate an optimization problem, which searches for the optimal placement of devices for the measurement of some member forces while all nodal coordinates are assumed to be measured. A heuristic approach called simulated annealing, with the initial solution determined by the stingy method, is adopted for solving this combinatorial problem.

10.3.1 Problem formulation

In the process of force identification of a prestressed pin-jointed structure, the key factors to be considered are (a) the precision of measurement, (b) the number of measurement devices, and (c) the locations of measurement devices. The study considers only the last two factors, since the precision of the measurement depends on the measurement device, which is out of the scope of this paper.

In practical applications of force identification, nodal coordinates can be easily measured with relatively small cost, while the measurement devices for member forces are much more expensive. Hence, we assume that all nodal coordinates are measured, whereas only a part of the member forces are to be measured.

From the definition of identification error in Eq. (10.13), we can see that the matrix $\mathbf{B}$ depends on the set of measurement members to be selected even for the case where the number of measurement devices is specified. Therefore, our problem is to find the optimal locations of measurement devices of member forces, which lead to minimum identification error E, with the fixed number $\bar{p}$ of devices. The problem is formulated as

$$\begin{aligned} &\text{minimize} \quad E \\ &\text{subject to} \quad p = \bar{p} \end{aligned} \tag{10.15}$$

Note that there is actually another inherent constraint: the matrix $\mathbf{D}^e$ has to be full-rank so as to have the least squares solution for the member forces to be estimated as in Eq. (10.2).

10.3.2 Solution process

The proposed problem in Eq. (10.15) is a typical combinatorial optimization problem, for which many heuristic methods have been presented. Simulated Annealing (SA) is one of the most popular approach that lead to approximate optimal solution within a practically acceptable computational cost. We modify SA to start from an initial solution found by the stingy method, which is a simple approach based on local search.

10.3.2.1 Simulated annealing

As its name implies, SA exploits an analogy between the metal annealing process and the search process of the best objective function in a general optimization problem (Kirkpatrick *et al.*, 1983). No sensitivity analysis is needed in the process of searching for the optimal solution. The major advantage of SA over other heuristic approaches is its ability to avoid being trapped at the local optimum.

The five important components involved in SA are: (a) feasible solutions, (b) initial solution, (c) transition of solutions, (d) cooling schedule, and (e) termination condition.

(a) Feasible Solutions:

For every feasible solution in our problem, the matrix $\mathbf{D}^e$ corresponding to the member forces to be estimated should be full-rank; i.e., $\text{rank}(\mathbf{D}^e) = m - p$. A new (candidate) solution can be generated from the current solution by randomly selecting and exchanging the members in the sets to be measured and to be estimated.

(b) Initial Solution:

The initial solution should also be feasible. The initial solutions are usually generated randomly. However, to ensure feasibility of the solution and to improve convergence property to the global optimum, we use the stingy method discussed later to determine the initial solution.

(c) Transition of Solutions

One of the main features of the SA is the transition to non-improving solution. The probability of acceptance of a neighborhood solution is defined as

$$P = \min\{1, e^{\Delta f_i / t_i}\} \tag{10.16}$$

where Δf_i is the increase of the objective value from the current solution in iteration i, and t_i is the control parameter known as *temperature*. Only when P is larger than a specified value $\bar{P}$, which is random value uniformly distributed in (0,1) in the study, transition of solution takes place. This way, convergence to a local optimal solution is possible to be avoided.

(d) Cooling Schedule

The temperature t_i determines the probability of the non-improving candidate solution to replace the current solution: lower temperature contributes to a lower acceptance probability. SA usually starts at a high initial temperature t_0, and then gradually decreases to a low temperature leading to convergence of the annealing. This process of decreasing temperature is called *cooling schedule* or *annealing schedule*. Azizi and Zolfaghari (2004) discussed several theoretical and empirical cooling schedules. Among them, we adopt the simple monotonic schedule as

$$t_i = \eta t_{i-1} \tag{10.17}$$

where $0 < \eta < 1$.

(e) Termination Condition

There are several criteria to terminate the algorithm. When the current temperature is smaller than the specified lower bound $\bar{t}$, it is possible that all the improving solutions in the neighborhood have been searched. If no improvement has been made during the specified number of iterations, the process can be regarded to be converged.

The process of SA adopted in the study is summarized as follows:

Algorithm 1 – Simulated annealing:

Step 0: *Initialization:*

Generate an initial solution. Specify the values of the cooling ratio η, initial temperature t_0, size of neighborhood n^s, and the termination parameters $\bar{t}$ and n^t. Set $i = 0$.

Step 1: *Local Search & Solution Update:*

Generate n^s candidate solutions in the neighborhood of the current solution, and move to the best one based on the acceptance criterion. Set $i =: i + 1$.

Step 2: *Cooling:*

If the solution is updated in Step 1, then reduce the temperature by Eq. (10.17); otherwise, do not modify the temperature.

Step 3: *Termination:*

If the temperature is lower than the specified bound $\bar{t}$, or there is not any new solution in Step 1 during n^t successive temperatures, then output the best solution and terminate the algorithm; otherwise, return to Step 1 with the updated temperature t_i.

The initial solution and the cooling schedule play critical roles in finding the (approximate) optimal solution. A faster cooling schedule may lead to faster termination but the final solution may not be close enough to the global solution. Accordingly, the SA starting from a random initial solution may need slower cooling schedule. However, in practical implementation of SA, value of η close to 1 may demand much computation cost. On the other hand, a better initial solution, which is closer to the optimal solution, may lead to faster convergence. Hence, it is more reliable to start the SA from a better initial solution, which is determined by the stingy method in the study.

10.3.2.2 Stingy Method

Zhang *et al.* (2004) developed several simple heuristic approaches, including the stingy method, to investigate the identification accuracy of force distribution of prestressed pin-jointed structures, where only the measurement errors of member forces are considered. It has been demonstrated that the stingy method has relatively high accuracy with small computation cost. Therefore, the stingy method can be effectively used for producing a good initial solution, rather than random solutions, to reduce computational cost as well as to improve accuracy in SA.

Stingy method is a basic heuristic approach, based on the local search, to combinatorial optimization problems. For the problem considered in this paper, it starts from a complete set of the possible measurement members, and successively removes the member with least contribution to the objective function from the current set of solutions, under the condition that the removal does not lead to an infeasible solution.

Let $\mathcal{I}$ denote the current set of measurement members, and p denote the size of $\mathcal{I}$. The stingy method is summarized as follows:

Algorithm 2 – Stingy method:

Step 0: Set $\mathcal{I} = \{1, 2, \ldots, m\}$. The forces of all members are to be measured; i.e., $p = m$.

Step 1 Find $k = \underset{j \in \mathcal{I}}{\operatorname{argmin}}(E_p^j - E_p^0)$, where E_p^0 and E_p^j denote the identification errors by the sets $\mathcal{I}$ and $\mathcal{I} - \{j\}$, respectively.

Step 2 If $p = \bar{p}$, then terminate the process; otherwise, set $\mathcal{I} := \mathcal{I} - \{k\}$ because it has the minimum contribution in $\mathcal{I}$ to reduction of the identification error. Set $i := i - 1$, and return to Step 1.

This way, we can find the $\bar{p}$ measurement members with the (approximately) minimal identification error for the optimization problem Eq. (10.15), which is used as the initial solution in the simulated annealing.

10.3.2.3 Improved simulated annealing

With the initial solution found by Algorithm 2, Step 0 of Algorithm 1 is then rewritten as follows

Algorithm 3 – Improved simulated annealing (ISA):

Step 0: *Initialization:*

Generate an initial solution by Algorithm 2. Specify the values of the cooling ratio η, initial temperature t_0, size of neighborhood n^s, and the termination parameters $\bar{t}$ and n^t. Set $i = 0$.

10.4 Numerical Examples

This section investigates the influence of the measurement errors of nodal coordinates and member forces on the identification error of the member forces, and is to demonstrate that the proposed improved simulated annealing (ISA) is more efficient and accurate than the conventional SA. The examples are investigated using MATLAB (Borse, 1997).

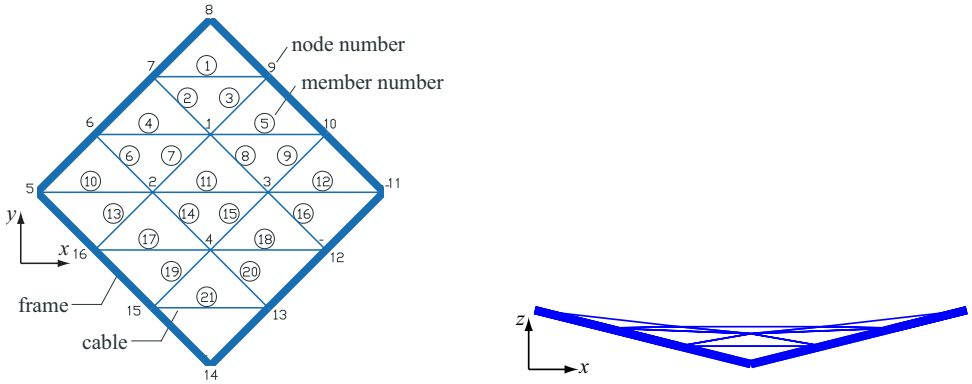

(a) top view (b) side view

Figure 10.1: A cable net with 21 members.

10.4.1 Cable Net Model

We first investigate the cable net model of an HP-shaped tension membrane structure as shown in Fig. 10.1. Although tension membrane structure is made of continuum membrane material, it can be discretized and substituted by a cable net model, e.g., as described by Maurin and Motro (1998). Hence, membrane structure can also be treated as a special kind of prestressed pin-jointed structure. Diagonal span length and height of the structure are respectively 16.0m and 2.0m.

The cable net model consists of four free nodes, 14 fixed nodes and 21 members. The maximum and minimum member forces in the model are 282.9kN and 400.0kN, respectively. The model consists of 9 independent modes of member forces, and hence, at least 9 independent measurement members are needed so as to make the matrix $\mathbf{D}^e$ to be full-rank.

10.4.1.1 Exact Solution

To investigate the exact influence of the number of measurement members on the identification error, enumeration method is applied first to have the exact solution for the problem (10.15). In order to find the optimal set of 9 measurement members for this relatively simple model, the number of combinations of 9 members out of 21 candidates is 293930. The computational cost increases exponentially when number of the members in the model becomes larger.

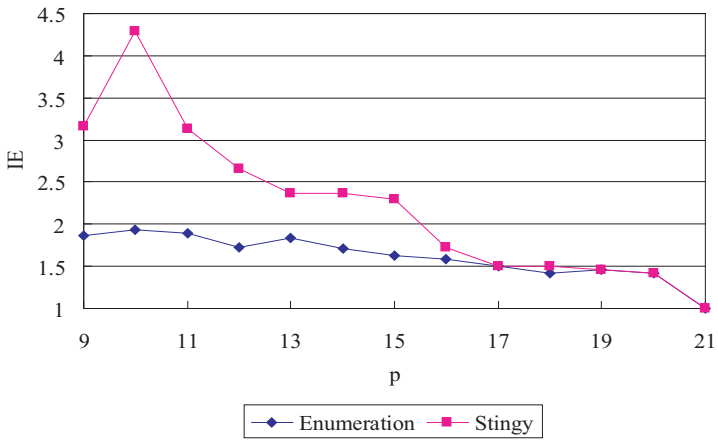

Figure 10.2: Optimal solutions for 21-member cable net. It shows performance of the enumeration method and stingy method in minimizing the identification error subjected to given number p of measurement devices.

Suppose that the variance of measurement error of each member force is $e_f = 1$, and the measurement errors of the nodal coordinates are neglected; i.e., $e_c = 0$. The relationships between the number p of measurement devices and the identification error derived by the enumeration method and the stingy method are plotted in Fig. 10.2. It can be observed from the figure that

[L1] There is a tendency for the enumeration method as well as the stingy method that the higher accuracy can be achieved by adding the measured members.

[L2] The stingy method has high accuracy especially when p is large.

10.4.1.2 Efficiency and Accuracy of Improved SA (ISA)

To investigate the efficiency and accuracy of the ISA in comparison to the conventional SA, the 21-member cable net in Fig. 10.1 is used again as an example structure.

The parameters for SA and ISA are specified as follows:

Table 10.1: Results by SA with random initial solution.

No. of Trials	1	2	3	4	5	6	Mean
Identification Error	1.9219	1.7302	1.7302	1.8252	1.8252	1.9219	1.8258
Computational Cost	24378	19941	16626	18768	16422	27795	20655

Table 10.2: Results by ISA with the initial solution by stingy method.

No. of Trials	1	2	3	4	5	6	Mean
Identification Error	1.7302	1.7302	1.8252	1.7302	1.8252	1.7302	1.7619
Computational Cost	18666	18513	17085	17901	15198	18411	17629

Table 10.3: Comparison of results by Enumeration, SA, Stingy and ISA for $\bar{p} = 12$ for the 21-member cable net model.

	Enumeration	Stingy	SA	ISA
Identification Error	1.7302	2.6607	1.8258	1.7619
Relative Error[a]	0%	53.78%	5.53%	1.83%
Computational Cost	293930	165	20655	17629
Relative Cost[b]	100%	0.056%	7.03%	6.0%

[a]Ratio of difference in the identification errors to the exact solution.
[b]Ratio of computational cost of each method to that of the enumeration method.

- Search the $n^s = 50$ neighborhood solutions of the current solution at each iteration;
- The initial temperature is $t_0 = 5$;
- The constant cooling ratio is $\eta = 0.99$;
- The termination parameters are $\bar{t} = 10^{-6}$ and $n^t = 5$.

The identification errors and computational costs by SA and ISA are listed in Tables 10.1 and 10.2, respectively. The results by the two methods are further investigated in Table 10.3 in comparison to the enumeration method and the stingy method to demonstrate their efficiencies and accuracies. It can also be observed from the results that ISA can find the strict optimal solution with higher frequency and slightly less computation cost than SA.

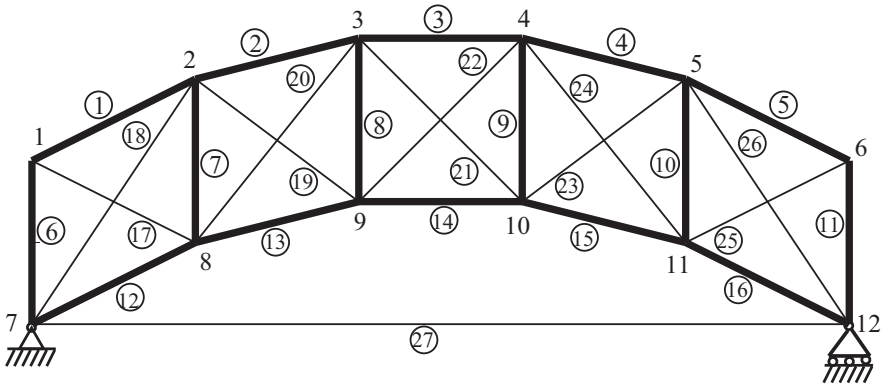

Figure 10.3: A two-dimensional tensegrity arch.

Hence, it might be possible for us to draw the conclusion that a better initial solution obtained by the stingy method, rather than a random one, is more reliable to achieve more accurate solution with higher efficiency.

10.4.2 Two-dimensional Tensegrity Arch

A two-dimensional tensegrity arch as shown in Fig. 10.3 is considered as another example structure. The structure consists of 12 nodes and 27 members. The span is 10.0m, and the height is 3.5m. Rigid-body motions of the structure in two-dimensional space are constrained by fixing node 7 in x- and y-directions, and node 12 in x-direction. The structure consists of six independent force modes in total.

Example 2-1: Suppose that we have 13 measurement devices for member forces; i.e., $\bar{p} = 13$. We first consider the case, where no measurement error exists in the nodal coordinates. For ISA, we set $t_0 = 10$, $\eta = 0.95$, and the same values for other parameters as in Section 6.1.

The optimal measurement members found by ISA are {2, 4, 13, 15, 17, 18, 20, 21, 22, 23, 25, 26, 27}, which are shown in dashed lines in Fig. 10.4. It is clear that locations of the measurements are symmetric, since the structure is symmetric.

Example 2-2: As the other example for the two-dimensional tensegrity arch, we set the variance of measurement error of each nodal coordinate e_c to 1.0mm,

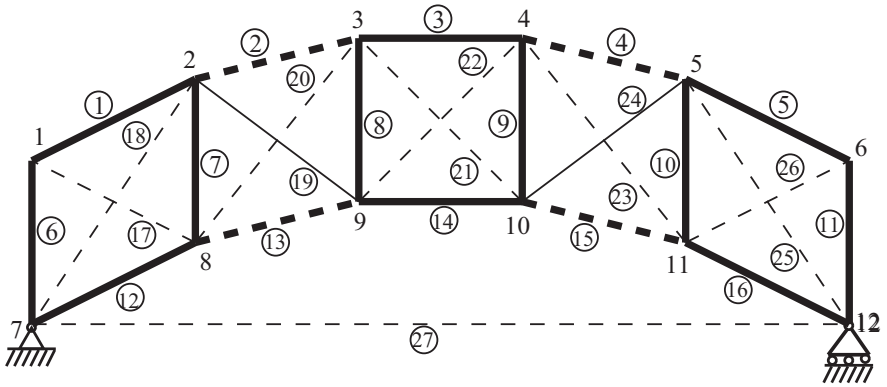

Figure 10.4: Ex. 2-1 of optimal measurement members ($\bar{p} = 13$). The dotted lines are the optimal members for measurement.

which is very small, because the devices for the measurement of nodal coordinates are of high accuracy.

Suppose that the maximum of absolute value of the member forces is 2.5697×10^3kN, 1.0% of which is set as their variance of measurement errors; i.e., $e_f = 25.697$kN.

ISA finds the optimal measurement members as {1, 3, 11, 12, 14, 16, 18, 19, 20, 22, 23, 24, 25}, which are shown in Fig. 10.5.

10.4.3 Three-dimensional Cable Dome

Fig. 10.6 shows a three-dimensional cable dome, consisting of 12 struts and 48 cables. The nodes of the structure are located on three circles with different radii, which are respectively set as 5.0m, 10.0m and 15.0m; and four different elevations of the circles are −1.0m, 0.0m, 1.0m and 2.0m.

The variance of each measurement error of the nodal coordinate e_c is set as $e_c = 1.0$mm, and that of the member force is $e_f = 0.5$kN, which is about 1.7% of the largest member force of the structure.

In practical applications, it might be more convenient to measure the forces in the cables rather than those in the struts, because the measurement devices can be imbedded into the cables more easily. Suppose that we have only 12

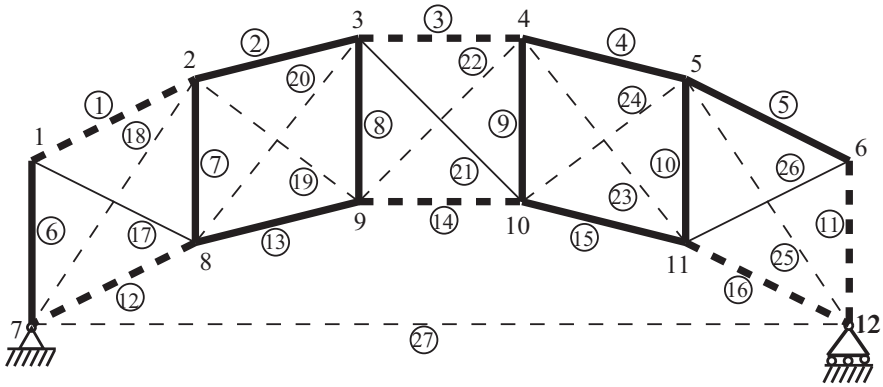

Figure 10.5: Ex. 2-2 of optimal measurement members ($\bar{p} = 13$). The dashed lines are the optimal members for measurement when measurement errors in nodal coordinates as well as in member forces are considered.

measurement devices, and the object of this example is to find 12 cables to be measured so as to minimize the identification error.

Example 3-1: Fig. 10.7(a) shows the cables to be measured which are determined by the stingy method. The identification error in this case is 1.1988.

Example 3-2: Use the measurement cables found in Example 3-1 as the initial solution for the simulated annealing. ISA finds the optimal locations of cables to be measured, which are shown in the dotted lines in Fig. 10.7(b). The identification error in this case is reduced to 1.0418, smaller than that by using stingy method only.

10.5 Discussions and Conclusions

In this study, we formulated the identification error for evaluation of the accuracy of the force distribution of prestressed pin-jointed structures. Measurement errors of both member forces and nodal coordinates are taken into consideration in the formulation.

In the optimization method for finding the optimal employment of measurement devices, the objective function is to minimize the identification error with specified number of devices. Preferences of employment of measurement devices to the members can also be easily taken into account—for some structures, it

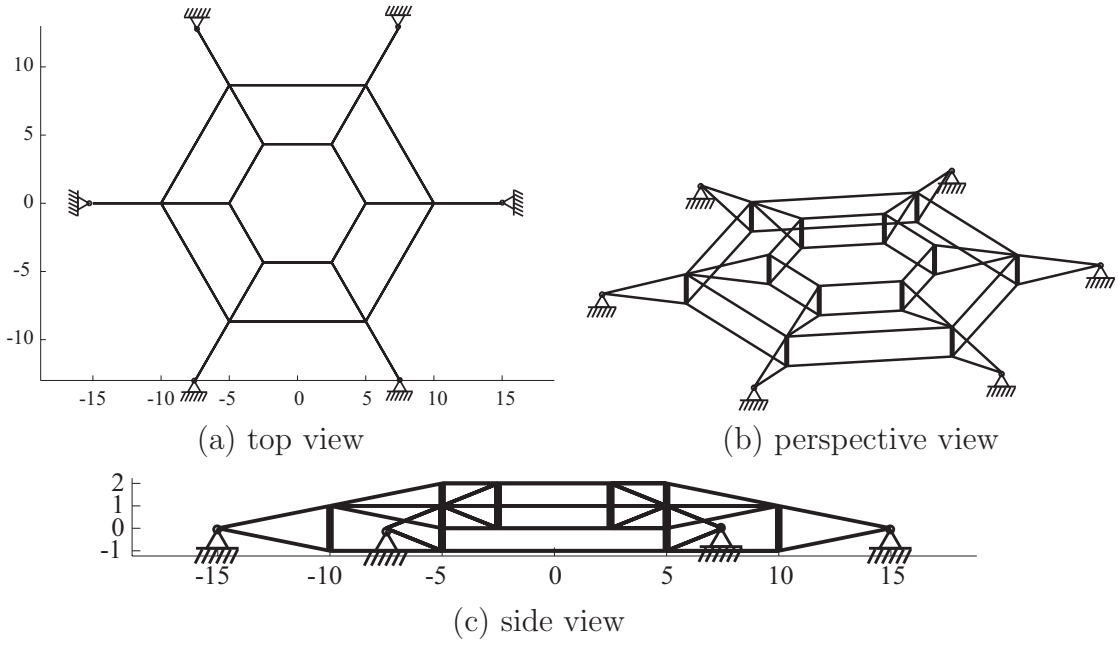

(a) top view (b) perspective view

(c) side view

Figure 10.6: A three-dimensional cable dome.

might be expected to measure only the member forces of cables, for instance. This gives more freedom to engineer to arrange measurement devices according to their distinct requirements, without suffering much lose in accuracy.

The basic idea of simulated annealing is adopted for the formulated combinatorial optimization problem. To have a better final solution, the simulated annealing method is improved by starting from the initial solution found by the stingy method, rather than a random initial solution. A number of numerical examples have been given to demonstrate the high efficiency and accuracy of the proposed method, and to illustrate the influence of measurement errors of nodal coordinates as well as member forces on the optimal employment of measurement devices for member forces.

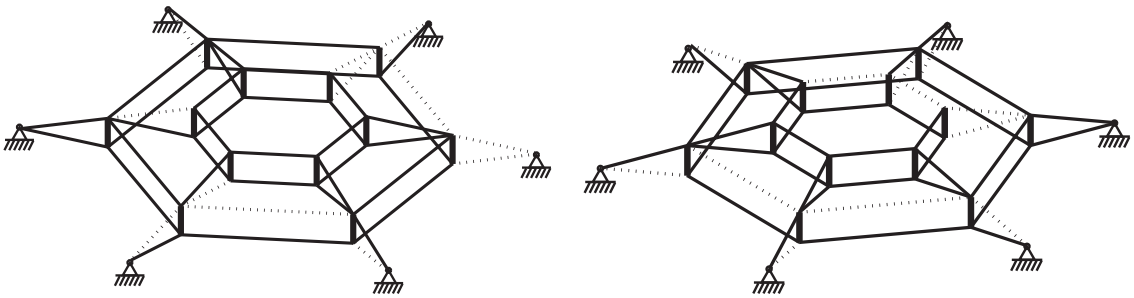

(a) measurement members by Stingy (b) measurement members by ISA

Figure 10.7: The optimal employment of measurement devices for cables of a three-dimensional cable dome. The dashed lines are the optimal members for measurement of member forces found by the stingy method and the improved simulated annealing (ISA).

Chapter 11

SUMMARIES

This chapter is to discuss and conclude our study on morphology and stability problems of tensegrity structures, and to look ahead further studies.

Tensegrity structures have not been well understood as they should, although a number of successful applications of their principles can be found in many different fields. Due to the subtle interplay between configuration and prestresses, the process of finding the self-equilibrated configuration, called morphology or form-finding, is a difficult task. Moreover, most tensegrity structures are not stable without prestresses, because of existence of mechanisms; meanwhile, prestresses may not always stiffen mechanisms so as to stabilize the structures.

The major objectives of the study are to provide efficient numerical and analytical methods for determination of self-equilibrated configurations of tensegrity structures, as well as to present stability conditions leading to deep insight of their structural properties. The proposed methods are demonstrated to be of high efficiency, and have excellent capacity in controlling geometrical and mechanical properties of the structures as well. The presented stability conditions are shown to be easy to use, and provide researchers the opportunity to have in-depth understanding of their distinct structural properties. To study these two major problems in the design of tensegrity structures in a systematic way, we have extensively made use of advanced knowledge in mathematics, such as graph theory, group representation theory and optimization method.

In summary, the study constructs a self-contained and fundamental knowledge system for design problem of tensegrity structures. It is also expected to lead to

thorough understanding of their distinct properties so as to benefit and guide further practical applications, whereas their principles are applicable.

Stability and morphology problems are no way separable in the design of tensegrity structures, although they are summarized separately in the follows. And some discussions on future study are given at the end of the chapter.

11.1 Stability

We presented a new way in Chapter 2 to obtain the stiffness matrices of a general pin-jointed structure. Using these formulations, three different stability criteria—stability, prestress stability, and super stability—were defined based on positive definiteness of the stiffness matrices: stability of a structure means that it has locally minimum energy, a prestress stable structure is stable in the deformation field spanned by the mechanisms, and a super stable structure is always stable regardless of its materials and level of prestresses. It is important to note that any stretched version of a super stable structure is also super stable. Further investigation showed that prestress stability is only necessary but not sufficient condition of stability, which was misunderstood before.

Pin-jointed structures were classified in a more logical way in Chapter 2, based on their stability properties: (1) trusses without prestresses, (2) tensile structures that carry only tension, and (3) tensegrity structures that carry both of compression and tension. Tensile and tensegrity structures are also called prestressed (pin-jointed) structures. It was shown that kinematical determinate trusses are stable, tensile structures are super stable, but stability of tensegrity structures are not apparent. This motivates the study on stability conditions for tensegrity structures in Chapter 3.

Stability of tensegrity structures were shown in Chapter 3 to be highly dependent on distribution of prestresses: prestress stable structures are stable only if level of prestresses is small enough. Sufficient conditions for super stability of tensegrity structures were further presented: (a) the geometry matrix is full-rank; (b) the force density matrix (or geometrical stiffness matrix) is positive semi-definite; (c) the force density matrix (or geometrical stiffness matrix) has maximum rank while satisfying the non-degeneracy condition for a free-standing

structure presented in Chapter 2. Condition (a) is the necessary condition for stability of a tensegrity structure, and was demonstrated to be equivalent to those obtained in structural rigidity theory in mathematics, and much easier to use as well. Conditions (a) and (b) are also the necessary conditions for super stability of a tensegrity structure.

The stiffness and force density matrices of symmetric structures can be written in block-diagonal forms by using group representation theory, which significantly reduces computational costs and may lead to in-depth understanding of the structures. We presented a direct strategy in Chapter 6 to analytically derive the diagonal blocks for a class of structures in general form, rather than dealing with individual structure as in conventional methods. The strategy enables us to find the conditions for prestress stability of prismatic tensegrity structures in Chapter 6 and for super stability of star-shaped tensegrity structures in Chapter 7: it was made clear for the first time that prestress stability of the structures that are not super stable is influenced by the height/radius ratio and connectivity of vertical cables; a star-shaped tensegrity structure without center members is guaranteed to be super stable if and only if it has odd number of struts and these struts are as close to each other as possible. Further investigation in Chapter 7 discovered that some star-shaped structures have multi-stable configurations, confirmed by numerical computations and physical models.

Optimization methods have also been extensively applied to stability investigation and design of tensegrity structures, in order to achieve novel and reasonable design. For the structures with multiple prestress modes, distribution of prestresses is a linear combination of these modes. Hence, we have the freedom to carefully select it satisfying self-equilibrium equations to let the structure have maximum stiffness. For this purpose and considering preference in design and construction, we presented a multi-objective optimization method to determine distribution of prestresses of a tensegrity structure, where its stiffness is to be maximized and the force deviation of prestresses from target values is to be minimized. To assist decision making, the curve of Pareto optimal solutions for these two objective functions was presented, since no simple optimal solution exists. Designers can have the freedom to choose a solution according to their preference as a trade-off between the objectives for the force design of the structure.

11.2 Morphology

Three different methods—adaptive force density method, direct approach and symmetry strategy—for morphology of tensegrity structures have been proposed. All of them are general methods, and applicable to different problems according to specific design requirements: the adaptive force density method is applicable to complex structure with high efficiency, and more importantly, it can ensure a stable solution in the form-finding process; the direct approach is good at controlling geometrical properties, such as member directions and symmetry properties; and the symmetry strategy extensively makes use of symmetry properties of the structure to provide analytical solutions.

The *adaptive force density method* presented in Chapter 4 makes use of the great advantage of the force density method in transforming non-linear equations into linear forms. The process of form-finding is divided into two design stages: (1) to adaptively find the feasible force densities that satisfy the non-degeneracy condition for general free-standing structures, and (2) to uniquely determine self-equilibrated configurations by specifying independent set of nodal coordinates. Geometrical and mechanical properties can be precisely controlled by respectively incorporating the constraints formulated in linear terms with respect to force densities and nodal coordinates into the two design stages. New configurations of a structure with given topology can be systematically found by modifying the variables, such as initial force densities, constraints and independent nodal coordinates. Moreover, super stability can also be ensured during the process by making the force density matrix positive semi-definite. The proposed method was demonstrated to be efficient for complex structures that have relatively large number of members. However, as the common shortcoming of the family of force density method, it cannot have direct controls over the prestresses and lengths of the members, because their ratios are involved in the process as variables.

To have some direct controls over geometrical properties of a tensegrity structure, we presented the *direct approach* in Chapter 5. It is an excellent application of graph theory, where structures are modeled as directed graphs. The method enables us to have the freedom of controlling member directions as well as force magnitudes. Hence, it is especially useful in the design of large span structures,

such as cable domes, for the purpose of meeting the requirements by the architectural designers and the structural engineers as well. The proposed method is of high efficiency because only linear equations need to be solved, and is capable of systematically searching for new configurations. However, when the structures become more complicated, there would be many variables that need to be specified by the designers, which might be considered as an extra burden.

For the structures with high symmetry, it was demonstrated to be sufficient to consider only the representative nodes in their morphology problem. This *symmetry strategy* can achieve the self-equilibrated configurations of the whole class of structures in a general form, e.g., the prismatic structures discussed in Chapter 7 and star-shaped structures in Chapter 8, both of which are of dihedral symmetry. Another good idea to make use of symmetry properties of a structure is to observe singularity of specific blocks of the symmetry-adapted force density matrix: in Chapter 6, we showed that self-equilibrated configurations of the structures with dihedral symmetry can also be analytically derived by considering singularities of the A_2 and E_1 blocks. Super stability is also possible to be ensured during the form-finding process by considering positive definiteness of other blocks of the matrix.

It is necessary to identify the distribution of prestresses, in construction, evaluation and adjustment of the structures, meanwhile, costs are expected to be as small as possible. For this purpose, we firstly presented the formulation for evaluation of identification error, where both measurement errors of prestresses and coordinates are taken into account. The identification error was utilized as an objective or constraint for finding the optimal members for measurement of prestresses: the objective function of the optimization problem is to minimize the number of measurement devices subject to a constraint on identification error, or to minimize the identification error when the number of devices is given. Preferences of employment of measurement devices to the members can also be taken into account, which gives more freedom to engineer in site, without suffering much lose in accuracy. To have a better solution, the simulated annealing method is improved by determining the initial solution by the stingy method, rather than starting from a random initial solution. The proposed method is demonstrated

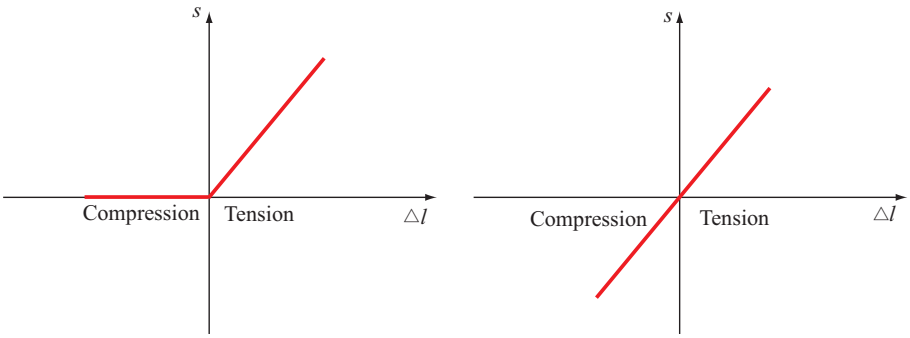

(a) cable (b) strut

Figure 11.1: Prestress and member length extension relation of the cables and struts in the elastic system. Cables have zero stiffness in compression, which may arise difficulties in stability investigation of the structures with unstressed cables.

to be of high efficiency, and has higher capability to find (near) optimal solutions compared to the method from a random initial solution.

11.3 Future Studies

Some further topics relevant to tensegrity structures are now under study, which will be outlined in this section. This include stability investigation of the structures consisting of unstressed cables, which have zero stiffness in compression, and morphology and stability of the structures that have symmetry of space group where translation operations are also involved.

11.3.1 Stability of Structures with Unstressed Cables

The stability of the tensegrity structures investigated so far is based on the assumption that all members have non-zero prestresses. Hence, stiffness of the members do not change for the elastic system in the field of small deformation. This assumption might be reasonable and acceptable for almost all tensegrity structures in practice.

However, in some cases, the fact that the cables cannot have stiffness in compression which has been ignored so far may dominate the stability problem of the structures. If the cables contain no stresses, and their lengths tend to be short-

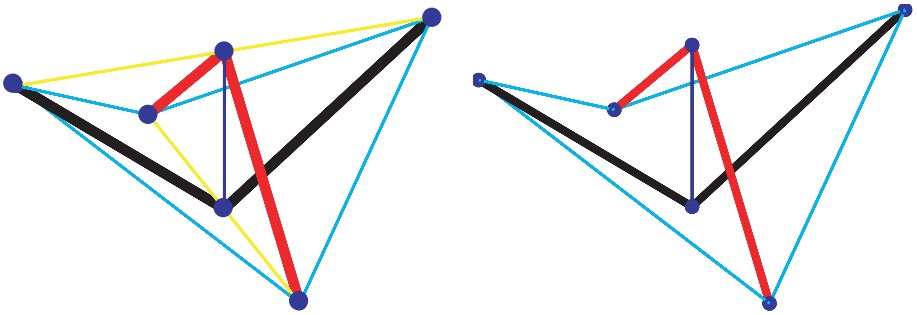

(a) initial structure (b) unstressed cables removed

Figure 11.2: The structure with some unstressed cables. The four members (cables) paralleling to xy-plane cannot carry prestresses, because the other three members connected to each of them are lying in the same plane.

ened, then the cables loss their resistant capability to that tendency, as shown in Fig. 11.1.

Consider, for example, the tensegrity structure as shown in Fig. 11.2.(a). The linearized cables in the top and the bottom cannot contain prestresses, because the other three members connected to a node fall into the same plane except for these cables. Rank investigation of the equilibrium matrix shows that the structure has one prestress mode and no mechanism. Hence, the structure seems to be stable if the material is stiff enough compared to the level of the prestresses.

However, in the discussions on the stability, we have assumed that all of the members are stressed such that the cables do not loss their stiffness even it is shorten by the small displacement. But in this case, the stiffness of the unstressed cables becomes zero if they are shortened.

Therefore, the stability investigation of the tensegrity structures should be extended to consider the material instability of the unstressed cables. Connelly and Whiteley (1996) gave a descriptive solution for the problem. But it is not easy to numerically implement.

From the viewpoint of energy, if there exists a small displacement that does not change the stressed members and shorten all of the unstressed cables, then the structure is unstable, because the strain energy of the structure is not changed so the structure with the present configuration does not has strictly local minimum energy.

Accordingly, we have the following strategies to investigate the stability of a tensegrity structure with some unstressed cables.

First Strategy : Assume that the unstressed cables can also have stiffness in compression to investigate the stability of the strengthened structure. If the strengthened structure is unstable, then the structure considering material instability of the cables cannot be stable; otherwise, we consider the second strategy.

Second Strategy : Find out whether there exists a displacement that does not change the stressed members and shortens the member lengths of the unstressed cables. If this displacement exists, then the structure is unstable; otherwise, it is stable.

Similar to the compatibility equation in Eq. (2.37), which relates the displacement $\mathbf{d}$ to the member extension $\mathbf{e}$ by the transpose of the equilibrium matrix for the whole structure, we can also write the following equations for the member extensions $\bar{\mathbf{e}}$ and $\hat{\mathbf{e}}$ for the stressed and unstressed members, respectively

$$\begin{aligned} \bar{\mathbf{D}}^\top \mathbf{d} &= \bar{\mathbf{e}} \\ \hat{\mathbf{D}}^\top \mathbf{d} &= \hat{\mathbf{e}} \end{aligned} \tag{11.1}$$

If the displacement $\mathbf{d}$ does not change the lengths of the stressed members, then $\bar{\mathbf{e}} = \mathbf{0}$; while $\hat{\mathbf{e}} \leq \mathbf{0}$ for the unstressed cables for the second strategy. Finding such a displacement can be formulated as the following optimization problem:

Optimization Problem 10.1

$$\begin{aligned} \text{Minimize} \quad & \hat{e} = \text{Max}(\hat{\mathbf{e}}) \\ \text{s.t.} \quad & \bar{\mathbf{D}}^\top \mathbf{d} = \mathbf{0} \\ & ||\mathbf{d}|| = 1 \end{aligned} \tag{11.2}$$

The problem can be solved by many existing approaches, for example the function $fmincon()$ with constraints in the optimization package of MATLAB. If the optimal solution $\hat{e}$ for the above optimization problem is equal to or smaller than zero; i.e., $\hat{e} \leq 0$, then the structure is unstable.

The solution of the Optimization Problem 10.1 for the structure in Fig. 11.2 shows that there exist displacements that make $\hat{e} < 0$. Note that this is only the

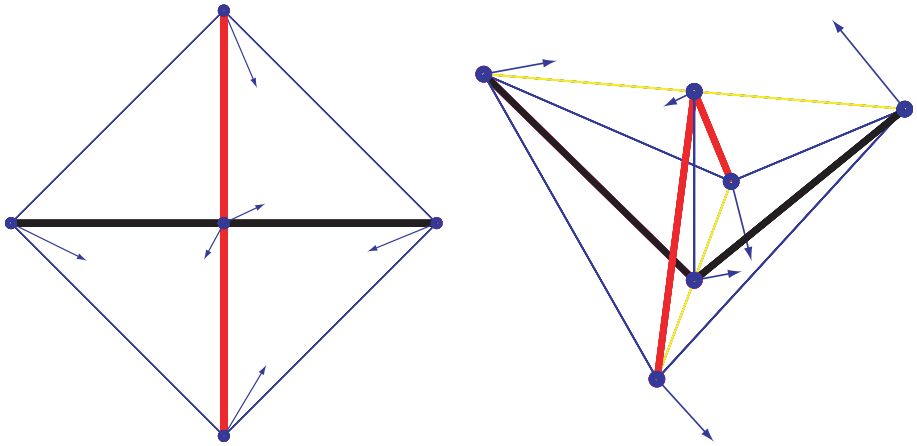

(a) top view (b) side view

Figure 11.3: One of the unstable mode of displacement of the structure in Fig. 11.2. The lengths of all stressed members remain unchanged, while some of the unstressed members (cables) are shortened by the unstable mode. Hence, strain energy of the structure does not change subject to the displacement, indicating that it is not stable.

solution of the optimization problem, which does not mean that this displacement is the only one that can make the structure change configuration without increasing its energy. The unstable displacement mode obtained by solving the optimization problem is shown in Fig. 11.3, where the directions and lengths of the arrows shows the directions and magnitudes of the displacement at the nodes.

It seems that we have a new and more comprehensible idea for the stability investigation of the tensegrity structures with unstressed cables in the filed of small deformation. But more careful considerations are needed in the future work in order to include all possibilities to obtain a general solution.

11.3.2 Structures with Space Symmetry

Besides applying the symmetry operations, such as rotations and reflections, in a point group to the nodes to obtain a structure with symmetry of that group, we can also used the translation involved in the space group. For example, the prismatic structure, can be translated in the z-direction and rotated so as to assemble together to obtain an infinite tensegrity tower.

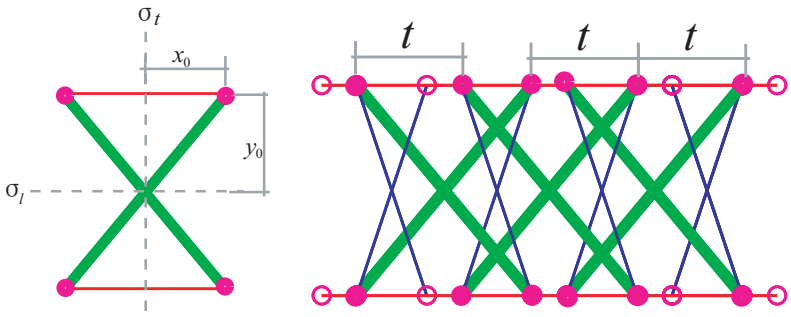

(a) unit cell (b) an example structure

Figure 11.4: Unit cell and translations of the two-dimensional tensegrity structure with space symmetry. Only translation operations are involved in this structure. A unit cell as in (a) consists of two horizontal cables and two crossing struts. The structure as in (b) is constructed by translations of the unit cell by t in x-direction.

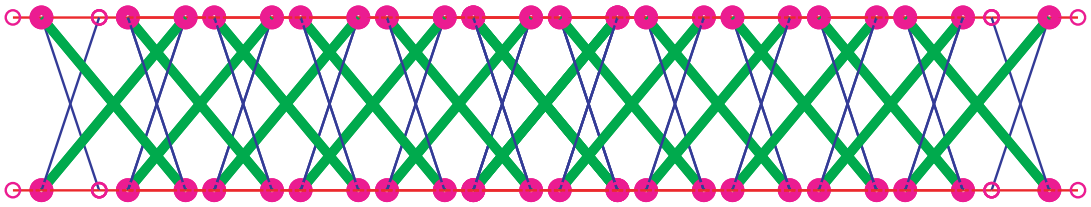

Figure 11.5: Example 1: self-equilibrated configuration of the structure when force density of the horizontal cable is given as $q_{h_2} = 2$.

For a simpler case, we consider only translation in one direction to the two-dimensional unit cell as shown in Fig. 11.4.(a). The unit cell itself has transverse and longitudinal reflection symmetries. It is translated t to the right and left of it as shown in Fig. 11.4.(b) and then goes on to form an infinite structure in two-dimensional space as in Fig. 11.5. Hence, it is sufficient to investigate the equilibrium of this reference node only.

Take a node of the unit cell as the *reference node*. The reference node is connected by two horizontal cables in x-direction, one strut and one vertical cables.

Denote the coordinate of the reference node as

$$\mathbf{X}_0 = \begin{pmatrix} x_0 \\ y_0 \end{pmatrix} \tag{11.3}$$

The representation matrices $\mathbf{R}_t$ and $\mathbf{R}_l$ corresponding to the transverse reflection σ_t and longitudinal reflection σ_l can be written as

$$\mathbf{R}_t = \begin{pmatrix} -1 & 0 \\ 0 & 1 \end{pmatrix} \text{ and } \mathbf{R}_l = \begin{pmatrix} 1 & 0 \\ 0 & -1 \end{pmatrix}$$

And the matrix representation of the translation in the x-direction can be written as

$$\mathbf{t} = t \begin{pmatrix} 1 \\ 0 \end{pmatrix}$$

where t is the unit translation in x-direction, and $\mathbf{t}$ is the unit translation vector.

There are two nodes connecting to the reference node as horizontal cables, and the coordinates of them can be written as

$$\mathbf{X}_{h_1} = \mathbf{R}_t\mathbf{X}_0 + \mathbf{t} \text{ and } \mathbf{X}_{h_2} = \mathbf{R}_t\mathbf{X}_0 + 2\mathbf{t}$$

and the two other nodes connecting to the reference node as strut and vertical cable can be written as

$$\mathbf{X}_s = \mathbf{R}_t\mathbf{R}_l\mathbf{X}_0 \text{ and } \mathbf{X}_v = \mathbf{R}_t\mathbf{R}_l\mathbf{X}_0 + \alpha\mathbf{t}$$

where α is an arbitrary integer, and the matrix representation $\mathbf{R}_t\mathbf{R}$ is actually the inversion of the reference node that

$$\mathbf{R}_t\mathbf{R}_l = -\mathbf{I}$$

which is the representation matrix of the two-fold rotation. By using these representation matrices and the translation vector, we can generate all the nodes of the infinite two-dimensional tensegrity structure.

The self-equilibrium equation of the reference node not being subjected to any external load can be written as

$$q_{h_1}(\mathbf{X}_{h_1} - \mathbf{X}_0) + q_{h_2}(\mathbf{X}_{h_2} - \mathbf{X}_0) + q_s(\mathbf{X}_s - \mathbf{X}_0) + q_v(\mathbf{X}_v - \mathbf{X}_0) = \mathbf{0} \qquad (11.4)$$

where q_{h_1}, q_{h_2}, q_s and q_v denote the force densities of the two horizontal cables, strut and vertical cable, respectively. From the definitions of the representation matrices and the translation vector, we may know that the self-equilibrium equations in x- and y-directions of the reference node are independent, so they

can be considered separately in each direction. The self-equilibrium equation in y-direction can be written as from the above equation

$$-2q_s y_0 - 2q_v y_0 = 0 \tag{11.5}$$

therefore, we may have

$$q_s = -q_v \tag{11.6}$$

irrespective of the coordinate y_0 of the reference node in y-direction.

Subsequently, the self-equilibrium equation in x-direction can be written as

$$q_{h_1}(-2x_0 + t) + q_{h_2}(-2x_0 + 2t) + \alpha q_v t = 0 \tag{11.7}$$

For simplicity, we set the force density of the vertical cable as +1. This will not reduce the generality of the solution since the force densities of the members of a self-equilibrated structure can be modified in scale. The coordinate of the reference node in x-direction can be then calculated as

$$x_0 = t(2q_{h_1} + q_{h_2} + \alpha)/2(q_{h_1} + q_{h_2}) \tag{11.8}$$

From the equation, we may get to know that the unit translation t should have the following relationship with the coordinate x_0 of the reference node in x-direction, in order to make the two nodes be in two different sides of the reference node to have the same signs of prestresses:

$$x_0 < t < 2x_0 \tag{11.9}$$

Therefore, we have the following relation for the force density q_{h_2} of the second horizontal cable

$$q_{h_2} > \alpha \tag{11.10}$$

When q_{h_2} is larger, t is closer to $2x_0$, and only if q_{h_2} becomes infinite, $t = 2x_0$ so that the nodes after translation will coincide with the original node.

Accordingly, x_0 can be determined by specifying the distance of translation and the values of the force densities of the two horizontal cables. There is no restrict for the determination of the y_0 so that it can be specified arbitrarily.

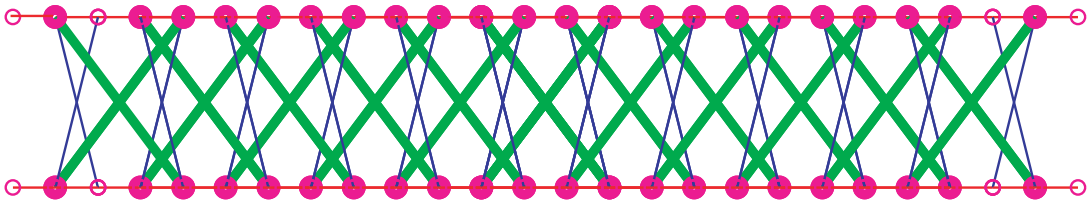

Figure 11.6: Example 2: self-equilibrated configuration of the structure when force density of the horizontal cable is given as $q_{h_2} = 3$.

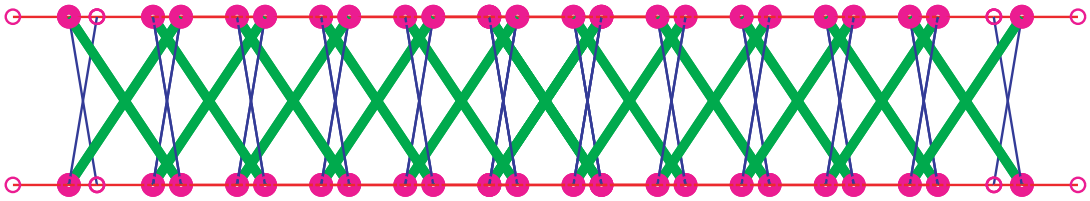

Figure 11.7: Example 3: self-equilibrated configuration of the structure when force density of the horizontal cable is given as $q_{h_2} = 5$.

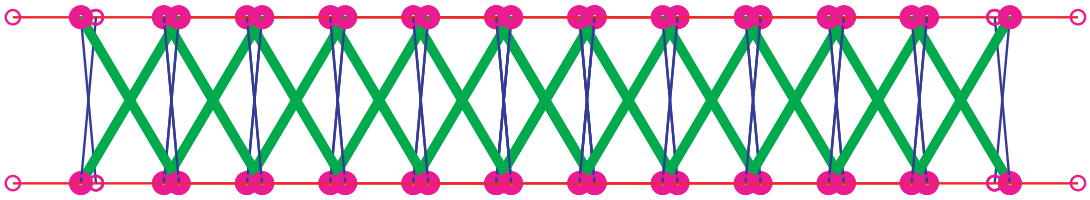

Figure 11.8: Example 4: self-equilibrated configuration of the structure when force density of the horizontal cable is given as $q_{h_2} = 10$.

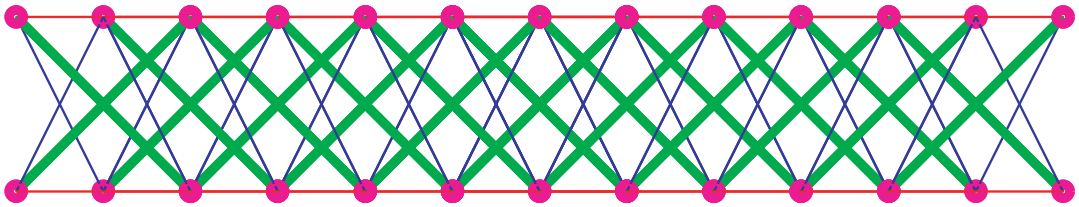

Figure 11.9: Example 5: self-equilibrated configuration of the structure when force density of the horizontal cable is given as $q_{h_2} = 1$.

Set $\alpha = 1$, and force density $q_{h_1} = 1$ for the first horizontal cable, now let us investigate the configuration of the structures with different force densities q_{h_2} of the second horizontal cable, which are listed in Figs. (11.6)–(11.9).

So far, we have obtained the self-equilibrium condition for the infinite two-dimensional tensegrity structure with space symmetry (translation in only one direction). However, we still have the following unsolve problems:

[L1] How to constrain the two ends of the structure if we do not want it to be infinite and want to have only a part of it to be used for some purposes?

[L2] Is the structure obtained super stable and prestress stable? Is there any simple method to analyze the stability of a structure with space symmetry.

[L3] How to extend the idea of the two-dimensional structure to a three-dimensional one?

Appendix A

REDUCED ROW-ECHELON FORM (RREF)

Any (possibly not square) finite matrix $\mathbf{A}$ can be reduced by a finite sequence of linear elementary row operation $\mathbf{E}_1, \mathbf{E}_2, \ldots, \mathbf{E}_l$, each one invertible, to a *Reduced Row-Echelon From* (RREF) $\mathbf{U} := \mathbf{E}_m \cdots \mathbf{E}_2 \mathbf{E}_1 \mathbf{A}$ characterized by the following three properties:

[L1] The first nonzero element in any nonzero row is 1.

[L2] The leading 1 of each nonzero row 1 appears in a column of which all the other elements are 0.

[L3] Each such leading 1 comes in a column after every preceding row's leading zeros.

Matrix $\mathbf{A}$ determines its RREF $\mathbf{U}$ uniquely, even though $\mathbf{A}$ does not determine uniquely the sequences of Elementary Row-Operations that reduce $\mathbf{A}$ to $\mathbf{U}$.

For example, the RREF of matrix

$$\mathbf{A} = \begin{pmatrix} 16 & 2 & 3 & 13 \\ 5 & 11 & 10 & 8 \\ 9 & 7 & 6 & 12 \\ 4 & 14 & 15 & 1 \end{pmatrix} \tag{A.1}$$

is

$$\mathbf{U} = \left(\begin{array}{ccc|c} 1 & 0 & 0 & 1 \\ 0 & 1 & 0 & 3 \\ 0 & 0 & 1 & -3 \\ \hline 0 & 0 & 0 & 0 \end{array}\right) \tag{A.2}$$

We can easily see that the rank of $\mathbf{U}$ is 3. Since the rank of $\mathbf{A}$ is unchanged by pre multiplication by invertible matrices, rank($\mathbf{A}$)=rank($\mathbf{U}$). From the fact that we have applied only row operations on $\mathbf{A}$ to get $\mathbf{U}$, we can know from $\mathbf{U}$ that the first three columns of $\mathbf{A}$ are independent.

Appendix B

SYMMETRY

B.1 Group

A mathematical group may be defined operationally as a set of elements that satisfy the following four general criteria:

[L1] Any two elements of the group must combine to give an element that is also a member of the group.

[L2] The associative law of combination must be satisfied.

[L3] The group must contain an element that commutes with all the other elements and also leaves them unchanged, which is call the *identity element*.

[L4] The inverse of every element in the group is also a member of the group.

The *order* of a group is the number of elements in the group.

There are basically two types of groups: point group and space group. *Point group* indicates that there is at least one point in the system which is not affected by any of the operations. If translational operations are allowed, the system can no longer be described by point symmetry. The symmetry groups that contain translational elements are referred to as *space groups*.

Hence, the dihedral group used in Chapters 6, 7 and 8 is a point group.

B.2 Symmetry Operations

A symmetry operation is an operation which when applied to a structure moves it in such a way that its final position is physically indistinguishable from its initial position. In the point group, there are five different types of symmetry operations that an isolated object may possess listed as follows:

[L1] E, *identical operation*:
Nothing will be done to the structure, so the structure is unchanged. The corresponding symmetry operation is called the identity.

[L2] C_n, *rotation operation*:
An operation of rotation of the structure counter-clockwise or clockwise about an axis. If a rotation by $2\pi/n$ brings the structure into coincidence with itself, the structure is said to have an n-fold rotation axis.

[L3] σ, *reflection operation*:
An operation of reflection about a plane.

(a) σ_v, *vertical plane of symmetry* contains the principal axis;

(b) σ_d, *dihedral plane of symmetry* contains the principal axis and in addition bisects pairs of two-fold axes which are perpendicular to the principal axis;

(c) σ_h, *horizontal plane of symmetry* is perpendicular to the principal axis;

[L4] S_n, *improper axis of rotation* (rotation-reflection operation)
The operation can be represented by the product of horizontal plane of symmetry σ_h and rotation C_n about the principle axis as

$$S_n = \sigma_h C_n \tag{B.1}$$

[L5] i, *inversion operation*:
If the origin of a Cartesian coordinate system is placed on the point of inversion, then for every point (x, y, z) in the system there must be a symmetry related point at $(-x, -y, -z)$.

Table B.1: Group multiplication table of group G.

	G_1	G_2	G_3	...
G_1	G_1G_1	G_1G_2	G_1G_3	...
G_2	G_2G_1	G_2G_2	G_2G_3	...
G_3	G_3G_1	G_3G_2	G_3G_3	...
...	...	...	...	...

B.3 Character and Representation

If we lay out a square array, labelling the rows and columns with the operations of the group and allowing the individual entries of the array to be the product of the corresponding operations of the group, we have a *group multiplication table*. Table B.1 shows the general format of the multiplication table of group G, where G_i is the element of the group. The product of two operations is to be defined as successive application of the two operations, the one to the *right* being carried out first.

Two groups are said to exhibit *isomorphism* if a one to one correspondence can be established between the elements of these two groups. In isomorphism, each element of one group is uniquely mirrored by an element of the other group. However, if two or more different elements of one group have the same image in the other group, then these two groups are said to exhibit *homomorphism*.

If R, P and Q are the elements of a group and have the following relation

$$R = Q^{-1}PQ \tag{B.2}$$

then we say that R is the *transform* of P by Q, or that P and R are *conjugate* to each other. The elements of a group which are conjugate to each other are said to form a *class*.

If a set of matrices can be found which form a group that obeys the group multiplication table for a given group, the matrices are said to form a *matrix representation* of that group.

A representation which can be reduced to a sum of other representations is called a *reducible representation*. Otherwise, it is a *irreducible representation*. Both of these two matrix representations are important to us: in Chapter 7, we use the irreducible representation matrices of the dihedral group to derive the

symmetry-adapted forms of the force density matrix and the stiffness matrices; and in Chapter 8 and 9, the reducible representation matrices of the A_2 and E_1 representations, which are respectively corresponding to the transformations about the z-axis and xy-plane, are used to carry out the self-equilibrium analysis.

We give out the three properties of the irreducible representation of a group without proof as:

[L1] If the irreducible representations of a group are one-dimensional, they must form a group in themselves;

[L2] The sum of the squares of the dimensions of the irreducible representations is equal to the order of the group.

[L3] There are as many irreducible representations for a group as there are classes.

A *character* is defined as the trace of an irreducible representation matrix, representing a given operation in a given group. The *character table* for a group lists the characters for the various operations associated with each irreducible representation.

An extremely important property of the matrices which multiply isomorphically to group operations is the fact that *their characters are invariant to a similarity transformation.*

B.4 Dihedral Group

Suppose that we have a regular n-gon in the xy-plane, with center at the origin of coordinates. Take the z-axis as the principal axis. When the n-gon is rotated about the z-axis through the angle $2k\pi/n$ $(k = 0, 1, 2, \ldots, n-1)$, it is carried into itself. All of these n rotations form a *cyclic group* of order n. Note that the rotation corresponding to $k = 0$ is the unit (identity).

If the surface of the n-gon is taken into account twice (both the top and the bottom), it is usually called a *dihedron.* Take any axis of the n-gon joining a vertex with the opposite vertex if n is even, or with the mid-point of the opposite

side if n is odd. When the xy-plane is rotated about this axis through the angles 0 and π, the n-gon is carried into itself too. There are n of these operations.

Therefore, the complete group of transformations carrying the n-gon dihedron into itself consists of $2n$ transformations as mentioned above. And the group constructed by these elements (transformations) is called the *dihedral group* of order $2n$, denoted as $\mathbf{D}_n$.

The symmetry elements of any point group can be produced from its generators. Any of the four basic symmetry elements can be used as generators, either alone or in combination. At most, three of these are sufficient to describe the point symmetry of any system. Table B.2 lists the generator for some common used point groups including the dihedral group interested in our study.

Table B.2: Generators for the various point group.

Group	$\mathbf{C}_n$	$\mathbf{S}_n$	$\mathbf{C}_{nv}$	$\mathbf{C}_{nh}$	$\mathbf{D}_n$	$\mathbf{D}_{nd}$
Generators	C_n	S_n	C_n, σ_v	C_n, σ_h	C_n, C_2	C_n, C_2, σ_d
Group	$\mathbf{T}$	$\mathbf{T}_d$	$\mathbf{T}_h$	$\mathbf{O}$	$\mathbf{O}_h$	$\mathbf{D}_{nh}$
Generators	C_2^z, C_3^{xyz}	S_4^z, C_3^{xyz}	C_2^z, C_3^{xyz}, i	C_4^z, C_3^{xyz}	C_4^z, C_3^{xyz}, i	C_n, C_2, σ_h

If the z-axis is selected as the principal axis for the axial point groups, the matrix representing a proper rotation $\mathbf{R}(C_n^1)$ in the three-dimensional Cartesian coordinate system can be written as

$$\mathbf{R}(C_n) = \mathbf{R}(C_n^1) = \begin{pmatrix} \cos(2\pi/n) & -\sin(2\pi/n) & 0 \\ \sin(2\pi/n) & \cos(2\pi/n) & 0 \\ 0 & 0 & 1 \end{pmatrix} \tag{B.3}$$

and the matrix representation $\mathbf{R}(C_2^x)$ for a twofold axis perpendicular to the principal axis and lying along the x-axis can be written as

$$\mathbf{R}(C_2^x) = \mathbf{R}(C_{21}) = \begin{pmatrix} 1 & 0 & 0 \\ 0 & -1 & 0 \\ 0 & 0 & -1 \end{pmatrix} \tag{B.4}$$

All the representations matrices can be generated by using these two matrices as

$$\mathbf{R}_{i+nj} = (\mathbf{R}(C_n))^i (\mathbf{R}(C_2^x))^j \tag{B.5}$$

where i runs from 0 to $n-1$ and j is equal to zero or one, and therefore, the subscript $i+nj$ of the matrix $\mathbf{R}_{i+nj}$ can represent the numbering of the matrix which is in the range from 0 to $2n-1$.

The irreducible representations and characters of the dihedral point groups (or subgroups) can be constructed in a straightforward manner. The basic requirement is that the character $[\chi(C_n)]^n$ must be equal to the character $\chi(E)$, which in turn equals unity. This yields the following results, for the group $\mathbf{D}_n$ we have

[L1] If n is even, there are four one-dimensional representations: two A representations, A_1 and A_2, two B representations, B_1 and B_2, and a set of two-dimensional E_k representations with k going from 1 to $n/2-1$.

[L2] If n is odd, there is no B representation, and the values of k for the E_k representations run from 1 to $(n-1)/2$.

The characters of the A_1 representation are all $+1$, while the characters of the A_2 are $+1$ for the cyclic subgroup $C_n^i (i = 0, 1, \ldots, n-1)$ about z-axis, and -1 for the two-fold rotations.

The characters of cyclic subgroup of the B representations, if it exists, alternate between $+1$ and -1; and the characters for the two-fold rotations alternate between $+1$ and -1 or -1 and $+1$.

The characters for the pairs of degenerate E_k representations are $[\exp(2\pi i/n)]^{jk}$ and $[\exp(-2\pi i/n)]^{jk}$, where k is the particular one of the E_k under consideration and j comes from the rotational elements C_n^j. Note also that the A and B representations are special cases of this, with k equal to zero and $n/2$, respectively. The generators of the two-dimensional representations can be written as follows in terms of 2-by-2 matrices

$$\mathbf{R}(E_k)_0 = \begin{pmatrix} \cos(2k\pi/n) & -\sin(2k\pi/n) \\ \sin(2k\pi/n) & \cos(2k\pi/n) \end{pmatrix} \text{ and } \mathbf{R}(E_k)_n = \begin{pmatrix} 1 & 0 \\ 0 & -1 \end{pmatrix} \tag{B.6}$$

All the two-dimensional irreducible representation matrices of the dihedral group can be generated by using the above two generators as

$$\mathbf{R}(E_k)_{i+nj} = (\mathbf{R}(E_k)_0)^i (\mathbf{R}(E_k)_n)^j \tag{B.7}$$

where i runs from 0 to $n-1$ and j is equal to 0 or 1.

Appendix C

LEAST SQUARES SOLUTION

For a linear equation

$$\mathbf{A}\mathbf{x} = \mathbf{b} \tag{C.1}$$

where $\mathbf{A} \in \Re^{m \times n}$ and $\mathbf{x} \in \Re^{n}$ denote the coefficient matrix and the unknown vector, respectively. Let r^A denote the rank of $\mathbf{A}$, therefore, we have $r^A \leq m$ and $r^A \leq n$.

From Eq. (C.1), we know that the equation has only one solution $\mathbf{x} = \mathbf{A}^{-1}\mathbf{b}$ if and only if $m = n = r^A$; the equation has infinite solutions while $r^A < n$ and no exact solution in the case of $m > n$ and $r^A = n$.

For the last case, we can have the error $\boldsymbol{\epsilon}$ of the solution $\bar{\mathbf{x}}$ as

$$\boldsymbol{\epsilon} = \mathbf{b} - \mathbf{A}\bar{\mathbf{x}} \tag{C.2}$$

The square of this error can be written as

$$\phi = \boldsymbol{\epsilon}^\top \boldsymbol{\epsilon} = (\mathbf{b} - \mathbf{A}\bar{\mathbf{x}})^\top (\mathbf{b} - \mathbf{A}\bar{\mathbf{x}}) \tag{C.3}$$

The following stationary condition of the square of error ϕ can be written as

$$\mathbf{A}^\top \mathbf{A}\bar{\mathbf{x}} - \mathbf{A}^\top \mathbf{b} = \mathbf{0} \tag{C.4}$$

Since we are discussing the case that $m > n$ and $r^A = n$, so rank of $\mathbf{A}^\top \mathbf{A}$ is r^A so that it is invertible. Therefore, the least square solution of Eq. (C.1) can be written as

$$\mathbf{x} = (\mathbf{A}^\top \mathbf{A})^{-1} \mathbf{A}^\top \mathbf{b} \tag{C.5}$$

Note here that $(\mathbf{A}^\top\mathbf{A})^{-1}\mathbf{A}^\top$ satisfies the definitions of Moore-Penrose matrix inverse, which are

$$\begin{aligned}(\mathbf{A}\mathbf{A}^-)^\top &= \mathbf{A}\mathbf{A}^- \\ (\mathbf{A}^-\mathbf{A})^\top &= \mathbf{A}^-\mathbf{A} \\ \mathbf{A}\mathbf{A}^-\mathbf{A} &= \mathbf{A} \\ \mathbf{A}^-\mathbf{A}\mathbf{A}^- &= \mathbf{A}^-\end{aligned} \tag{C.6}$$

where $(\,)^-$ denotes the Moore-Penrose matrix inverse, so $(\mathbf{A}^\top\mathbf{A})^{-1}\mathbf{A}^\top$ can be written in terms of Moore-Penrose matrix inverse $\mathbf{A}^-$ for simplification that Eq. (C.5) becomes

$$\mathbf{x} = \mathbf{A}^-\mathbf{b} \tag{C.7}$$

Bibliography

Atkins, P.W., Child, M.S. and Phillips, C.S.G., 1970. Tables for Group Theory. Oxford University Press. 6.2.2

Altmann, S.L. and Herzig, P., 1994. Point-group Theory Tables. Clarendon Press, Oxford. 6.4, 7.2.2

Azizi, N., Zolfaghari, S., 2004. Adaptive temperature control for simulated annealing: a comparative study. Computers & Operations Research. 31, 2439–2451. 10.3.2.1

Barnes, M. R., 1999. Form finding and analysis of tension structures by dynamic relaxation. Int. J. Space Struct. 14(2), 89–104. 1.2.2

Group Theory and Chemistry. Clarendon Press, Oxford, 1973. 4.2.3.2, 6.2, 7.4.2.1

Borse, G. J., 1997. Numerical Method with MATLAB. International Thomson Publishing Inc. 5.3.1, 9.3, 10.4

Caspar, D.L.D., and Klug, A., 1962. Physical principles in the constructurion of regular viruses. Proceedings of Cold Spring harbor Symposium on Quantitative Biology. 27, 1-24. 1.1.5

Calladine, C.R., 1978. Buckminster Fuller's "tensegrity" structures and Clerk Maxwell's rules for the construction of stiff frames. Int. J. Solids Struct. 14, 161–172. 2.5.1, 2.5.1, 6.5.3

Calladine, C.R. and Pellegrino, S., 1991. First-order infinitesimal mechanisms. Int. J. Solids Struct., 27, 505–515. 1.2.3, 3.3.2

Calladine, C.R. and Pellegrino, S., 1992. Further remarks on first-order infinitesimal mechanisms. Int. J. Solids Struct., 29, 2119–2122. 3.3.2

Chan, W., Arbelaez, D., Bossens, F., Skleton, R.E., 2004. Active vibration control of a three-stage tensegrity structure. SPIE 11th Annual International Symposium on Smart Structures and Materials, San Diego, California, USA. 1.1.4

Connelly, R., 1982. Rigidity and energy. Invent. Math. 66(1), 11–33. 1.2.3, 2.2.2, 3.2, 3.2.2, 3.2.2

Connelly, R. and Back, A., 1998. Mathematics and tensegrity. American Scientist, 86, 142–151. 4.1, 7.2.3

Connelly, R. and Terrell, M., 1995. Globally rigid symmetric tensegrities. Structural Topology, 21, 59–78. 1.2.2, 4.4.3.2, 7, 7.1, 7.2.4, 7.4.1, 7.6

Connelly, R. and Whiteley, W., 1996. Second-order rigidity and prestress stability for tensegrity frameworks. SIAM J. Discrete Mathematics, (9)3, 453–491. 1.2.2, 1.2.3, 2.5.2.3, 11.3.1

Connelly, R., 1999. Tensegrity Structures: Why are they Stable? Rigidity Theory and Applications, edited by Thorpe and Duxbury, Kluwer/Plenum Publishers, 47–54. 1.2.3, 3.3.1, 1

Donev, A., Torquato, S., Stillinger, F. H., Connelly, R., 2004. A linear programming algorithm to test for jamming in hard-sphere packings. J. Comp. Phys., 197, 139–166. 1.1.6

El-Lishani, Sana; Nooshin, H.; Disney, P., 2005 Investigating the Statical Stability of Pin-jointed Structures Using Genetic Algorithm Int. J. Space Structures, 20(1), 2005, 53–68. 9.1

Fowler, P.W. and Guest, S.D., 2000. A symmetry extension of Maxwell's rule for rigidity of frames. Int. J. Solids Struct., 37, 1793-1804. 6.3.2

Fuller, R. B., 1975. Synergetics, Explorations in the Geometry of Thinking. Collier Macmillan, London. 1.1.1

Guest, S.D., 2006. The stiffness of prestressed frameworks: a unifying approach. Int. J. Solids Struct., 43, 842-854 2.4, 3.3.2

Harary, F., 1969. Graph Theory. Addison-Wesley, Reading, MA. 2.1.2, 4.2.3.2

S. H. Juan and J. M. M. Tur, 2007. Tensegrity frameworks: Static analysis review. Mechanism and Machine Theory, Available online. 1.2.2

Horn, R.A. and Johnson, C.R., 1990. Matrix Analysis. 10.2.2

Ingber, D.E., 1993. Cellular tensegrity: defining new rules of biological design that govern the cytoskeleton. J. Cell Science. 104, 613–627. 1.1.5

Ingber, D.E., 1998. The architecture of life. Scientific American, January, 48–57. 1.8

Kangwai, R.D., Guest, S.D. and Pellegrino, S., 1999. Introduction to the analysis of symmetric structures. Computers and Structures 71(2), 671–688. 6.1, 7.4.2.1

Kangwai, R.D. and Guest, S.D., 2000. Symmetry adapted equilibrium matrices. Int. J. Solids Struct., 37, 1525–1548. 6.5.1, 7.4.2.1

Kaveh, A., 1992. Structural Mechanics: Graph and Matrix Methods. Wiley, NY. 2.1.2

K. Kawaguchi and S. Ohya, 2004. Preliminary Report of Observation of Real Scale Tensegrity Skeletons under Temperature Change. Proc. of Symposium of Internatinal Association for Shell and Spatial Structures (CD-ROM), Montpellier, France, Sep. 2004. 1.1.3.2

K. Kawaguchi and Y. Suzuki, 2005. Extraction of selstress modes and inextentional displacement modes of tensegrity structures by group theory. J. Struct. Constru. Eng., AIJ, No. 597, 77–84. 6.5.1

Kettle, S.F.A., Symmetry and Structure, 2nd ed. John Wiley & Sons Ltd, West Sussex, England, 1995. 6.2, 6.3.2, 6.3.2, 7.2.1

Kirkpatrick, S., Gelatt, C.D., Jr., Vecchi, M.P., 1983. Optimization by simulated annealing. Science. 220(4598), 671–680. 10.3.2.1

Lay, D.C., 1996. Linear algebra and its applications, 2nd ed. Pergamon Press, Oxford. 4.3.1

Livesley, R.K., 1975. Matrix Methods of Structural Analysis, 2nd Edn. Reading, MA Addison-Wesley. 2.5.1

Masic, M., Skelton, R.E., Gill, P.E., 2005. Algebraic tensegrity form-finding. Int. J. Solids Struct. 42(16-17), 4833–4858 . 2.4

Maurin, B., Motro, R., 1998. The surface stress density method as a form-finding tool for tensile membranes. Engineering Structures. 20(8), 712–719. 2.2.2, 10.4.1

Maxwell, J.C., 1864. On the calculation of the equilivrium and stiffness of frames. Phil. Mag. 27, 294 (paper XXVI in Collected Papers, Cambridge 1890). 1.1.1

Motro, R., 1984. Forms and forces in tensegrity systems, in: H.Nooshin, ed.. Proc. 3rd Int. Conf. on Space Struct., Elsevier, Amsterdam. 180–185. 1.2.2

Motro, R., 1992. Tensegrity systems: the state of the art. Int. J. Space Structures. 7(2), 75–83. 1.1.2

Motro, R., 1996. Structural morphology of tensegrity systems. Int. J. Space Structures. 11(1&2), 233–240. 1.1.2

Motro, R., Tensegrity : structural systems for the future. London : Kogan Page Science, 2003. 1.1.2, 9.3

Murakami, H., 2001. Static and dynamic analyses of tensegrity structures. Part 1. Nonlinear equations of motion. Int. J. Solids Struct. 40, 6347–6367. 2.4

Pellegrino, S., 1986. Mechanics of kinematically indeterminate structures. Ph.D. dissertation. University of Cambridge, U.K. 1.2.2

Pellegrino, S., Calladine, C.R., 1986. Matrix analysis of statically and kinematically indetermined frameworks. Int. J. Solids and Struct. 22(4), 409–428. 2.5.1

Pugh, A., 1976. An introduction to Tensegrity. University of California Press, Berkeley, California. 1.2.2

Schek, H. J., 1974. The force density method for form finding and computation of general networks. 1.2.2, 2.2.2, 2, 4.1

Sultan, C., Corless, M., Skelton, R.E., 2001. The prestressability problem of tensegrity structures: some analytical solutions. Int. J. Solids and Struct. 38, 5223–5252. 1.2.2

Sultan, C., Corless, M., Skelton R.,E., 2002. Symmetrical reconfiguration of tensegrity structures. International Journal of Solids and Structures. 39, 2215–2234. 4.4.1

Thompson, J.M.T. and Hunt, G.W., 1984. Elastic Instability Phenomena. John Wiley, Chichester. 1.2.1, 2.5.2.1

Tibert, G., Pellegrino, S., 2003. Review of form-finding methods for tensegrity structures. Int. J. Space Struct. 18(4), 209–223. 1.2.2

Vassart, N. and Motro, R., 1999. Multiparametered formfinding method: application to tensegrity systems. Int. J. Space Struct. 14(2), 147–154. 1.2.2, 4.1

Weiss, P., 2004. Candy science: M&Ms pack more tightly than spheres. Science News, 165(7), 102. 1.1.6

Weisstein, E.W., 1999. Affine transformation. MathWorld, http://mathworld.wolfram.com/AffineTransformation.html 3.1

Zhang, J.Y., Ohsaki, M. and Araki, Y., 2004. Optimal measurement positions for identifying stress distribution of membrane structures using cable net approximation. Proc. Third China-Japan-Korea Joint Symposium on Optimization of Structural and Mechanical Systems (CJK-OSM3), Kanazawa, Japan, 547–552. 10.1, 10.3.2.2

Zhang, L., Maurin, B. and Motro, R., 2006. Form-finding of nonregular tensegrity systems. J. Structrual Engineering. 1435–1440. 1.2.2

Zhu, L.P., Elishakoff, I. and Starnes, Jr., J. H., 1996. Derivation of multidimensional ellipsoidal convex model for exprimental data, Mathematical and Computer Modeling, 24(2), 103–114. 10.2.2